Mg(II) Heterodinuclear Catalysts for the Synthesis of Oxygenated Polymers

Gloria Rosetto

University of Oxford

Department of Chemistry

Merton College

March 2022

A thesis submitted in partial fulfilment of the requirements for the degree of Doctor of Philosophy in Chemistry

Per la mia famiglia

Declaration

All work presented in this thesis was carried out at the University of Oxford or the University of Konstanz, by the author, unless otherwise stated.

Gloria Rosetto

Abstract

The thesis describes the use of heterodinuclear Mg(II)M(II) complexes (M = transition metals) as catalysts for the ring-opening copolymerisation (ROCOP) of epoxides and anhydrides, and epoxides and CO_2.

Chapter 1 provides an introduction to ROCOP, outlining the mechanism and catalyst developments, with a particular focus on epoxides and CO_2. Routes towards the construction of ROCOP-derived block copolymers, and the concept of switch catalysis are also described.

Chapter 2 details the ROCOP of norbornene anhydride (NA) and cyclohexene oxide (CHO) for a series of heterodinuclear Mg(II)M(II) complexes, were M = first row transition metals. A representative rate law is proposed on the basis of kinetic experiments for the most active complex, Mg(II)Co(II). Subsequently, monomer insertion selectivity for ROCOP of tricyclic anhydride (TCA), cyclohexene oxide (CHO), and CO_2 is determined for complexes Zn(II)Zn(II), Mg(II)Mg(II), Mg(II)Zn(II) and Mg(II)Co(II). It is found that Zn(II)Zn(II) selectively forms poly(TCA-*alt*-CHO), Mg(II)Zn(II) forms poly((TCA-*alt*-CHO)-*ran*-cyclohexene carbonate), and Mg(II)Mg(II) and Mg(II)Co(II) selectively form poly(cyclohexene carbonate) (PCHC).

Chapter 3 describes the synthesis of multi-block copolymers, up to heptablock, of PCHC and PE in one-pot by changing the headspace between CO_2 and N_2 gas at 1 bar, using the Mg(II)Co(II) catalyst. Switch catalysis is also used to make a pentablock polymer, the final block afforded by the ring-opening polymerisation of ε-caprolactone (CL).

Chapter 4 details the synthesis of and characterisation of a Mg(II)Co(II) complex with organometallic co-ligands. It is demonstrated that when using this complex for the ROCOP of CO_2 and epoxides, in addition with bifunctional protic chain transfer agents, high molar

mass polycarbonates with monodisperse distributions are yielded. Mechanical data is obtained for a high molar mass poly(vinyl-cyclohexene carbonate) (PvCHC).

Chapter 5 details the synthesis and characterisation of Ni(II) phenoxyiminato complexes, and their application in ethylene polymerisation under various conditions. Three different strategies towards Ni(II) alkoxide complexes are attempted, as they can operate as initiators for either ROP or ROCOP processes.

Chapter 6 summarises the key findings of the thesis and suggests future research which could follow the work described.

Chapter 7 provides experimental details for Chapters 2–5.

Appendix contains supplementary figures and data for Chapters 2–5.

Acknowledgements

First, I would like to thank Professor Charlotte Williams for the opportunity to work in her research group and her guidance throughout my PhD. Thank you for all the support and encouragement during both high and low times. Thank you also to Professor Stefan Mecking and his team for hosting me in your group and helping me in my research. I am also very thankful to Siam Chemical Group (SCG) for funding my PhD.

I am grateful to all the Williams group members who have made the PhD research experience enjoyable. I am fortunate to have shared the time with many talented, inspiring and friendly people. In particular, thanks to the post docs who assisted and taught me in the lab: Dr Ryan Kerr (fun SCG times), Dr Arron Deacy, Dr Georgina Gregory, and Dr Fernando Vidal. Thank you Ryan for persisting with my occasionally dubious crystal samples. I should also mention Dr Andreas Phanopolous, Dr Greg Sulley, and Ron from facilities for helping me design and build my beloved triple-manifold steel line.

A shoutout to my best friend and collaborator Sarah Kakadellis who has supported me in many other ways during the PhD. I am forever grateful for our exchanges on plastics and our many wholesome rendez-vous.

Grazie mamma, papá, Gaia (e Kiko!) per il vostro supporto immenso. Thank you dad for our chemistry discussions and for always believing in me. The last, but not least, word goes to Wilf, who brought calm amongst the chaos. Thank you for spending hours reading my thesis and encouraging me during the writing, I couldn't have done it without you.

Abbreviations

Å	Angstrom
AGE	Allyl Glycidyl Ether
AH	Anhydride
alt	alternating
Ar	Aryl
A. U.	Arbitrary Units
b	block
β-BL	β-butyrolactone
BDI	β-Diimine
BO	Butylene Oxide
μ_B	Bohr Magneton
BPA	Bisphenol-A
BPA-PC	Bisphenol-A Polycarbonate
Bu	Butyl
C	Celsius
ca.	circa
cat.	Catalyst
CHD	Cyclohexene-1,2-diol
CHO	Cyclohexene Oxide
COD	Cyclooctadiene
Conv.	Conversion
CPO	Cyclopentene Oxide
Cp	Cyclopentadienyl

CTA	Chain Transfer Agent
CV	Cyclic Voltammetry
$Đ$	Dispersity
DBU	1,8-Diazabicyclo[5.4.0]undec-7-ene
DCM	Dichloromethane
DGA	Diglycolic Anhydride
DFT	Density Functional Theory
Dipp	2,4-Diisopropylphenyl
DMAP	4-Dimethylaminopyridine
DOSY	Diffusion Ordered Spectroscopy
$\overline{DP}$	Degree of Polymerisation
DSC	Differential Scanning Calorimetry
ECH	Epichlorohydrin
equiv.	Equivalents
CL	ε-Caprolactone
DL	ε-Decalactone
Et	Ethyl
g	gram
GPC	Gel Permeation Chromatography
h	hour
IR	Infrared
^{i}Pr	Isopropyl
K	Kelvin
k	Rate Constant

kcal	kilocalories
kg	kilogram
k_{obs}	Observed Rate Constant
k_p	Polymerisation Rate Coefficient
L	Ligand
LO	Limonene Oxide
min	minute
μ	Magnetic Moment
M	Metal
MA	Maleic Anhydride
MALDI	Matrix Assisted Laser Desorption Ionisation
Me	Methyl
mg	milligram
MHz	Megahertz
mol	mole
M_n	Number Average Molecular Mass
Mt	Megatonne
NA	Norbornene Anhydride
NMR	Nuclear Magnetic Resonance
OAc	Acetate
P	Polymer chain
PA	Phthalic Anhydride
PBL	Poly(butyrolactone)
PC	Polycarbonate

PCHC	Poly(cyclohexene carbonate)
PCL	Polycaprolactone
PDL	Polydecalactone
PE	Poly(tricyclic anhydride-*alt*-cyclohexene oxide)
PE'	Poly(phthalic anhydride-*alt*-cyclohexene oxide)
PE"	Polyethylene
PET	Polyethylene Terephthalate
Ph	Phenyl
PLC	Poly(limonene carbonate)
PO	Propylene Oxide
PPC	Poly(propylene carbonate)
ppm	Parts Per Million
PPNCl	Bis(triphenylphosphine)iminium chloride
PS	Polystyrene
PvCHC	Poly(vinyl-cyclohexene carbonate)
R	Generic Substituent
r	ratio
r	random
RDS	Rate Determining Step
ROCOP	Ring-Opening Copolymerisation
ROP	Ring-Opening Polymerisation
s	second
SA	Succinic Anhydride
SQUID	Superconducting Quantum Interference Device

t	time
T	Temperature
^{t}Bu	*tert*-butyl
TCA	Tricyclic Anhydride
T_d	Decomposition Temperature
TEB	Triethylborane
T_g	Glass Transition Temperature
TGA	Thermogravimetric Analysis
THF	Tetrahydrofuran
TIBA	Triisobutylaluminium
T_m	Melting Temperature
TM	Transition Metal
TMEDA	Tetramethylethylenediamine
ToF	Time of Flight
TOF	Turn-over Frequency
TON	Turnover Number
TS	Transition State
vCHO	4-Vinyl-1-cyclohexene oxide
vs.	versus
VT	Variable Temperature
X	Generic co-ligand
XRD	X-ray Diffraction

List of Figures, Schemes, and Tables

Chapter 1: Introduction

Chapter 2: Investigation of Mg(II)M(II) Complexes for Epoxide/anhydride ROCOP and their Selectivity in Terpolymerisations with CO_2

Chapter 3: Multi-block Copolymers Derived from CO_2

Chapter 6: Thesis Conclusions and Outlook

Table of Contents

Chapter 1

Introduction

1.1 Sustainable Polymeric Materials

Synthetic polymers, in particular plastics, are omnipresent in our daily lives, with many applications ranging from food packaging to bulletproof vests. Despite their high utility and low cost, the production and disposal of plastics is currently unsustainable, as they are synthesised from fossil fuels and recycling at scale is limited. In 2018, it was estimated that out of the 360 Mt of plastics produced, 20 % was sent to landfill, 20 % was leaked into the environment, and only 8 % underwent closed-loop recycling.[1-2] Hence, there is a growing interest in developing more sustainable polymers derived from renewable monomers that can be triggered to degrade at their end of life, once recovered or in the natural environment.[3] Monomer sourcing and degradability are equally important; replacing a petroleum-derived monomer with a renewable alternative that is chemically equivalent may still result in a polymer that takes thousands of years to degrade and contribute to the large volumes of plastic waste. A further challenge when designing new sustainable materials is that they must possess similar property profiles to petrochemical derived polymers they are intended to replace.

1.2 CO_2-based Polymers

Fixation of carbon dioxide from our atmosphere, either into geological storages, or transformation into products, is of growing importance in light of the link between the soaring levels of CO_2 in our atmosphere and climate change.[4] One method of utilising CO_2 is as a C_1 source in the production of polymers. Ring-opening copolymerisation (ROCOP) of epoxides and carbon dioxide to make polycarbonates (PCs) is one such process (Scheme 1.1a), resulting in 20–50 wt% incorporation of CO_2 in the polymer backbone, significantly reducing the greenhouse gas emissions associated with polymer production.[5-7] It has also been possible to apply CO_2 captured directly from flue gas in the polymerisation.[8] Other

advantages are that CO_2 is abundant, non-toxic, cheap, and the resulting polycarbonates can be biodegradable and biocompatible.[9-10] In comparison, an industrially relevant polycarbonate, BPA-PC, is typically synthesised *via* condensation polymerisation of petrochemical derived bisphenol-A (BPA) and phosgene (Scheme 1.1b). BPA-PC has faced increasing safety concerns, as phosgene is a highly toxic nerve gas, and BPA is an endocrine disruptor.[11-12] Furthermore, the synthesis requires high temperatures (280–300 ˚C) and vacuum conditions, and is not atom-economical, as two equivalents of HCl are formed as the by-product.[13]

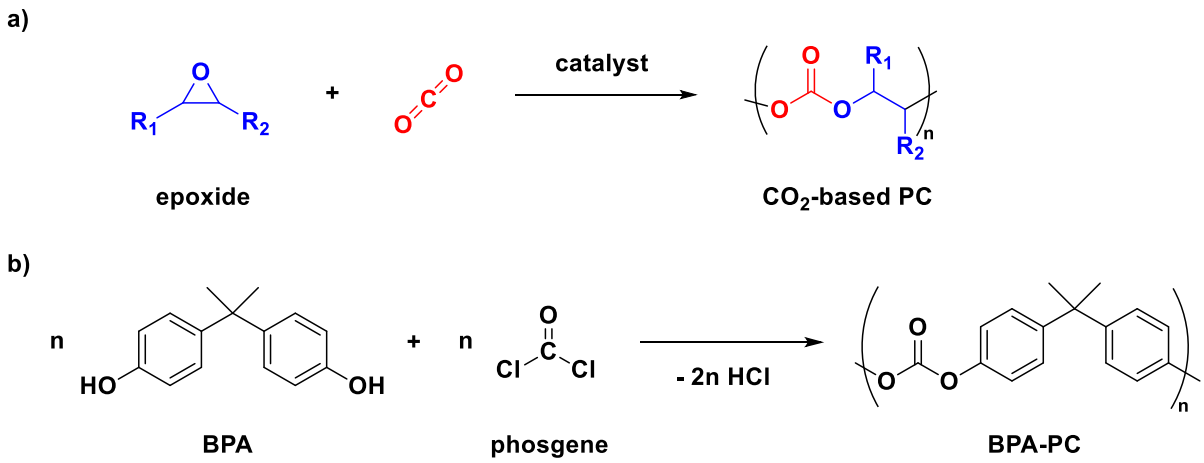

Scheme 1.1: Schematic for a) CO_2-based polycarbonate and b) the synthesis of conventional BPA-PC.

Carbon dioxide is inherently stable and hence requires activation with efficient chemical species; catalysts play a crucial role in the potential for the production of copolymers from CO_2.[14] Inoue and co-workers first demonstrated the coupling reaction of epoxides with CO_2 in 1969, using a mixture of diethylzinc and water.[15] Many more discoveries of efficient catalyst systems followed since, driven by this green chemical transformation. Initially this comprised of heterogeneous catalysts, which had improved activity, although their precise nature and active sites were ill-defined,[16-20] making rational catalyst design challenging. In the last two decades, homogeneous metal-based catalysts, and more recently metal-free examples, have been found to exhibit high activities and polymerisation control (*vide*

infra).[21-26] Contemporary research is focussing on the development of faster and more selective catalysts, with the ability of enchaining a wider choice of epoxide co-monomers producing diverse polycarbonate with a wide range of material properties.

1.2.1 CO_2/Epoxide ROCOP Mechanism

The general proposed mechanism for the ROCOP of CO_2/epoxide catalysed by a homogeneous metal complex [M] with initiating group X (usually halide, alkoxide, or acetate) is described in Figure 1.1.[24] The initiation step involves the ring-opening of the epoxide by a nucleophilic X group, usually an acetate or halide co-ligand, to generate a metal alkoxide. Subsequently, the CO_2 inserts into the alkoxide to generate a metal carbonate, which is typically the catalytic resting state. The cycle propagates by nucleophilic attack on the epoxide, typically the rate-determining step (RDS), regenerating a metal alkoxide species which inserts CO_2, thus leading to alternating copolymerisation. Two undesired side reactions are cyclic carbonate formation from back-biting, and sequential ring-opening of epoxide yielding ether linkages. The key criteria for assessing catalyst performance is the polymerisation activity, measured by turn-over frequency (TOF), and selectivity, measured by % carbonate *vs.* % ether and % cyclic carbonate *vs.* % polycarbonate. For controlled polymerisations, the initiation occurs more rapidly than propagation, leading to a degree of polymerisation ($\overline{DP}$) dependent on the ratio of monomer to catalyst concentration. Polymerisations are typically found to be living as there is no chain termination step.

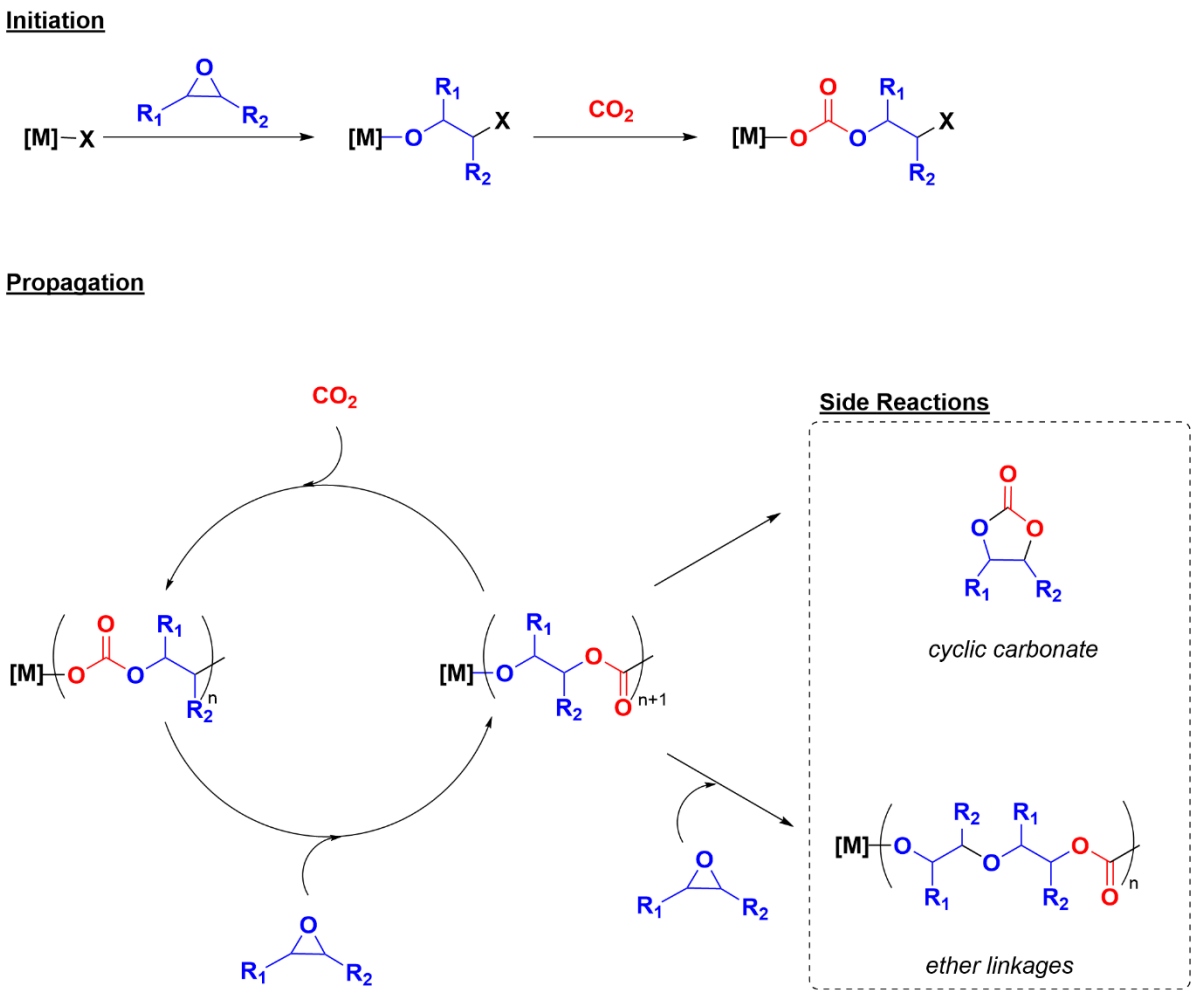

Figure 1.1: Mechanism for the alternating copolymerisation of CO_2 and epoxides.

Chain transfer reactions may occur if the reaction is exposed to alcohol or water to form a hydroxyl terminated polymer chain and a new metal alkoxide/hydroxide species, which can initiate new chains and propagate; the process is reversible, so the polymer chain growth can be renewed.[7] This can arise from contaminants introduced from the start or during the polymerisation, such as diols formed by hydrolysing the monomer and water in the CO_2, or can be deliberately added as a chain transfer agent (CTA) to control the chain end.

Chain transfer reactions result in the reduction of M_n as new chains are initiated. Another direct consequence of adventitious CTAs is the formation of bimodal molar mass distributions. Given that most catalyst species are monofunctional initiators (acetate or halide), and diols (from hydrolised epoxide by water) are bifunctional, the latter will have double the molar mass, as the polymer chains grow at the same rate (Figure 1.2). The two distributions also have different end group chemistries, as the higher molar mass features telechelic α,ω-hydroxy terminated chains, whereas the lower mass features α-X,ω-hydroxy terminated chains (where X is the catalyst initiating species). Whilst this is not necessarily detrimental to the polymerisation catalysis, there are some applications where having only one type of end group is essential. This includes the construction of more complex structures, such as tri-block polymers (*vide infra*). Adding multiple equivalents (>10 equiv.) of bifunctional CTA with respect to catalyst will produce predominantly telechelic α,ω-hydroxy end-capped chains and thus will supress the lower mass distribution. However, as mentioned previously, this will result in a significant decrease in molar mass, meaning this strategy cannot be adopted when high molar mass polymers are targeted. An alternative approach is to use catalysts that do not feature initiating co-ligands, which are typically organometallic aryl or alkyl groups.[27-28] In this scenario, CTA alcohols with the desired functionalities can be deliberately added to the polymerisation, which will generate metal alkoxide species *in situ* to initiate the polymerisation as normal.

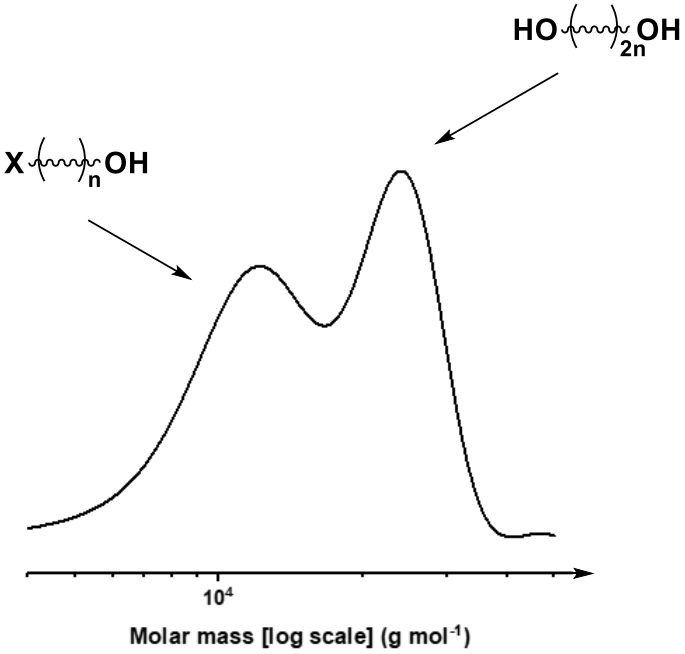

Figure 1.2: An example of a bimodal polymer molar mass distribution measured by gel permeation chromatography (GPC) for a polycarbonate produced by ROCOP of epoxide/CO_2.

A range of epoxides have been employed for ROCOP with CO_2, and the resulting polycarbonates have different thermal and mechanical properties depending on the epoxide utilised (Figure 1.3).[24, 29] The most common epoxides are cyclohexene oxide (CHO), propylene oxide (PO), and limonene oxide (LO). CHO is an inexpensive, commercially available epoxide which is typically used to benchmark the performance of new catalysts, as rates are typically high and the propensity of back biting is low (due to steric reasons).[21] PO is a commodity chemical, and the resulting poly(propylene carbonate) (PPC) is being investigated for the production of polyurethanes. LO is a commercially available epoxide derived from waste citrus peel, meaning that PLC can be made entirely from renewable feedstocks.[30] Other epoxides that have been investigated include: epichlorohydrin (ECH), butylene oxide (BO), allyl glycidyl ether (AGE), and cyclopentene oxide (CPO).[31]

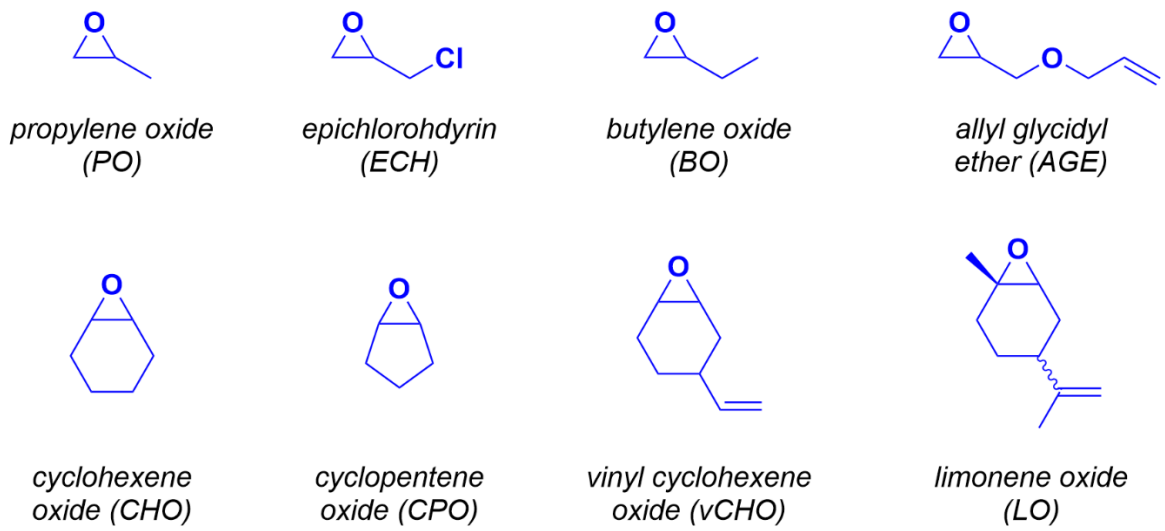

Figure 1.3: Common epoxides employed in ROCOP with CO_2.

1.2.2 Metal-based Catalysts

Metal-based complexes for the ROCOP of CO_2/epoxide feature a range of metals from across the periodic table, including Mg(II),[32-33] Zn(II),[34-37] Cr(III),[38-39] Mn(III),[40-42] Fe(II/III),[43-45] Co(II)/(III),[46-48] Ni(II),[42, 49] Cu (II),[42, 50] Al(III),[51-52] In(III),[53] and lanthanides[54] with a variety of ancillary ligand scaffolds. The catalysts most relevant to the thesis are discussed below; the reader is directed to reviews providing further details on the full range of metal complexes reported for CO_2/epoxide ROCOP.[25, 55]

In 1998, Coates and co-workers discovered highly active zinc β-diimine complexes ([Zn(BDI)(OAc)], Figure 1.4a) for CHO/CO_2 ROCOP.[56] The complexes exist in an equilibrium between monomeric and dimeric species in the solid state and in solution, which is influenced by temperature, concentration, and the size of the R substituents on the *ortho*- and *para*- positions of the phenyl substituent of the ligand.[57] It was found that in catalysis, the complex functions through dimerization of two [Zn(BDI)] molecules to yield the active species, implied by the ligand-dependent variation of the order in catalyst between 1.0 and 1.8.[58] The optimum activity was observed for a loosely bound dimer, displaying a TOF of

729 h^{-1} (50 ˚C, 7 bar CO_2) together with excellent copolymer selectivity (99 % carbonate linkages) and polymerisation control ($Đ$ = 1.15). In the case of tightly bound dimers (small R groups) or monomeric species (from larger R groups), inferior catalytic activity was observed. Furthermore, at higher temperatures and lower catalyst concentrations, dissociation to inactive monomeric species are favoured.

Metal(III)-salen or porphyrin catalyst systems containing Co(III) and Cr(III) centres, which are typically used with a nucleophilic co-catalyst, often an ionic compound (e.g. bis(triphenylphosphine)iminium chloride, [PPNCl]) or an organic base (e.g. diazabicycloundecene (DBU)), have also been widely studied (Figure 1.4b).[21] Kinetic studies revealed that the order in catalyst is typically between 1 and 2, indicative that the catalysts operate *via* a bimetallic and/or monometallic mechanism in the rate-limiting step.[21, 59] There is also a rate dependence on the concentration of the co-catalyst, implying it is also part of the RDS. Hence, the activity for these systems falls with catalyst loading below a critical ion-pair concentration. To address this limitation, researchers have designed ligands in which the co-catalyst is attached to the ancillary ligand (Figure 1.4c).[48, 60-62] Indeed, they lead to superior performance in both rates and selectivity compared to their bi-component counterparts, amongst the highest in the field. This strategy has also been applied to porphyrin-derived catalysts (Figure 1.4d).[51]

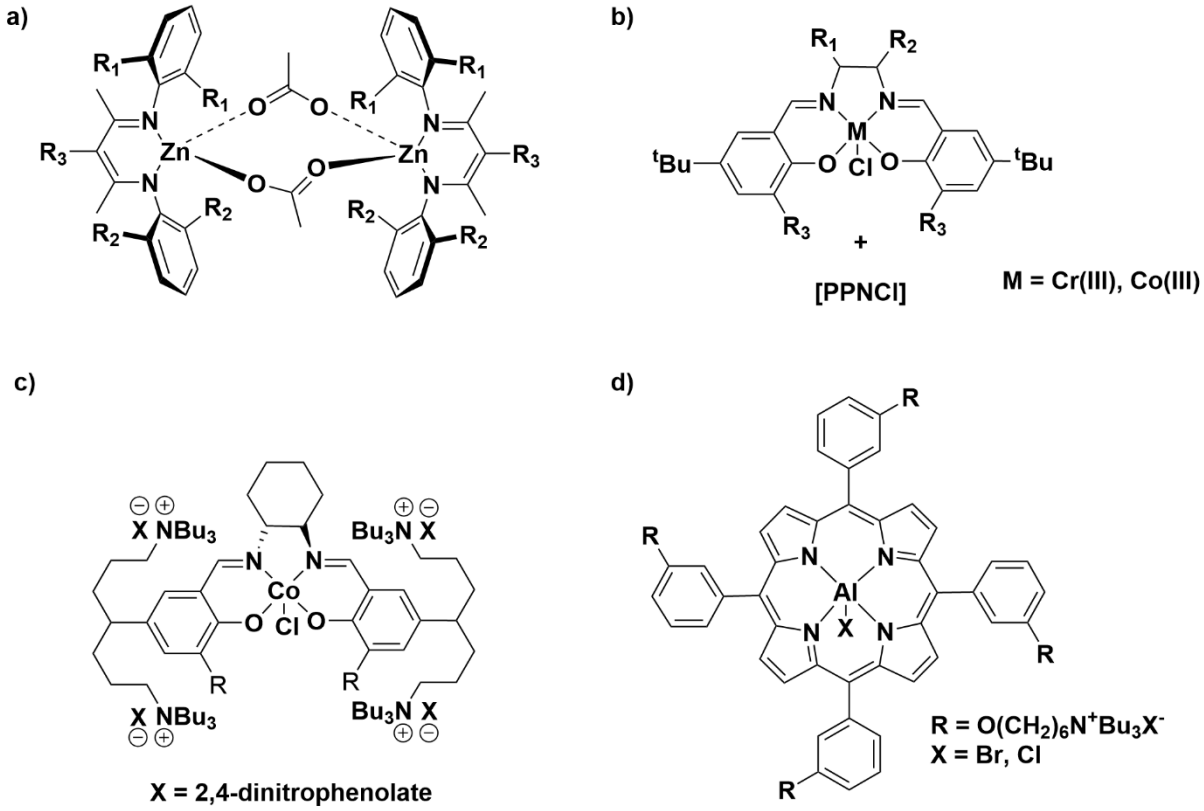

Figure 1.4: a) [Zn(BDI)] complex with acetate co-ligands.[56] b) Metal salen catalyst system.[63] c) Example of a salen-type complex with tethered co-catalyst.[48] d) Example of a metal porphyrin complex with tethered co-catalyst.[51]

The apparent bimetallic mechanism observed for [Zn(BDI)] catalysts prompted the development of several dinuclear Zn(II) complexes, with the intention of resolving the aforementioned drawbacks.[37, 64-66] In 2009, our group reported a Zn(II)Zn(II) catalyst featuring a macrocyclic diphenolate tetraamine ancillary ligand, which showed moderate activity for copolymerisation of CHO and CO_2 at 1 bar pressure (TOF = 18 h^{-1}, 80 ˚C) (Figure 1.5a).[67] At the time, low pressure CO_2 catalysts were uncommon.

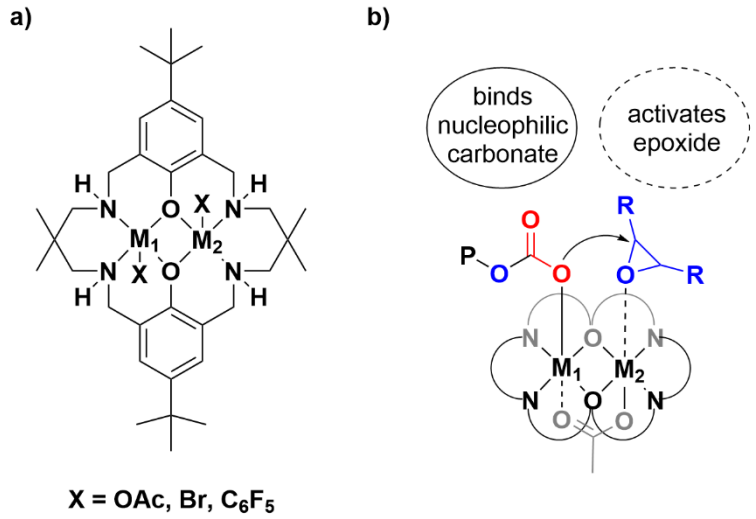

Figure 1.5: a) Homo- and heterodinuclear catalysts with various metals, reported by our group.[32, 45, 47, 67-70] b) Schematic depicting the distinct roles for each metal.

Subsequent studies with different metal centres were conducted, using Mg(II)Mg(II) (TOF = 35 h^{-1}), Co(II)Co(II) (TOF = 161 h^{-1}), and Fe(III)Fe(III) (TOF = 6 h^{-1}), under the same experimental conditions.[32, 45, 47] Kinetic investigations, coupled with DFT calculations, supported a chain shuttling mechanism where, for each monomer insertion, the polymer moves between the two metal centres (Figure 1.5b).[71] This led to further investigation into heterodinuclear catalysts, to substantiate whether each metal has a distinct role in the catalysis. A heterodinuclear Mg(II)Zn(II) catalyst showed enhanced catalytic activity compared to the homodinuclear Zn(II)Zn(II) and Mg(II)Mg(II) complexes.[68] The improvement in performance suggests intermetallic synergy in catalysis, supporting the idea that the two metals have distinct mechanistic roles. Later, a heterodinuclear Mg(II)Co(II) catalyst showed excellent activity and polycarbonate selectivity at 1 bar (TOF = 1205 h^{-1}, 120 ˚C) and 20 bar CO_2 pressure (TOF = 12,460 h^{-1}, 140 ˚C),[70] which, compared to the homodinuclear Mg(II)Mg(II) and Co(II)Co(II) catalysts, was four and two times faster, respectively. Detailed kinetic analyses showed that the Mg(II) ion reduces the transition state entropy (M_2 in Figure 1.5b) of the rate determining step, while the Co(II) carbonate is more nucleophilic, in turn lowering the transition state enthalpy (M_1, Figure 1.5b).

More recently, it was found that the Mg(II)Fe(II) metal variant was equally active at 1 bar of CO_2, which is a significant result as iron is more earth abundant and not widely reported for its use in ROCOP catalysis.[42] Whilst these examples of heterodinuclear complexes demonstrate metal synergy in ROCOP, it is not always the case that they are more active compared to their homodinuclear analogues. For a series of Zn(II)M complexes, where M = Group 1 or 2 metals, all performed worse than Zn(II)Zn(II).[69]

1.2.3 Organocatalysts

Organocatalysts, in the form of Lewis acid/base pairs, are of interest as they can be air stable and are often commercially available. They may operate differently compared to transition metal catalysts, allowing for different regio-, stereo-, or enantio- selectivity. It should be noted that some organocatalysts are toxic,[72] expensive, and corrosive, although there are reports that have focussed on environmentally friendly and cost-effective processes.[73-74]

The first example of metal-free CO_2/epoxide ROCOP was demonstrated by Feng and Gnanou in 2016, using triethyl borane (TEB) and phosphonium salts (e.g. [PPNCl]) (Figure 1.6a).[75] They found that two equivalents of TEB to PPNCl were necessary to achieve high activities for the copolymerisation of CO_2 and CHO. A subsequent DFT study suggested that TEB has two distinct roles in this catalysis: one as epoxide activator and the other as a stabiliser for the growing carbonate anion, which in turn prevents backbiting reactions.[76] The optimised catalyst component loadings afforded a TOF value of 148 h^{-1} and >99 % polycarbonate selectivity (80 ˚C, 10 bar CO_2). Since this discovery, several other Lewis pairs showed good activity and selectivity using a variety of epoxides, some of the best catalysts were tethered systems (Figure 1.6b).[77-80]

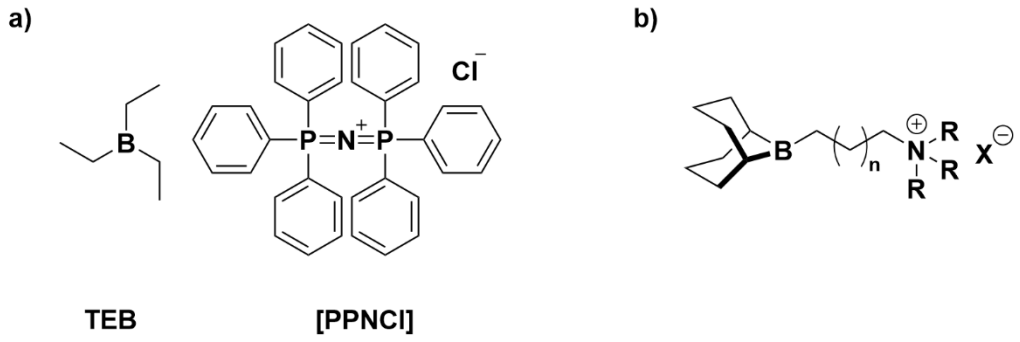

Figure 1.6: a) Organocatalyst developed by Feng and Gnanou.[75] b) Example of a tethered organocatalyst developed by Wu.[73]

1.2.4 Polycarbonate Properties

The thermal and mechanical data for the most commonly investigated CO_2-derived polycarbonates are presented in Table 1.1, with BPA-PC and atactic polystyrene (PS-at) included for comparison. Poly(cyclohexene carbonate) (PCHC) is widely synthesised within academic research, as CHO is used as a benchmark epoxide for catalyst development, although characterisation studies of the polymer itself are limited.[81] One study of high molar mass PCHC (M_n = 252 kg mol^{-1}, $Đ$ = 6) revealed that it is a stiff, brittle material, with a small strain at break of 1–2 % (Table 1.1).[82] Poly(propylene carbonate) (PPC) has gained more industrial interest as the epoxide is produced at scale,[83] and its material properties make it suitable as a polyol for polyurethane production.[84-85] The material is more flexible, with a strain at break up to 1200 %, and has a mid-range tensile strength (7–30 MPa) (Table 1.1). Poly(limonene carbonate) (PLC) is entirely renewable and has attractive material properties as an emerging plastic. Greiner and colleagues were able to synthesise high molar mass (M_n = 53 kg mol^{-1}) PLC which possesses a high glass transition temperature (T_g) of 130 ˚C, high tensile strength (55 MPa), and optical transparency (94 %); its properties are close to BPA-PC.[86] In later studies, the pendant double bond moiety in PLC was post-functionalised, resulting in thermoplastic elastomers and antimicrobial materials.[87] Beyond altering the

epoxide, another strategy to modify the properties of CO_2-based polycarbonates, without the use of additives, is to incorporate them in block copolymers.

Table 1.1: Material properties of polycarbonates.

Polymer	T_g (°C)[a]	T_d (°C)[b]	Young's Modulus (GPa)	Strain at break (%)	Tensile Strength (MPa)	Ref.
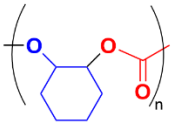 **PCHC**	115	280	2.5–3.7	1.1–2.3	40–44	82,88
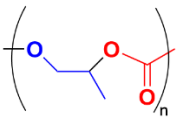 **PPC**	42	195	0.7–1.4	600–1200	7–30	89,90
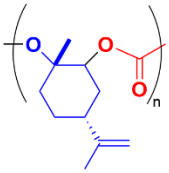 **PLC**	130	223	0.95	15	55	86
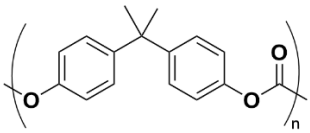 **BPA-PC**	145–150	320	2.1–2.4	65–107	60–121	91,92
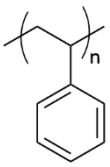 **PS-at**	100	325	3.2–3.4	3.4	35–55	91

[a] T_g = glass transition temperature. [b] T_d = onset decomposition temperature.

1.3 Polyesters *via* ROCOP

The related alternating copolymerisation of epoxide and cyclic anhydride (AH) yields polyesters. Many active catalysts for CO_2/epoxide ROCOP are also effective for

anhydride/epoxide ROCOP, although not always *vice versa*.[24] Heterodinuclear metal catalysts have also shown high activities in such reactions; Diment *et al.* has recently reported an Al(III)K(I) catalyst with field leading rates.[93]

The catalytic cycle is similar to that discussed for epoxide/CO_2 ROCOP (Figure 1.1) and includes initiation, propagation, chain transfer reactions, and polyether formation as side reaction. The main difference is that no backbiting into cyclic product is typically observed, due to higher barriers for this pathway.[23] As with epoxide/CO_2, epoxide ring-opening and insertion is typically the RDS.

There is greater potential for structural diversities for polyesters, compared to polycarbonates, as both co-monomers can be altered. These could include aliphatic or aromatic units (Figure 1.7), depending on the desired application. The most commonly employed anhydride is phthalic anhydride (PA), which is typically used to benchmark catalyst performance, and is produced at scale.[94]

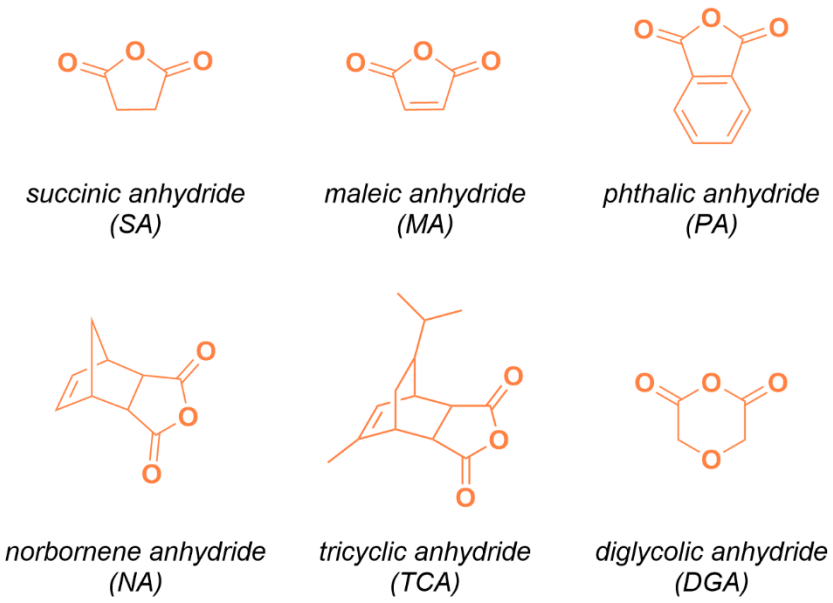

Figure 1.7: Selected anhydrides used in ROCOP with epoxides.

1.4 Block Copolymers

1.4.1 Methods Towards CO_2-based Block Polymers

In order to expand the use of CO_2-based polycarbonates in materials with improved functionality, more diverse polymeric structures need to be synthesised.[95] Constructing block polymers is a useful method, and can be executed through various strategies, which are presented in Figure 1.8. Each method can be applied to ROCOP,[95-96] allowing for the preparation of block copolymers in one-pot without additional purification steps. Each method has its own benefits and limitations, which are dependent on the monomers and catalysts used.

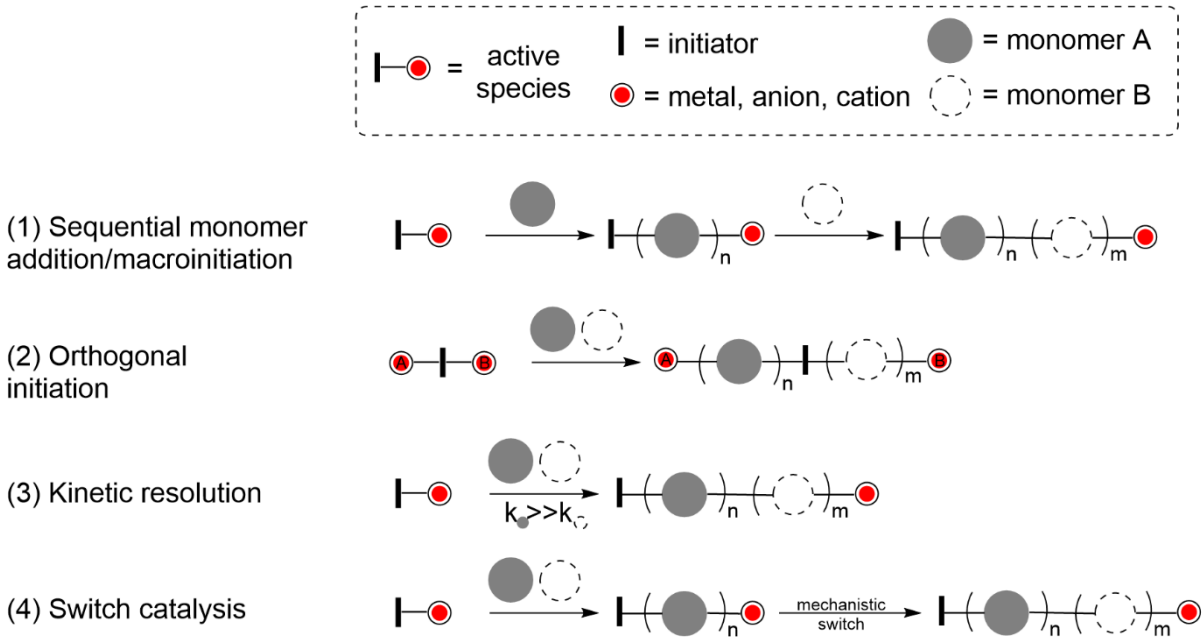

Figure 1.8: Different methods for accessing diblock copolymers. Adapted from literature.[97]

The most widely applied strategy is sequential monomer addition (1), which is utilised with many polymerisation types. Once monomer A is depleted, its polymer serves as a macroinitiator for the subsequently added monomer, which initiates the polymerisation from the chain end. Orthogonal initiation (2) relies on a bifunctional initiating species, or

catalysts, which are capable of performing two distinct polymerisations at the same time, with precise matching of monomer to initiating site. Examples include block copolymers which combine radical polymerisation and CO_2/epoxide ROCOP.[98-100] When, from a mixture, enchainment of only one monomer from the chain end is preferred ($k_A >> k_B$), blocks can be formed by kinetic resolution (3), on the basis that once the favoured monomer is depleted, the secondary monomer will be enchained. The reactivity ratio ($r_A = r_{AA}/r_{AB}$) gives an indication whether a particular monomer will homopolymerise or copolymerise in the presence of another monomer; when r > 1, homopolymerisation may occur. The pairing of monomers and their reactivity ratios are important to determine the resulting block structure, as tapering or random enchainment may result if k_A and k_B are not sufficiently different. For perfectly alternating ROCOP reactions described earlier, the reactivity ratio of epoxide, anhydride and CO_2 is zero, as self-enchainment is disfavoured. Finally, switch catalysis (4) applies a single catalyst to switch between different polymerisation cycles (e.g. ROCOP of epoxide/heteroallene and ring-opening polymerisation (ROP) of lactones) depending on the chain-end group chemistry, in turn selectively enchaining monomers from mixtures.[101]

1.4.2 ROCOP-derived Block Copolymers

Putting these strategies into practice and controlling the block sequences and the precise placement of monomers can be challenging. In terms of controlling block sequence in polyesters, Coates and co-workers developed high activity Al(III) catalysts for epoxide/anhydride ROCOP, accessing tri-block copolymers by sequential monomer addition of different anhydrides, and applied orthogonal post-functionalisation reactions to install alternating sequences of imine and alkyl group substituents.[102] Examples incorporating CO_2 include a study by Wu and co-workers, where they prepared self-healable thermoplastic elastomers from CO_2/epoxide derived polycarbonates by copolymerising allyl glycidyl ether (AGE) and CO_2 followed by CHO and CO_2 (by sequential monomer addition),

and placing dynamic cross-linking moieties to the AGE side-chains.[103] The materials showed a Young's modulus of 10 MPa and excellent elastic recovery. In two separate studies, Darensbourg and co-workers prepared amphiphilic and self-healing triblock copolymers by sequential polymerisation of PO and AGE with CO_2, followed by post-modification by thiol-ene click chemistry.[104-105]

Catalyst selection is important when targeting block copolymers, in particular for the selective enchainment of monomers from a mixture.[14, 106-107] Being able to switch between two polymerisation cycles is a useful tool to access different polymer block chemistries. In 2008, Coates and co-workers pioneered a synthesis of CO_2-based block copolymers by exploiting kinetic resolution polymerisation with a [Zn(BDI)] catalyst.[97] Terpolymerisation of a mixture of diglycolic anhydride (DGA), CHO and CO_2 resulted in poly(ester-*b*-carbonate); epoxide/anhydride ROCOP selectively occurred to make polyester until full conversion of the anhydride before any polycarbonate was produced (Figure 1.9). This was rationalised by >2000-fold faster insertion rate for DGA *vs.* CO_2 insertion ($k_1 > k_2$) into the propagating zinc alkoxide intermediate.

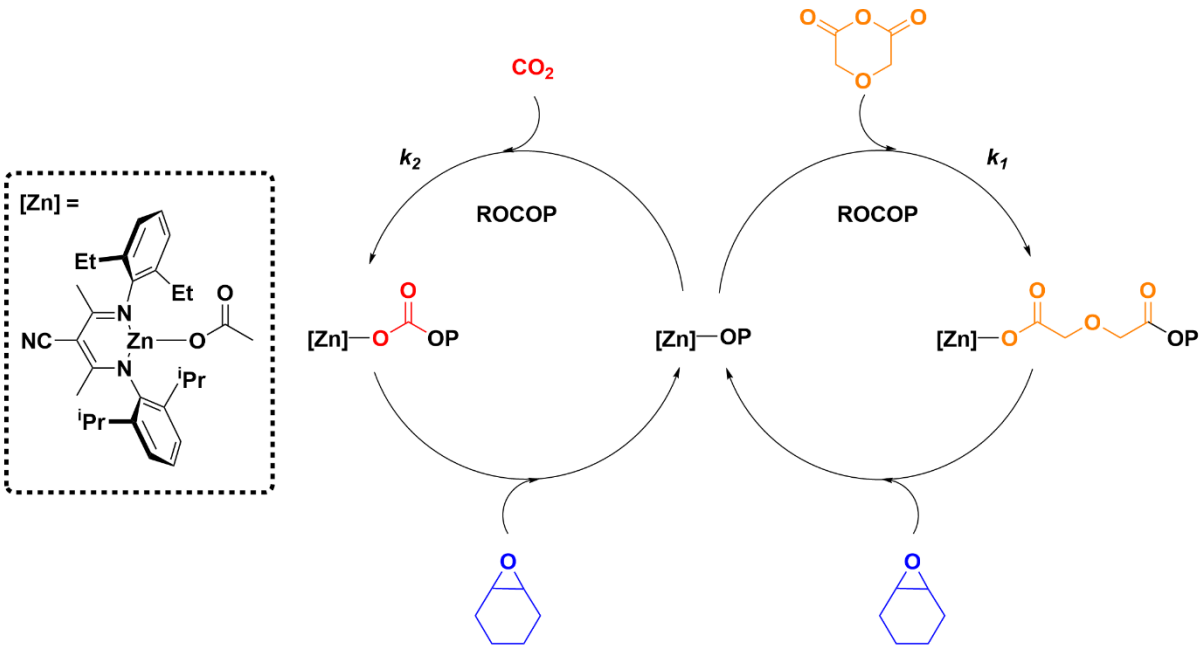

Figure 1.9: Terpolymerisation of DGA, CHO, and carbon dioxide using a zinc β-diimine catalyst.[97] P = polymer chain.

From then, many other catalysts exhibiting the same controlled selectivity between CO_2 *vs.* anhydride have been reported, including homogeneous mono-,[60, 108-110] dinuclear metal catalysts,[111-112] and organocatalysts.[113] A notable exception was the ROCOP of CO_2, tricyclic anhydride (TCA), and CHO with a Mg(II)Mg(II) catalyst, reported by our group, where polycarbonate is selectively formed rather than polyester.[112]

An example of a functional polymer using this strategy is reported by Meng and co-workers, who polymerised quadricomponent mixtures of PO, CHO, PA, and CO_2 with an organocatalyst to selectively form poly(ester-*b*-carbonate) polymers with little tapering.[114] The materials showed high tensile strength (54 MPa) with variable T_g between 86–115 ˚C depending on the monomer feed ratio, properties that are competitive with polystyrene.

1.4.3 Switch Catalysis as a Route to Block Copolymers

In 2014, our group reported a new type of switchable polymerisation catalysis, whereby a Zn(II)Zn(II) catalyst, from a mixture of CHO, CO_2 and ε-caprolactone (CL) monomers,

displayed an unexpected orthogonal reactivity dependent on the zinc-polymer end group chemistry; zinc-alkoxides reacted with CO_2 or CL, but not with epoxide, and zinc-carbonates ring-opened epoxide, but not CL (Figure 1.10).[115] Therefore, from this mixture, the catalyst delivered well controlled poly(ester-*b*-carbonates); lactone ROP was only possible when CO_2 was removed from the reaction, as CO_2 insertion into the zinc-alkoxide is faster. A year later, the same selectivity and block structures were observed when mixtures of epoxide, anhydride and lactone were polymerized by the Zn(II)Zn(II) catalyst.[116] This discovery implied that a single catalyst can be directed between different polymerisation cycles while selecting for particular monomers.[117] The chemoselective switch can occur by monomer depletion in the polymerisation, or exogenously by removal or addition of monomer.

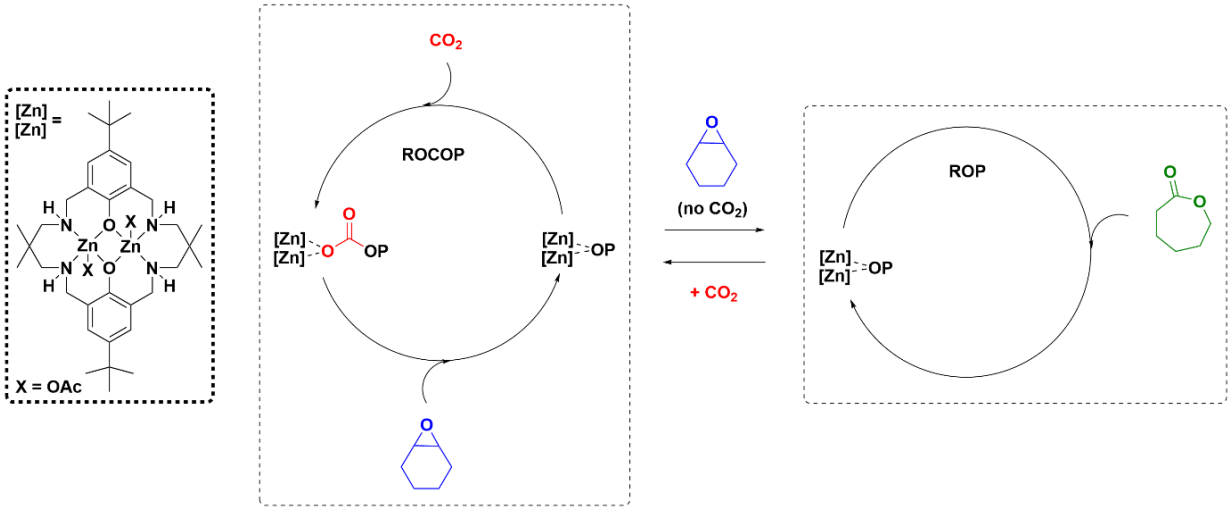

Figure 1.10: The switch mechanism between ROCOP and ROP with a Zn(II)Zn(II).[115] P = polymer chain.

In 2016, a combined experimental and computational investigation provided understanding of the orthogonal reactivity between mixtures of epoxide (CHO), anhydride (PA), and CO_2, and lactone (CL) using the Zn(II)Zn(II) complex as a model catalyst; despite the lower energy barrier to CO_2 insertion into the zinc-alkoxide compared to anhydride insertion (10.9 kcal mol^{-1} and 18.8 kcal mol^{-1}, respectively), experimentally the polyester block formed before the polycarbonate (Figure 1.11).[118] It was rationalised that the zinc-carboxylate

intermediate is significantly more stable than the corresponding zinc-carbonate, and that CO_2 insertion would be expected to be reversible under the polymerization conditions. Therefore, the relative monomer insertion order was anhydride > carbon dioxide > lactone into the zinc alkoxide intermediate.

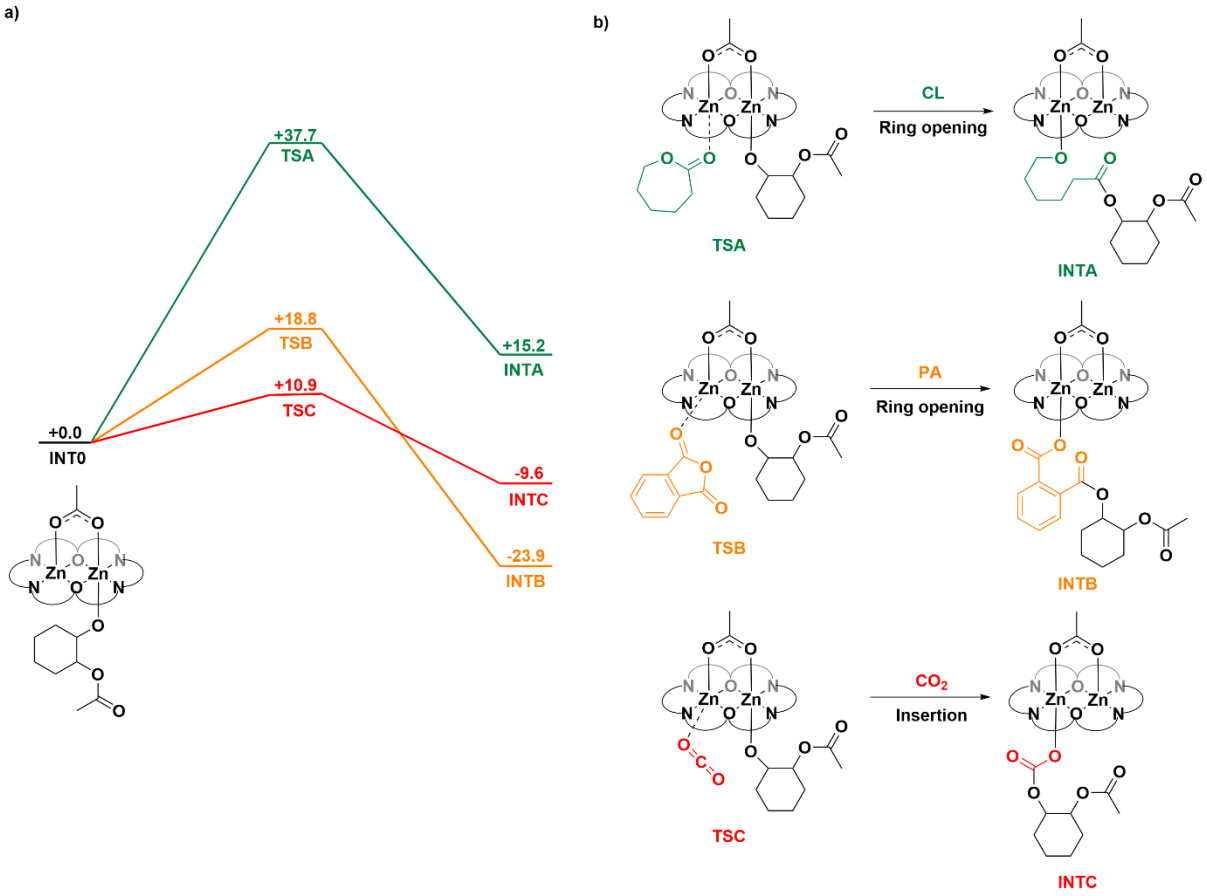

Figure 1.11: a) Density functional theory (DFT) (ΔG kcal mol^{-1}) energy profiles for the insertions of monomers into the zinc-alkoxide intermediate: CO_2 (red), PA (orange) and CL (green). b) Illustration of the transition states and intermediates upon monomer insertion.[118] TS = transition state, INT = intermediate.

Subsequently, it was shown that a range of other metal[119-123] and organocatalysts[124-125] obeyed the same monomer sequence selectivity 'rules', and that switchable catalysis could be applied to a range of different epoxides, anhydrides, lactones and heterocycles.[107] Heterogeneous catalysts are typically an exception, which result in ill-controlled random or tapered polymers,[126-128] although materials with properties of interest can still be made.[129-130]

Switch catalysis enables the construction of block copolymers that may be difficult or impossible by other means. In particular, they often employ commercial, bio-, or waste-derived monomers, and thus show improved sustainability in comparison to conventional petroleum-derived polymers.[131-133] They also feature ester, carbonate, and ether bonds, which are susceptible to hydrolyses or biodegradation reactions.[134] This is an important consideration for chemical recycling, *i.e.* depolymerisation to monomers, or for degradation in the environment if appropriate disposal fails.[135]

Examples of switch catalysis in block copolymer synthesis include a study by Sulley *et al.* in which a Mg(II)Zn(II) organometallic catalyst was employed for the synthesis of high molar mass poly(carbonate-*b*-ester-*b*-carbonate) triblock copolymers.[28] The first block was afforded from the ring-opening polymerisation of ε-decalactone (DL) to form an α,ω-hydroxyl end-capped polyester, and from the chain end PCHC was grown. Depending on the polyester:polycarbonate block ratio, the polymers were thermoplastic elastomers, pressure-sensitive adhesives, or toughened plastics. Using a similar method, triblock copolymers with PA/CHO as the ROCOP-derived block yielded thermoplastic elastomers with high strain at break (1900 %), moderate Young's moduli (1.5–5.0 MPa), and high tensile strength (2.0–6.5 MPa).[136] Rieger and co-workers prepared poly(ester-carbonates) featuring either PCHC or PCL as the hard block and poly(hydroxy butyrate) (PHB) as the soft block using a [Zn(BDI)] catalyst.[137] Statistical polymers and perfect blocks were accessed depending on the CO_2 pressure applied in the polymerisation. The polymer specimens showed strain at break values between 13–18 %, depending on PHB content, which are higher than the PCHC or PLC homopolymers.[121] With a variety of catalysts and monomers available, many applications remain to be explored. In particular, finding new CO_2-based block polymers which can overcome the material weaknesses of the homopolymers.

1.5 Aims

The thesis will focus on the ROCOP of CO_2/epoxide and anhydride/epoxide with various heterodinuclear Mg(II)M(II) complexes. From the current developments in ROCOP catalysis, the areas of interest are summarised in Figure 1.12 and listed below:

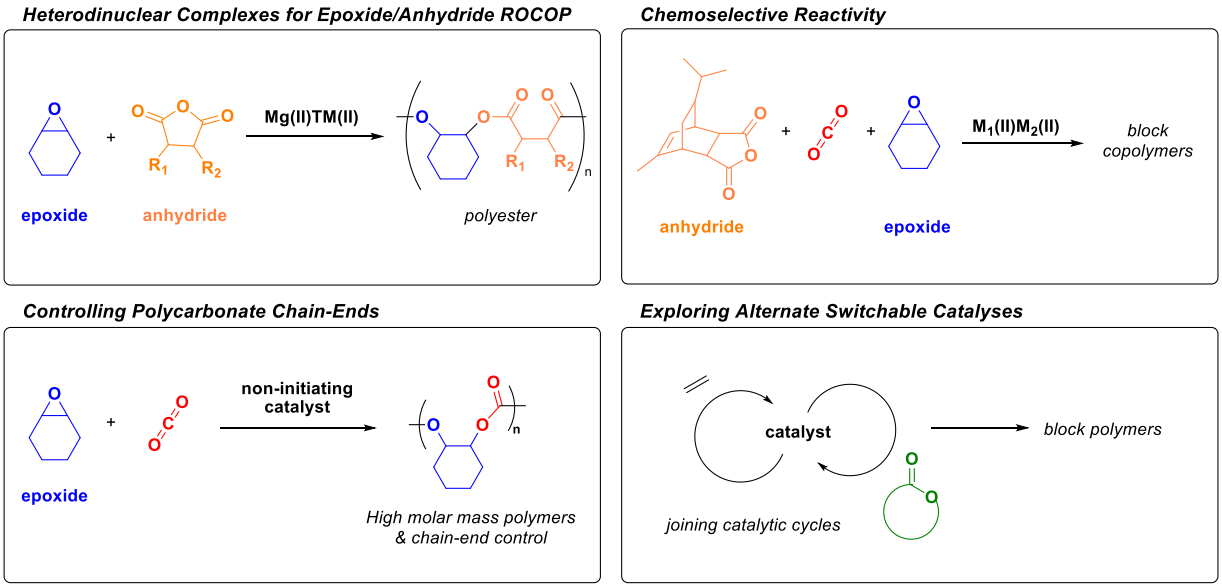

Figure 1.12: Overview of the thesis.

1. The effect of the divalent transition metal (TM) partner in Mg(II)M(II) heterodinuclear complexes in the copolymerisation of anhydride and epoxide. Reis *et al.* reported a series of Mg(II) and first row TM(II) heterodinuclear complexes for CO_2/CHO ROCOP, finding that Mg(II)Co(II) and Mg(II)Fe(II) were the most active.[138] The goal of this work is to reveal whether similar activity trends are observed for anhydride/epoxide ROCOP.
2. Determining the selectivity in CO_2/anhydride/epoxide ROCOP using heterodinuclear Mg(II) complexes. Saini *et al.* reported unusual orthogonal monomer selectivity between a Mg(II)Mg(II) and Zn(II)Zn(II) catalyst in the copolymerisation of TCA/CHO/CO_2.[112] The activity and selectivity will be further

explored with Mg(II) heterodinuclear complexes to better understand this phenomenon.

3. Exploiting monomer selectivity in the polymerisation of higher order structures, such as multi-block copolymers with more than 3 blocks, which could deliver better materials and access new phase separated nanostructures. The uncommon selectivity observed for Mg(II)-containing dinuclear catalysts, where CO_2/epoxide ROCOP occurs prior to anhydride/epoxide ROCOP, means that the polymerisation can be controlled by changing the head-space gas. This is a facile method to produce such structures, as sequential monomer addition of liquid or solid monomers is likely to introduce impurities. ROCOP-derived multi-block copolymers will be prepared, as they have the potential of tempering brittleness, improving processability, and enhancing material properties.[117]
4. Development of organometallic heterodinuclear catalysts for CO_2/epoxide ROCOP which are fully end-group selective. End-group fidelity is crucial to access pure block polymers, and to synthesise monomodal high molar mass polymers. Almost all current ROCOP catalysts feature monofunctional initiators, in the form of acetate or chloride moieties, provided from either the co-ligand or co-catalyst. The presence of water or diol impurities in the monomers will, as a consequence, produce bimodal polymer molar mass distributions, as diol-initiated chains grow at twice the rate of the monofunctional chains. A catalyst system that does not possess initiating moieties is required, such that added alcohols function as the sole initiators in the polymerisation. Currently, Zn(II)Zn(II) and Mg(II)Zn(II) dinuclear catalysts featuring C_6F_5 or C_6H_5 co-ligands have been established, however they are slower catalysts for CO_2/epoxide ROCOP than recently reported Mg(II)Co(II) catalyst.

5. New switch catalysis processes. Switching between ethylene polymerisation and epoxide/anhydride ROCOP or lactone ROP could deliver new products, perhaps introducing degradable linkages to short oligo-olefin blocks. Ni(II) catalysts will be explored for both ethylene polymerisation of ring-opening polymerisations.

1.6 References

1. World Economic Forum; Ellen MacArthur Foundation *The New Plastics Economy: Rethinking the future of plastics*; 2016.

2. Conversio Market & Strategy GmbH *Global Plastics Flow*; 2018.

3. Schneiderman, D. K.; Hillmyer, M. A., *Macromolecules* **2017,** *50* (10), 3733-3749.

4. Lashof, D. A.; Ahuja, D. R., *Nature* **1990,** *344* (6266), 529-531.

5. Hepburn, C.; Adlen, E.; Beddington, J.; Carter, E. A.; Fuss, S.; Mac Dowell, N.; Minx, J. C.; Smith, P.; Williams, C. K., *Nature* **2019,** *575* (7781), 87-97.

6. Artz, J.; Müller, T. E.; Thenert, K.; Kleinekorte, J.; Meys, R.; Sternberg, A.; Bardow, A.; Leitner, W., *Chem. Rev.* **2018,** *118* (2), 434-504.

7. Darensbourg, D. J., *Green Chem.* **2019,** *21* (9), 2214-2223.

8. Chapman, A. M.; Keyworth, C.; Kember, M. R.; Lennox, A. J. J.; Williams, C. K., *ACS Catal.* **2015,** *5* (3), 1581-1588.

9. Feng, J.; Zhuo, R.-X.; Zhang, X.-Z., *Prog. Polym. Sci.* **2012,** *37* (2), 211-236.

10. Liang, X.; Tan, F.; Zhu, Y., *Front. Chem.* **2021,** *9*, 647245.

11. Hoekstra, E. J.; Simoneau, C., *Crit. Rev. Food Sci. Nutr* **2013,** *53* (4), 386-402.

12. Cywar, R. M.; Rorrer, N. A.; Hoyt, C. B.; Beckham, G. T.; Chen, E. Y. X., *Nat. Rev. Mater.* **2022,** *7* (2), 83-103.

13. Woo, B.-G.; Choi, K. Y.; Song, K. H.; Lee, S. H., *J. Appl. Polym. Sci.* **2001,** *80* (8), 1253-1266.

14. Zhang, X.; Fevre, M.; Jones, G. O.; Waymouth, R. M., *Chem. Rev.* **2018,** *118* (2), 839-885.

15. Inoue, S.; Koinuma, H.; Tsuruta, T., *J. Polym. Sci., Part B: Polym. Lett.* **1969,** *7* (4), 287-292.

16. Ree, M.; Hwang, Y.; Kim, J.-S.; Kim, H.; Kim, G.; Kim, H., *Catal. Today* **2006,** *115* (1), 134-145.

17. Klaus, S.; Lehenmeier, M. W.; Herdtweck, E.; Deglmann, P.; Ott, A. K.; Rieger, B., *J. Am. Chem. Soc.* **2011,** *133* (33), 13151-13161.

18. Sun, X.-K.; Zhang, X.-H.; Liu, F.; Chen, S.; Du, B.-Y.; Wang, Q.; Fan, Z.-Q.; Qi, G.-R., *J. Polym. Sci., Part A: Polym. Chem.* **2008,** *46* (9), 3128-3139.

19. Varghese, J. K.; Park, D. S.; Jeon, J. Y.; Lee, B. Y., *J. Polym. Sci., Part A: Polym. Chem.* **2013,** *51* (22), 4811-4818.

20. Chen, S.; Qi, G.-R.; Hua, Z.-J.; Yan, H.-Q., *J. Polym. Sci., Part A: Polym. Chem.* **2004,** *42* (20), 5284-5291.

21. Darensbourg, D. J., *Chem. Rev.* **2007,** *107* (6), 2388-2410.

22. Chisholm, M. H.; Zhou, Z., *J. Mater. Chem.* **2004,** *14* (21), 3081-3092.

23. Plajer, A. J.; Williams, C. K., *Angew. Chem. Int. Ed.* **2022,** *61* (1), e202104495.

24. Paul, S.; Zhu, Y.; Romain, C.; Brooks, R.; Saini, P. K.; Williams, C. K., *Chem. Commun.* **2015,** *51* (30), 6459-6479.

25. Kozak, C. M.; Ambrose, K.; Anderson, T. S., *Coord. Chem. Rev.* **2018,** *376*, 565-587.

26. Trott, G.; Saini, P. K.; Williams, C. K., *Philos. Trans. R. Soc. A* **2016,** *374* (2061), 20150085.

27. Romain, C.; Garden, J. A.; Trott, G.; Buchard, A.; White, A. J. P.; Williams, C. K., *Chem. Eur. J.* **2017,** *23* (30), 7367-7376.

28. Sulley, G. S.; Gregory, G. L.; Chen, T. T. D.; Peña Carrodeguas, L.; Trott, G.; Santmarti, A.; Lee, K.-Y.; Terrill, N. J.; Williams, C. K., *J. Am. Chem. Soc.* **2020,** *142* (9), 4367-4378.

29. Wang, Y.; Darensbourg, D. J., *Coord. Chem. Rev.* **2018,** *372*, 85-100.

30. Ciriminna, R.; Lomeli-Rodriguez, M.; Demma Carà, P.; Lopez-Sanchez, J. A.; Pagliaro, M., *Chem. Commun.* **2014,** *50* (97), 15288-15296.

31. Scharfenberg, M.; Hilf, J.; Frey, H., *Adv. Funct. Mater.* **2018,** *28* (10), 1704302.

32. Kember, M. R.; Williams, C. K., *J. Am. Chem. Soc.* **2012,** *134* (38), 15676-15679.

33. Xiao, Y.; Wang, Z.; Ding, K., *Macromolecules* **2006,** *39* (1), 128-137.

34. de la Cruz-Martínez, F.; Martínez de Sarasa Buchaca, M.; Martínez, J.; Tejeda, J.; Fernández-Baeza, J.; Alonso-Moreno, C.; Rodríguez, A. M.; Castro-Osma, J. A.; Lara-Sánchez, A., *Inorg. Chem.* **2020,** *59* (12), 8412-8423.

35. Nakano, K.; Nozaki, K.; Hiyama, T., *J. Am. Chem. Soc.* **2003,** *125* (18), 5501-5510.

36. Trott, G.; Garden, J. A.; Williams, C. K., *Chem. Sci.* **2019,** *10* (17), 4618-4627.

37. Kissling, S.; Lehenmeier, M. W.; Altenbuchner, P. T.; Kronast, A.; Reiter, M.; Deglmann, P.; Seemann, U. B.; Rieger, B., *Chem. Commun.* **2015,** *51* (22), 4579-4582.

38. Ni, K.; Kozak, C. M., *Inorg. Chem.* **2018,** *57* (6), 3097-3106.

39. Darensbourg, D. J.; Mackiewicz, R. M.; Billodeaux, D. R., *Organometallics* **2005,** *24* (1), 144-148.

40. Robert, C.; Ohkawara, T.; Nozaki, K., *Chem. Eur. J.* **2014,** *20* (16), 4789-4795.

41. Sugimoto, H.; Ohshima, H.; Inoue, S., *J. Polym. Sci., Part A: Polym. Chem.* **2003,** *41* (22), 3549-3555.

42. Reis, N. V.; Deacy, A. C.; Rosetto, G.; Durr, C. B.; Williams, C. K., *Chem. Eur. J.* **2022,** *28*, e202104198.

43. Nakano, K.; Kobayashi, K.; Ohkawara, T.; Imoto, H.; Nozaki, K., *J. Am. Chem. Soc.* **2013,** *135* (23), 8456-8459.

44. Taherimehr, M.; Al-Amsyar, S. M.; Whiteoak, C. J.; Kleij, A. W.; Pescarmona, P. P., *Green Chem.* **2013,** *15* (11), 3083-3090.

45. Buchard, A.; Kember, M. R.; Sandeman, K. G.; Williams, C. K., *Chem. Commun.* **2011,** *47* (1), 212-214.

46. Cohen, C. T.; Chu, T.; Coates, G. W., *J. Am. Chem. Soc.* **2005,** *127* (31), 10869-10878.

47. Kember, M. R.; Jutz, F.; Buchard, A.; White, A. J. P.; Williams, C. K., *Chem. Sci.* **2012,** *3* (4), 1245-1255.

48. Seong, J. E.; Na, S. J.; Cyriac, A.; Kim, B.-W.; Lee, B. Y., *Macromolecules* **2010,** *43* (2), 903-908.

49. Lin, P.-M.; Chang, C.-H.; Chuang, H.-J.; Liu, C.-T.; Ko, B.-T.; Lin, C.-C., *ChemCatChem* **2016,** *8* (5), 984-991.

50. Tsai, C.-Y.; Huang, B.-H.; Hsiao, M.-W.; Lin, C.-C.; Ko, B.-T., *Inorg. Chem.* **2014,** *53* (10), 5109-5116.

51. Deng, J.; Ratanasak, M.; Sako, Y.; Tokuda, H.; Maeda, C.; Hasegawa, J.-y.; Nozaki, K.; Ema, T., *Chem. Sci.* **2020,** *11* (22), 5669-5675.

52. Peña Carrodeguas, L.; González-Fabra, J.; Castro-Gómez, F.; Bo, C.; Kleij, A. W., *Chem. Eur. J.* **2015,** *21* (16), 6115-6122.

53. Thevenon, A.; Cyriac, A.; Myers, D.; White, A. J. P.; Durr, C. B.; Williams, C. K., *J. Am. Chem. Soc.* **2018,** *140* (22), 6893-6903.

54. Asaba, H.; Iwasaki, T.; Hatazawa, M.; Deng, J.; Nagae, H.; Mashima, K.; Nozaki, K., *Inorg. Chem.* **2020,** *59* (12), 7928-7933.

55. Coates, G. W.; Moore, D. R., *Angew. Chem. Int. Ed.* **2004,** *43* (48), 6618-6639.

56. Cheng, M.; Lobkovsky, E. B.; Coates, G. W., *J. Am. Chem. Soc.* **1998,** *120* (42), 11018-11019.

57. Cheng, M.; Moore, D. R.; Reczek, J. J.; Chamberlain, B. M.; Lobkovsky, E. B.; Coates, G. W., *J. Am. Chem. Soc.* **2001,** *123* (36), 8738-8749.

58. Moore, D. R.; Cheng, M.; Lobkovsky, E. B.; Coates, G. W., *J. Am. Chem. Soc.* **2003,** *125* (39), 11911-11924.

59. Ohkawara, T.; Suzuki, K.; Nakano, K.; Mori, S.; Nozaki, K., *J. Am. Chem. Soc.* **2014,** *136* (30), 10728-10735.

60. Jeon, J. Y.; Eo, S. C.; Varghese, J. K.; Lee, B. Y., *Beilstein J. Org. Chem* **2014,** *10*, 1787-1795.

61. S, S.; Min, J. K.; Seong, J. E.; Na, S. J.; Lee, B. Y., *Angew. Chem. Int. Ed.* **2008,** *47* (38), 7306-7309.

62. Nakano, K.; Kamada, T.; Nozaki, K., *Angew. Chem. Int. Ed.* **2006,** *45* (43), 7274-7277.

63. Darensbourg, D. J.; Mackiewicz, R. M.; Phelps, A. L.; Billodeaux, D. R., *Acc. Chem. Res.* **2004,** *37* (11), 836-844.

64. Xiao, Y.; Wang, Z.; Ding, K., *Chem. Eur. J.* **2005,** *11* (12), 3668-3678.

65. Piesik, D. F. J.; Range, S.; Harder, S., *Organometallics* **2008,** *27* (23), 6178-6187.

66. Lee, B. Y.; Kwon, H. Y.; Lee, S. Y.; Na, S. J.; Han, S.-i.; Yun, H.; Lee, H.; Park, Y.-W., *J. Am. Chem. Soc.* **2005,** *127* (9), 3031-3037.

67. Kember, M. R.; Knight, P. D.; Reung, P. T. R.; Williams, C. K., *Angew. Chem. Int. Ed.* **2009,** *48* (5), 931-933.

68. Garden, J. A.; Saini, P. K.; Williams, C. K., *J. Am. Chem. Soc.* **2015,** *137* (48), 15078-15081.

69. Deacy, A. C.; Durr, C. B.; Garden, J. A.; White, A. J. P.; Williams, C. K., *Inorg. Chem.* **2018,** *57* (24), 15575-15583.

70. Deacy, A. C.; Kilpatrick, A. F. R.; Regoutz, A.; Williams, C. K., *Nat. Chem.* **2020,** *12* (4), 372-380.

71. Buchard, A.; Jutz, F.; Kember, M. R.; White, A. J. P.; Rzepa, H. S.; Williams, C. K., *Macromolecules* **2012,** *45* (17), 6781-6795.

72. Nachtergael, A.; Coulembier, O.; Dubois, P.; Helvenstein, M.; Duez, P.; Blankert, B.; Mespouille, L., *Biomacromolecules* **2015,** *16* (2), 507-514.

73. Yang, G.-W.; Zhang, Y.-Y.; Xie, R.; Wu, G.-P., *J. Am. Chem. Soc.* **2020,** *142* (28), 12245-12255.

74. Patil, N.; Bhoopathi, S.; Chidara, V.; Hadjichristidis, N.; Gnanou, Y.; Feng, X., *ChemSusChem* **2020,** *13* (18), 5080-5087.

75. Zhang, D.; Boopathi, S. K.; Hadjichristidis, N.; Gnanou, Y.; Feng, X., *J. Am. Chem. Soc.* **2016,** *138* (35), 11117-11120.

76. Zhang, D.-D.; Feng, X.; Gnanou, Y.; Huang, K.-W., *Macromolecules* **2018,** *51* (15), 5600-5607.

77. Zhang, J.; Wang, L.; Liu, S.; Li, Z., *Angew. Chem. Int. Ed.* **2022,** *61* (4), e202111197.

78. Naumann, S.; Dove, A. P., *Polym. Chem,* **2015,** *6* (17), 3185-3200.

79. Yang, G.-W.; Xu, C.-K.; Xie, R.; Zhang, Y.-Y.; Zhu, X.-F.; Wu, G.-P., *J. Am. Chem. Soc.* **2021,** *143* (9), 3455-3465.

80. Wang, Y.; Zhang, J.-Y.; Yang, J.-L.; Zhang, H.-K.; Kiriratnikom, J.; Zhang, C.-J.; Chen, K.-L.; Cao, X.-H.; Hu, L.-F.; Zhang, X.-H.; Tang, B. Z., *Macromolecules* **2021,** *54* (5), 2178-2186.

81. Spyridakou, M.; Gardiner, C.; Papamokos, G.; Frey, H.; Floudas, G., *ACS Applied Polymer Materials* **2022,** *4* (5), 3833-3843.

82. Koning, C.; Wildeson, J.; Parton, R.; Plum, B.; Steeman, P.; Darensbourg, D. J., *Polymer* **2001,** *42* (9), 3995-4004.

83. Leow, W. R.; Lum, Y.; Ozden, A.; Wang, Y.; Nam, D.-H.; Chen, B.; Wicks, J.; Zhuang, T.-T.; Li, F.; Sinton, D.; Sargent, E. H., *Science* **2020,** *368* (6496), 1228-1233.

84. Langanke, J.; Wolf, A.; Hofmann, J.; Böhm, K.; Subhani, M. A.; Müller, T. E.; Leitner, W.; Gürtler, C., *Green Chem.* **2014,** *16* (4), 1865-1870.

85. Alagi, P.; Ghorpade, R.; Choi, Y. J.; Patil, U.; Kim, I.; Baik, J. H.; Hong, S. C., *ACS Sustain. Chem. Eng.* **2017,** *5* (5), 3871-3881.

86. Hauenstein, O.; Reiter, M.; Agarwal, S.; Rieger, B.; Greiner, A., *Green Chem.* **2016,** *18* (3), 760-770.

87. Hauenstein, O.; Agarwal, S.; Greiner, A., *Nat. Commun.* **2016,** *7* (1), 11862.

88. Kernbichl, S.; Rieger, B., *Polymer* **2020,** *205*, 122667.

89. Luinstra, G. A., *Polym. Rev.* **2008,** *48* (1), 192-219.

90. Song, P.; Ran, B.; Shang, Y.; Kang, L.; Chen, Y.; Sun, L., *Adv. Ind. Eng. Polym. Res.* **2019,** *2* (4), 161-166.

91. CHEMnetBASE - Polymers: a Property Database. http://poly.chemnetbase.com/faces/polymers/PolymerSearch.xhtml (accessed Feb 22).

92. Zhang, X.; Liu, Y.; Li, X.; Liu, X.; Jian, X.; Wang, J., *International Journal of Polymer Science* **2022,** *2022*, 9255159.

93. Diment, W. T.; Gregory, G. L.; Kerr, R. W. F.; Phanopoulos, A.; Buchard, A.; Williams, C. K., *ACS Catal.* **2021,** *11* (20), 12532-12542.

94. Merchant Research and Consulting Ltd. https://mcgroup.co.uk/researches/phthalic-anhydride-pa (accessed 2022).

95. Zhang, Y.-Y.; Wu, G.-P.; Darensbourg, D. J., *Trends Chem.* **2020,** *2* (8), 750-763.

96. Li, Y.; Zhang, Y.-Y.; Hu, L.-F.; Zhang, X.-H.; Du, B.-Y.; Xu, J.-T., *Prog. Polym. Sci.* **2018,** *82*, 120-157.

97. Jeske, R. C.; Rowley, J. M.; Coates, G. W., *Angew. Chem. Int. Ed.* **2008,** *47* (32), 6041-6044.

98. Wang, Y.; Zhao, Y.; Ye, Y.; Peng, H.; Zhou, X.; Xie, X.; Wang, X.; Wang, F., *Angew. Chem. Int. Ed.* **2018,** *57* (14), 3593-3597.

99. Fu, C.; Xu, J.; Kokotovic, M.; Boyer, C., *ACS Macro Lett.* **2016,** *5* (4), 444-449.

100. Zhang, Y.-Y.; Yang, G.-W.; Wu, G.-P., *Macromolecules* **2018,** *51* (10), 3640-3646.

101. Stößer, T.; Chen, T. T. D.; Zhu, Y.; Williams, C. K., *Philos. Trans. R. Soc. A* **2018,** *376* (2110), 20170066.

102. Sanford, M. J.; Van Zee, N. J.; Coates, G. W., *Chem. Sci.* **2018,** *9* (1), 134-142.

103. Yang, G.-W.; Wu, G.-P., *ACS Sustain. Chem. Eng.* **2019,** *7* (1), 1372-1380.

104. Wang, Y.; Fan, J.; Darensbourg, D. J., *Angew. Chem. Int. Ed.* **2015,** *54* (35), 10206-10210.

105. Yang, G.-W.; Zhang, Y.-Y.; Wang, Y.; Wu, G.-P.; Xu, Z.-K.; Darensbourg, D. J., *Macromolecules* **2018,** *51* (4), 1308-1313.

106. Zhu, N.; Hu, X.; Fang, Z.; Guo, K., *Prog. Polym. Sci.* **2021,** *117*, 101397.

107. Darensbourg, D. J., *Inorg. Chem. Front.* **2017,** *4* (3), 412-419.

108. Koning, C. E.; Sablong, R. J.; Nejad, E. H.; Duchateau, R.; Buijsen, P., *Prog. Org. Coat.* **2013,** *76* (12), 1704-1711.

109. Huijser, S.; HosseiniNejad, E.; Sablong, R.; de Jong, C.; Koning, C. E.; Duchateau, R., *Macromolecules* **2011,** *44* (5), 1132-1139.

110. Darensbourg, D. J.; Poland, R. R.; Escobedo, C., *Macromolecules* **2012,** *45* (5), 2242-2248.

111. Saini, P. K.; Romain, C.; Zhu, Y.; Williams, C. K., *Polym. Chem,* **2014,** *5* (20), 6068-6075.

112. Saini, P. K.; Fiorani, G.; Mathers, R. T.; Williams, C. K., *Chem. Eur. J.* **2017,** *23* (18), 4260-4265.

113. Zhang, J.; Wang, L.; Liu, S.; Kang, X.; Li, Z., *Macromolecules* **2021,** *54* (2), 763-772.

114. Ye, S.; Wang, W.; Liang, J.; Wang, S.; Xiao, M.; Meng, Y., *ACS Sustain. Chem. Eng.* **2020,** *8* (48), 17860-17867.

115. Romain, C.; Williams, C. K., *Angew. Chem. Int. Ed.* **2014,** *53* (6), 1607-1610.

116. Zhu, Y.; Romain, C.; Williams, C. K., *J. Am. Chem. Soc.* **2015,** *137* (38), 12179-12182.

117. Deacy, A. C.; Gregory, G. L.; Sulley, G. S.; Chen, T. T. D.; Williams, C. K., *J. Am. Chem. Soc.* **2021,** *143* (27), 10021-10040.

118. Romain, C.; Zhu, Y.; Dingwall, P.; Paul, S.; Rzepa, H. S.; Buchard, A.; Williams, C. K., *J. Am. Chem. Soc.* **2016,** *138* (12), 4120-4131.

119. Stößer, T.; Mulryan, D.; Williams, C. K., *Angew. Chem. Int. Ed.* **2018,** *57* (51), 16893-16897.

120. Diment, W. T.; Stößer, T.; Kerr, R. W. F.; Phanopoulos, A.; Durr, C. B.; Williams, C. K., *Cat. Sci. Tech.* **2021,** *11* (5), 1737-1745.

121. Kernbichl, S.; Reiter, M.; Mock, J.; Rieger, B., *Macromolecules* **2019,** *52* (21), 8476-8483.

122. Plajer, A. J.; Williams, C. K., *Angew. Chem. Int. Ed.* **2021,** *n/a* (n/a).

123. Stößer, T.; Sulley, G. S.; Gregory, G. L.; Williams, C. K., *Nat. Commun.* **2019,** *10* (1), 2668.

124. Li, H.; He, G.; Chen, Y.; Zhao, J.; Zhang, G., *ACS Macro Lett.* **2019,** *8* (8), 973-978.

125. Li, C.; Dang, Y.-F.; Wang, B.; Pan, L.; Li, Y.-S., *Macromolecules* **2021,** *54* (13), 6171-6181.

126. Liu, Y.; Deng, K.; Wang, S.; Xiao, M.; Han, D.; Meng, Y., *Polym. Chem,* **2015,** *6* (11), 2076-2083.

127. Liu, Y.; Huang, K.; Peng, D.; Wu, H., *Polymer* **2006,** *47* (26), 8453-8461.

128. Liu, Y.; Xiao, M.; Wang, S.; Xia, L.; Hang, D.; Cui, G.; Meng, Y., *RSC Adv.* **2014,** *4* (19), 9503-9508.

129. Subhani, M. A.; Köhler, B.; Gürtler, C.; Leitner, W.; Müller, T. E., *Angew. Chem. Int. Ed.* **2016,** *55* (18), 5591-5596.

130. Dienes, Y.; Leitner, W.; Müller, M. G. J.; Offermans, W. K.; Reier, T.; Reinholdt, A.; Weirich, T. E.; Müller, T. E., *Green Chem.* **2012,** *14* (4), 1168-1177.

131. Zhu, Y.; Romain, C.; Williams, C. K., *Nature* **2016,** *540* (7633), 354-362.

132. Delidovich, I.; Hausoul, P. J. C.; Deng, L.; Pfützenreuter, R.; Rose, M.; Palkovits, R., *Chem. Rev.* **2016,** *116* (3), 1540-1599.

133. Stadler, B. M.; Wulf, C.; Werner, T.; Tin, S.; de Vries, J. G., *ACS Catal.* **2019,** *9* (9), 8012-8067.

134. Diaz, C.; Mehrkhodavandi, P., *Polym. Chem*, **2021,** *12* (6), 783-806.

135. Coates, G. W.; Getzler, Y. D. Y. L., *Nat. Rev. Mater.* **2020,** *5* (7), 501-516.

136. Gregory, G. L.; Sulley, G. S.; Carrodeguas, L. P.; Chen, T. T. D.; Santmarti, A.; Terrill, N. J.; Lee, K.-Y.; Williams, C. K., *Chem. Sci.* **2020,** *11* (25), 6567-6581.

137. Kernbichl, S.; Reiter, M.; Adams, F.; Vagin, S.; Rieger, B., *J. Am. Chem. Soc.* **2017,** *139* (20), 6787-6790.

138. Reis, N. V. Homogeneous catalysts for the ROCOP of CO2 and epoxides. University of Oxford, 2020.

Chapter 2

Investigation of Mg(II)M(II) Complexes for Epoxide/Anhydride ROCOP and their Selectivity in Terpolymerisations with CO_2

Work described in this chapter appears in:

Heterodinuclear Mg(II)M(II) (M = Cr, Mn, Fe, Co, Ni, Cu and Zn) Complexes for the Ring Opening Copolymerization of Carbon Dioxide/Epoxide and Anhydride/Epoxide

N. V. Reis, A. C. Deacy, G. Rosetto, C. B. Durr, C. K. Williams, *Chem. Eur. J.*, **2022**, *28*, e202104198

Mg(II) heterodinuclear catalysts delivering carbon dioxide derived multi-block polymers

G. Rosetto, A. C. Deacy, C. K. Williams, *Chem. Sci.*, **2021**, *12*, 12315–12325

2.1 Introduction

In 2015, our group demonstrated that a heterodinuclear Mg(II)Zn(II) supported by a diphenolate tetraamine macrocycle ligand displayed much greater activities for CO_2/epoxide and anhydride/epoxide ROCOP than the homodinuclear Zn(II)Zn(II) and Mg(II)Mg(II) metal analogues.[1] Further optimisation of the metal combinations let to the development of a Mg(II)Co(II) complex which showed even greater activity (TOF_{MgZn} = 98 h^{-1} *vs.* TOF_{MgCo} = 455 h^{-1} at 1 bar CO_2 pressure, 80 ˚C).[2-3] An experimental investigation into its mechanism indicated that the synergy arises from the metals playing different roles in the rate determining step of the polymerisation cycle (see Chapter 1, Section 1.2.2). This discovery naturally led to the study of other metal combinations with Mg(II) and transition metals (TM(II)) to assess whether they would show similar competitive rates and synergy in CO_2/epoxide ROCOP. A series of Mg(II)M(II) complexes, where M = Mg (**1**), Cr (**2**) , Mn (**3**), Fe (**4**), Co (**5**), Ni (**6**), Cu (**7**), Zn (**8**), were synthesised and fully characterised by Dr. Natalia Reis (Figure 2.1).[4-5]

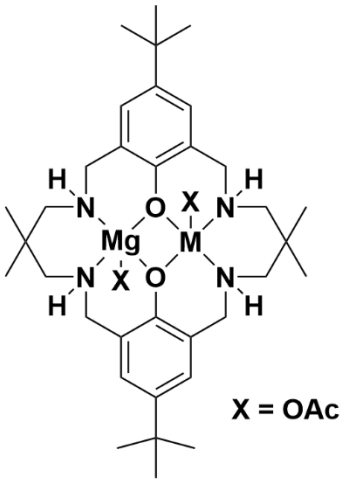

M(II)	#
Mg	1
Cr	2
Mn	3
Fe	4
Co	5
Ni	6
Cu	7
Zn	8

Figure 2.1: Structure of Mg(II)M(II) **1**–**8** studied in this chapter.

Their activities for CHO and CO_2 (1 bar pressure) ROCOP at 100 ˚C in neat conditions were compared to the homodinuclear Mg(II)Mg(II). All showed a good performance and high

polycarbonate selectivity, except **3** and **7**, which gave 10 % *trans*-cyclic carbonate. There are evident metal dependent differences in productivity; complexes **4** and **5** featuring Co(II) and Fe(II) showed the highest activities, with TOFs of 1056 h^{-1} and 1071 h^{-1} respectively. Overall, the mid-transition metals perform better, as seen in the volcano plot of M(II) metal *vs.* polymerisation propagation rate constants obtained experimentally.

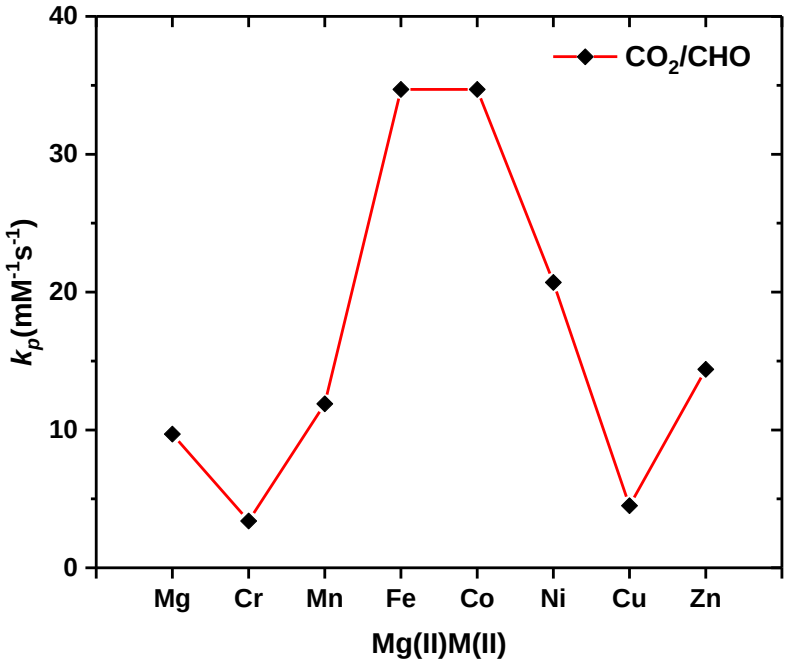

Figure 2.2: Plot of the polymerisation rate coefficient (k_p) for the ring opening copolymerisation of CO_2 and CHO using Mg(II)M(II) catalysts **1**–**8**.[4]

Frequently, catalysts active for CO_2/epoxide ROCOP are also active for epoxide/anhydride ROCOP, although their relative performance may differ.[6-8] Versatile catalysts that are effective for both processes are important for applications, such as block copolymer synthesis.[8-9] In relation to this, Saini *et al.* found that catalyst **1** and the di-zinc complex (**9**) have orthogonal polymerisation reactivity for a mixture of epoxide, a sterically hindered tricyclic anhydride (TCA) and carbon dioxide (1 bar pressure); **1** selectively copolymerised CO_2/epoxide to form polycarbonate, whilst **9** exclusively formed polyester.[10] This was an unexpected result as, according to the switch catalysis "rules", the anhydride ROCOP should

be thermodynamically more favourable (see Chapter 1, Section 1.4.3).[11] However, it is apparent that both anhydride and metal choice will affect the order of monomer enchainment. Selectivity in switch catalysis is an important consideration, as it determines the sequence of block copolymers if performed in one-pot. Hence, the selectivity of more active catalysts should be explored.

2.2 Aims

In this chapter, the ring-opening copolymerisation of CHO and norbornene anhydride (NA) catalysed by Mg(II)Mg(II) (**1**) and seven Mg(II)M(II) (**2**–**8**) (M = Cr, Mn, Fe, Co, Ni, Cu, Zn) complexes will be carried out to assess their relative activities (Figure 2.3a). Norbornene anhydride was chosen due to its commercial availability and versatility as an anhydride, as it displays higher polymerisation rates compared to other bulkier substrates, and provides an internal alkene susceptible to post-functionalisation.[12-13] The reactions will be monitored by *in situ* IR spectroscopy until 100 % conversion of the anhydride is reached. The rate law for the catalyst with the highest activity will be established, by experimentally determining the order in catalyst, epoxide, and anhydride.

The most active catalysts for both ROCOP cycles will also be tested for polymerisation in a one-pot mixture of CO_2, anhydride, and epoxide, to establish the selectivity with respect to the monomers (Figure 2.3b). Tricyclic anhydride (TCA), a bio-derived Diels-Alder adduct of cyclic monoterpene and maleic anhydride, will be used as the anhydride, given its precedence in causing orthogonal selectivity between catalysts.[10, 14]

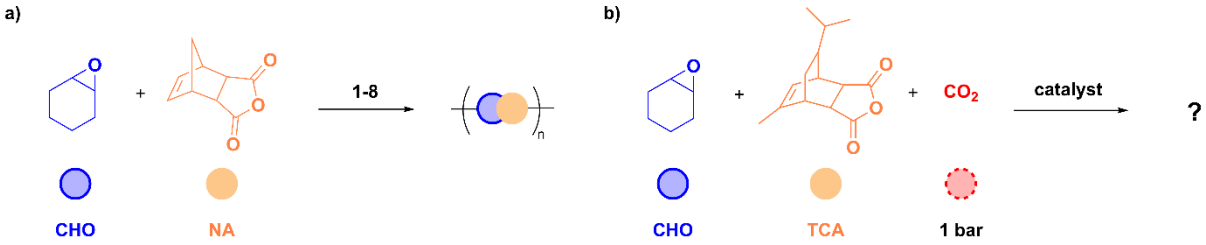

Figure 2.3: Aims for Chapter 2. a) ROCOP of NA and CHO with catalysts **1**–**8**. b) ROCOP of CHO, TCA and CO_2 (at 1 bar).

2.3 Heterodinuclear Catalysts for the ROCOP of NA and CHO

2.3.1 NA/CHO ROCOP

In order to assess the epoxide/anhydride ROCOP activity, complexes **1**–**8** were tested for the copolymerisation of CHO and NA at a catalyst loading of 0.05 mol % in neat epoxide (9.9 M) with 20 equivalents of CHD as chain transfer agent, at 100 ˚C (Table 2.1). The reactions were monitored by *in situ* IR spectroscopy. By plotting absorbance of the anhydride signal (C=O stretch, 1785 cm^{-1}) against time, a rate coefficient, k_{obs} (s^{-1}) was extracted by taking the gradient between 20–80 % anhydride conversion (Figures S2.1–S2.7) to account for induction periods. In turn, the polymerisation propagation rate coefficient (k_p) was determined from the pseudo first-order rate coefficient (k_{obs}) by dividing by the relevant catalyst concentration (this assumes first order dependence on the catalyst, *vide infra*). Reactions were run to full conversion of anhydride, which was identified when the IR signal intensity decreased below 0.05 A.U., further confirmed by ^{1}H NMR spectroscopy.

Table 2.1: Results for NA/CHO ROCOP using catalysts **1–8** and leading catalysts in the field.[a]

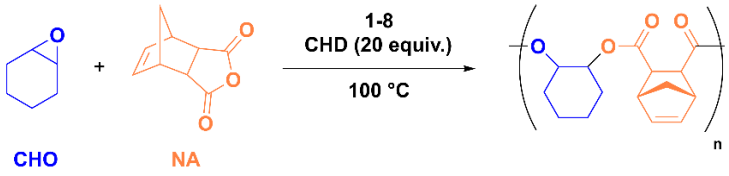

Entry	Mg(II)M(II) M, catalyst #	Conv. (%)[b]	TON[c]	TOF (h^{-1})[d]	k_p ($mM^{-1}s^{-1}$)[e]	k_{rel}[f]	M_n [Đ] (kg mol^{-1})[g]
1	Mg, **1**	> 99	100	71	8.7	1.0	1.6 [1.15]
2	Cr, **2**	> 99	100	54	6.6	0.8	*n.d*
3	Mn, **3**	> 99	100	272	33.5	3.9	1.4 [1.14]
4	Fe, **4**	> 99	100	109	13.4	1.5	1.3 [1.15]
5	Co, **5**	> 99	100	610	75.2	8.6	1.5 [1.14]
6	Ni, **6**	> 99	100	244	30.1	3.5	1.4 [1.15]
7	Cu, **7**	> 99	100	170	21.2	2.4	1.2 [1.15]
8	Zn, **8**	> 99	100	186	23.0	2.6	1.3 [1.14]
9[h,15]	(ONSO)Cr(III)Cl/DMAP	77	192	288	-	-	6.4 [1.26]
10[i,13]	(salophen)Cr(III)Cl/PPNCl	97	243	49	-	-	3.0 [1.12]
11[j,16]	(salen[CyPr]$^+$)Al(III)Cl_2	51	204	34	-	-	8.2 [1.24]
12[k,17]	(*o*-van)Al(III)K(I)$(OAc)_2$	33	133	266	-	-	4.5 [1.10]

[a] Reaction conditions: [cat.]:[CHD]:[NA]:[CHO] = 1:20:100:2000; 0.05 mol% catalyst loading (4.9 mM), neat CHO (3.2 mL, 9.9 M), 100 °C. [b] Expressed as a percentage of epoxide conversion against the theoretical maximum (100 %). [c] Turn over number (TON) = number of moles of monomer converted / number of moles of catalyst. [d] Turn over frequency (TOF) = TON / hour. [e] k_p = rate coefficient = k_{obs} / [cat.]^1 where k_{obs} is calculated from the gradient of the plot of [NA] *vs.* time (s). [f] k_{rel} = relative rate coefficient = $k_{p(MgM)}$ / $k_{p(MgMg)}$. [g] Determined by GPC analysis in THF, calibrated with narrow-M_n polystyrene standard; dispersity values in parentheses. [h] Reaction conditions: [cat.]:[DMAP]:[NA]:[CHO] = 1:1:250:250 in toluene (2 mL), 110 °C. [i] Reaction conditions: $[cat.]_0$:$[DMAP]_0$:$[NA]_0$:$[CHO]_0$ = 1:1:250:250 in toluene, 110 °C. [j] Reaction conditions: [cat.]:[NA]:[CHO] = 1 : 400 : 2000, 0.05 mol % catalyst loading, neat CHO (9.9 M), 60 °C. [k] Reaction conditions: [cat.]:[NA]:[CHO] = 1:400:2000, 0.05 mol %, neat CHO (9.9 M), 100 °C. For reported catalyst structures, entries 9–13, see Figure S2.9.

All complexes are catalytically active and show excellent selectivity for polyester (> 99%), as no ether linkages were detected in the ^{1}H NMR spectra of the resulting polyesters. Molar mass values analysed by GPC were around 1.3 kg mol^{-1} and monodisperse (Đ < 1.2) (Figure S2.8). Complex **5** (Mg(II)Co(II)) was the most active (Table 2.1, Entry 5, TOF = 610 h^{-1}), followed by **3** (Mg(II)Mn(II), Table 2.1, Entry 3, TOF = 272 h^{-1}) and **6** (Mg(II)Ni(II), Table

2.1, Entry 6, TOF = 244 h^{-1}). In contrast to the previous study, the activity of **4** (Mg(II)Fe(II)) was not similar to that of **5**, instead displaying a moderate TOF of 109 h^{-1} (Table 2.1, Entry 4). Overall, the order in metal reactivity was Co > Mn ~ Ni > Zn ~ Cu > Fe > Mg > Cr (Figure 2.4).

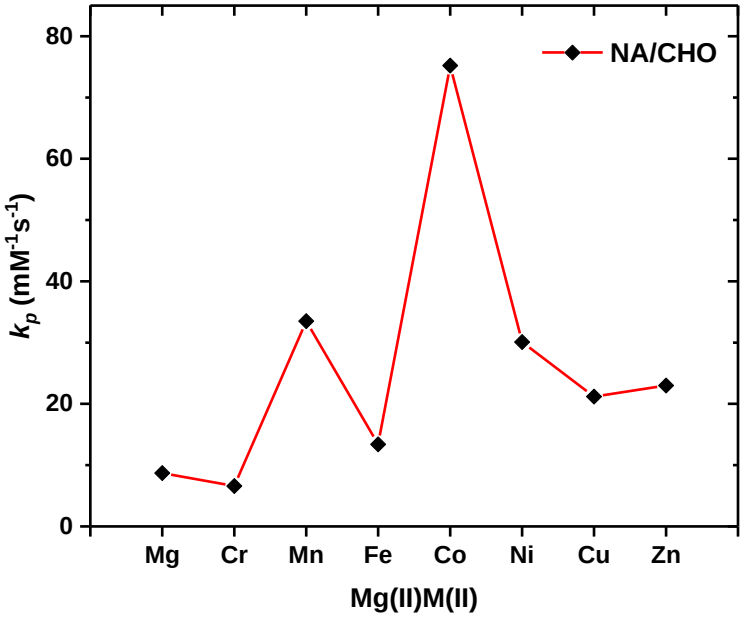

Figure 2.4: Plot of the polymerisation rate coefficient (k_p) for the ring opening copolymerisation of NA and CHO using Mg(II)M(II) catalysts **1–8.**

In comparison to the wider field, complex **5** shows good activity for NA/CHO ROCOP. It exhibits a TOF ~12x greater than the commercial [(salen)Cr(III)Cl]DMAP catalyst system (Table 2.1, Entry 9, [cat.]:[PPNCl]:[NA]:[CHO] = 1:1:250:250 in toluene (2 mL), TOF = 49 h^{-1}, 110 ˚C) and double the activity to a sulphur modified salen [(ONSO)Cr(III)Cl]/DMAP] (Table 2.1, Entry 10, [cat.]:[PPNCl]:[NA]:[CHO] = 1:1:250:250 in toluene (2 mL), TOF = 289 h^{-1}, 110 ˚C), both at 10 times lower loading.[13, 15] Catalyst **5** does not require a co-catalyst, hence high activities can be achieved at low loadings, in contrast to bicomponent systems. Systems which tether the co-catalyst, such as [(salen[CyPr]$^{+}$)Al(III)Cl], also avoid this issue. The Al(III) catalyst shows a lower TOF for NA/CHO ROCOP (Table 2.1, Entry 11, [cat.]:[NA]:[CHO] = 1: 400: 2000, TOF = 34 h^{-1}, 60 ˚C), although it is applied at a lower

temperature (60 *vs.* 100 ˚C), hence it cannot be fairly compared.[16] A recent report of a heterodinuclear Al(III)/K(I) complex [(*o*-van)Al(III)K(I)$(OAc)_2$] for ROCOP of NA/CHO resulted in a TOF half that of **5** under equivalent conditions (Table 2.1, Entry 12, [cat.]:[NA]:[CHO] = 1:400:2000, TOF = 266 h^{-1}, 100 ˚C).[17]

2.3.2 Rate Law

Subsequent kinetic investigations were undertaken with catalyst **5**, as it was the most active out of the series. Several reactions, outlined below, were monitored by *in situ* IR spectroscopy to determine the rate law. For anhydride, a linear decrease in NA concentration over time was observed, indicative of a zeroth order in NA concentration (Figure 2.5a). This finding is consistent with CO_2 concentration in CO_2/epoxide ROCOP,[2] and for other dinuclear catalysts.[18]

The order in catalyst was determined by taking the pseudo rate coefficients (k_{obs}) for the catalyst concentration range 2–5 mM ([CHO] = 9.9 M, [NA]:[CHO] = 1:20), and plotting them against each other. A linear relationship was established between them (Figure 2.5b), and a logarithmic plot gave a gradient close to 1 (Figure 2.5c), indicating a first order dependence of catalyst concentration in the polymerisation.

Lastly, the order in epoxide was found by an integrated rate treatment of a reaction conducted in toluene, where epoxide is the limiting reagent. An exponential fit to the data was applied across the entire conversion range, suggesting a first order dependence in epoxide (Figure 2.5d) . Hence, the rate law is proposed as:

$$rate = k_p[cat.]^1[epoxide]^1[anhydride]^0$$

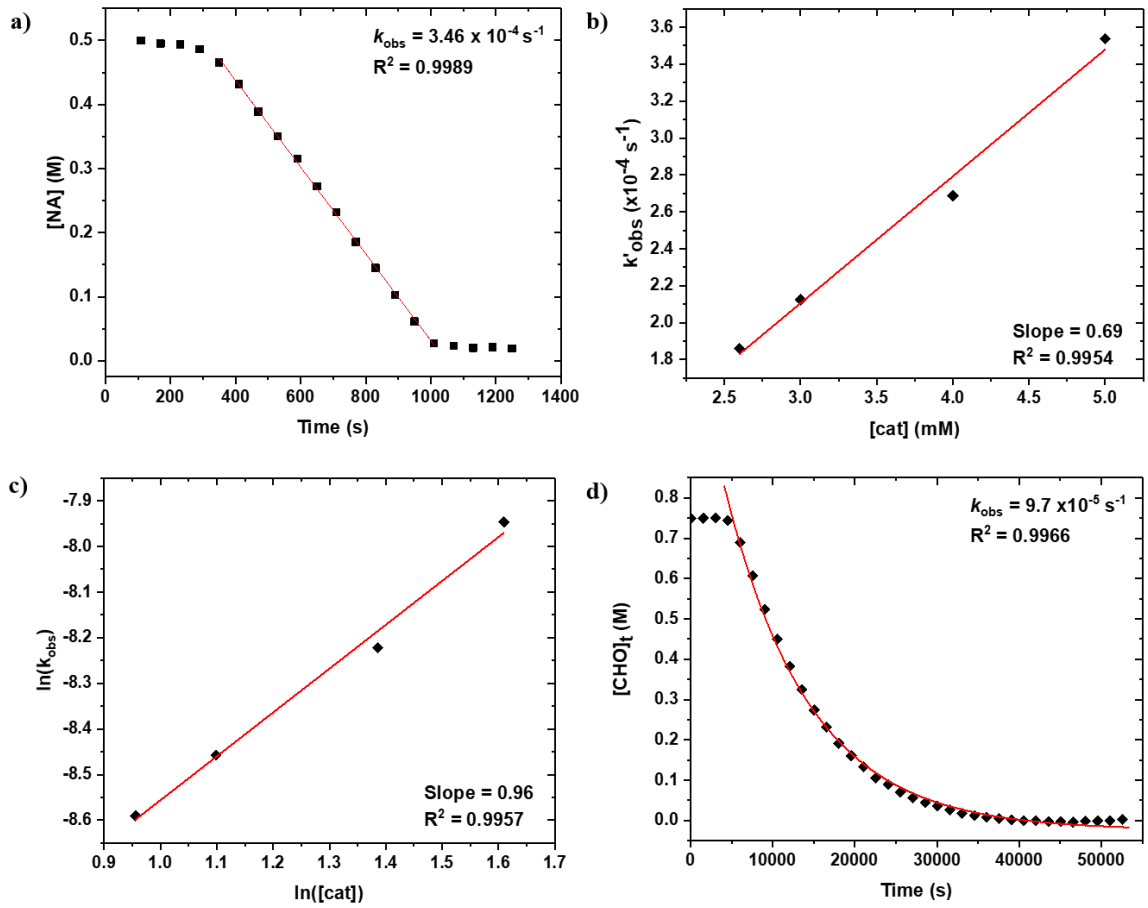

Figure 2.5: Reaction kinetic plots that determine the order in a) anhydride concentration (0 order). Reaction conditions: [cat.]:[CHD]:[NA]:[CHO] = 1:20:100:2000, [cat.] = 4.9 mM, 100 °C. b) and c) catalyst concentration (first order). Reaction conditions: $[cat.]_{x\text{-}y}$:[CHD]:[NA]:[CHO] = 1-2:20:100:2000, $[cat.]_{x\text{-}y}$ = 2.5 mM (x)–5mM (y), 100 °C. d) CHO order (first order) [cat.]:[CHD]:[NA]:[CHO] = 1:20:180:50, $[cat.]_0$ = 5mM in toluene (total volume 1.6 mL), 100 °C.

The rate law implies that the rate determining step involves both catalyst and epoxide, and is hence the insertion of CHO into transition metal-carboxylate bond (Figure 2.6). This is the same rate law found for CO_2/epoxide ROCOP, which may explain why the reactivity trends between the two polymerisations are similar, as the reactions involve similar rate determining steps. In the case of Mg(II)Fe(II), the low reactivity may be tentatively attributed to its decomposition by diacid impurities present in the anhydride. This proposal comes from an observation in the synthesis of homodinuclear Fe(II)Fe(II) complex, where an Fe(II) centre readily oxidised to Fe(III) in the presence of acetic acid.[4] In turn, the

oxidation to Fe(III) may lead to an inactive species. To confirm this hypothesis, the oxidised species Mg(II)Fe(III) should be synthesised and tested for this catalysis.

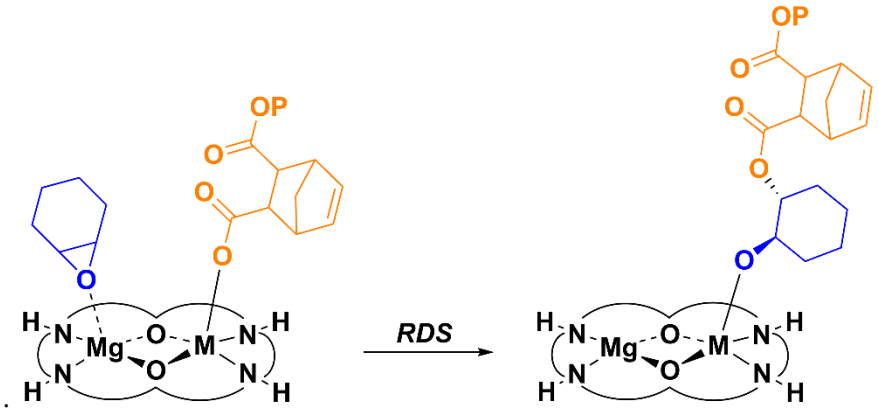

Figure 2.6: Illustration of the rate determining step of CHO/NA ROCOP catalysed by heterodinuclear Mg(II)M(II) complexes, implied by kinetic analysis of **5**. P = polymer.

The structure-activity study has shown that mid-period transition metals are better partners with Mg(II) in ROCOP catalysis. Overall, there is no direct correlation between activity and fundamental parameters for transition metals, such as Lewis acidity, oxophilicity and bond dissociation energy.[4, 19] It is proposed that Mg(II), being the stronger Lewis Acid, binds the epoxide, whilst the other metal bears the carboxylate polymeryl chain end. A faster epoxide insertion would require epoxide activation by a strong Lewis acid and a weaker or more nucleophilic metal-carboxylate bond. Such qualities are influenced by various factors, including vicinal metal effects and ligand field stabilisations; hence, it is unlikely to correlate directly to a single fundamental parameter.

Similarly, a study by Nozaki, Mashima and co-workers looked at the influence of different lanthanide M(III) metals (M(III) = La, Ce, Pr, Nd, Eu, or Gd) on CO_2/epoxide ROCOP, which also had little success in correlating the TOF with various parameters of lanthanide ions.[20]

2.4 M(II)M(II) Catalyst Selectivity for the One-pot Reaction of Epoxide, Anhydride, and CO_2

Motivated by the work of Saini *et al.*, in which Mg(II)Mg(II) and Zn(II)Zn(II) exhibited orthogonal reactivity in ROCOP,[10] it was apparent that the selectivity of the class of macrocyclic catalysts in the terpolymerisation of epoxide, anhydride, and CO_2 is dependent on the choice of metal centres. Given that several Mg(II)M(II) complexes have proven to be more active for both CO_2/epoxide and anhydride/epoxide ROCOP in comparison to the homodinuclear Mg(II)Mg(II) (**1**) complex, their selectivity for these copolymerisations should be probed. An evident choice was **5** (Mg(II)Co(II)), as it was most active for both polymerisation cycles. Complex **8** (Mg(II)Zn(II)) was also included in the study, since it would represent one of each metal in the previous study. Polymerisations with the homodinuclear complexes **1** and Zn(II)Zn(II) (**9**) were also repeated for direct comparison (Figure 2.7).

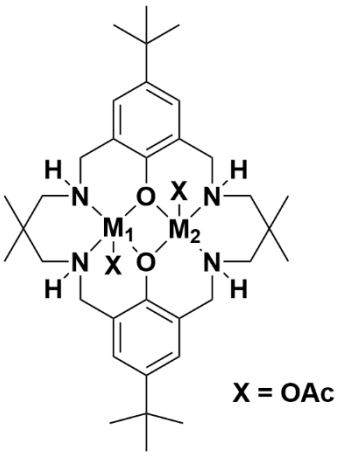

M_1(II)	M_2(II)	#
Zn	Zn	9
Mg	Mg	1
Mg	Zn	8
Mg	Co	5

Figure 2.7: Structure and numbering system for the complexes used in Section 2.4.

Each catalyst was exposed to 100 equiv. of tricyclic anhydride (TCA), 2000 equiv. of neat CHO, 10 equivalents of cyclohexene diol (CHD) as CTA, and 1 bar pressure of CO_2, at 100 ˚C. The selectivity of the catalysts was established by monitoring the reactions with *in situ* IR spectroscopy, by measuring the change in absorption intensity of the polycarbonate

(1230 cm^{-1}) and anhydride (1780 cm^{-1}) resonance over time. ^1H NMR spectroscopy was additionally used to quantify the formation of polymer.

Table 2.2: Catalyst selectivity data for the polymerisation of a mixture of TCA, CHO, and CO_2 at 1 bar pressure using **1**, **5**, **8**, and **9**.[a]

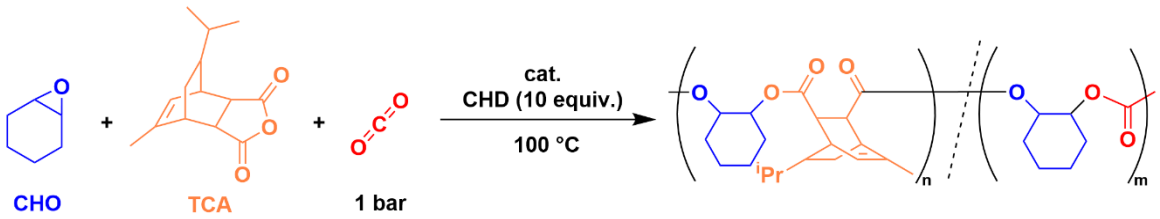

Entry	Catalyst	Time (h)	TON[b]		TOF (h^{-1})[c]		Composition (%)		M_n [$Đ$] (kg mol^{-1})[d]
			TCA	CHO	TCA	PCHC	PE	PCHC	
1	**ZnZn, 9**	7.7	82	82	11	0	100	0	1.7 [1.16]
2	**MgMg, 1**	1.5	0	168	0	112	0	100	2.3 [1.15]
3	**MgZn, 8**	1.5	100	407	67	205	25	75	4.8 [1.14]
4	**MgCo, 5**	1.0	0	640	0	640	0	100	7.2 [1.13]

[a] Polymerisation conditions: [cat.]:[CHD]:[TCA]:[CHO] = 1:10:100:2000, 100 °C, 1 bar CO_2. [b] Turnover number (TON), number of moles of TCA or CHO consumed/number of moles of catalyst. Moles consumed determined from the ^1H NMR spectrum by comparing normalized integrals for polycarbonate (4.6 ppm), CHO (3.12 ppm), TCA (5.78 ppm), and PE (5.70–5.80 and 4.6 ppm) resonances. [d] Turnover frequency (TOF), TON / time (h). [c] Determined by GPC, in THF, calibrated with narrow molar mass polystyrene standards (Figures S2.28–S2.31).

Consistent with the prior report, catalyst **9** showed selective formation of poly(TCA-*alt*-CHO) (denoted PE) (Figures S2.10 and S2.11) whereas **1** displayed the opposite reactivity, forming poly(cyclohexene carbonate) (PCHC) exclusively (Table 2.2, Entry 1 and 2, and Figure S2.12 and S2.13).[10] Interestingly, **8** showed simultaneous formation of PE and PCHC linkages (Table 2.2, Entry 3 and Figure S2.14), with a ratio of 1:3 PE:PCHC, determined by ^1H NMR spectroscopy (Figure 2.8). The result implies preference for CO_2 insertion although with competitive anhydride insertion. After purification of the polymer, the ratio remained unchanged, supporting the formation of a random copolymer. A single diffusion coefficient was observed by ^1H DOSY analysis, which is also in agreement with the formation of a random copolymer structure rather than PE and PCHC homopolymers (Figure S2.15). In the

$^{13}C\{^{1}H\}$ NMR spectrum, new signals shouldering the polyester carbonyl resonance (169 ppm) were also observed, which were attributed to the random CO_2 incorporation (Figure S2.16).[21] Catalyst **5** showed equivalent selectivity to **1**, only forming PCHC and exhibiting no conversion of the anhydride (Table 2.2, Entry 4 and Figure S2.17). Under these reaction conditions, it displays ~6 times the activity of **1** (TOF_{MgMg} = 112 h^{-1} *vs.* TOF_{MgCo} = 640 h^{-1}), consistent with the previously established rate enhancement through metal synergy between Mg(II) and Co(II) within the macrocyclic framework.

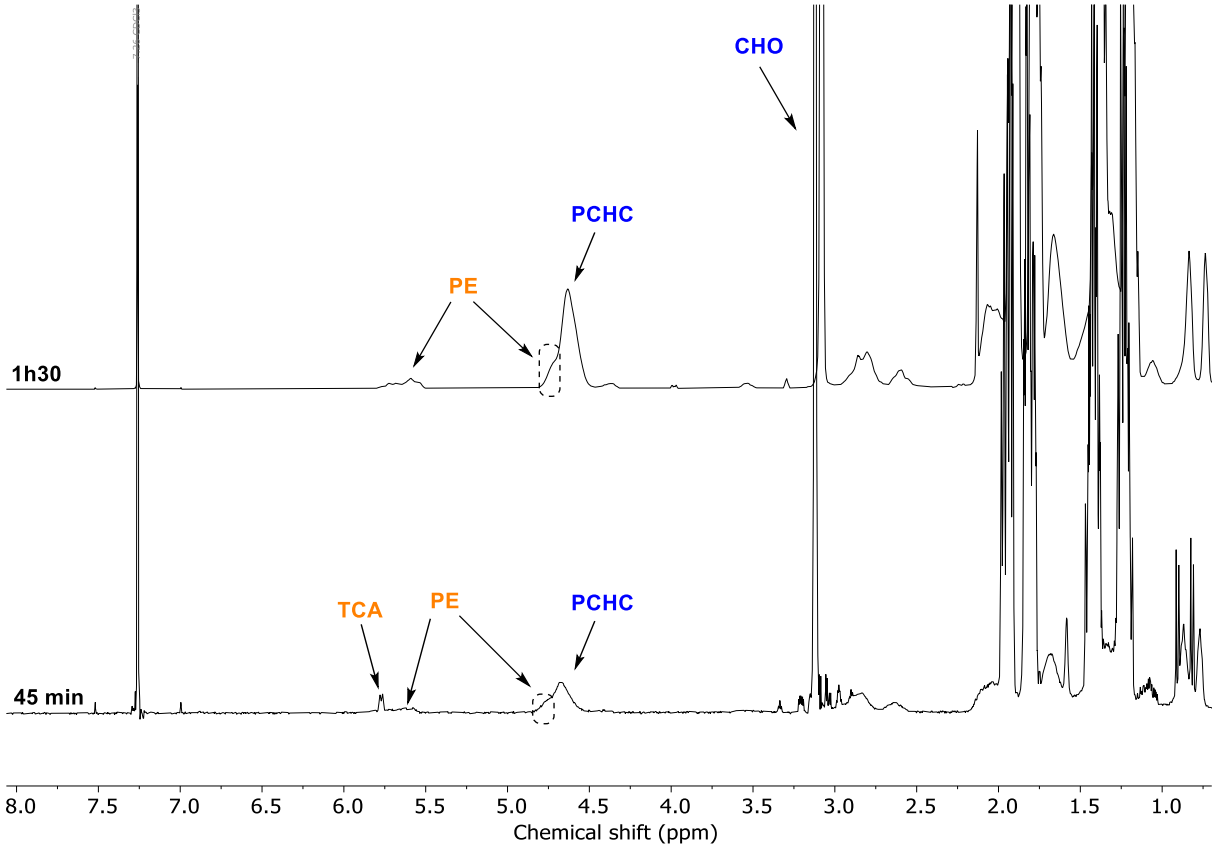

Figure 2.8: ^{1}H NMR spectra ($CDCl_3$, 400 MHz) of aliquots showing simultaneous formation of PCHC and PE using catalyst **8**.

Table 2.3: Catalyst selectivity data for polymerisation of a mixture of PA, CHO, and CO_2 at 1 bar pressure using **1**, **5**, **8**, and **9**.[a]

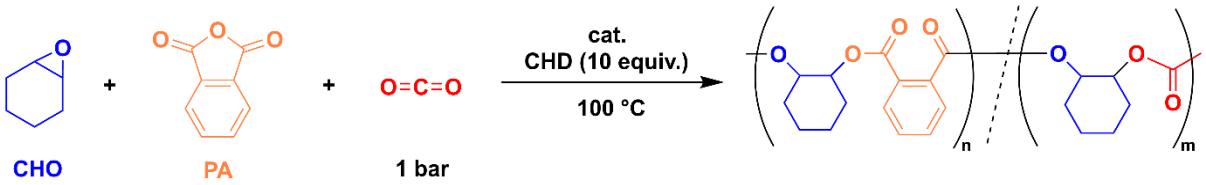

Entry	Catalyst	Time (h)	TON[b]		TOF (h^{-1})[c]		Composition (%)		M_n [$Đ$] (kg mol^{-1})[d]
			PA	CHO	PE'	PCHC	PE'	PCHC	
1	**ZnZn, 9**	5.7	70	70	13	0	100	0	1.3 [1.19]
2	**MgMg, 1**	1.0	62	180	62	118	34	64	2.3 [1.14]
3	**MgZn. 8**	0.5	52	52	104	0	100	0	3.2 [1.11]
4	**MgCo, 5**	1.0	95	530	95	435	18	82	5.3 [1.09]
5[e]	**MgCo, 5**	0.6	30	1440	50	2350	2	98	5.4 [1.25]

[a] Polymerisation conditions: [cat.]:[CHD]:[PA]:[CHO] = 1:10:100:2000, 100 °C, 1 bar CO_2. [b] Turnover number (TON), number of moles of PA or CHO consumed / number of moles of catalyst. Moles consumed determined from the ^{1}H NMR spectrum by comparing normalized integrals for polycarbonate (4.6 ppm), CHO (3.12 ppm), PA (7.90 ppm), and PE' (7.50 and 5.14 ppm) resonances. [d] Turnover frequency (TOF), TON / time (h). [c] Determined by GPC, in THF, calibrated with narrow molar mass polystyrene standards (Figures S2.32–S2.36). [e] [cat.]:[CHD]:[PA]:[CHO] = 1:10:100:6000 20 bar CO_2.

To better understand the differences in the catalyst selectivities, the sterically hindered anhydride was replaced with a bicyclic, planar anhydride, phthalic anhydride (PA), which is also commercial and used at scale in polymer production.[22] Applying the same reaction conditions, catalyst **8** and **9** resulted in the formation of poly(PA-*alt*-CHO) (denoted as PE') (Table 2.3, Entry 1 and 3, Figures S2.19–S2.21). However, with catalysts **1** and **5**, random copolymers of ~1:4 ester:carbonate ratio were formed; this implies that CO_2 and PA insertion is competitive, although CO_2 is still favoured (Table 2.3, Entry 2 and 4). For this random copolymer, characteristic peaks of PCHC (4.61 ppm), PE' (5.13 ppm), and junction units (4.98 and 4.47 ppm) were observed in the ^{1}H NMR spectrum, which were used to determine the polymer composition (Figure 2.9 and Figure S2.23).

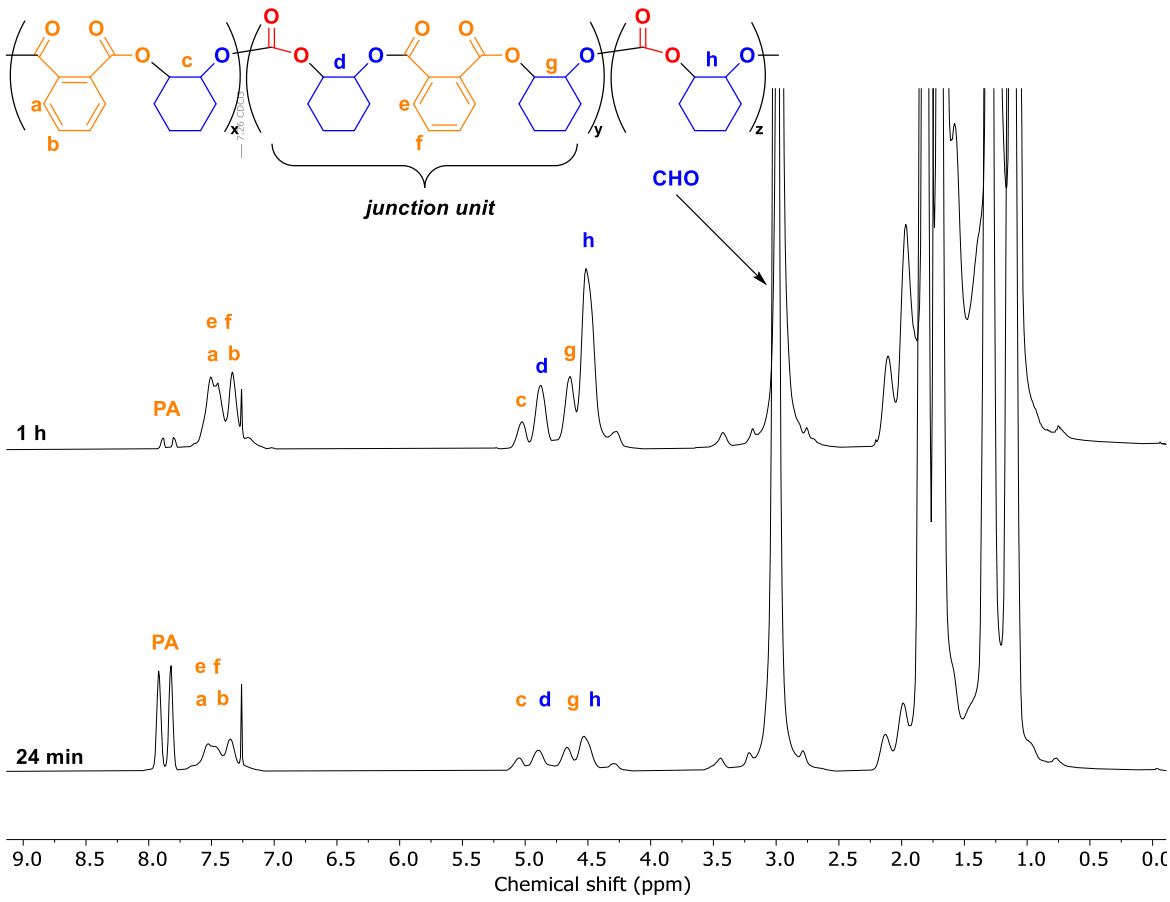

Figure 2.9: ^{1}H NMR spectra ($CDCl_3$, 400 MHz) of aliquots showing simultaneous formation of PCHC and PE' using catalyst **5**.

In situ IR spectroscopy also showed the simultaneous consumption of PA (1779 cm^{-1}) and formation of polycarbonate (1230 cm^{-1}) (Figure S2.22). ^{1}H DOSY analysis of the purified polymers displays a single diffusion coefficient, indicative of a random copolymer (Figure S2.24). Additional distinctive carbonyl resonances at 154 ppm in the $^{13}C\{^{1}H\}$ NMR spectrum agrees with the formation with random copolymer formation (Figure S2.25). Catalyst **5** shows a significant but slower rate for PA insertion compared to CO_2 at 1 bar pressure. It was envisaged that by increasing the CO_2 pressure, the insertion ratio may shift further towards CO_2. The reaction was run in a reactor at 20 bar pressure of CO_2 at 100 ˚C ([**5**]:[PA]:[CHO] = 1:100:6000) and was monitored by *in situ* IR spectroscopy (Table 2.3, Entry 5 and Figure S2.26). The polymerisation resulted in nearly quantitative formation of PCHC, with only 2 % of polyester linkages present in the polymer backbone, as determined

by analysis of the ^{1}H NMR spectrum of an aliquot (Figure S2.27). After 35 minutes, the pressure of the reactor was released to < 1 bar of CO_2, triggering the consumption PA into a random copolymer of CO_2, PA, and CHO, as confirmed by ^{1}H NMR spectroscopy. Residual carbon dioxide still dissolved in the reaction mixture competes with anhydride insertion, which is why a random copolymer is still obtained.[23] With an improved experimental set up, where CO_2 can be removed more effectively from the reaction mixture, there is a higher chance of obtaining a perfect poly(PE'-*b*-PCHC-*b*-PE') block copolymer using catalyst **5**.

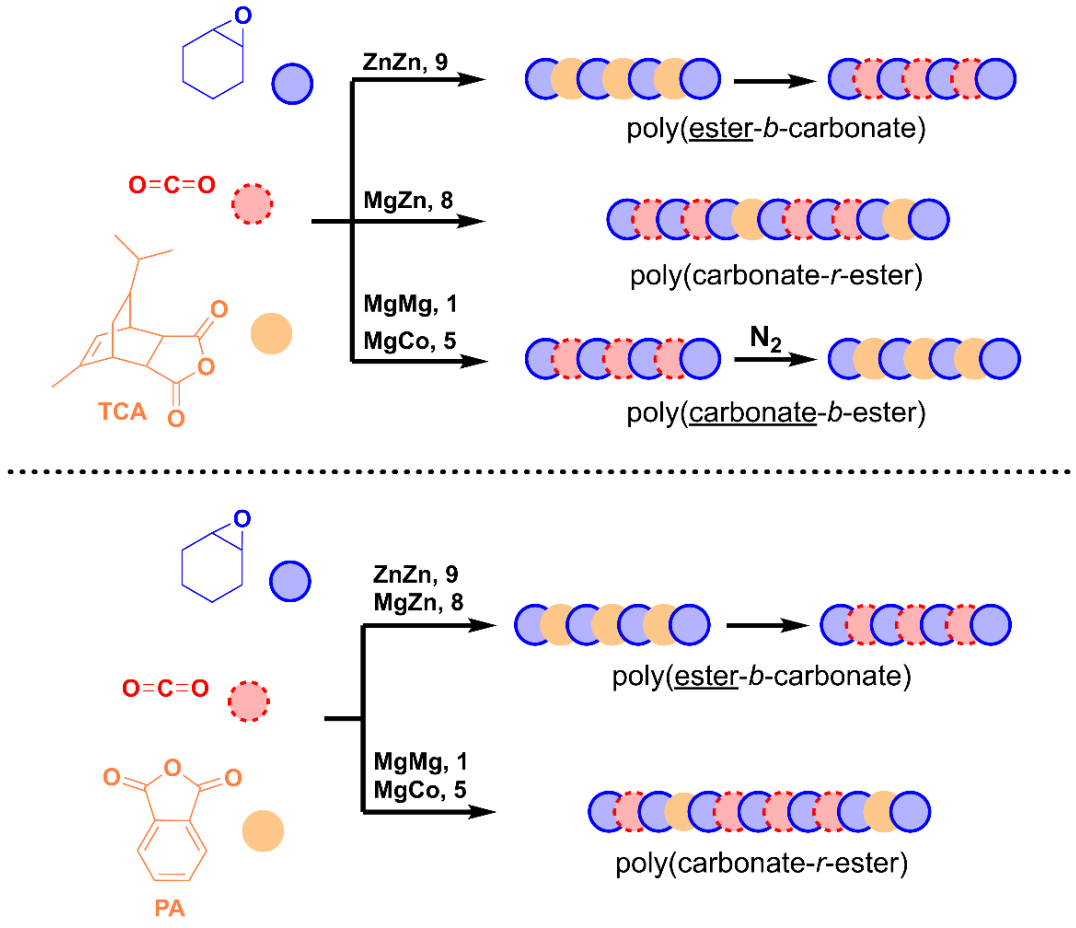

Figure 2.10: Summary of the selectivity of catalysts **1**, **5**, **8**, and **9** when exposed to a mixture of CHO, TCA or PA, and 1 bar of CO_2.

A pictorial summary of the possible different block architectures with the catalyst and monomer combinations described in this section are outlined in Figure 2.10. This assumes

that for systems in which anhydride/epoxide ROCOP is favoured, after full consumption of the anhydride under CO_2, polycarbonate formation would follow, and for those where CO_2/anhydride ROCOP is favoured, anhydride/epoxide enchainment commences once CO_2 is removed and replaced by a N_2 atmosphere.

2.4.1 Mechanism and Discussion

From this study, it can be concluded that CO_2 insertion rates into a chain end are metal dependent, and follow the order Mg(II)Co(II) > Mg(II)Mg(II) > Mg(II)Zn(II) > Zn(II)Zn(II). In particular, Mg(II) appears to play an important role in this phenomenon, as catalysts featuring Mg(II) favour CO_2 insertion. The polymerisation cycles share a common alkoxide intermediate, and in both cases the epoxide insertion is rate limiting (Figure 2.10). The insertion of the anhydride and CO_2 is the product determining step which is pre-rate limiting.[21] As mentioned previously, experimental evidence suggests that for complex **5**, in CO_2/epoxide catalysis, the metals have differentiated roles; Mg(II) activates the epoxide and Co(II) coordinates the carbonate.[2] The rate determining step involves CHO insertion into the Co-carbonate bond; its high rate compared to other metal combinations is owed to its enhanced nucleophilicity. The pre-rate determining step involves CO_2 inserting into the Mg-alkoxide bond. Since this step determines selectivity, it may explain why the Mg(II) centre in the catalyst plays a significant role here. It is difficult to measure these insertion rates, as they are pre-limiting in catalysis (k_2 and k_3 in Figure 2.11), although they can be qualitatively inferred from the monomer selectivity in the polymerisations.

The choice in anhydride also evidently skews k_3; for the sterically hindered TCA, k_3 is significantly reduced compared to PA, and hence the selectivity towards polycarbonate is favoured. For complex **9,** CO_2 insertion into the Zn-alkoxide bond is slower relative to

anhydride insertion ($k_3 > k_2$). This is also the case for most catalysts in the field that have reported this related terpolymerisation.[24-30]

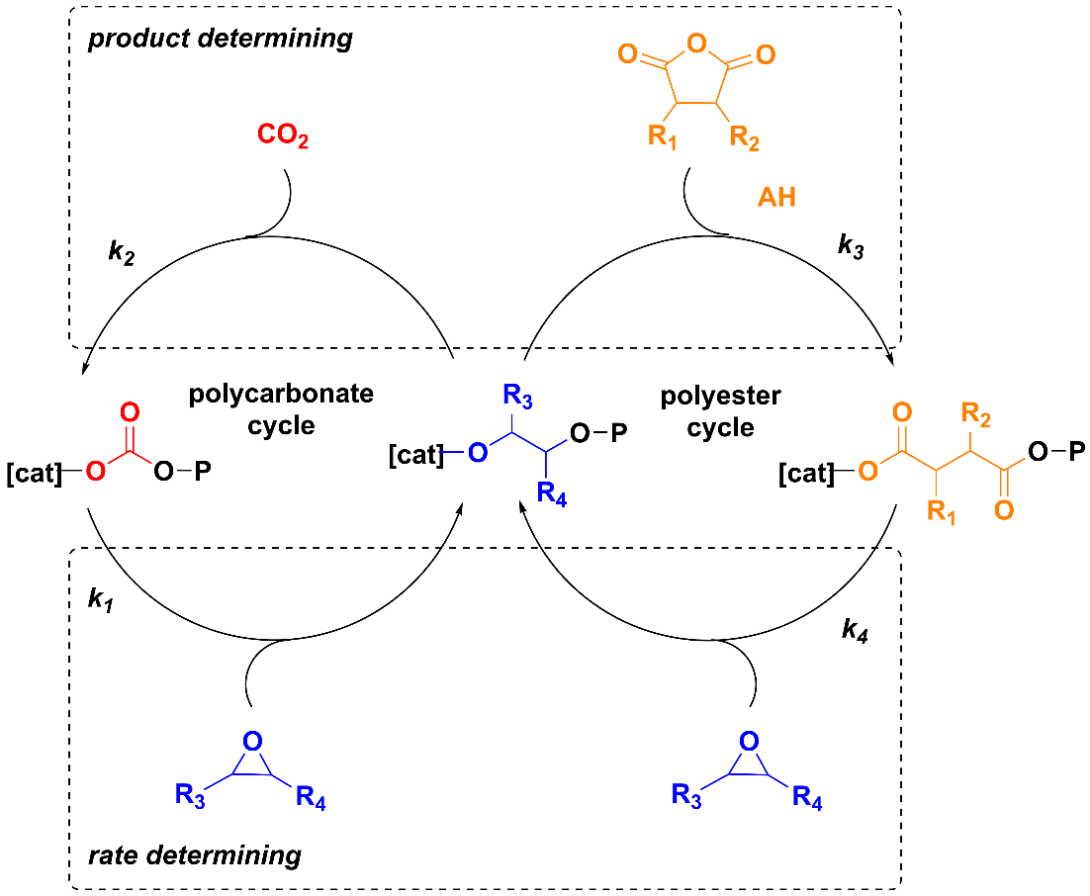

Figure 2.11: Scheme for the catalytic cycles of the ROCOP of epoxide/CO_2 and epoxide/anhydride, linked by a common metal alkoxide intermediate.

There are few other examples of competitive CO_2 insertions for this terpolymerisation. Recently, Feng and co-workers reported specific conditions at which random copolymers from mixtures of PA/CHO/CO_2 are formed with a triethylborane (TEB) and PPNCl catalyst combination.[31] These reactions were run at 10 bar of CO_2, which only reached the randomised enchainment when ratios of PPNCl:TEB:PA:CHO were in the range 1:3:50–80:200, *i.e.* at very high loading of catalyst relative to PA. Attempts at reducing the loading led to catalyst deactivation. Furthermore, this result was clearly quite fine-tuned since Li and co-workers reported the same terpolymerisation at 1 bar of CO_2 ($TOF_{CHO/PA}$ = 100 h^{-1},

[PPNCl]:[TEB]:[PA]:[CHO], 1:0.5:50:500), which formed the expected poly(ester-*b*-carbonate).[30] The organocatalyst system has rather low activity ($TOF_{CHO/PA}$ = 5 h^{-1}, $TOF_{CHO/CO2}$= 3.5 h^{-1}, [PPNCl]:[TEB]:[PA]:[CHO] = 1:3:80:200, 16 h, 10 bar of CO_2, 80 ˚C), especially in comparison to **5** ($TOF_{CHO/PA}$ = 95 h^{-1}, $TOF_{CHO/CO2}$ = 640 h^{-1}, [**5**]:[CHD]:[AH]:[CHO] = 1:10:100:2000, 100 ˚C, 1 bar CO_2). Coates and co-workers found that at CO_2 pressure over 27 bar, CO_2 was incorporated randomly into the DGA/CHO polyester, using [Zn(II)BDI] as catalyst.[21] Several heterogeneous catalysts have also reported uncontrolled random, tapered, and gradient terpolymerisation of anhydride, epoxide, and CO_2 at pressures above 35 bar.[32-34] For example, the terpolymerisation of PO, PA, and CO_2 using the zinc glutarate (ZnGA) catalyst ([PA]:[PO] = 1:8, 50 bar CO_2, 75 ˚C) resulted in a random copolymer, although it displayed a greater propensity for CO_2 insertion.[33] To date, complexes **1** and **5** are the only reported catalysts that can form a perfect poly(carbonate-*b*-ester) block copolymer, from the one-pot mixture of epoxide, anhydride, and CO_2, at any given CO_2 pressure. This result has implications in controlling block structure in complicated architectures, as the polycarbonate block formation can be exogenously triggered by a CO_2 atmosphere. This will be further explored in Chapter 3. As summarised in Figure 2.10, the desired block architecture can be tailored with the choice in catalyst and monomers.

2.5 Summary and Outlook

2.5.1 Summary

In this chapter, a series of Mg(II)M(II) (M = Mg, Cr, Mn, Fe, Co, Ni, Cu, Zn) dinuclear complexes were tested for the copolymerisation of NA and CHO. It was found that the Mg(II)Co(II) combination gave the highest activity, with neighbouring mid-transition metals also performing well compared to the homodinuclear Mg(II)Mg(II) complex. The

Mg(II)Fe(II) complex performed poorly, which was contrary to the result obtained for CO_2/CHO ROCOP in a previous study, in which it exhibited a TOF similar to Mg(II)Co(II). This was tentatively attributed to its sensitivity towards diacid impurities present in the anhydride. No clear trend between transition metal properties and activity for ROCOP could be drawn. Nevertheless, catalysts with competitive rates compared to literature examples were identified.

The second part of the chapter explored the effect of choice in metal combination on the selectivity in ROCOP catalysis from a mixture of CO_2, CHO, and anhydride. It was found that, depending on the homo- and heterodinuclear metal combinations applied (Mg(II)Mg(II), Zn(II)Zn(II), Mg(II)Zn(II) and Mg(II)Co(II)), the monomer enchainment order varied to give different block structures. Using a bio-derived tricyclic anhydride, TCA, Zn(II)Zn(II) yielded poly(ester-*b*-carbonate), Mg(II)Mg(II) or Mg(II)Co(II) catalysts delivered poly(carbonate-*b*-ester) and Mg(II)Zn(II) a random copolymer. This phenomenon is rationalised by competing CO_2 and anhydride insertion into the common alkoxide intermediate, where the order in rate of CO_2 insertion follows Mg(II)Co(II) > Mg(II)Mg(II) > Mg(II)Zn(II) > Zn(II)Zn(II). The result obtained for Mg(II)Co(II) is of particular interest, as it is a highly active and selective catalyst for polycarbonate formation, making it a suitable candidate for making block copolymers efficiently in one-pot. To date, only the Mg(II)Mg(II) and Mg(II)Co(II) display such selectivity for ROCOP, where it is usually found that anhydride/epoxide enchainment is favoured and occurs selectively.

2.5.2 Outlook

The work described in this chapter presents several avenues for further research, with an eye towards further elucidation of the catalytic mechanism. Whilst the work presented here

demonstrates a marked dependence on catalytic rates and selectivity with M(II) selection, further areas for investigation that may shed light on this phenomenon are:

- Mg(II)M(II) catalyst activity:
    - To confirm the low activity of Mg(II)Fe(II) for the ROCOP of NA and CHO, the complex could be exposed to anhydrides that are more rigorously purified in excess, to detect any decomposition. Furthermore, the one-pot reaction of anhydride/CO_2/epoxide can confirm whether the rate of CO_2/epoxide is significantly compromised in the presence of anhydride.
    - Cr(III) salen catalyst systems are well known to be highly active for both CO_2/epoxide and anhydride/epoxide ROCOP.[8, 35] It would be worth attempting the synthesis of a Mg(II)Cr(III) to assess whether the activity of the Cr(III) centre is enhanced by the neighbouring Mg(II) centre.
- M(II)M(II) catalyst terpolymerisation selectivity:
    - More metal combinations already studied for ROCOP could be tested to better establish the selectivity trends between metals.
    - Model CO_2 and anhydride insertion reactions could be performed to measure the insertion rates directly. For UV-vis active complexes, stopped-flow UV-vis data can be used to determine insertion kinetics.[36]

2.6 References

1. Garden, J. A.; Saini, P. K.; Williams, C. K., *J. Am. Chem. Soc.* **2015,** *137* (48), 15078-15081.

2. Deacy, A. C.; Kilpatrick, A. F. R.; Regoutz, A.; Williams, C. K., *Nat. Chem.* **2020,** *12* (4), 372-380.

3. Trott, G.; Garden, J. A.; Williams, C. K., *Chem. Sci.* **2019,** *10* (17), 4618-4627.

4. Reis, N. V. Homogeneous catalysts for the ROCOP of CO2 and epoxides. University of Oxford, 2020.

5. Reis, N. V.; Deacy, A. C.; Rosetto, G.; Durr, C. B.; Williams, C. K., *Chem. Eur. J.* **2022,** *28*, e202104198.

6. Hosseini Nejad, E.; van Melis, C. G. W.; Vermeer, T. J.; Koning, C. E.; Duchateau, R., *Macromolecules* **2012,** *45* (4), 1770-1776.

7. Darensbourg, D. J., *Chem. Rev.* **2007,** *107* (6), 2388-2410.

8. Paul, S.; Zhu, Y.; Romain, C.; Brooks, R.; Saini, P. K.; Williams, C. K., *Chem. Commun.* **2015,** *51* (30), 6459-6479.

9. Chen, T. T. D.; Zhu, Y.; Williams, C. K., *Macromolecules* **2018,** *51* (14), 5346-5351.

10. Saini, P. K.; Fiorani, G.; Mathers, R. T.; Williams, C. K., *Chem. Eur. J.* **2017,** *23* (18), 4260-4265.

11. Romain, C.; Zhu, Y.; Dingwall, P.; Paul, S.; Rzepa, H. S.; Buchard, A.; Williams, C. K., *J. Am. Chem. Soc.* **2016,** *138* (12), 4120-4131.

12. Fieser, M. E.; Sanford, M. J.; Mitchell, L. A.; Dunbar, C. R.; Mandal, M.; Van Zee, N. J.; Urness, D. M.; Cramer, C. J.; Coates, G. W.; Tolman, W. B., *J. Am. Chem. Soc.* **2017,** *139* (42), 15222-15231.

13. Baumgartner, R.; Song, Z.; Zhang, Y.; Cheng, J., *Polym. Chem*, **2015,** *6* (19), 3586-3590.

14. Dakshinamoorthy, D.; Weinstock, A. K.; Damodaran, K.; Iwig, D. F.; Mathers, R. T., *ChemSusChem* **2014,** *7* (10), 2923-2929.

15. Han, B.; Zhang, L.; Yang, M.; Liu, B.; Dong, X.; Theato, P., *Macromolecules* **2016,** *49* (17), 6232-6239.

16. Abel, B. A.; Lidston, C. A. L.; Coates, G. W., *J. Am. Chem. Soc.* **2019,** *141* (32), 12760-12769.

17. Diment, W. T.; Gregory, G. L.; Kerr, R. W. F.; Phanopoulos, A.; Buchard, A.; Williams, C. K., *ACS Catal.* **2021,** *11* (20), 12532-12542.

18. Saini, P. K.; Romain, C.; Zhu, Y.; Williams, C. K., *Polym. Chem*, **2014,** *5* (20), 6068-6075.

19. Moltved, K. A.; Kepp, K. P., *The Journal of Physical Chemistry C* **2019,** *123* (30), 18432-18444.

20. Asaba, H.; Iwasaki, T.; Hatazawa, M.; Deng, J.; Nagae, H.; Mashima, K.; Nozaki, K., *Inorg. Chem.* **2020,** *59* (12), 7928-7933.

21. Jeske, R. C.; Rowley, J. M.; Coates, G. W., *Angew. Chem. Int. Ed.* **2008,** *47* (32), 6041-6044.

22. Merchant Research and Consulting Ltd. https://mcgroup.co.uk/researches/phthalic-anhydride-pa (accessed 2022).

23. Raman, S. K.; Raja, R.; Arnold, P. L.; Davidson, M. G.; Williams, C. K., *Chem. Commun.* **2019,** *55* (51), 7315-7318.

24. Darensbourg, D. J.; Poland, R. R.; Escobedo, C., *Macromolecules* **2012,** *45* (5), 2242-2248.

25. Longo, J. M.; Sanford, M. J.; Coates, G. W., *Chem. Rev.* **2016,** *116* (24), 15167-15197.

26. Ye, S.; Wang, W.; Liang, J.; Wang, S.; Xiao, M.; Meng, Y., *ACS Sustain. Chem. Eng.* **2020,** *8* (48), 17860-17867.

27. Chang, C.-H.; Tsai, C.-Y.; Lin, W.-J.; Su, Y.-C.; Chuang, H.-J.; Liu, W.-L.; Chen, C.-T.; Chen, C.-K.; Ko, B.-T., *Polymer* **2018,** *141*, 1-11.

28. Pappuru, S.; Chakraborty, D., *Eur. Polym. J.* **2019,** *121*, 109276.

29. Huijser, S.; HosseiniNejad, E.; Sablong, R.; de Jong, C.; Koning, C. E.; Duchateau, R., *Macromolecules* **2011,** *44* (5), 1132-1139.

30. Zhang, J.; Wang, L.; Liu, S.; Kang, X.; Li, Z., *Macromolecules* **2021,** *54* (2), 763-772.

31. Chidara, V. K.; Boopathi, S. K.; Hadjichristidis, N.; Gnanou, Y.; Feng, X., *Macromolecules* **2021,** *54* (6), 2711-2719.

32. Liu, Y.; Deng, K.; Wang, S.; Xiao, M.; Han, D.; Meng, Y., *Polym. Chem,* **2015,** *6* (11), 2076-2083.

33. Liu, Y.; Xiao, M.; Wang, S.; Xia, L.; Hang, D.; Cui, G.; Meng, Y., *RSC Adv.* **2014,** *4* (19), 9503-9508.

34. Liu, Y.; Huang, K.; Peng, D.; Wu, H., *Polymer* **2006,** *47* (26), 8453-8461.

35. Darensbourg, D. J.; Mackiewicz, R. M.; Phelps, A. L.; Billodeaux, D. R., *Acc. Chem. Res.* **2004,** *37* (11), 836-844.

36. Heimann, J. E.; Bernskoetter, W. H.; Hazari, N., *J. Am. Chem. Soc.* **2019,** *141* (26), 10520-10529.

Chapter 3

Multi-block Copolymers Derived from CO_2

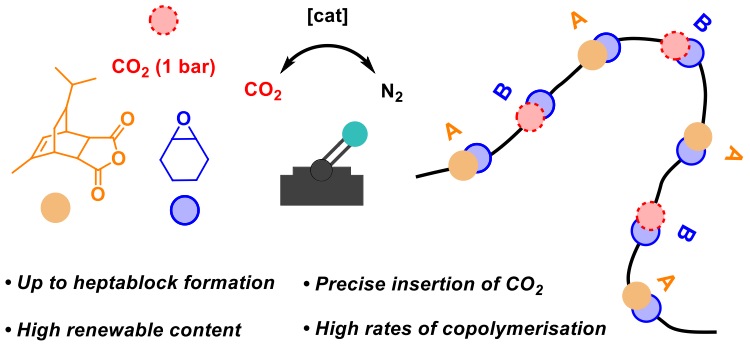

Work described in this chapter appears in:

Mg(II) heterodinuclear catalysts delivering carbon dioxide derived multi-block polymers

G. Rosetto, A. C. Deacy, C. K. Williams, *Chem. Sci.*, **2021**, *12*, 12315–12325

3.1 Introduction

Most prior research on oxygenated di-block and multi-block polymers is focussed around polyester and polyethers, with very few examples including CO_2 in the monomer mixture.[1-6] Most likely this is a result of a limited range of carbon dioxide/epoxide ROCOP catalysts and technical complexities in controlling the gas atmosphere since many catalysts require high pressures and use of stainless-steel reactors. Thus, there is a lack of examples of multi-block polymers derived from CO_2, in particular where carbon dioxide copolymerisation can be switched multiple times to build up multi-block structures.[7] Only one prior report from our group presents a BCACB pentablock structure combining blocks derived by lactone ROP (C), epoxide/anhydride (A) and epoxide/carbon dioxide (B) ROCOP using an organometallic di-Zn(II) catalyst.[8]

By using catalysts that are active and highly selective for CO_2 insertion at 1 bar pressure, it is envisaged that multi-block polycarbonate-based copolymers can be prepared in one pot by introducing CO_2 at various stages throughout the polymerisation. In 2017, Saini *et al.* showed that a Mg(II)Mg(II) complex (**1**) has a higher selectivity for polycarbonate formation over polyester when a sterically hindered anhydride is used for the polyester segment. This makes it a suitable candidate for yielding such multi-block polymers, although the turn-over frequency (TOF) is limited to < 100 h^{-1} at 1 bar of CO_2.

3.2 Aims

The aim of this chapter is to employ the Mg(II)Co(II) complex (**5**), which was identified as a highly active and selective catalyst for CO_2/epoxide ROCOP in Chapter 2, for the synthesis of multi-block copolymers of polycarbonate and polyester.

From a mixture of epoxide and anhydride, by cycling between CO_2 and N_2 gas atmospheres, catalyst **5** will switch between two different polymerisation cycles to yield multi-block

copolymers. Altering the number of gas switches over the course of the reaction allows for targeting of multi-block structures. This will determine the block sequence length; one, two, and three switches will yield tri-, penta-, and heptablock copolymers when a bifunctional CTA is employed (1,2-cyclohexane diol (CHD), will be used in this work). The selectivity throughout the polymerisation steps will be analysed by *in situ* IR spectroscopy and CO_2 mass flow measurement, as well as ^{1}H NMR spectroscopy. The exclusive formation of block copolymers will be proven by GPC and DOSY NMR. The concept will be expanded to include a third polymerisation cycle, ROP of lactones. In all cases, monomers that are potentially bio-derived will be used, namely CHO, TCA, CO_2, ε-caprolactone (CL), and ε-decalactone (DL). [9-13]

3.3 Triple-manifold Steel Schlenk Line

For this investigation, a triple-manifold stainless steel Schlenk line was constructed allowing for reactions to be subjected to nitrogen, carbon dioxide, and vacuum atmospheres (Figure 3.1). The set-up includes a pressure controller and mass flow meter, so the CO_2 flow can be monitored. The Swagelok fixed steel tubing was chosen as it ensures air tightness and a water-free system, which should aid in introducing less protic impurities in the polymerisation reactions. To confirm this, a test polymerisation of CO_2/CHO was run under equivalent conditions using a glass set-up and compared to the steel one, at a loading of 2000 equiv. of CHO with respect to catalyst **5**, at 100 ˚C for 2.5 h. The CO_2 mass flow was measured on the steel line and *in situ* IR spectroscopy on the glass line, to monitor polycarbonate formation (Figure 3.2b). For both polymerisations, after 1 h, the reaction rate began to plateau due to diffusion limitations. After 2.5 h, the mixtures were analysed by ^{1}H NMR spectroscopy and GPC. Both reactions reached 27 % conversion of the epoxide, although by GPC the molar mass was significantly higher for the reaction run on the steel

line (Figure 3.2a). The bimodality is inherent, arising from initiation from the catalyst's acetate groups (low mass fraction) and protic impurities present in the monomers which can be bifunctional (high mass fraction). The more initiators and chain transfer agents in the polymerisation, the lower the molar mass. Hence, there appear to be fewer impurities for the reaction in the steel line. Furthermore, the polymerisation conducted on the glass line produced a dark yellow coloured mixture, whereas on the steel line it was significantly paler, which could suggest that fewer impurities are present.

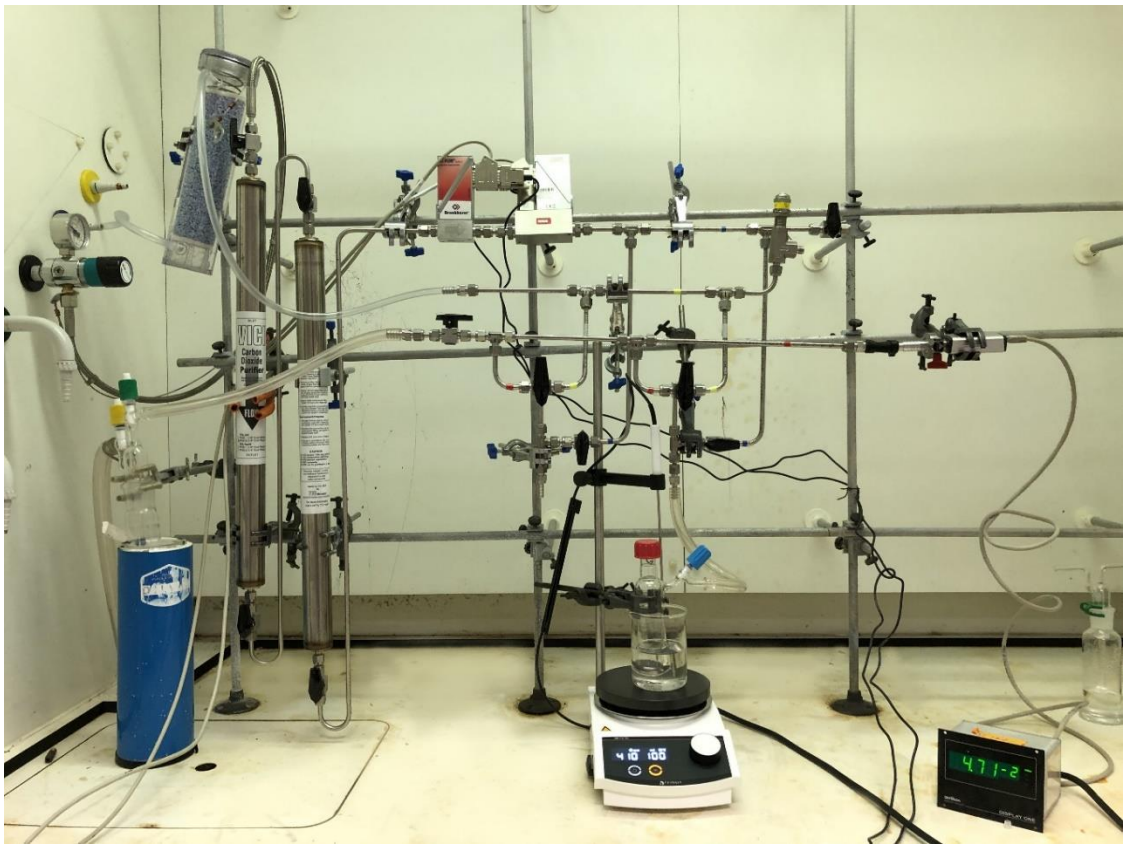

Figure 3.1: Photograph of the triple-manifold steel Schlenk line built for the work presented in this chapter.

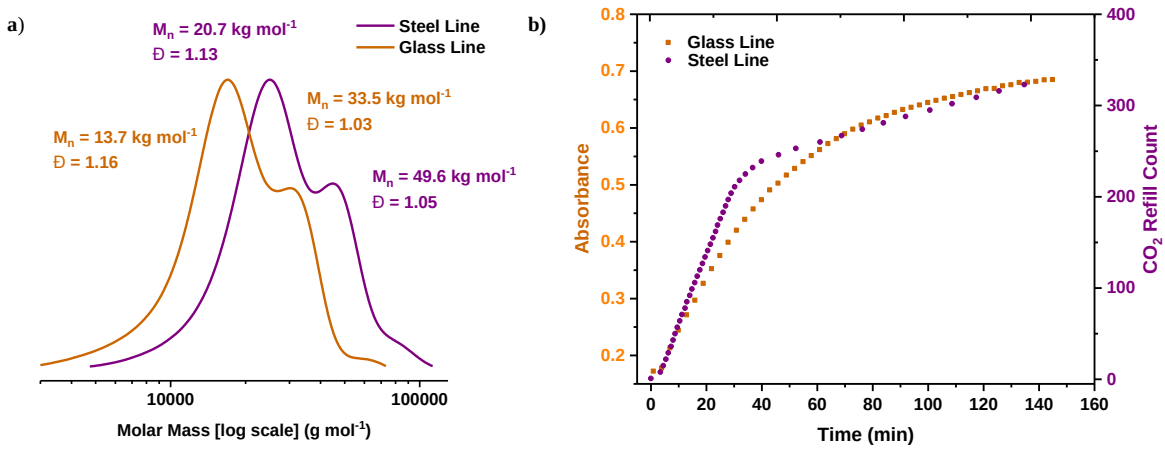

Figure 3.2: a) GPC analysis of the polycarbonate synthesised using the steel line (purple) and glass line (orange). b) Absorbance *vs.* time graph of polycarbonate formation measured by *in situ* IR spectroscopy at 1233 cm^{-1} obtained on the glass Schlenk line (orange) and CO_2 refill count *vs.* time measured by the mass flow meter on the steel Schlenk line (purple).

3.4 Synthesis of Multi-block Poly(carbonate-*b*-ester)s

Using the stainless steel apparatus, mixtures of catalyst **5**, TCA, CHO, and toluene were combined and exposed to CO_2 at 1 bar pressure; toluene was used to balance a diffusion limited rate, caused by solution viscosity, and rate law dependence on epoxide concentration (rate is maximised with higher epoxide concentration) (Scheme 3.1). A ten-fold excess *vs.* catalyst of 1,2-cyclohexane diol (CHD) was added to exclusively form α,ω-hydroxyl-telechelic polymers. The polymerisation reactions were monitored by regular removal of aliquots prior to switching reaction gas; it was found that roughly ~6 vacuum/gas cycles were sufficient to switch gas atmospheres. The anhydride loading and gas switches timing were chosen such that each block displayed a degree of polymerisation ($\overline{DP}$) > 6. This value was previously determined to be the minimum block length for a 7-block copolymer with 99 % fidelity, given narrow dispersity molar mass distributions.[14] In all cases, polymerisations were monitored by CO_2 mass flow measurements as well as *in situ* IR, and polymer formation was confirmed by ^1H NMR spectroscopy and GPC analysis of the aliquots taken.

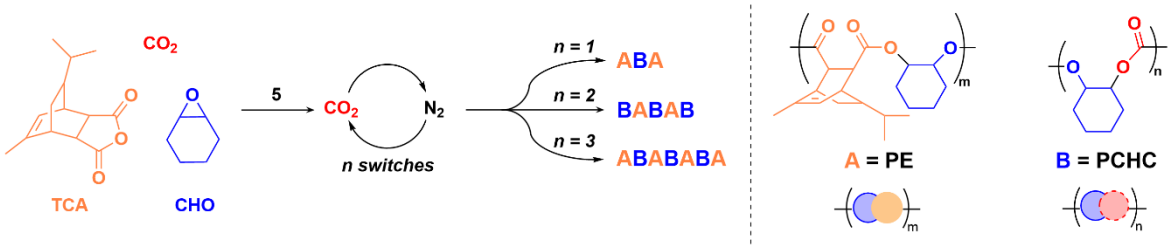

Scheme 3.1: Illustrative schematic for the synthesis of polycarbonate and polyester derived multi-block copolymers, enabled by cycling between CO_2 and N_2 gas and using complex **5** as the catalyst. The polymerisations were conducted at 100 ˚C and 1 bar of either CO_2 or N_2 in 4 M of CHO in toluene with 10 equiv. of CHD *vs.* catalyst.

Table 3.1: Data for multi-block polymer formation from TCA, CHO and 1 bar CO_2 with catalyst **5**.

Entry	Block Polymer Structure	Gas	Time (h)	TON[d]		Block Polymer Composition (%)		M_n [$Đ$] (kg mol^{-1})[e]	$\overline{DP}$[f]	T_g (˚C)[g]
				TCA	CHO	PE	PCHC			
1[a]	ABA	CO_2	1.3	0	740	0	100	6.7 [1.15]	74	121
		N_2	1.2	200	940	21	79	9.1 [1.17]	10	
2[b]	BABAB	CO_2	1.0	0	750	0	100	5.7 [1.13]	75	122
		N_2	2.3	300	1050	29	71	9.4 [1.17]	15	
		CO_2	1.7	300	1777	17	83	14.0 [1.12]	37	
3[c]	ABABABA	CO_2	1.6	0	1020	0	100	6.0 [1.14]	102	130
		N_2	2.2	360	1380	26	74	11.1 [1.11]	18	
		CO_2	1.7	360	2520	14	82	17.4 [1.09]	57	
		N_2	4.5	600	2700	20	80	19.9 [1.07]	12	

All entries run at 100 ˚C at 1 bar pressure of CO_2, 4 M CHO in toluene. [a] [**5**]:[CHD]:[TCA]:[CHO] = 1:10:200:2000. [b] [**5**]:[CHD]:[TCA]:[CHO] = 1:10:300:3000. [c] [**5**]:[CHD]:[TCA]:[CHO] = 1:10:600:6000. [d] Turnover Number (TON), number of moles of TCA or CHO consumed / number of moles of catalyst. Moles consumed determined from the ^{1}H NMR spectrum by comparing normalised integrals for PCHC (4.6 ppm), CHO (3.12 ppm), TCA (5.75 ppm) and PE (5.68 ppm) resonances. [e] Determined by GPC, in THF, calibrated with narrow molar mass polystyrene standards. [f] Determined from TON /number of growing chains (initiated by CHD only). [g] Value for multi-block polymer determined by DSC, at 20 ˚C/min heating rate, and taken from the second heating/cooling cycle.

Firstly, in order to target a triblock copolymer, the reaction was conducted with a single gas switch, starting with CO_2 for 1.3 h then switching to N_2. Based on the earlier work in Chapter 2, it was predicted that an ABA triblock copolymer would form (A = polyester, B = polycarbonate), as a result of the faster CO_2 insertion compared to anhydride. Aliquot analysis after 1.3 h under CO_2 showed the selective formation of polycarbonate (PCHC) by

^{1}H NMR spectroscopy (Figure 3.4), with a molar mass of 6.7 kg mol^{-1} (Table 3.1, entry 1, Figure 3.3b). A linear increase in the intensity of the polycarbonate stretching frequency was also observed by *in situ* IR spectroscopy (Figure 3.3a). A plot of the CO_2 re-pressurising events, indicative of CO_2 consumption, over time, also displayed a linear increase (Figure S3.1). Upon changing the gas to N_2, polycarbonate formation halted, and polyester (PE) formation commenced, as seen from the decrease in the TCA monomer's stretching frequency at 1783 cm^{-1}, which was converted to polyester formation in Figure 3.3a. An aliquot taken after 1.2 h confirmed this, as the anhydride's sharp doublet peak at 5.77 ppm turned into a broader signal (5.50–5.90 ppm), indicative of its polymerisation (Figure 3.4). The formation of an ABA-block copolymer was confirmed by an increase in molar mass to 9.1 kg mol^{-1} and from a single diffusion coefficient for all signals by ^{1}H DOSY analysis (Figure S3.2).

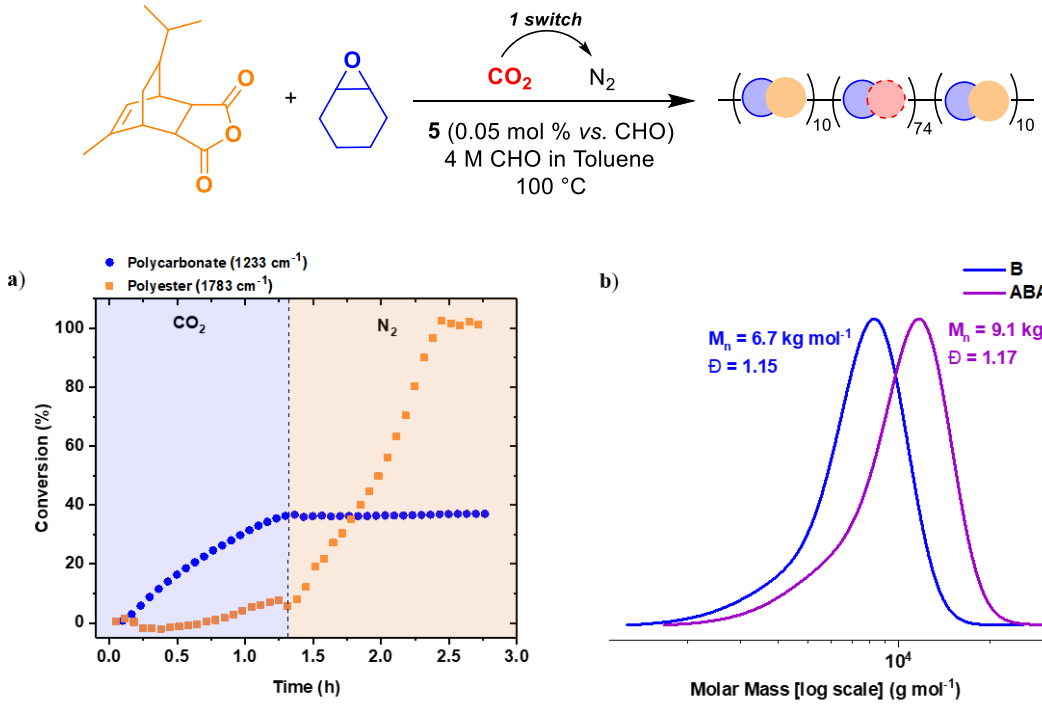

Figure 3.3: Scheme and supporting data for the selective polymerisation of CHO, TCA, and CO_2 to form an ABA triblock copolymer. Polymerisation conditions: [**5**]:[CHD]:[TCA]:[CHO] = 1:10:200:2000, 1 bar CO_2, 100 ˚C, 4 M CHO in toluene. $\overline{DP}$ of each block is denoted in the bracket subscripts. a) Conversion *vs.* time plot using data from *in situ* IR spectroscopy and calibrated using ^{1}H NMR spectroscopy (Figure 3.4), illustrating block formation under the two reaction atmospheres. b) GPC analysis of the aliquots removed at the end of each stage of the polymerisation.

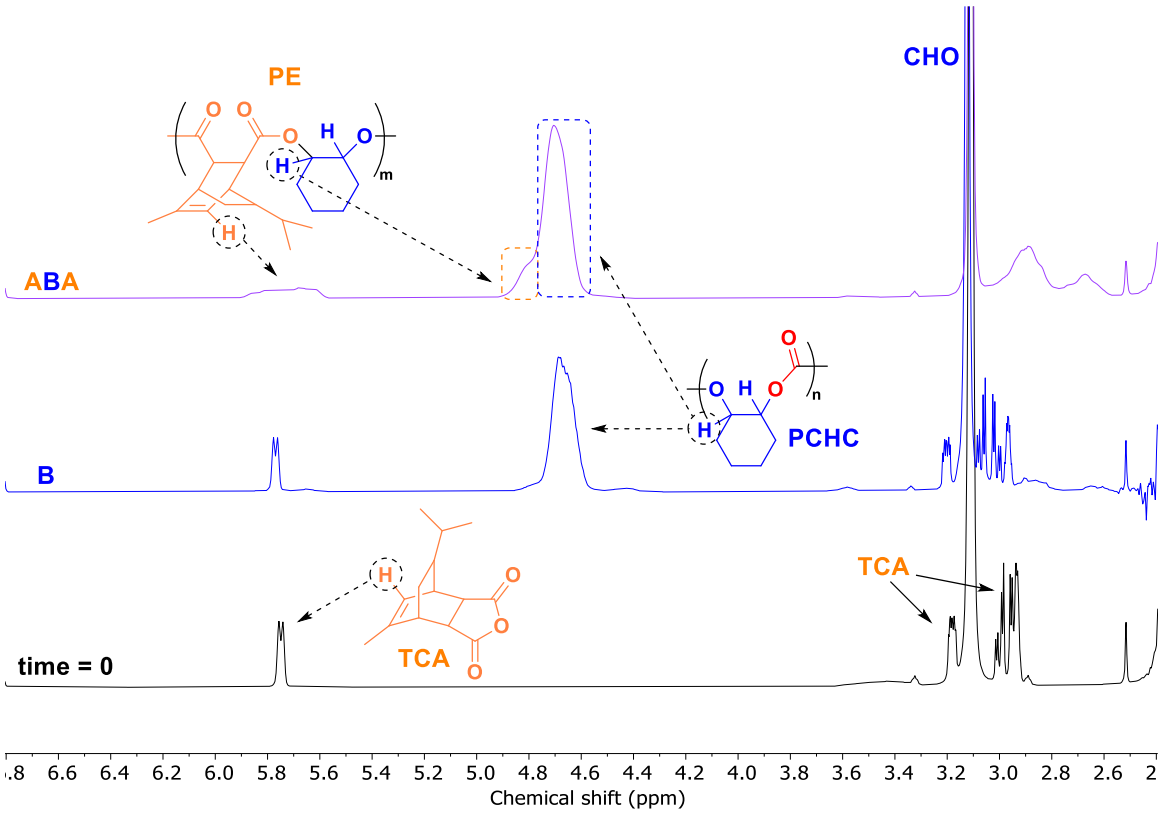

Figure 3.4: Selected region of the ^{1}H NMR spectra throughout polymerisation stages, illustrating the change in the resonances of monomers and polymer.

Next, a BABAB pentablock copolymer was targeted, by starting the reaction under a CO_2 atmosphere and performing two gas switches, first to N_2 and subsequently back to CO_2 (Table 3, entry 2). In the first stage, under CO_2, polycarbonate formation occurred, as indicated by aliquot analysis (Figure S3.3) and *in situ* IR spectroscopy (Figure 3.5a). On switching to N_2 for 2.3 h, the complete consumption of anhydride was observed by a plateau in the anhydride conversion by *in situ* IR spectroscopy. The intermediary ABA triblock polymer showed a molar mass of 9.4 kg mol^{-1} (Figure 3.5b). Lastly, the reaction atmosphere was switched back to CO_2, triggering the formation of polycarbonate to form a BABAB pentablock polymer with a molar mass of 14.0 kg mol^{-1} (Figure 3.5b).

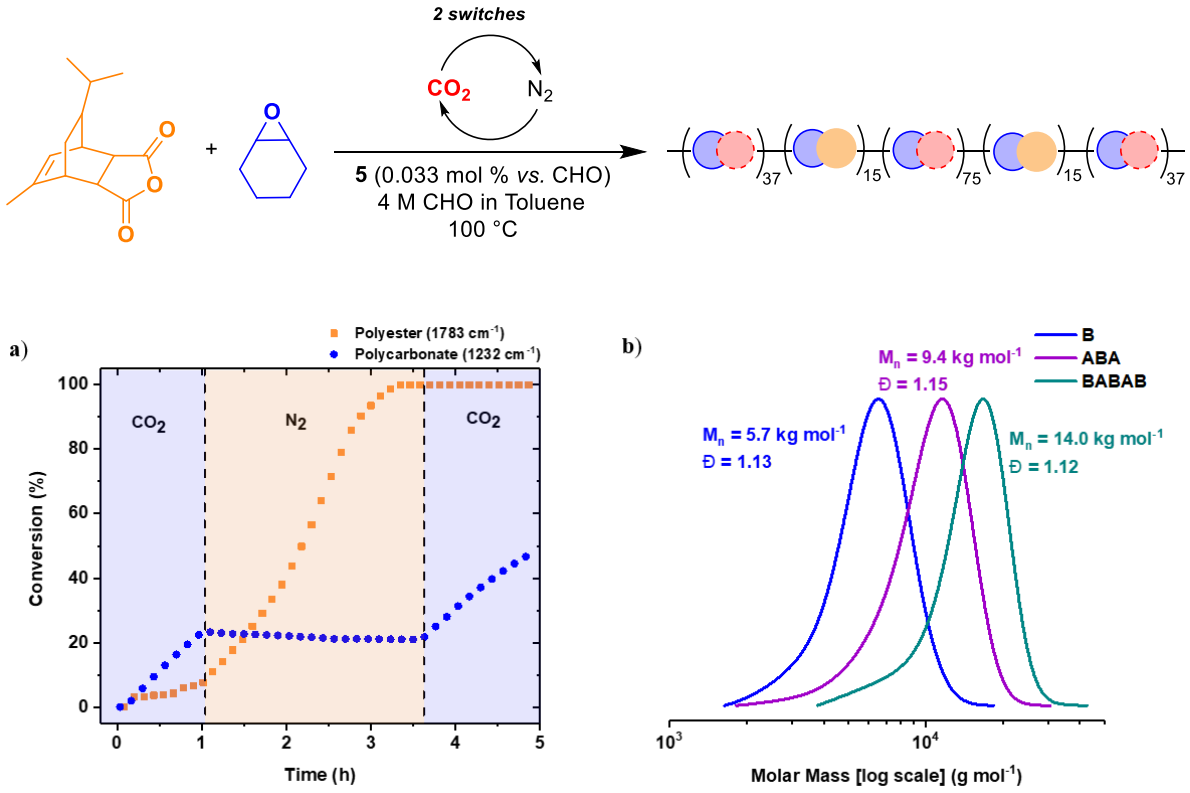

Figure 3.5: Scheme and supporting data for the selective polymerisation of CHO, TCA, and CO_2 to form an BABAB pentablock polymer. Polymerisation conditions: [**5**]:[CHD]:[TCA]:[CHO] = 1:10:300:3000. 1 bar CO_2, 100 ˚C. 4 M CHO in toluene. $\overline{DP}$ of each block is denoted in the bracket subscripts. a) Conversion *vs.* time plot using data from *in situ* IR spectroscopy and calibrated using ^{1}H NMR spectroscopy (Figure S3.3), illustrating block formation under the two reaction atmospheres. b) GPC analysis of the aliquots removed at the end of each stage of the polymerisation.

Finally, a heptablock copolymer (ABABABA) was targeted by employing a third gas switch during the course of the reaction (Table 3.1, entry 3). After the first gas exchange, the TCA was allowed to reach 60 % conversion, after 2.2 h under N_2. By replacing the gas with CO_2, polycarbonate formation resumed readily; *in situ* IR spectroscopy further confirmed the selectivity throughout the polymerisation as the gases were switched between carbon dioxide and nitrogen (Figure 3.6a and b). Block polymer formation was confirmed through ^{1}H NMR spectroscopy (Figure S3.4), and GPC analysis (Figure 3.6b), with the systematic increase in polymer molar mass and narrow distributions at each stage, reaching 19.9 kg mol^{-1} .

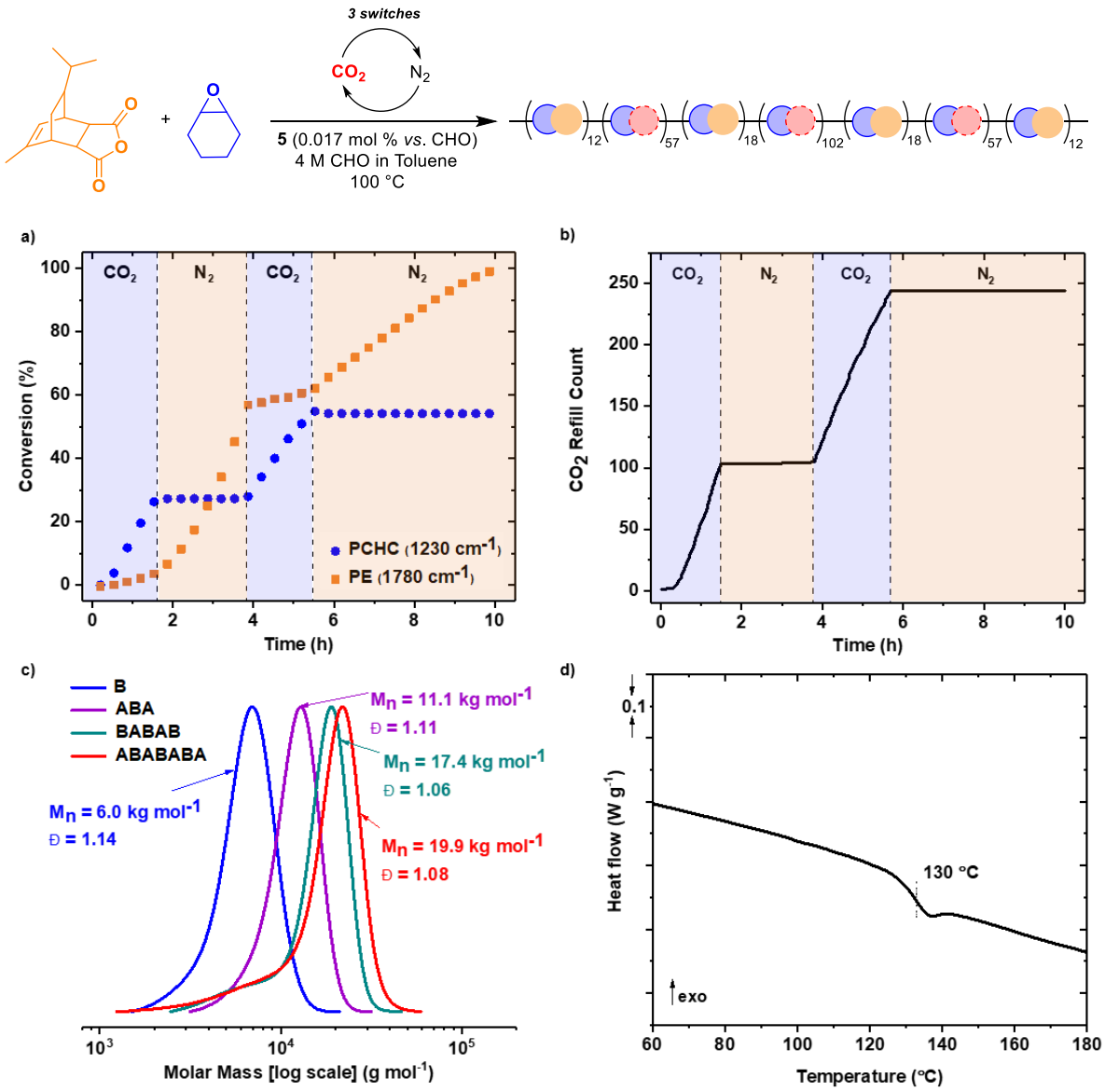

Figure 3.6: Data supporting the selective catalysis of CHO, TCA, and CO_2 to form an ABABABA heptablock polymer. Polymerisation conditions: [**5**]:[CHD]:[TCA]:[CHO] = 1:10:600:6000. 1 bar CO_2, 100 ˚C, 4 M CHO in toluene. a) *In situ* IR spectroscopy data used to plot conversion of monomer into polymer over time, calibrated using ^{1}H NMR spectroscopy (Figure S3.4), showing the selective formation of polycarbonate and polyester blocks. b) The mass-flow metre output is used to determine the frequency of CO_2 refill into the reaction vessel, directly relating to the consumption of CO_2. c) Analysis of the reaction aliquots by GPC, showing continual evolution of molar mass after each block is formed whilst maintaining a narrow dispersity. d) DSC data for the purified heptablock polymer, determined at 20 ˚C/min heating rate, and taken from the second heating/cooling cycle.

Lower molar mass tailing apparent in the GPC trace of the third stage and fourth stages may arise from minor contamination from acetate-initiated chains and/or from slower initiation from polymeric cyclohexanol end-capped chains. At lower molar mass, the separation

between acetate and cyclohexane diol-initiated chains is small and the former is "hidden" under the curve of the main distribution. At higher molar masses, the separation increases, resulting in two distinct peaks. Despite using a 10-fold excess in CHD, it may not be sufficient to fully supress the second distribution. However, if more CHD is added, which also acts as a chain transfer agent (CTA), overall lower molar masses would result. Notwithstanding, the ratio between the peaks is 1:8, and hence the shouldering peak is not significant.

The three new multi-block polymers were also analysed by DSC, each of them displaying a single glass transition temperature (T_g), indicative of amorphous polymers with miscible block components (Figure 3.6d, Figure S3.5 and S3.6). The T_g values increase with the number of blocks, although this may correspond with increase in molecular weight (Table 3.1). The T_g values are above 100 ˚C, and are consistent with previously reported values for PCHC (115 ˚C)[15] and PE (118–126 ˚C).[1, 16-17] Such polymers with high glass transition temperatures are useful compared to aliphatic polyesters obtained from ROP of lactones; their moderate/low T_g can result in softening in the temperature range of use.[18]

These results demonstrate a novel route for the selective polymerisation of epoxide, anhydride, and CO_2 to synthesise multi-block copolymers using a single catalyst. To date, only the Mg(II)-containing catalysts **1** and **5** display the unique selective enchainment of epoxide and CO_2 (at 1 bar pressure) over anhydride, when using a sterically hindered anhydride (see Chapter 2). Complex **5** is the most suitable for subsequent investigations as its activity for the ROCOP of CO_2/CHO is 6-fold higher compared to **1**. Most other catalysts in the literature show the opposite selectivity, preferentially inserting anhydride over CO_2, even when using high CO_2 pressures.[19-25] To obtain the same block order with such catalysts, a sequential monomer addition procedure would be required, which is both procedurally more demanding, and may introduce impurities that could initiate new chains.

There are a few other reports that utilise CO_2 to trigger chemoselective copolymerisations, which include work by Rieger and co-workers, using β-butyrolactone (BBL), epoxide and CO_2 at 40 bar pressure, and from Chen and co-workers, using lactide, propylene oxide (PO), and CO_2 at 20 bar pressure.[26-27] In the former example, utilising a [(BDI^{CF3})Zn(N(SiMe$_3$)$_2$)] catalyst, the terpolymerisation of BBL, CHO and CO_2 can be regulated by the presence of CO_2 in the reaction mixture.[26] Applying 40 bar pressure of CO_2 to the monomer mixture affords copolymerisation of CHO and CO_2 exclusively, and upon releasing CO_2, the ROP of BBL was initiated. As also demonstrated in this work, CO_2 can act as a reversible switching agent, and hence multi-block polymers with thermoplastic elastomer properties may be synthesised.[28] In the latter example, it was found that the DBU/^{i}PrOH catalytic system became inactive for lactide ROP under CO_2.[27] This observation led to the design of a tandem catalyst system with the addition of a (salen)-Cr(III)Cl complex, which from a mixture of PO and lactide under CO_2, formed poly(propylene carbonate) (PPC) exclusively. Exchanging the CO_2 gas to argon triggered growth of polylactide from the PPC chain end to make a block copolymer, with the potential of forming multi-block copolymers if multiple gas switches are performed. Again, this is an example of using CO_2 as a reversible switch to control the polymer enchainment sequence. The main advantage in the study described herein is that autoclave use for high pressure gases is not required, and that rates and tolerance of catalysts are high across all reactions where switches are used.

3.5 Pentablock Copolymers from CO_2/Anhydride/Epoxide/Lactone

In 2016, a DFT study published by our group predicted that, when using a di-Zn(II) catalyst (complex **9**) from a mixture of four monomers (PA, carbon dioxide, CHO, and CL), should enchain in a specific order to form a CBABC-pentablock structure (A = poly(PA-*alt*-CHO), B = PCHC, and C = polycaprolactone, PCL).[29] The insertion selectivity of the different monomers into the common zinc alkoxide intermediate was established to arise due to both

kinetic (insertion barriers) and thermodynamic (linkage stabilities) factors (Chapter 1, Figure 1.11). A follow-up experimental study in 2018 reported difficulties to achieve this prediction when ε-decalactone (DL) was used, as the PCHC chain end underwent backbiting to form cyclic carbonate faster than initiation of DL ROP.[8] An alternative monomer addition order was therefore used to prevent backbiting; carbon dioxide was introduced to the polymerisation after ROCOP of PA/CHO and ROP of DL, forming a BCACB structure (A = poly(PA-*alt*-CHO), B = PCHC, and C = polydecalactone, PDL). This was the first example of linking the three different polymerisation cycles in one-pot.

It was postulated that by using catalyst **5**, which shows enhanced carbon dioxide/anhydride selectivity, other pentablock polymers could be accessed, such as the CABAC pattern. Given that PCHC formation occurs before PE (when TCA is used as anhydride), the aforementioned issue of backbiting may be avoided as lactone ROP initiates from a polyester chain end.

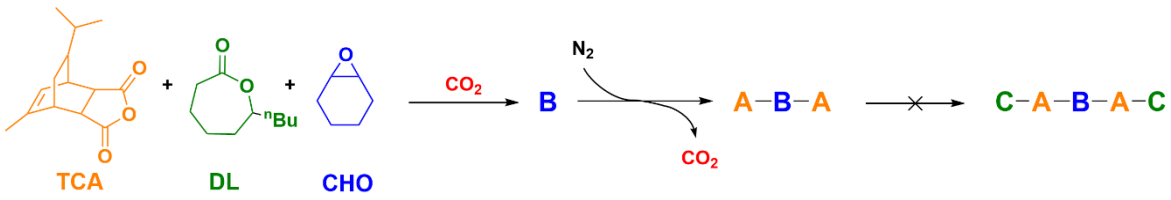

Scheme 3.2: Attempted polymerisation of tetracomponent mixture using gas switches. Polymerisation conditions: [**5**]:[CHD]:[TCA]:[DL]:[CHO] = 1:10:100:100:2000, 1 bar of CO_2 at 100 ˚C.

In order to investigate the synthesis of a pentablock copolymer featuring a lactone block, catalyst **5** was combined in solution with TCA (100 equiv.), DL (100 equiv.), CHO (~2000 equiv.), CHD (10 equiv.) at 1 bar pressure of CO_2 at 100 ˚C (Scheme 3.2). As observed without the presence of DL, the catalysis began with polycarbonate formation, which was followed by the PE block once the headspace was exchanged to N_2. Once the anhydride was fully consumed, the reaction stopped, with no detectable polymerisation of DL by either *in*

situ IR or ^{1}H NMR spectroscopy, even after 8 h with heating. ^{1}H NMR analysis of the reaction at this point showed that the only polymeric species was the ABA polymer. A new low intensity signal at 4.93 ppm, attributed to *trans*-cyclohexene carbonate (~1 %) was also observed (Figure S3.7). It was an unexpected occurrence, as the signal only appeared after complete conversion of the anhydride. Hence, cyclic product formation does not arise from degradation of the PCHC block's chain end, but rather from the low levels of CO_2 still dissolved in solution. This residual CO_2 preferentially inserts into the PE block zinc alkoxide chain end-group, degrading to cyclic carbonate and thus preventing DL ROP initiation. A more rigorous method for removing CO_2 from the reaction solution was attempted by employing 3 freeze-pump-thaw cycles, however it was still not sufficient to remove the residual CO_2 and enable the ROP of DL.

To confirm this hypothesis, TCA, DL, CHO and CHD with catalyst **5** were heated to 100 ˚C, which successfully formed a CAC triblock copolymer. Aliquot analysis by ^{1}H NMR and GPC confirmed the formation of PE followed by PDL blocks (Figures S3.8 and S3.9). This experiment confirms that initiation of PDL ROP from a poly(TCA-*alt*-CHO) chain end is feasible, and that it is not inhibited by chain end-group sterics/rigidity limiting pentablock formation.

To further examine the importance of ROP initiation rates for pentablock formation, DL was replaced by CL, which propagates by a primary alkoxide and is thus faster.[30] Furthermore, there are existing reports for switch catalysis using mixtures of CL, CHO, and CO_2 to form block copolymers.[31-32]

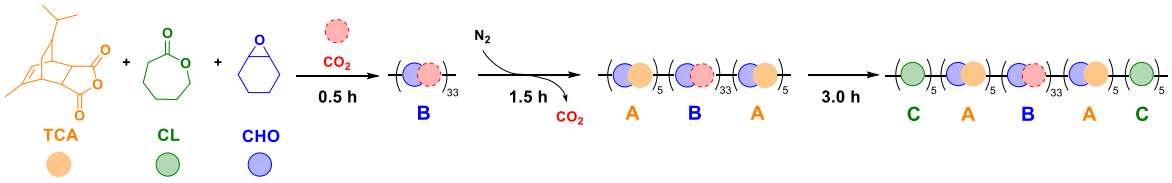

Scheme 3.3: Illustration of the polymerisation of the tetracomponent monomer mixture of TCA, CL, CHO, and CO_2. Block polymer structures are simplified as coloured balls representing the different monomers. $\overline{DP}$ of each block denoted on brackets.

Table 3.2: Data for the formation of a pentablock polymer from TCA, CHO, CL and CO_2 using catalyst **5**.[a]

Entry	Reaction Gas	Time (h)	TON[b]			TOF (h^{-1})[c]	M_n [$Đ$] (kg mol^{-1})[d]
			TCA	CL	CHO		
1	CO_2	0.5	0	0	325	650	3.5 [1.08]
2	N_2	1.5	100	0	425	67	5.2 [1.19]
3	N_2	3.0	100	86	425	29	6.1 [1.34]

[a] [**5**]:[CHD]:[TCA]:[CL]:[CHO] = 1:10:100:200:2000, 100 ˚C, Entry 1 under 1 bar of CO_2 for 0.5 h, Entry 2 under 1 bar of N_2 for 1.5 h and 3 for 3.0 h. [b] Turnover number (TON), number of moles of TCA or CHO consumed / number of moles of catalyst. Moles consumed determined by ^{1}H NMR, by comparison of the relative integrals of the resonances due to monomer (TCA: 5.73 ppm, CHO: 3.08 ppm, CL: 4.18 ppm) and polymer (PE: 4.63 ppm, PCHC: 4.63 ppm, PCL: 4.02 ppm). [c] Turnover frequency (TOF), TON / time (h). [d] Measured by GPC, in THF, using narrow MW polystyrene standards to calibrate the instrument.

Complex **5** was combined with TCA (100 equiv.), CL (200 equiv.), CHO (~2000 equiv.) and 1 bar pressure CO_2 at 100 ˚C. Consistent with previous experiments, PCHC formation occurred first (Table 3.2, entry 1). After 0.5 h, the carbon dioxide was exchanged to N_2, allowing the ROCOP of TCA/CHO to occur. An aliquot after 1.5 h showed full conversion of the anhydride by ^{1}H NMR spectroscopy (Figure 3.8) and an increase in molar mass from 3.5 kg mol^{-1} to 5.2 kg mol^{-1} by GPC (Table 3.2, entry 2 and Figure 3.9). Shortly after, an aliquot revealed the formation of PCL from the appearance of a broad triplet at 4.05 ppm (Figure 3.8). The final aliquot was taken after 4.5 h under N_2, at 43 % conversion of the CL monomer; the ROP of CL in making the pentablock was significantly slower (TOF = 29 h^{-1}) compared to that of CL homopolymerisation (TOF = >6000 h^{-1}, [**5**]:[CHD]:[CL]:[CHO] = 1:10:200:2000, T = 100 ˚C). This is most likely due to slow initiation and propagation of CL ROP, inhibited by the CO_2 still present in the reaction solution.

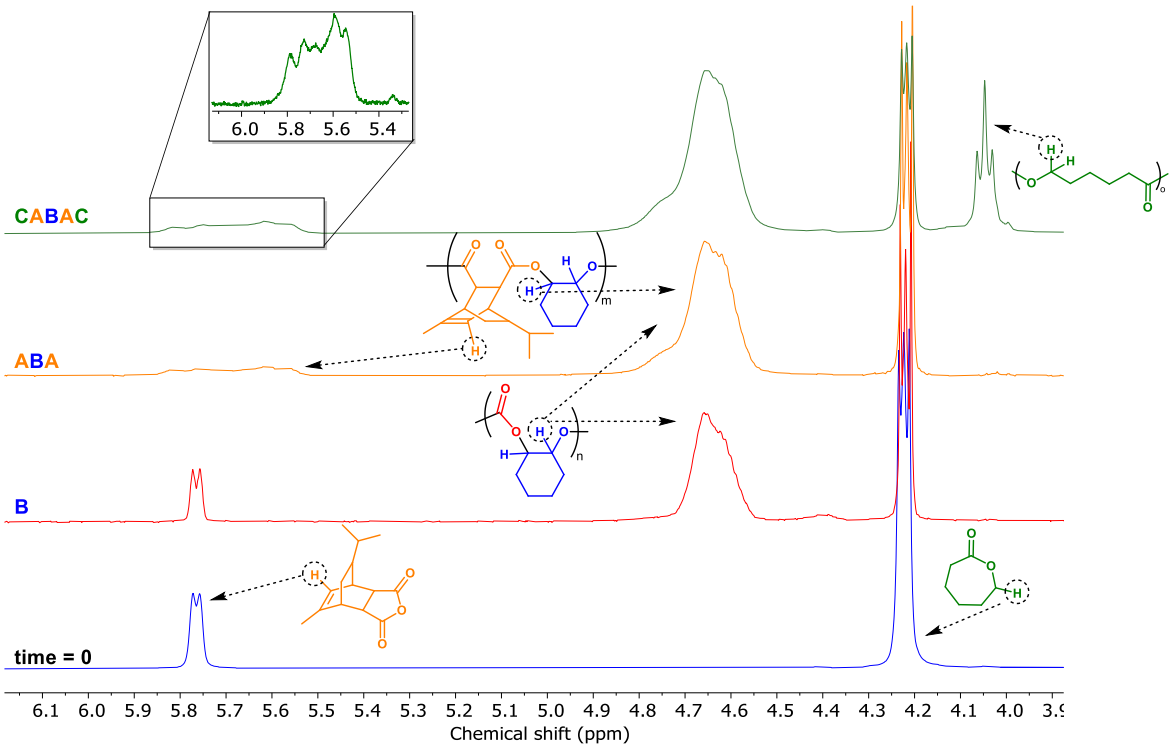

Figure 3.7: Stacked plot of selected region of ^{1}H NMR spectra illustrating the changes in various resonances throughout the polymerisation reaction, demonstrating the formation of the three different blocks. Spectrum at time = 0 is the mixture before polymerisation. The first block is formed is PCHC (B), shown by the resonance at 4.6 ppm. The second is PE (B), shown by the loss of the sharp doublet corresponding to the TCA monomer's alkene proton into a broad polymer signal at 5.8 ppm. The final block in green is denoted by the new signal at 4.0 ppm. The full spectrum can be found in Figure S3.10.

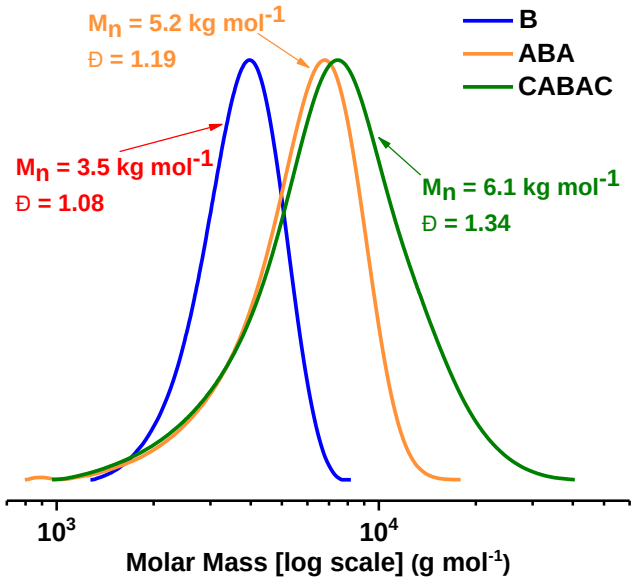

Figure 3.8: GPC traces of aliquots removed at the different stages of the polymerisation reaction (corresponding to entries 1, 2 and 3 in Table 3.2) and showing the formation of PCHC, PE-PCHC-PE, and PCL-PE-PCHC-PE-PCL.

The GPC of the final polymer shows a molar mass of 6.1 kg mol^{-1} and a broader dispersity of 1.34. This can be attributed to slower rates of initiation *vs.* propagation in CL ROP, which occur from a secondary cyclohexanol group and a primary hydroxyl group respectively.[30] This polymerisation reaction could not be monitored by *in situ* IR spectroscopy due to the weak and overlapping signal of both CL and PCL. The purified pentablock polymer was analysed by DSC and showed a single T_g value at 86 ˚C (Figure S3.11), characteristic of miscible blocks in the polymer and demonstrating how incorporating a "soft" aliphatic polyester block can significantly alter polymer properties; the ABA triblock copolymer from Section 3.3 at a similar molar mass displayed a T_g of 120 ˚C. Block formation was also confirmed by DOSY analysis of the purified polymer (Figure S3.12)

Overall, the characterisation data presented is consistent with the formation of a pentablock copolymer. It presents a considerable improvement to the aforementioned BCACB copolymer (A = PE', B = PCHC, C = PDL).[8] Firstly, the anhydride used here, TCA, is fully bio-renewable, whilst commercial PA is fossil-based with only a potential renewable

route.[33-34] With regards to polymerisation rates, both PE and PCHC ROCOP cycles are significantly faster for this work using catalyst **5**, even under more dilute conditions (2000 *vs.* 1000 equiv. of CHO), compared to using the organometallic Zn(II)Zn(II) catalyst; here, the TOF for TCA/CHO ROCOP was 67 h^{-1} and CO_2/CHO ROCOP was 650 h^{-1}, whereas for the latter catalyst PA/CHO ROCOP was 27 h^{-1} and CO_2/CHO ROCOP was 6 h^{-1}, 100 times slower. Furthermore, complex **5** is able to reproduce the BCACB order in monomer enchainment. Conversely, the Zn(II)Zn(II) catalyst could not make the CABAC polymer sequence as it does not exhibit the same selectivity as **5**, as seen in Chapter 2, and hence it is less versatile.

The proposed mechanism is outlined in Figure 3.10. All three polymerisation cycles are linked by an alkoxide intermediate where the relative insertion rates, which govern the block copolymer structure, follow the order CO_2 >TCA > CL. This is a different result to what was predicted by the DFT study using a Zn(II)Zn(II) complex as catalyst and PA, CHO, carbon dioxide, and CL as model monomer substrates.[29] This work demonstrates that the choice of central metals as well as anhydride can alter the insertion barriers into the metal alkoxide and linkage stabilities of the products. In turn, this changes the catalyst's selectivity. Experimentally, DL ROP was not possible in this one-pot procedure as the propagation rate k_5 was slower than the back-biting side reaction, which was also observed for Zn(II)Zn(II).[8]

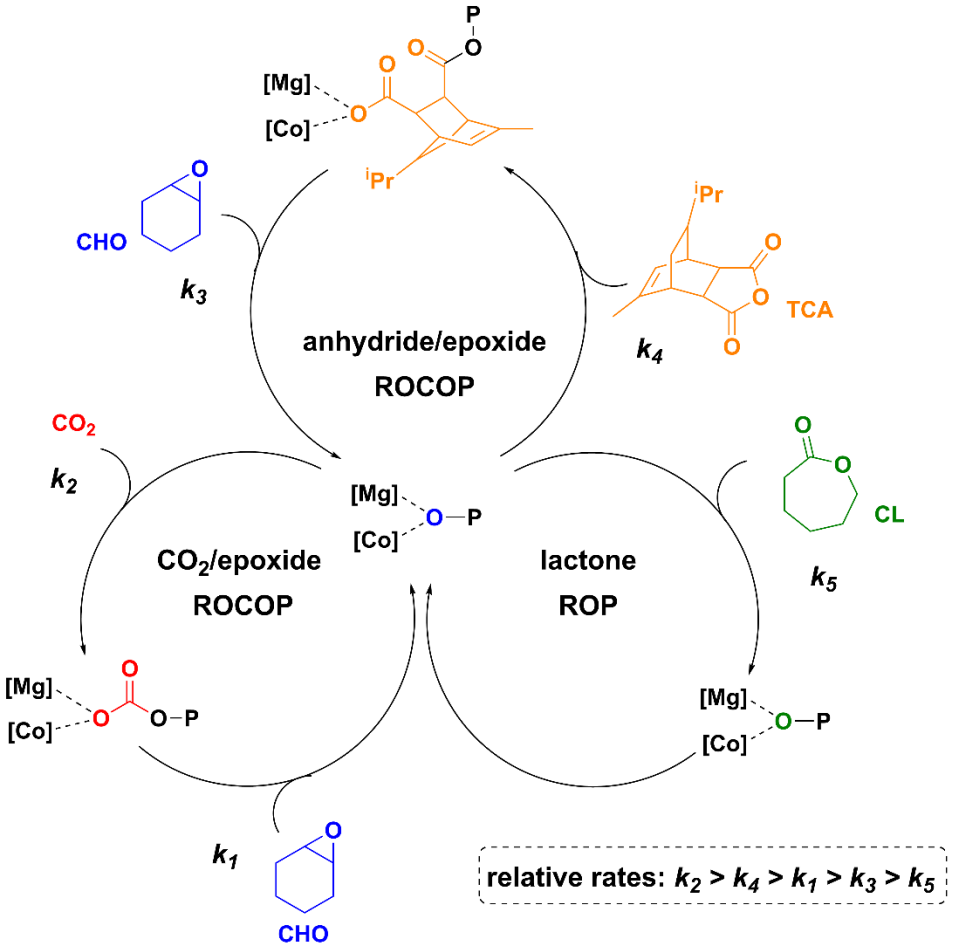

Figure 3.9: Proposed catalytic cycle for the polymerisation of CO_2, CHO, TCA, and CL. P = growing polymer chain.

3.6 Summary and Outlook

3.6.1 Summary

In summary, multi-block copolymers featuring carbonate and ester linkages have been synthesised by using simple gas exchanges to switch polymerisation cycles. The catalyst employed, featuring Mg(II) and Co(II) as metal centres, showed strong preference for carbon dioxide *vs.* anhydride insertion; this unique feature enabled precise carbonate linkage placement to form multi-block polymer architectures. In addition to high selectivity, this catalyst displayed high polymerisation rates across both polymerisation cycles, achieving up to 6-fold improvement compared to the analogous di-Mg(II) catalyst. It also selectively enchained a mixture of four monomers (cyclohexene oxide, tricyclic anhydride, carbon

dioxide, and caprolactone) to make a pentablock copolymer in a different sequence, and at higher rates, to what was previously reported.[8] Furthermore, the monomers employed can be fully derived from renewable feedstocks, which is an important consideration for making sustainable polymers.[9-13]

3.6.2 Outlook

The work presented in this chapter is primarily focused on the catalytic concept, with ample space for further material studies. In the future, rheology, degradation chemistry, and addition of functional substituents should be investigated for these precisely controlled multi-block polymers. These polymers are significant in the context of materials as by tailoring the composition of the monomer mixture, molar mass, chain end-group chemistry and glass transition temperature of the polymer can be controlled as desired. Selecting monomer combinations that lead to immiscible block segments could for example result in thermoplastic elastomers. Assessment of the benefits of multiblock polymers should be further explored, as there is precedence in material improvement.[35-36]

3.7 References

1. Saini, P. K.; Fiorani, G.; Mathers, R. T.; Williams, C. K., *Chem. Eur. J.* **2017,** *23* (18), 4260-4265.

2. Virachotikul, A.; Laiwattanapaisarn, N.; Wongmahasirikun, P.; Piromjitpong, P.; Chainok, K.; Phomphrai, K., *Inorg. Chem.* **2020,** *59* (13), 8983-8994.

3. Chidara, V. K.; Boopathi, S. K.; Hadjichristidis, N.; Gnanou, Y.; Feng, X., *Macromolecules* **2021,** *54* (6), 2711-2719.

4. Li, Y.; Zhang, Y.-Y.; Hu, L.-F.; Zhang, X.-H.; Du, B.-Y.; Xu, J.-T., *Prog. Polym. Sci.* **2018,** *82*, 120-157.

5. Li, C.; Dang, Y.-F.; Wang, B.; Pan, L.; Li, Y.-S., *Macromolecules* **2021,** *54* (13), 6171-6181.

6. Sulley, G. S.; Gregory, G. L.; Chen, T. T. D.; Peña Carrodeguas, L.; Trott, G.; Santmarti, A.; Lee, K.-Y.; Terrill, N. J.; Williams, C. K., *J. Am. Chem. Soc.* **2020,** *142* (9), 4367-4378.

7. Diaz, C.; Mehrkhodavandi, P., *Polym. Chem*, **2021,** *12* (6), 783-806.

8. Chen, T. T. D.; Zhu, Y.; Williams, C. K., *Macromolecules* **2018,** *51* (14), 5346-5351.

9. Thaore, V.; Chadwick, D.; Shah, N., *Chem. Eng. Res. Des.* **2018,** *135*, 140-152.

10. Dakshinamoorthy, D.; Weinstock, A. K.; Damodaran, K.; Iwig, D. F.; Mathers, R. T., *ChemSusChem* **2014,** *7* (10), 2923-2929.

11. Zhu, Y.; Romain, C.; Williams, C. K., *Nature* **2016,** *540* (7633), 354-362.

12. Winkler, M.; Romain, C.; Meier, M. A. R.; Williams, C. K., *Green Chem.* **2015,** *17* (1), 300-306.

13. Poland, S. J.; Darensbourg, D. J., *Green Chem.* **2017,** *19* (21), 4990-5011.

14. Gody, G.; Zetterlund, P. B.; Perrier, S.; Harrisson, S., *Nat. Commun.* **2016,** *7* (1), 10514.

15. Koning, C.; Wildeson, J.; Parton, R.; Plum, B.; Steeman, P.; Darensbourg, D. J., *Polymer* **2001,** *42* (9), 3995-4004.

16. Van Zee, N. J.; Coates, G. W., *Angew. Chem. Int. Ed.* **2015,** *54* (9), 2665-2668.

17. Sanford, M. J.; Peña Carrodeguas, L.; Van Zee, N. J.; Kleij, A. W.; Coates, G. W., *Macromolecules* **2016,** *49* (17), 6394-6400.

18. Koleske, J. V.; Lundberg, R. D., *Journal of Polymer Science Part A-2: Polymer Physics* **1972,** *10* (2), 323-337.

19. Darensbourg, D. J.; Poland, R. R.; Escobedo, C., *Macromolecules* **2012,** *45* (5), 2242-2248.

20. Longo, J. M.; Sanford, M. J.; Coates, G. W., *Chem. Rev.* **2016,** *116* (24), 15167-15197.

21. Ye, S.; Wang, W.; Liang, J.; Wang, S.; Xiao, M.; Meng, Y., *ACS Sustain. Chem. Eng.* **2020,** *8* (48), 17860-17867.

22. Chang, C.-H.; Tsai, C.-Y.; Lin, W.-J.; Su, Y.-C.; Chuang, H.-J.; Liu, W.-L.; Chen, C.-T.; Chen, C.-K.; Ko, B.-T., *Polymer* **2018,** *141*, 1-11.

23. Pappuru, S.; Chakraborty, D., *Eur. Polym. J.* **2019,** *121*, 109276.

24. Huijser, S.; HosseiniNejad, E.; Sablong, R.; de Jong, C.; Koning, C. E.; Duchateau, R., *Macromolecules* **2011,** *44* (5), 1132-1139.

25. Zhang, J.; Wang, L.; Liu, S.; Kang, X.; Li, Z., *Macromolecules* **2021,** *54* (2), 763-772.

26. Kernbichl, S.; Reiter, M.; Adams, F.; Vagin, S.; Rieger, B., *J. Am. Chem. Soc.* **2017,** *139* (20), 6787-6790.

27. Hu, C.; Duan, R.; Yang, S.; Pang, X.; Chen, X., *Macromolecules* **2018,** *51* (12), 4699-4704.

28. Kernbichl, S.; Reiter, M.; Mock, J.; Rieger, B., *Macromolecules* **2019,** *52* (21), 8476-8483.

29. Romain, C.; Zhu, Y.; Dingwall, P.; Paul, S.; Rzepa, H. S.; Buchard, A.; Williams, C. K., *J. Am. Chem. Soc.* **2016,** *138* (12), 4120-4131.

30. Zhu, Y.; Romain, C.; Poirier, V.; Williams, C. K., *Macromolecules* **2015,** *48* (8), 2407-2416.

31. Paul, S.; Romain, C.; Shaw, J.; Williams, C. K., *Macromolecules* **2015,** *48* (17), 6047-6056.

32. Romain, C.; Williams, C. K., *Angew. Chem. Int. Ed.* **2014,** *53* (6), 1607-1610.

33. Giarola, S.; Romain, C.; Williams, C. K.; Hallett, J. P.; Shah, N., *Chem. Eng. Res. Des.* **2016,** *107*, 181-194.

34. Shao, X.; Su, L.; Zhang, J.; Tian, Z.; Zhang, N.; Wang, Y.; Wang, H.; Cui, X.; Hou, X.; Deng, T., *ACS Sustain. Chem. Eng.* **2021,** *9* (43), 14385-14394.

35. Grune, E.; Appold, M.; Müller, A. H. E.; Gallei, M.; Frey, H., *ACS Macro Lett.* **2018,** *7* (7), 807-810.

36. Bates, F. S.; Hillmyer, M. A.; Lodge, T. P.; Bates, C. M.; Delaney, K. T.; Fredrickson, G. H., *Science* **2012,** *336* (6080), 434.

Chapter 4

A Novel Catalyst with Non-initiating Co-ligands for CO_2/Epoxide ROCOP Yielding High Molar Mass Polymers

4.1 Introduction and Aims

There is growing interest in developing novel catalysts for the ROCOP of epoxides and CO_2 as a strategy to fix CO_2 into a value-added product.[1-2] Since the discovery of this process by Inoue in 1969,[3] research has been focussing on enhancing polymerisation rates, polycarbonate selectivity, and cost effectiveness of catalysts.[4-6] In all of these examples, polymer molar masses have been low and/or bimodal. This is because most catalysts can initiate polymerisation with anionic moieties (e.g. $^{-}$OAc and Cl^{-}), and any protic impurity in CO_2 or the epoxide can act as an initiator and/or chain transfer agent (CTA).[7-9] This results in bimodal molar mass distributions as the diol/water-initiated chains display twice the molar mass of a catalyst-initiated chain (Figure 4.1).

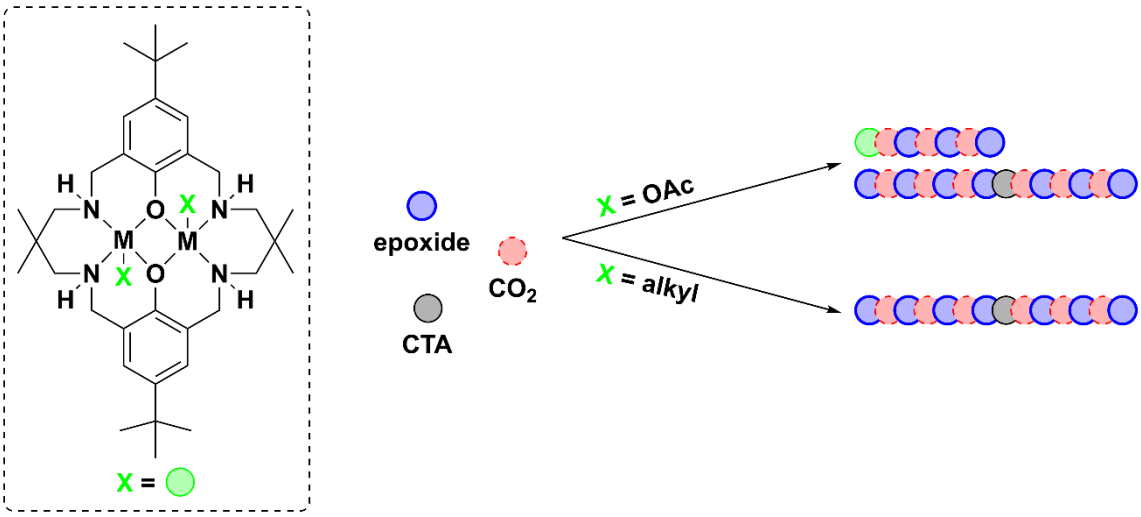

Figure 4.1: Effect of catalyst initiating group X on the polycarbonate synthesised by ROCOP of epoxides and CO_2.

Under these conditions, the resulting materials are inherently impure as a mixture of mono and dihydroxyl telechelic chains. This can become problematic when block copolymers are targeted, as both diblock and triblock polymers will be formed, which may exhibit different material properties. There have been attempts to tackle this issue, which focus on either monomer purification methods to reduce diol concentrations, which is difficult to achieve at

the ppm level, or by tailored catalyst design.[10-14] Using a catalyst that does not carry an initiating moiety, such as an alkyl group, means that added diols can be used exclusively as the initiators. The first report was from our group in 2017, when [Zn(II)Zn(II)X_2] catalysts where X = C_6H_5 and C_6F_5 were synthesised to investigate aryl co-ligand reactivity with CO_2 and in polymerisation catalysis.[15] Later, Sulley *et al.* synthesised an [Mg(II)Zn(II)X_2] catalyst (X = C_6F_5), which was more catalytically active compared to the Zn(II)Zn(II) complex.[16] Once protonated, the HC_6F_5 is innocent in the polymerisation. Whilst this development was successful in making high molar mass functional materials (70 kg mol^{-1} triblock copolymer with up to 30 kg mol^{-1} PCHC content), it remains a relatively slow catalyst for CO_2/epoxide ROCOP.[10] As seen in Chapters 2 and 3, Co(II) was found to display enhanced synergy with Mg(II) in ROCOP catalysis, exhibiting much faster rates compared to Zn(II), due to the increased nucleophilicity of the Co-carbonate propagating species.[17] Therefore, a logical next step would be to prepare an organometallic Mg(II)Co(II)X_2 catalyst. This should show high selectivity, activity, and high loading tolerance to access high molar mass polycarbonates.

4.3 Synthesis, Characterisation, and Reactivity of Organometallic Mg(II)Co(II) Complex

4.3.1 Synthetic Routes Towards Heterodinuclear Complex

The pentafluorophenyl X group was targeted as the labile non-initiating co-ligand as it was successful in the di-Zn(II) and Mg(II)Zn(II) catalysts.[10, 15] An analogous synthetic route to that used for [LMgZn(C_6F_5)$_2$] was taken, using cobalt bispentafluorophenyl to as the second metal precursor (Scheme 4.1).[10]

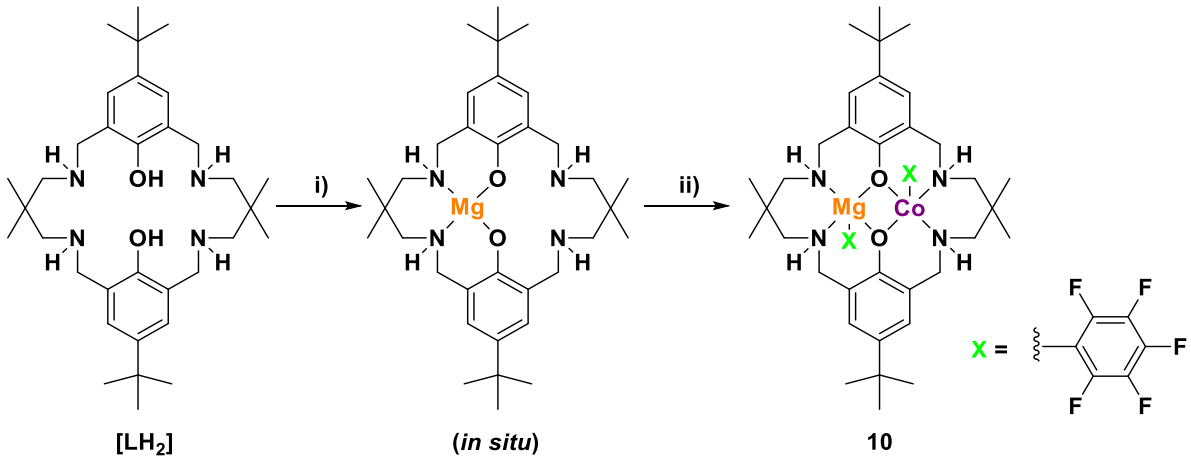

Scheme 4.1: i) $[Mg\{N(SiMe_3)_2\}_2]$, THF, 2 h at RT. ii) $[Co(C_6F_5)_2(THF)_2]$, 16 h at RT, 12 h at −30 ˚C, 53 % yield.

Cobalt bispentafluorophenyl was synthesised according to a literature procedure, by reacting $CoBr_2$ with the pentafluorophenyl Grignard, $BrMgC_6F_5$.[18-19] The complex exists as either a dioxane or THF adduct. The resultant compound, $[Co(C_6F_5)_2(THF)_2]$, was recrystallised twice from a 1:6 THF:hexane mixture before use. Single crystals, suitable for XRD, were afforded *via* the same method. The solid-state molecular structure of the compound showed a tetrahedral Co(II) centre with two C_6F_5 and two donor THF co-ligands (Figure S4.1 and Table S4.1 for bond lengths and angles). The structure of $[Co(C_6F_5)_2(THF)_2]$ had not previously been confirmed, so this report could assist others using it.

A 1:1 molar ratio of the macrocyclic ligand $[LH_2]$, prepared according to a previous literature procedure,[20] and $[Mg\{N(SiMe_3)_2\}_2]$ were combined at RT in anhydrous THF for 2 hours, forming the mono-magnesium chelate *in situ* ([LMg]). Subsequently, a solution of $[Co(C_6F_5)_2(THF)_2]$ (1 equiv.) in THF was added dropwise and stirred for 16 h at RT, with the reaction solution first turning an aquamarine colour before then gradually turning dark brown. The reaction was then cooled to –30 ˚C for 24 h, allowing the precipitation of $[LCoMg(C_6F_5)_2]$ (**10**) as a purple crystalline solid (53 % yield). Elemental analysis of the

complex could not be obtained due to its high sensitivity to moisture and oxygen, resulting in decomposition during transit.

4.3.2 X-ray Crystallography

Single crystals of **10** suitable for X-ray diffraction were isolated *via* crystallisation from a saturated THF solution at −30 ˚C. The solid-state structure of the compound shows the desired heterodinuclear complex, with a C_6F_5 co-ligand at each metal (Figure 4.2).

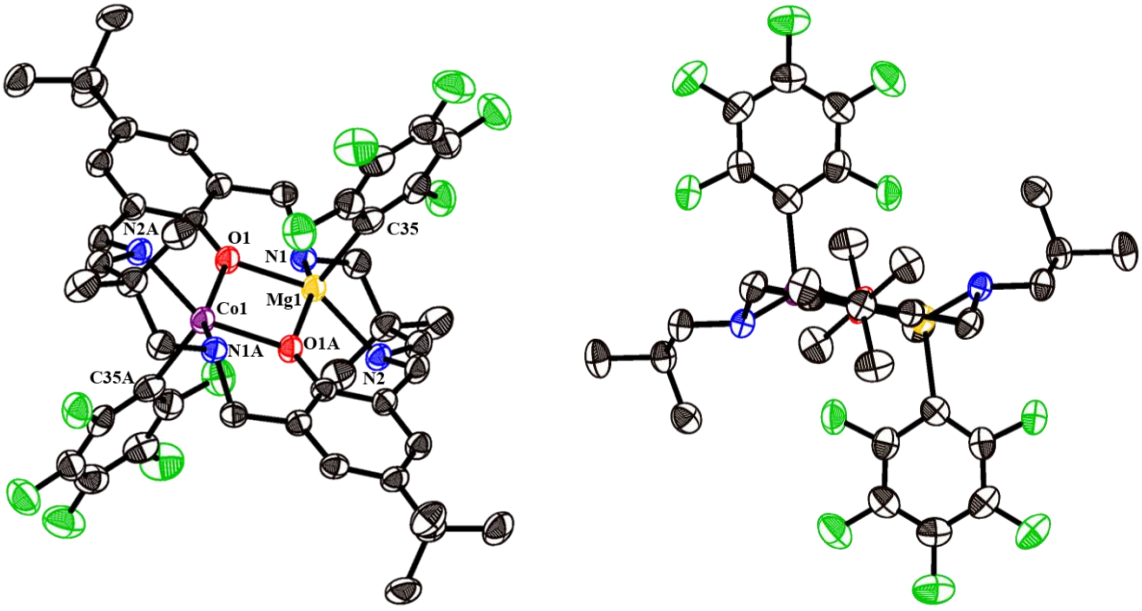

Figure 4.2: ORTEP diagram for the molecular structure of **10**. H atoms and two THF molecules have been omitted for clarity. Thermal ellipsoids at 50 % probability level. Figure on the right shows the "S" shape of the ligand. Co = purple, Mg = yellow, O = red, N = blue, F = green, C = grey.

The asymmetric unit represents half of the structure as a result of positional disorder, where one of the metal centres is calculated to have 50 % occupancy of Mg(II) and Co(II). The ligand scaffold adopts an "S" shape, which is analogous to the di-Zn complex with the same co-ligands.[15] In contrast, the analogous Mg(II)Co(II) acetate complex **5** exists as a dimer in the solid state, with the ligand adopting a "bowl" shape.[21] The Co(II) centre is pentacoordinate and adopts a distorted square pyramidal geometry, with an average basal

angle of 149˚. There are few examples of this geometry for Co(II) complexes.[22] The intermetallic distance is 3.098 Å, similar to **5** (3.037(3) Å).[21] The Co–C bond is significantly longer compared to the bonds in $[Co(C_6F_5)_2(THF)_2]$ (2.182(14) *vs.* 2.030(4) Å). There are no apparent F-metal or F-HN interactions (F---HN(2) = 3.311 Å), only H-bonding of a THF molecule to each NH of the ligand scaffold (O---HN = 2.116 Å). A summary of the key bond lengths and angles can be found in Table 4.1.

Table 4.1: Key bond lengths and angles in the solid-state structure of **10**.

Bond	**Length (Å)**	**Bond**	**Angle (˚)**
Co(1)-O(1)	2.050(12)	O(1)-Co(1)-N(1A)	150.9(7)
Mg(1)-O(1)	2.010(2)	O(1A)-Co(1)-N(2A)	147.7(7)
Co(1)-C(35A)	2.182(14)	O(1A)-Mg(1)-N(1)	150.4(14)
Mg(1)-C(35)	2.160(3)	O(1)-Mg(1)-N(2)	146.8(14)

4.3.3 NMR Spectroscopy

The ^{1}H NMR spectrum of complex **10**, in toluene-d_8, shows peaks in the paramagnetic region, ranging from −55 to 270 ppm, indicative of a Co(II) species (Figure S4.2). There are 13 sharp signals, although *J*-coupling information is lost due to the short relaxation times inherent to paramagnetic compounds,[23] and two broader signals (>200 Hz). Hence, the spectrum could not be completely assigned. The total number of signals, 15, matches what would be expected for the ligand in an asymmetric environment (excluding the ligand NH proton). The ^{19}F{^{1}H} NMR spectrum shows the presence of only three peaks; two broad singlets at −155 ppm and −65 ppm (both with a linewidth of 111 Hz), and a triplet at −154 ppm (Figure 4.3). The peaks integrate 4:2:2, respectively. The lack of a second set of co-ligand peaks and the integration pattern is unexpected. Two scenarios are possible for these observations:

a) A fluxional ring-exchange process occurs in solution which causes the resonances from the two co-ligands to average.

b) The fluorines closest to the paramagnetic Co(II) centre, either *via* through-bond or through-space interactions, denoted **u**, **v**, and **x**, are not observed by ^{19}F NMR spectroscopy due to fast nuclear relaxation.

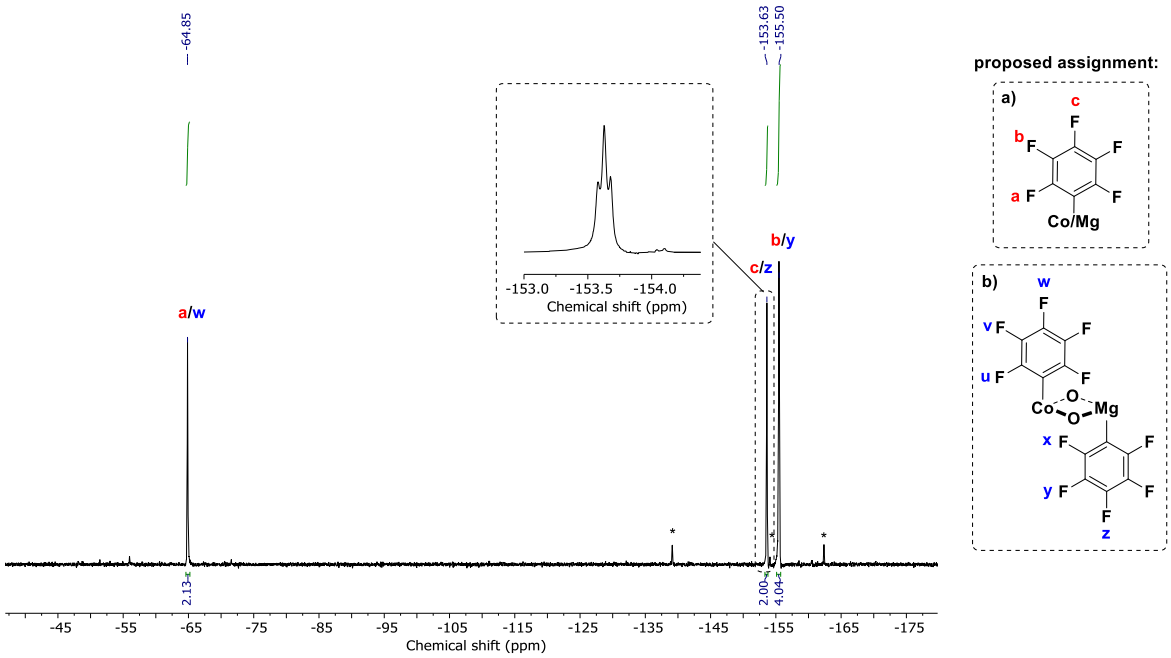

Figure 4.3: ^{19}F{^{1}H} NMR spectrum (toluene-d_8, 377 MHz) of complex **10**. Resonances of traces of HC_6F_5 denoted by *. Proposed assignments based on points a) and b).

These hypotheses were investigated further *via* ^{19}F{^{1}H} COSY NMR spectroscopy (Figure S4.3) and ^{19}F{^{1}H} VT NMR spectroscopy at −60 ˚C (Figure S4.4). The low temperature ^{19}F{^{1}H} NMR spectrum supports hypothesis a), as it shows splitting of signal **a**, which is assigned to the *ortho*-F as it is the most affected by the paramagnetic centre. This peak integrates to 2 due to fast relaxation of the nucleus. Resonances **b** and **c** are assigned based on the relative integration. However, the Mg(II)Zn(II) analogue does not show fluxional behaviour at room temperature.[10] The ^{19}F COSY spectrum supports hypothesis b). It shows that the resonance at -65 ppm does not couple to the other nuclei (Figure S4.3), suggesting

it may be **w** and that **u** and **v** are not detected in the spectrum. The fluorine resonances at -155 and -154 ppm couple, indicating they are on the same ring, and hence are assigned as **y** and **z**. Fluorine **x** is most likely affected by through-space interactions with the paramagnetic Co(II) centre,[24] as the distance is ~3 Å in the crystal structure, and thus not observed in the spectrum. These assignments also explain the relative integrations of the resonances. Additional experiments, such as $^{13}C\{^{19}F\}$ and ^{19}F HSQC NMR spectroscopy may give further insight into this uncertainty.

Over time, signals for pentafluorobenzene (HC_5F_6) appear in the $^{19}F\{^{1}H\}$ NMR spectrum at room temperature (Figure S4.5), which arise from hydrogen abstraction from the solvent or potentially the N–H of the ligand. The complex is hence unstable in solution. This is not expected to be a concern for catalysis, as the co-ligand should be instantly reactive with the added alcohol to form the alkoxide initiator (*vide infra*).

4.3.4 Super Conducting Quantum Interference Device (SQUID) Magnetometry

The complex was further analysed by super conducting quantum interference device (SQUID) magnetometry. The magnetic susceptibility of **10,** in the solid state, was studied using SQUID at an applied magnetic field of 0.1 T and between 8 and 350 K. The complex behaves as a typical paramagnet throughout the temperature range measured. Its magnetic susceptibility was corrected for diamagnetic contributions (χ_{dia} = −4.84 x 10^{-4} emu) and converted to molar magnetic susceptibility (χ_m) (by multiplying by the molar mass). A plot of $1/\chi_m$ against temperature (T) displayed a linear relationship between 50 and 300 K (Figure 4.4a), indicating that it obeys the Curie-Weiss law (Equation 4.1). From the linear fit, the Curie (C) and Weiss (θ) constants were extracted, as the inverse of the slope and the x-intercept, respectively.

$$\chi_m = \frac{C}{T-\theta} \qquad \text{Equation 4.1}$$

The values of C and θ are 3.28 emu K mol^{-1} and −15.2 K, respectively. The χ_mT product remains constant from room temperature to 100 K, which is consistent with non-interacting Co(II) centres. The observed rapid decrease below 100 K is most likely due to the magnetic anisotropy inherent to the Co(II) centres, reaching a value of 0.4 cm^3 K mol^{-1} at 2 K (Figure 4.4b). At room temperature (300 K), the χ_mT value is 3.12 cm^3 K mol^{-1}. This matches well with other reported high spin Co(II) complexes with high magnetic anisotropy and significant orbital contribution (2.1–3.4 cm^3).[25-27] Using the equation for calculating the effective magnetic moment (μ_{eff}) (Equation 4.2), a value of 4.99 μ_B was obtained.

$$\mu_{eff} = 2.828\sqrt{\chi_m T} = 4.99\ \mu_B \qquad \text{Equation 4.2}$$

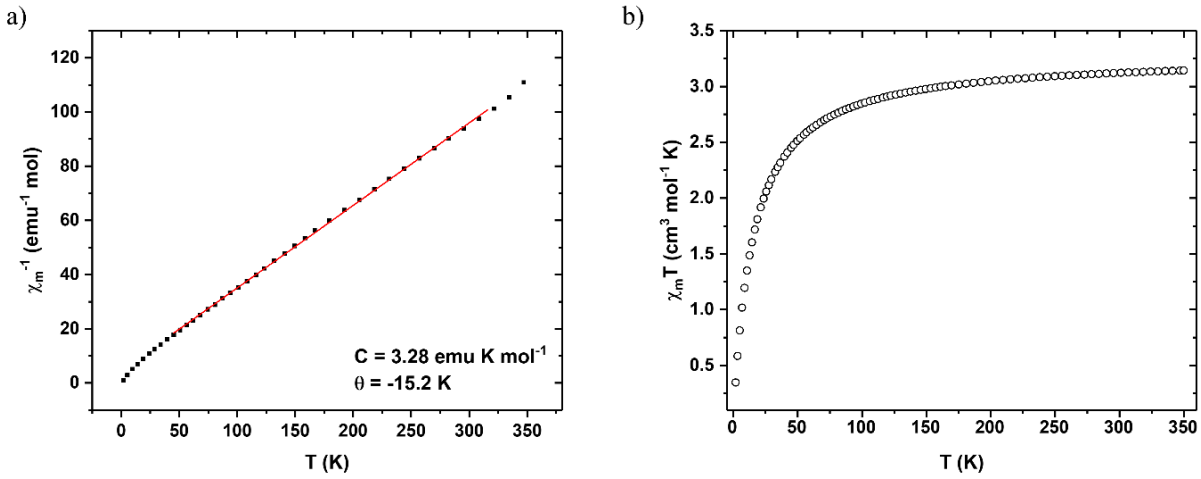

Figure 4.4: a) Inverse susceptibility against temperature χ_m^{-1} *vs.* T for complex **10**. b) χ_mT *vs.* T plot for complex **10**.

This value is comparable to complex **5** (μ_{eff} = 4.75 μ_B), which indicates that it has a high spin d^7 Co(II) centre.[21] The spin-only value (μ_{SO}) for a complex with 3 unpaired electrons is 3.87 μ_B (S = 3/2, g = 2), which is much lower than the experimental value obtained (4.99 μ_B), again due to 2nd order spin-orbit coupling.

The electronic configuration and population of energy levels can be postulated using molecular orbital diagrams calculated by Rossi and Hoffmann.[28] The authors report the *d*

orbital energy levels of a general square pyramidal ML_5 complex with respect to its basal angle (Figure 4.5a). From the crystal structure of **10**, an angle of around 150˚ was obtained, hence the energy levels can be proposed by extrapolation from the MO diagram. Assuming a relatively small ligand field splitting for the Co(II) complex, three unpaired electrons would result, which aligns well with the measured magnetic moment. Jurca *et al.* also report a simplified model, based on DFT calculations, of the *d*-orbital energy diagram associated with distortions in square-based pyramid geometries.[26] The model is in good agreement with Rossi and Hoffman; the cobalt in **10** sits above the chelating ONON mean plane by 0.55 Å, measured from the solid state structure, a pronounced distortion that leads to the identical orbital configuration in Figure 4.5b.

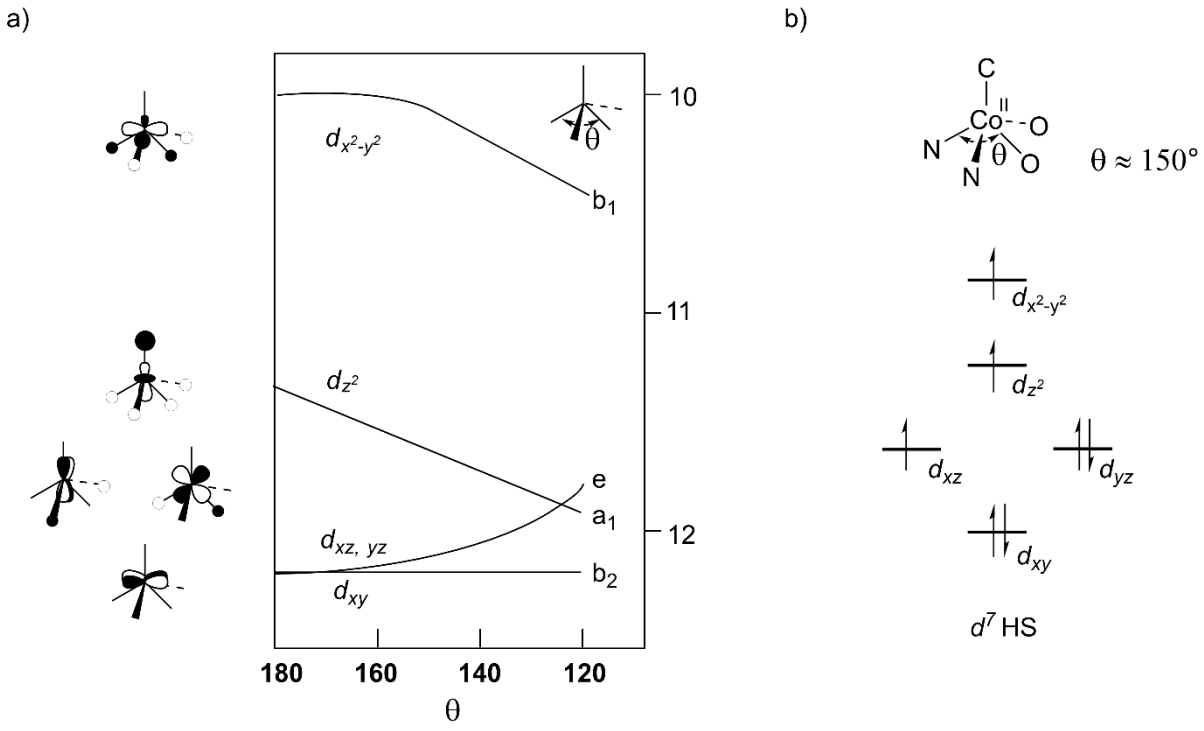

Figure 4.5: a) Calculated energies in eV for an ML_5 complex as a function of basal angle, θ. Adapted from reference.[28] b) Proposed electronic configuration for complex **10**.

It is worth noting that there are few examples Co(II) alkyl complexes.[19, 29-30] This is primarily because they tend to be prone to β-hydride elimination and thus are inherently unstable,

which is why **10** is a relatively stable complex. Organometallic Co(III) chemistry is more common and widely explored given the involvement of organocobalt(III) species in certain biological processes, for example in vitamin B12.[31]

4.3.5 Cyclic Voltammetry

To gain further insight into the heterodinuclear nature of **10**, cyclic voltammetry was investigated. Experiments were conducted in THF, using [^{n}Bu$_4$N][PF$_6$] (0.1 M) as the electrolyte. Measurements were referenced internally to the ferrocene ($FeCp^{+}$/FeCp) reduction potential.

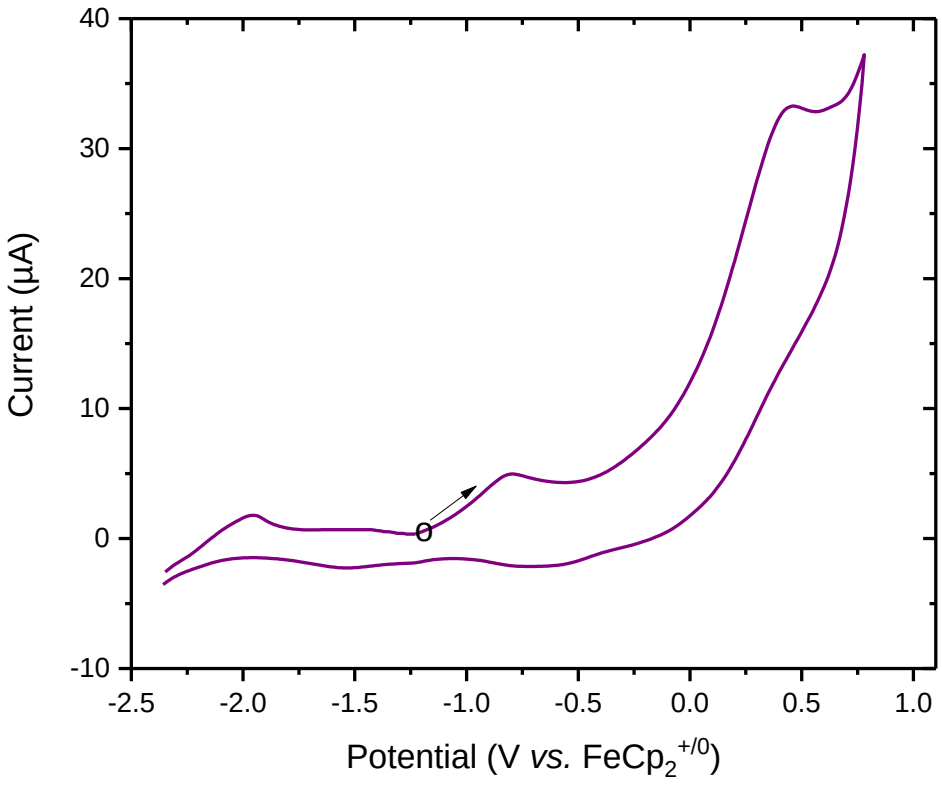

Figure 4.6: CV curve of **10** in THF with 0.1 M [^{n}Bu$_4$N][PF$_6$] at a scan rate of 0.1 V s^{-1}, referenced to $FeCp_2^{+}$/$FeCp_2$. Circle and arrow indicate start and direction of the measurement, respectively.

Two oxidation events were found in the CV curve, at −0.819 V and 0.39 V (Figure 4.6). They are assigned to [MgCo^{II}]/[MgCo^{III}]$^{+}$ and phenolate ligand oxidation, at E_{pa} = −0.819

V and E_{pa} = 0.39 V, respectively, given that Mg(II) is not oxidised (for complex **1**, only a ligand oxidation event is observed).[32] There are no apparent associated reductions in the reverse scan, suggesting that the $[MgCo^{III}]^+$ product is unstable. Hence, the oxidation feature at –2.0 V was not assigned. A similar result was observed for complex **5** under identical conditions; it possesses a similar electrochemical profile, with only two oxidations detected and no associated reductions.[32] The ligand oxidation of **5** was similarly observed at E_{pa} = 0.35 V. The oxidation of $[MgCo^{II}]/[MgCo^{III}]^+$ was at E_{pa} = −0.06 V, which is higher compared to **10**, signifying that **10** is more readily oxidised. This may explain the inherent instability of the complex and observed decomposition in solution. The Co(II) centre in **10** may also be more electron-rich compared to **5** as the OAc is more electron withdrawing. Overall, the similarity to **5** and the presence of a single Co^{II}/Co^{III} oxidation supports a heterodinuclear complex.

4.3.6 Stoichiometric Reactions

In order to test the lability and reactivity of the aryl co-ligand, stoichiometric reactions using **10** were performed. The most important reactions are with alcohols, since these are proposed to generate the polymerisation initiating species, and its reaction with CO_2. They were monitored by ^{19}F NMR spectroscopy, since it is easier to analyse compared to ^{1}H NMR spectroscopy, due to the paramagnetic nature of the complex. Therefore, an alcohol with a fluorine substituent was chosen, 4-fluorophenol. Complex **10** was reacted with 2 equivalents of 4-fluorophenol, in toluene-d_8, in a Young's tap NMR tube (Figure 4.7). The solution instantly turned from light purple to bright pink. The $^{19}F\{^{1}H\}$ NMR spectrum showed the formation of HC_6F_5, *i.e.* the product of alcoholysis, as well as new resonances at −56.1 and −132.0 ppm with 1:1 integration. The signals are tentatively assigned to a 4-fluorophenoxide ligand coordinated to Mg(II) and Co(II).

Next, the *in situ* generated alkoxide solution was exposed to 1 bar of CO_2, after 3 freeze-pump-thaw cycles to remove the nitrogen atmosphere. The solution underwent a rapid colour change to pale pink/orange. This colour change is also observed when a solution of epoxide, complex and alcohol is exposed to a CO_2 atmosphere (*vide infra*). In the $^{19}F\{^1H\}$ NMR spectrum, the lower field peak shift disappears, and the other shifts to −114.6 ppm (Figure S4.6); this value is close to the resonance for the corresponding fluorinated aryl carbonate in chloroform-*d*,[33] suggesting CO_2 insertion was successful.

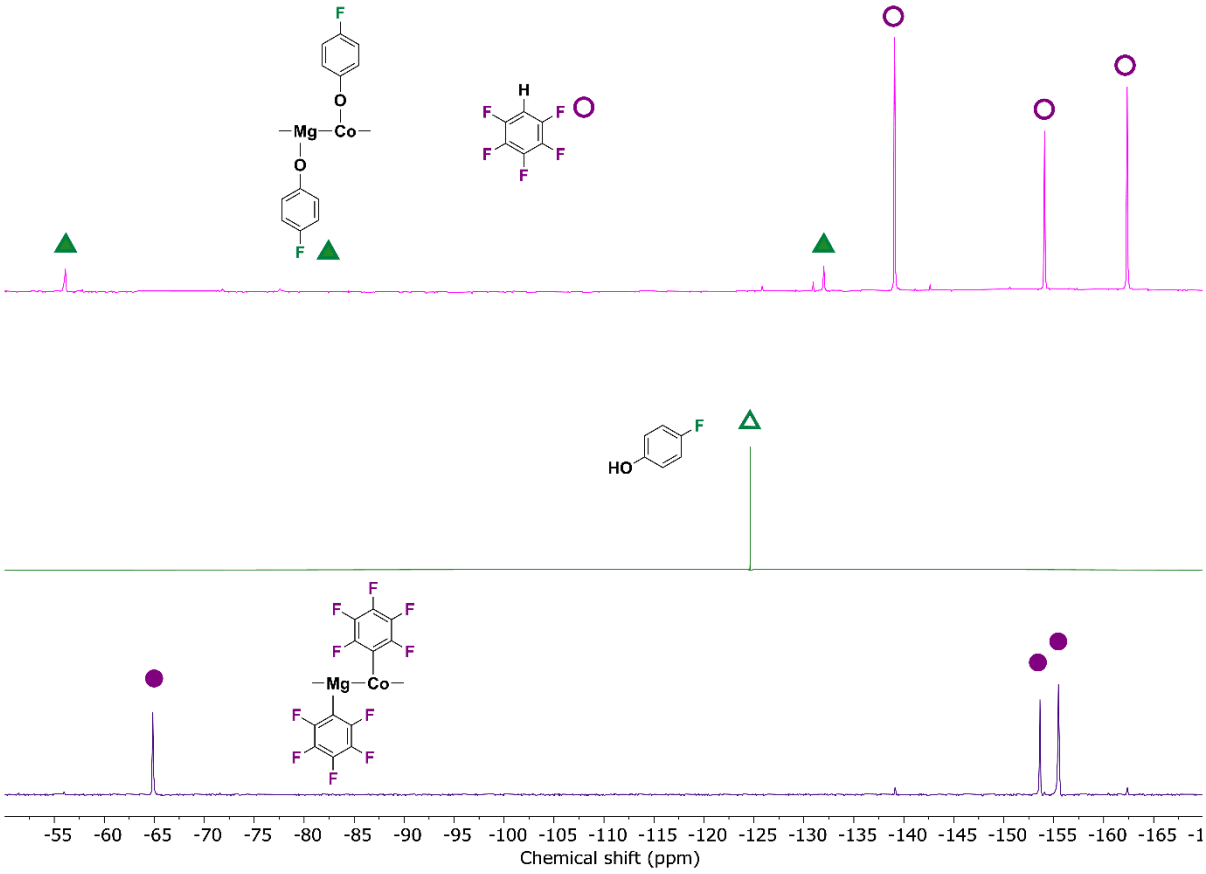

Figure 4.7: Stacked plot of $^{19}F\{^1H\}$ NMR spectra (toluene-d_8, 377 MHz) of **10** (bottom), 4-fluorophenol (middle), and the reaction between them (top).

To assess whether CO_2 could directly insert into the M-C_6F_5 bonds of compound **10**, a further experiment was undertaken. A Young's tap NMR tube of **10**, dissolved in toluene-d_8, was charged with 1 bar of CO_2 after 3 freeze-pump-thaw cycles to remove N_2 atmosphere. The solution changed colour from light purple to pale yellow. The $^{19}F\{^1H\}$ NMR spectrum

after the colour change only showed the presence of HC_6F_5, indicating that no insertion took place. It seems most likely that hydrolysis of the aryl group was triggered by traces of water present in the CO_2.

Whilst the general mechanism for epoxide/CO_2 ROCOP of these dinuclear catalysts is well understood, the structures of the intermediates are not elucidated. Synthesising model compounds could consolidate mechanistic understanding.[34] Metal carboxylate species have been isolated, but metal alkoxide and carbonates are less known.[21, 35-36] Complexes with bidentate/chelating co-ligands, such as acetates, are not easily displaced, whereas organometallic ligands are. Hence, complex **10** provides an opportunity to access such intermediary structures.

4.3.7 Homodinuclear Compound

Previous research into heterodinuclear catalysts suggests that mixed-metal complexes are generally more thermodynamically stable than their homodinuclear counterparts.[37] Nevertheless, each metal combination is unique and so proof of heterodinuclear stability is always desirable. Whilst the characterisation and stability data for **10** are highly suggestive of a heterodinuclear complex, characterisation of, and subsequent comparison to the homodinuclear analogues may further strengthen the claim.

To form the Co(II)Co(II) complex, two equivalents of $[Co(C_6F_5)_2(THF)_2]$ were added to a cold (−30 ˚C) suspension of the macrocycle in toluene-d_8. The mixture was stirred at room temperature, gradually turning to a homogeneous bright purple solution within 10 minutes. The crude reaction mixture was transferred to a Young's tap NMR tube. The crude $^{19}F\{^1H\}$ NMR spectrum of the reaction shows a single resonance, at −71.32 ppm, as the major product, and HC_6F_5 as by-product (Figure S4.7). The ^1H NMR spectrum shows 9 sharp paramagnetic resonances between −75 and +271 ppm, indicative of a symmetric ligand

environment (Figure S4.8). The single resonance for the C_6F_5 group bound to Co(II) is curious and not easy to rationalise. Further VT NMR spectroscopy using different solvents may provide further insights.

Crystals suitable for XRD were afforded by cooling the toluene-d_8 solution to −30 ˚C. The solid-state structure confirms a dinuclear Co(II) complex with a C_6F_5 group coordinated to each metal (Figure S4.9). The structure is similar to **10**; it possesses an intermetallic distance of 3.095 Å, adopts an "S" shape ligand conformation, and shows Co–C bond lengths of 2.104 Å (Table S4.3).

4.4 CO_2 Copolymerisation Experiments

4.4.1 CO_2/Epoxide ROCOP at 1 bar of CO_2

The new heterodinuclear complex **10** was tested for the ROCOP of CO_2 and cyclohexene oxide (CHO). In particular, it was important to evaluate its activity compared to **5** and its ability to form high molar mass polycarbonate with polymerisation control.

Firstly, in order to assess the ability of complex **10** to provide effective end group control, PCHC samples catalysed by both complex **10** and **5** were analysed by MALDI-ToF mass spectrometry (Figure 4.8). A low molar mass PCHC sample, prepared using a [**10**]:[CHD]:[CHO] ratio of 1:4:2000 in toluene at 80 ˚C for 10 minutes, shows a single distribution of α,ω-dihydroxy telechelic polymer chains, initiated solely from CHD (Figure 4.8a and b). The colour changes observed upon adding CHD to the solution of **10** in CHO and toluene (bright pink), and subsequent exposure to CO_2 (pale yellow/pink), corresponded with those in the stoichiometric reactions of **10** (Section 4.3.6). The MALDI-ToF data provides good evidence that the organometallic co-ligands are not initiators for the polymerisation; initiation is exclusively from the added CHD. In contrast, under identical

conditions, a mixture of two distributions is observed when complex **5** is used as the catalyst, namely α,ω-dihydroxy telechelic and α-acetal-ω-hydroxy chains, as it features initiating acetate groups (Figure 4.8c and d).

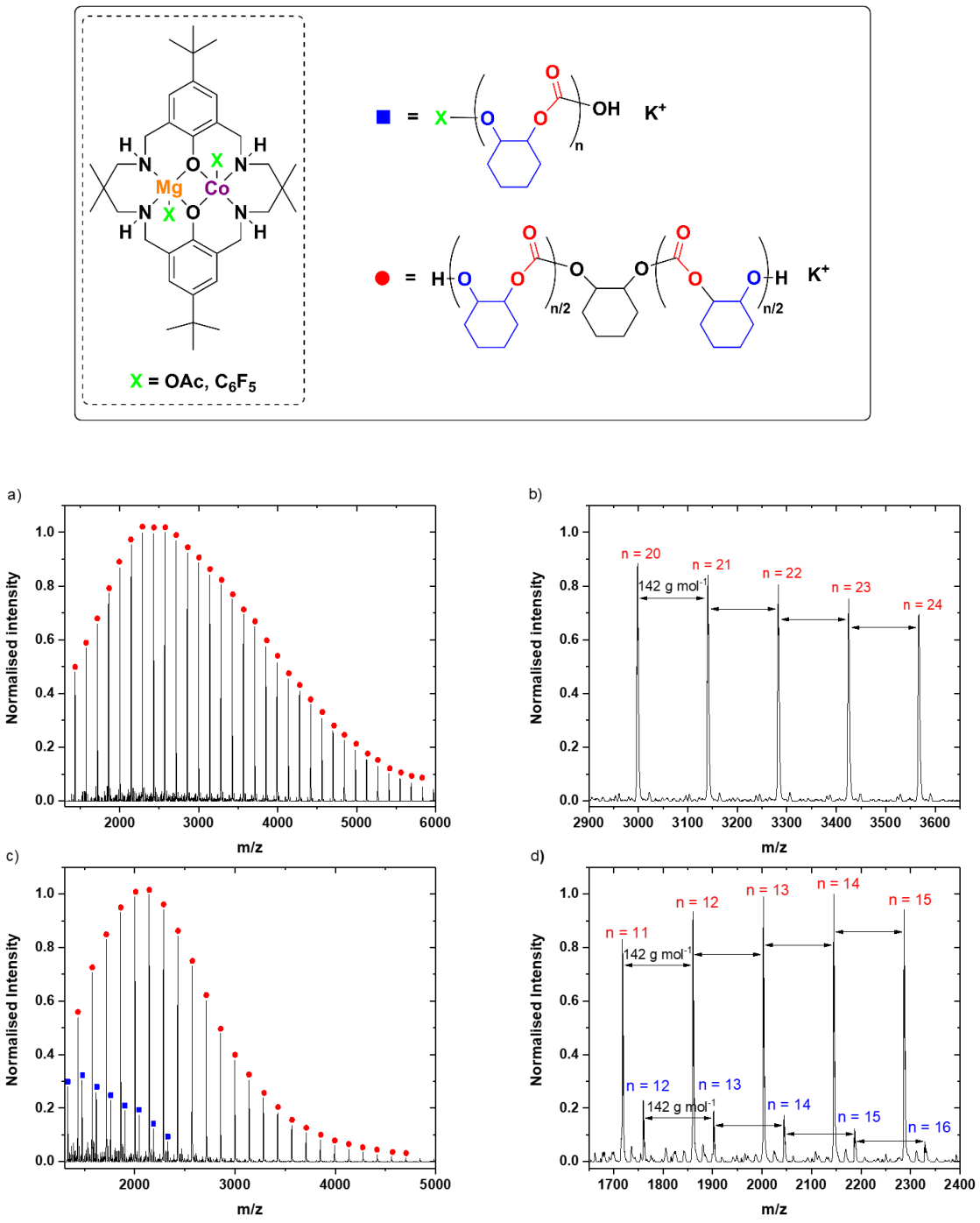

Figure 4.8: a) MALDI-ToF analysis of PCHC catalysed by **10** with 4 equivalents of CHD. b) Section of the MALDI-ToF in a). c) MALDI-ToF analysis of PCHC catalysed by **5.** (d) Section of the MALDI-ToF in c). Distributions end capped with CHD are denoted with ● and acetate end capped with ■.

Table 4.2: Data for the ROCOP of vCHO and CO_2 at 1 bar pressure with catalysts **5** and **10**.[a]

Polymer #	Co-ligand	vCHO Equiv.	Solvent	Time (h)	vCHO conv. (%)[b]	TOF (h^{-1})[c]	$M_{n,exp}$ [$Đ$] (kg mol^{-1})[d]	$M_{n,theo}$ (kg mol^{-1})[e]
P1	OAc	2000	Neat	1	33	660	16.7 [1.19]	27.7
P2	C_6F_5	2000	Neat	1	30	600	22.2 [1.08]	25.2
P3		6000	Neat	3	26	480	27.5 [1.14]	65.5
P4		2000	Toluene (4 M)	3	44	293	28.6 [1.10]	37.0

[a] Polymerisation conditions: 0.008 mmol of catalyst, 0.032 mmol of CHD, 1 bar of CO_2, 100 ˚C. [b] Determined by ^{1}H NMR spectroscopy. [c] TON divided by time. [d] Determined by GPC analysis in THF using a narrow polystyrene standard. [e] Determined by multiplying the TON by the molar mass of the repeat unit divided by the number of initiators

Once chain-end control was established, different conditions for the ROCOP of epoxide and CO_2 at 1 bar pressure were investigated with complex **10**. The epoxide was changed to 4-vinyl-cyclohexene oxide (vCHO) as this epoxide is easier to purify than CHO, and allows for polymer post-functionalisation *via* the double bond.[38-41] At a catalyst to epoxide ratio of 1:2000 and with 4 equivalents of cyclohexene diol (CHD) at 100 ˚C, the reaction after 1 h reached 30 % conversion of epoxide, with a TOF of 600 h^{-1} (Table 4.2, entry 2). The selectivity for carbonate linkages was excellent (> 99 %), and no cyclic carbonate was observed (by ^{1}H NMR spectroscopy). This performance is comparable to the acetate catalyst **5**, under identical conditions (Table 4.2, entry 1, TOF = 660 h^{-1}), signifying that the aryl co-ligands do not influence the polymerisation kinetics. The data is reassuring, as the true active species should be equivalent for both complexes **5** and **10**, although the initiation time for each complex may differ.[42] A stark difference in polycarbonate molar mass is seen by GPC, however; the reaction with complex **5** has 6 initiators, two of which are monofunctional, and hence leads to a bimodal molar mass distribution centred at 16.7 kg mol^{-1} (Figure 4.9a). In contrast, catalyst **10** has 4 bifunctional initiators, and produces a monodisperse distribution at 22.2 kg mol^{-1} (Figure 4.9b).

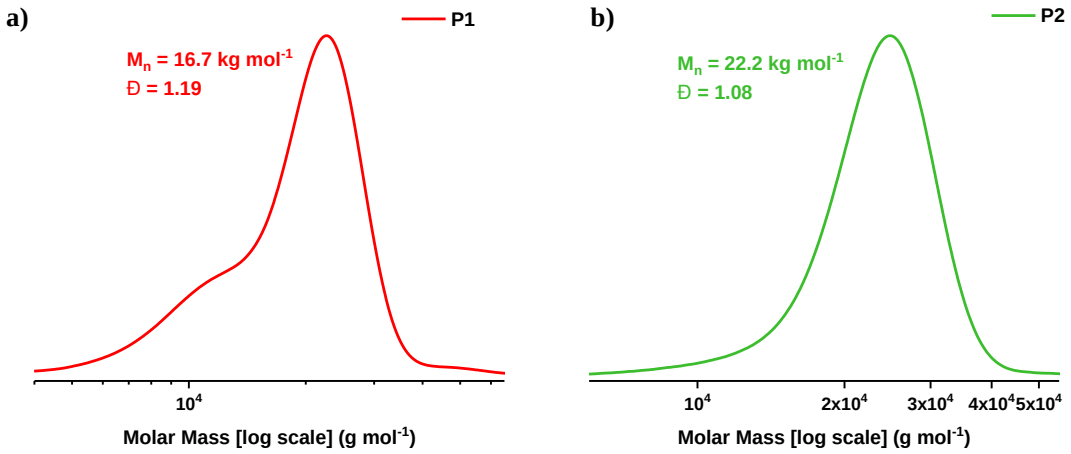

Figure 4.9: GPC analysis of a) **P1** and b) **P2**.

It is apparent that at lower catalyst loadings, the discrepancy between theoretical and experimental molar mass increases, most likely due to the higher concentration of diol (as impurities) present in the epoxide relative to the catalyst, which function as chain transfer agents (Table 4.2, **P3** and **P4**). Diluting the reaction in toluene results in a higher epoxide conversion, although with a drop in the activity, primarily due to the first order rate dependence of epoxide (TOF = 293 h^{-1}, Table 4.2, **P4**). The resulting polycarbonate M_n was 28 kg mol^{-1}. From these experiments, it is apparent that the molar mass does not continue to increase much with added monomer/solvent or with time, most likely this is because of diffusion and CO_2 solubility limitations under these experimental conditions.

4.4.2 CO_2/Epoxide ROCOP at 20 bar of CO_2

The copolymerisation was also tested in a reactor at 20 bar pressure of CO_2, which is expected to overcome diffusion and solubility limitations.[43] The polymerisations were carried out with 3 M vCHO or CHO in toluene, with 4 equivalents of CTA, at 80 ˚C, and at 0.017 to 0.010 mol % catalyst loading with respect to epoxide.

Table 4.3: Data for the copolymerisation of vCHO or CHO and CO_2 at 20 bar pressure using catalyst **10**.[a]

Polymer #	Epoxide	Epoxide equiv.	Time (h)	Epoxide Conversion (%)[b]	M_n [$Đ$] (kg mol^{-1})[c]
P5	vCHO	6000	18	33	70.7 [1.15]
P6	vCHO	6000	30	97	128.6 [1.10]
P7	vCHO	10000	30	95	162.8 [1.17]
P8	CHO	10000	18	94	121.6 [1.09]

[a] Polymerisation conditions: 0.008 mmol of **10**, 0.032 mmol of CHD, 3 M epoxide in toluene, 20 bar of CO_2, 80 ˚C. [b] Determined by ^{1}H NMR spectroscopy. [c] Determined by GPC analysis, in THF, using a narrow polystyrene standard.

At 0.017 mol % catalyst loading, the conversion of epoxide reached 33 % after 18 h (Table 4.3, **P5**). A polycarbonate molar mass of 70.7 kg mol^{-1} ($Đ$ = 1.15) was obtained. Repeating the experiment for 30 h allowed full conversion of the epoxide (97 %) and an increase in PvCHC molar mass to 128.6 kg mol^{-1} (Table 4.3, **P6**). A small low molar mass shoulder is apparent, at 35 kg mol^{-1} ($Đ$ = 1.15), most likely from the formation of new chains once the reaction becomes diffusion limited. Decreasing the loading further, to 0.01 mol % catalyst loading, led to a polymer molar mass of 162.8 kg mol^{-1} with a polydispersity of 1.17 (Table 4.3, **P7**). This is the highest molar mass PvCHC polymer reported to date. Figure 4.10 depicts the increase in PvCHC molar mass of polymers **P4**–**P7** that have been synthesised under different conditions.

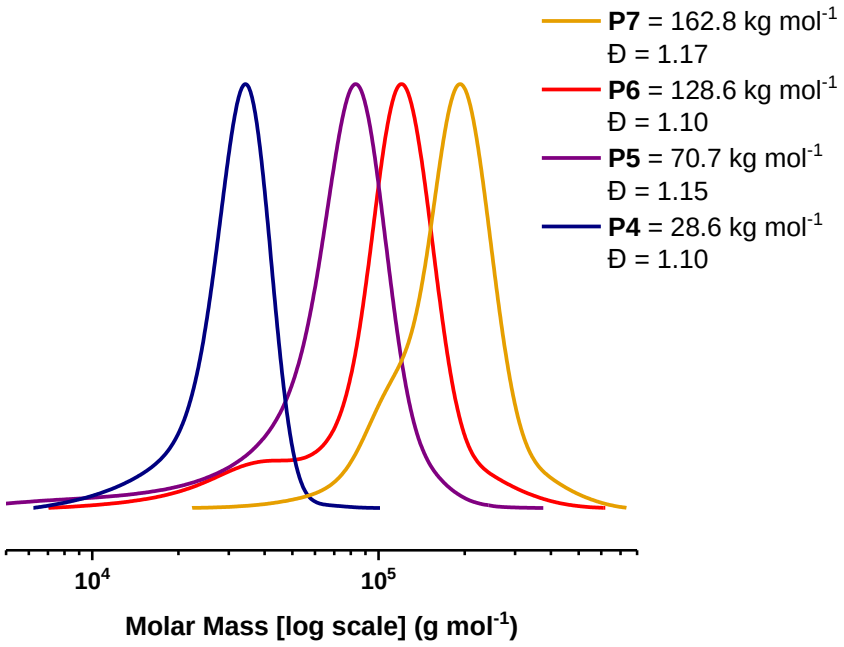

Figure 4.10: GPC analysis of the PvCHC polymers **P4**–**P7**.

The same polymerisation conditions were attempted with CHO as the epoxide monomer. In addition to cyclohexene diol and water, mono-cyclohexanol impurities are often present in CHO, which cannot be removed from a single distillation over CaH_2 as the drying agent.[44] Given that the strategy of this work is to use deliberate addition of diols as initiators, the presence of any monofunctional hydroxyl impurities may lead to bimodal molar mass distributions. Treating the CHO monomer with ^{n}BuLi as the drying agent, followed by a distillation under reduced pressure, was sufficient to successfully remove the mono-hydroxyl containing impurity, as seen indirectly by MALDI-ToF analysis of PCHC samples catalysed by **10** (Figure 4.10).

The polymerisation of this CHO with CO_2 using complex **10**, after 18 h, reached 94 % conversion of CHO after 18 h (Table 4.3, **P8**). Analysis of the resulting polymer by GPC showed a monomodal distribution of 121.6 kg mol^{-1} with a polydispersity of 1.09 (Figure

S4.9). The very narrow polydispersity signifies the high level of polymerisation control and purity of the monomer.

4.4.3 Thermal and Mechanical Properties of Polymers

The synthesis of high molar mass polymers provided a unique opportunity to investigate their material properties. Polymers **P4**–**P8** were precipitated twice from acidified methanol, and subsequently passed through a silica column to remove traces of catalyst. The purified polymers were then dried in a vacuum oven, and were isolated as white solids. Analysis by DSC showed that the glass transition temperatures (T_g) of the PvCHC polymers **P4**–**P7** were similar (within error), averaging at 115 ˚C, in close agreement with literature values (Table 4.4, Figure S4.11).[45] The fact that the T_g values do not increase with M_n suggests that the masses are already above entanglement.[46] By thermogravimetric analysis (TGA), the onset decomposition temperatures (T_d) were also the same, averaging at 273 ˚C (Table 4.4, Figure S4.12).

Table 4.4: Glass transition (T_g) temperature and onset decomposition temperature (T_d) for polymers **P4**–**P8**.

Polymer	M_n [$Đ$] (kg mol^{-1})[a]	T_g (˚C)[b]	T_d (˚C)[c]
P4	28.6 [1.10]	116	274
P5	70.7 [1.15]	114	274
P6	128.6 [1.10]	117	273
P7	162.8 [1.17]	118	270
P8	121.6 [1.09]	126	253

[a] Determined by GPC analysis in THF using a narrow polystyrene standard. [b] Determined by DSC at a heating rate of 20 ˚C/min from the second cycle. [c] Determined by TGA under a nitrogen atmosphere measured at 10 ˚C/min.

Polymers **P7** and **P8** were processed using a hot-press into a dog bone shape for tensile testing. To get homogeneously moulded samples of **P7**, the polycarbonate was pressed at 125 ˚C for 3 h. Analysis of the heated polymer revealed that it was no longer fully soluble in THF and chloroform. This suggests that partial cross-linking of the double bond occurred

during heating of the polymer sample. Hence, no tensile measurements were obtained, as the material physically changed upon heating. This was also reported for poly(limonene carbonate) (PLC), which possesses a terminal alkene;[14] a solution for the study was to hydrogenate the limonene oxide alkene prior to copolymerisation with CO_2, or to add an antioxidant such as Irganox®.[14]

Another strategy for sample preparation is solution casting of polymer films. Polycarbonates with low molar masses typically make poor films as they are very brittle.[14] Slow evaporation of **P7** in either DCM or toluene yielded transparent films, which were cut to size and shape for tensile testing (Figure 4.11). For **P8**, homogeneous films could not be obtained this way owing to the brittle nature of the material.

Figure 4.11: Dog bone shape of **P7**.

The tensile measurement data is summarised in Figure 4.12. Polymer **P7** exhibits a strain at break at 18.8 %, the tensile strength is 22.5 MPa, Young's modulus is 1.00 GPa, and the toughness is 3.6 MPA. The necking behaviour, which is observed as the flat region between the yield and breaking point, is indicative of ductility. The commercial polymers polyethylene terephthalate (PET) and bisphenol-A polycarbonate (BPA-PC) show the same behaviour, and are described as hard, strong, and tough plastics.[47] Compared to these commercial polymers, **P7** is a weaker material, as the strain at break for PET and BPA-PC are 3 and 20 times larger respectively, and 2–4 times the Young's modulus.[48] The tensile data for **P7** are similar to that reported by Greiner and co-workers for high molar mass PLC (M_n = 53.4 kg mol^{-1}, Young's modulus = 0.95 GPa, strain at break = 15 %), although the

material is much tougher (tensile strength = 55 MPa), as a result of the additional methyl groups on the cyclohexyl backbone.[12] Whilst PLC is a 100 % renewable polymer, it faces several challenges regarding catalysis and polymer processability. Only two classes of catalysts have been reported to copolymerise limonene oxide and CO_2 at high pressures, namely an Al(III) trisphenolate complex and [Zn(BDI)] catalysts,[49-50] the latter able to make block copolymers with other ROP cycles.[51-52] In terms of PLC's processability, the onset degradation (225 ˚C) is close to the glass transition temperature ($T_g \approx 130$ ˚C), and its melt viscosity is high, restricting most engineering applications.[12] There have been efforts to remediate the issue with chain end-capping agents and additives, although the addition of additive decreases the tensile strength (≈ 22 MPa).[12, 53] Therefore, vCHO could be used as a model substrate instead of LO, due to its ease of polymerisation and reasonable processing temperature window without the need for additives (although this requires further investigation).

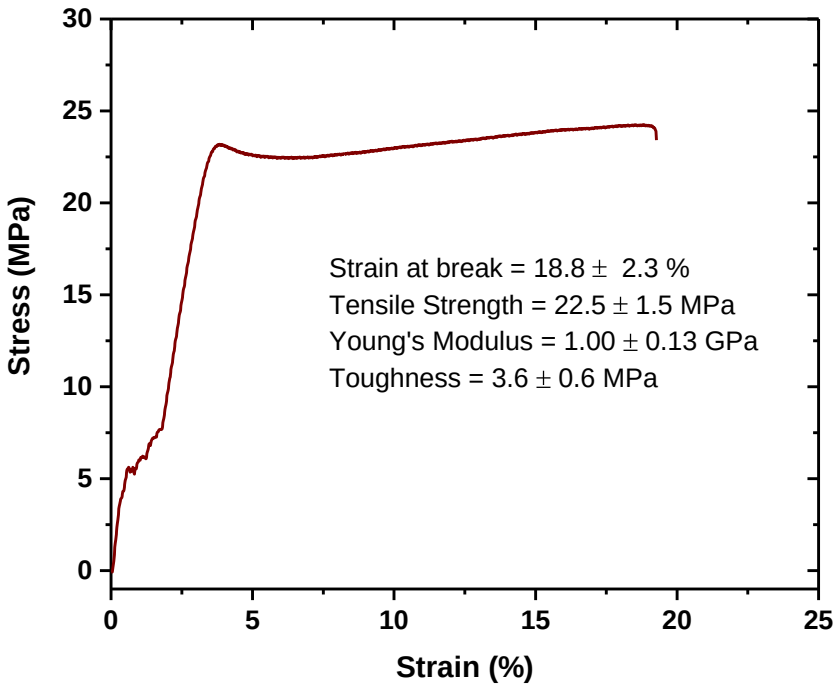

Figure 4.12: Stress-strain curve (representative of three repeats) of **P7**.

4.4 Discussion

The molar masses of the polymers catalysed by **10** are high compared to typical values in the field, which are typically in the polyol regime (< 20 kg mol^{-1}). Whilst this is not necessarily a negative outcome, as polyols are used in polyurethane production,[54-56] higher molar mass polymers are desirable to make materials. Most attempts at reaching high molar mass polycarbonate result in multimodal distributions, owing to mixed initiators in the polymerisation, and in some cases loss of catalytic activity at low catalyst loadings. However, there have been advancements on this front, using several different strategies.

Greiner and co-worker's report on high molar mass PLC demonstrated the importance epoxide purity in achieving higher molar masses and improved material properties.[12] A monomodal ($Đ$ = 1.10) distribution of 53.4 kg mol^{-1} was reached using [(BDI)Zn(OAc)] (Figure 4.13). The LO was pre-treated with NaH and MeI, which masks hydroxyls by *O*-methylation, and distilled to obtain a pure monomer as characterised by gas chromatography (GC). Rieger *et al.* used a similar catalyst, [(BDI^{CF3})Zn($N(SiMe_3)_2$)] (Figure 4.13), to scale-up the synthesis of PCHC (50 g of CHO, 10 bar of CO_2 in a 1 L Buchi reactor) at a [epoxide]:[catalyst] ratio of 2500:1, reporting a bimodal molar mass polymer (275 kg mol^{-1}, $Đ$ = 1.42) with a large dispersity owing to the impurities in CHO.[14] On the other hand, Feng and co-workers reported the effect of CO_2 drying agents on the molar mass and modality of its distribution for PCHC using triethyl borane (TEB) and PPNCl (Figure 4.13) as the catalytic system.[13] From the drying agents tested, bubbling CO_2 in triisobutylaluminium (TIBA) was found to be the only effective method to produce monomodal ultra-high molar mass PCHC, up to 450 kg mol^{-1} with a dispersity of 1.31 ([TEB]:[PPNCl]:[CHO] = 2:1:16000, 10 bar of CO_2, 80˚ C). No material properties were reported for their resulting PCHC samples. Whilst applying TIBA as a drying agent gave field leading molar masses,

the reagent reacts violently in contact with water and air, and is corrosive, making it difficult to handle safely and to use at a larger scale. Furthermore, the catalyst does not have chain-end control as it initiates *via* the chloride of the PPNCl co-catalyst. More recently, Li and co-workers employed a binary organocatalyst comprising of organophosphazenes and TEB for the copolymerisation of CO_2 and diverse epoxides.[57] Out of three organophosphazenes tested, the one with a relatively lower basicity and large molecular size, C_3N_3-Py-P_3 (Figure 4.13), exhibited the highest catalytic activity and selectivity for polycarbonate (TOF = 95 h^{-1}, [CHO]:[base]:[alcohol]:[TEB] = 500:1:2:6, 1 bar CO_2, 25 ˚C). Having demonstrated effective chain end control *via* MALDI-ToF spectrometry, they aimed for higher activities and molar mass polymers. The pressure of CO_2 was increased to 10 bar and CHO was distilled 3 times over NaH (as opposed to once from CaH_2), obtaining a polymer with a very high molar mass of 275.5 kg mol^{-1}, albeit with a bimodal distribution, reflected in the large polydispersity of 1.59 ([CHO]:[base]:[alcohol]:[TEB] = 24000:1:1:2, 10 bar CO_2, 80 ˚C).

By using complex **10**, high molar mass polycarbonates can be obtained in a simple and efficient manner, at very low loadings of catalyst ([epoxide]:[catalyst] = 10000:1) and with safer monomer purification methods (MeI is a carcinogen and TIBA is highly pyrophoric).

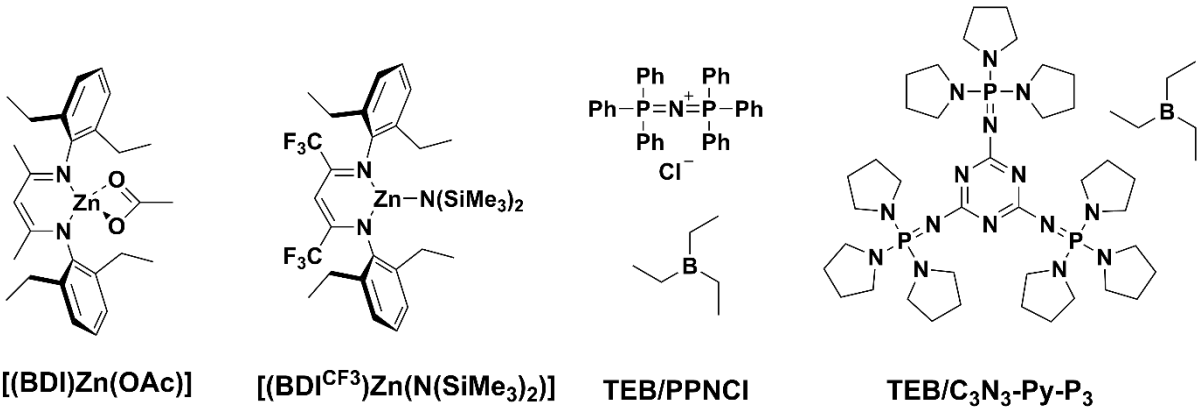

Figure 4.13: Structures of literature catalysts which have achieved the synthesis of high molar mass polycarbonates.

4.5 Summary and Outlook

4.5.1 Summary

In this chapter, a novel Mg(II)Co(II) complex with organometallic co-ligands (**10**) was synthesised and characterised, and then applied in CO_2/epoxide ROCOP. **10** was successfully characterised by XRD, NMR spectroscopy, SQUID magnetometry, and cyclic voltammetry. The complex is a rare example of a Co(II) organometallic. The organometallic co-ligands were installed as they are non-initiating in catalysis, allowing for chain-end control. Given that the CO_2 and epoxide monomers contain traces of diol impurities, these were deliberately added as initiators to give high molar mass polymers with monomodal distributions. It exhibited almost identical polymerisation rates compared to **5**, indicative of the same propagating species. Analysis by MALDI-ToF of a low molar mass PCHC sample revealed the presence of a single distribution, corresponding to α,ω-dihydroxy PCHC initiated by CHD. It was therefore possible to synthesise high molar mass PCHC and PvCHC ([**10**]:[CHD]:[epoxide] = 1:4:10000, 20 bar of CO_2, 80 ˚C), resulting in a molar mass of 121.6 and 162.8 kg mol^{-1}, respectively. The heterodinuclear organometallic catalyst is both highly active for CO_2/epoxide ROCOP and does not initiate polymerisation, features which are not common in other literature catalysts. The tensile properties of the PvCHC polymer with the highest M_n, **P7**, shows that it is less brittle than PCHC, and could potentially be used as a model for PLC.

4.5.2 Outlook

The presence of readily cleavable co-ligands is attractive for both the synthesis of high molar mass polymers and further studies of reaction intermediates during the catalysis, which would strengthen reaction mechanism claims.

To complete the study on organometallic homodinuclear complexes, the Mg(II)Mg(II) complex with C_6F_5 co-ligands should be synthesised and characterised. A similar synthetic route with $Mg(C_6F_5)_2$ should be applied, or *via* transmetallation of [LMgMgBr_2], a compound already reported,[16] with the appropriate metal alkyl reagent.

The current investigation can be extended to examine the effect of polycarbonate molar mass and modality on the tensile properties, to understand whether monomodal, high molar mass polymers offer any benefits. This would require analysing **P4**–**P6** and high molar mass polymers with bimodal distributions synthesised using complex **5**.

To further improve the tensile properties and processability of the polycarbonate polymers, short chain plasticisers, synthesised from the same catalyst, can be explored. Upon blending, these samples may provide ductility to the brittle polycarbonate material.[46, 53] Another option includes using low T_g macroinitiators, such as a short chain of PCL or poly(ethylene glycol) (PEG), at a composition at which the blocks are still miscible. There are existing studies of such materials, although the M_n is typically low (< 50 kg mol^{-1}).[10, 58]

Another industrially relevant polycarbonate is poly(propylene carbonate) (PPC), synthesised from the ROCOP of CO_2 and propylene oxide (PO). Catalyst **10** is inactive for this polymerisation, whereas the macrocyclic Co(III)K(I) heterodinuclear catalyst with acetate co-ligands published by our group shows excellent activity and selectivity.[59] This Co(III)K(I) catalyst suffers the same drawbacks as complex **5,** as it possesses initiating acetate co-ligands. Modifying the complex to possess non-initiating co-ligands would be beneficial to synthesise monodisperse, high molar mass PPC polymer and block co-polymers. As mentioned previously, Co(III) alkyls are more commonly found in the literature, suggesting that this modification is synthetically viable.

4.6 References

1. Hepburn, C.; Adlen, E.; Beddington, J.; Carter, E. A.; Fuss, S.; Mac Dowell, N.; Minx, J. C.; Smith, P.; Williams, C. K., *Nature* **2019,** *575* (7781), 87-97.

2. Grignard, B.; Gennen, S.; Jérôme, C.; Kleij, A. W.; Detrembleur, C., *Chem. Soc. Rev.* **2019,** *48* (16), 4466-4514.

3. Inoue, S.; Koinuma, H.; Tsuruta, T., *J. Polym. Sci., Part B: Polym. Lett.* **1969,** *7* (4), 287-292.

4. Poland, S. J.; Darensbourg, D. J., *Green Chem.* **2017,** *19* (21), 4990-5011.

5. Kozak, C. M.; Ambrose, K.; Anderson, T. S., *Coord. Chem. Rev.* **2018,** *376*, 565-587.

6. Zhang, D.; Boopathi, S. K.; Hadjichristidis, N.; Gnanou, Y.; Feng, X., *J. Am. Chem. Soc.* **2016,** *138* (35), 11117-11120.

7. Darensbourg, D. J.; Wu, G.-P., *Angew. Chem. Int. Ed.* **2013,** *52* (40), 10602-10606.

8. Kember, M. R.; Williams, C. K., *J. Am. Chem. Soc.* **2012,** *134* (38), 15676-15679.

9. Darensbourg, D. J., *Chem. Rev.* **2007,** *107* (6), 2388-2410.

10. Sulley, G. S.; Gregory, G. L.; Chen, T. T. D.; Peña Carrodeguas, L.; Trott, G.; Santmarti, A.; Lee, K.-Y.; Terrill, N. J.; Williams, C. K., *J. Am. Chem. Soc.* **2020,** *142* (9), 4367-4378.

11. Chen, T. T. D.; Zhu, Y.; Williams, C. K., *Macromolecules* **2018,** *51* (14), 5346-5351.

12. Hauenstein, O.; Reiter, M.; Agarwal, S.; Rieger, B.; Greiner, A., *Green Chem.* **2016,** *18* (3), 760-770.

13. Jia, M.; Hadjichristidis, N.; Gnanou, Y.; Feng, X., *ACS Macro Lett.* **2019**, 1594-1598.

14. Kernbichl, S.; Rieger, B., *Polymer* **2020,** *205*, 122667.

15. Romain, C.; Garden, J. A.; Trott, G.; Buchard, A.; White, A. J. P.; Williams, C. K., *Chem. Eur. J.* **2017,** *23* (30), 7367-7376.

16. Garden, J. A.; Saini, P. K.; Williams, C. K., *J. Am. Chem. Soc.* **2015,** *137* (48), 15078-15081.

17. Kember, M. R.; Jutz, F.; Buchard, A.; White, A. J. P.; Williams, C. K., *Chem. Sci.* **2012,** *3* (4), 1245-1255.

18. Smith, C. F.; Tamborski, C., *J. Organomet. Chem.* **1971,** *32* (2), 257-262.

19. Royo, P.; Vazquez, A., *J. Organomet. Chem.* **1981,** *204* (2), 243-247.

20. Kember, M. R.; Knight, P. D.; Reung, P. T. R.; Williams, C. K., *Angew. Chem. Int. Ed.* **2009,** *48* (5), 931-933.

21. Deacy, A. C. Understanding Metal Synergy in Heterodinuclear Catalysts for CO2/Epoxide Copolymerization. University of Oxford, 2019.

22. Stalick, J. K.; Corfields, P. W. R.; Meek, D. W., *Inorg. Chem.* **1973,** *12* (7), 1668-1675.

23. Lehr, M.; Paschelke, T.; Trumpf, E.; Vogt, A.-M.; Näther, C.; Sönnichsen, F. D.; McConnell, A. J., *Angew. Chem. Int. Ed.* **2020,** *59* (43), 19344-19351.

24. Pell, A. J.; Pintacuda, G.; Grey, C. P., *Prog. Nucl. Magn. Reson. Spectrosc.* **2019,** *111*, 1-271.

25. Mabbs, F. E.; Manchin, D. J., *Magnetism and Transition Metal Complexes*. Dover Publications: 2008.

26. Jurca, T.; Farghal, A.; Lin, P.-H.; Korobkov, I.; Murugesu, M.; Richeson, D. S., *J. Am. Chem. Soc.* **2011,** *133* (40), 15814-15817.

27. Atanasov, M.; Aravena, D.; Suturina, E.; Bill, E.; Maganas, D.; Neese, F., *Coord. Chem. Rev.* **2015,** *289-290*, 177-214.

28. Rossi, A. R.; Hoffmann, R., *Inorg. Chem.* **1975,** *14* (2), 365-374.

29. Hay-Motherwell, R. S.; Wilkinson, G.; Hussain, B.; Hursthouse, M. B., *Polyhedron* **1990,** *9* (7), 931-937.

30. Zhu, D.; Janssen, F. F. B. J.; Budzelaar, P. H. M., *Organometallics* **2010,** *29* (8), 1897-1908.

31. Demarteau, J.; Debuigne, A.; Detrembleur, C., *Chem. Rev.* **2019,** *119* (12), 6906-6955.

32. Deacy, A. C.; Kilpatrick, A. F. R.; Regoutz, A.; Williams, C. K., *Nat. Chem.* **2020,** *12* (4), 372-380.

33. Matić, M.; Katić, M.; Denegri, B.; Kronja, O., *J. Org. Chem.* **2017,** *82* (15), 7820-7831.

34. Lidston, C. A. L.; Abel, B. A.; Coates, G. W., *J. Am. Chem. Soc.* **2020,** *142* (47), 20161-20169.

35. Trott, G. Heterodinuclear Catalysts for CO2/Epoxide Copolymerisations. University of Oxford, 2018.

36. Reis, N. V. Homogeneous catalysts for the ROCOP of CO2 and epoxides. University of Oxford, 2020.

37. Deacy, A. C.; Durr, C. B.; Garden, J. A.; White, A. J. P.; Williams, C. K., *Inorg. Chem.* **2018,** *57* (24), 15575-15583.

38. Yi, N.; Chen, T. T. D.; Unruangsri, J.; Zhu, Y.; Williams, C. K., *Chem. Sci.* **2019,** *10* (43), 9974-9980.

39. Chang, C.-H.; Tsai, C.-Y.; Lin, W.-J.; Su, Y.-C.; Chuang, H.-J.; Liu, W.-L.; Chen, C.-T.; Chen, C.-K.; Ko, B.-T., *Polymer* **2018,** *141*, 1-11.

40. Zhang, H.; Liu, B.; Ding, H.; Chen, J.; Duan, Z., *Polymer* **2017,** *129*, 5-11.

41. Zhang, J.-F.; Ren, W.-M.; Sun, X.-K.; Meng, Y.; Du, B.-Y.; Zhang, X.-H., *Macromolecules* **2011,** *44* (24), 9882-9886.

42. Trott, G.; Garden, J. A.; Williams, C. K., *Chem. Sci.* **2019,** *10* (17), 4618-4627.

43. Foltran, S.; Cloutet, E.; Cramail, H.; Tassaing, T., *J. Supercrit. Fluids* **2012,** *63*, 52-58.

44. Deng, J.; Ratanasak, M.; Sako, Y.; Tokuda, H.; Maeda, C.; Hasegawa, J.-y.; Nozaki, K.; Ema, T., *Chem. Sci.* **2020,** *11* (22), 5669-5675.

45. Lin, P.-M.; Chang, C.-H.; Chuang, H.-J.; Liu, C.-T.; Ko, B.-T.; Lin, C.-C., *ChemCatChem* **2016,** *8* (5), 984-991.

46. Koning, C.; Wildeson, J.; Parton, R.; Plum, B.; Steeman, P.; Darensbourg, D. J., *Polymer* **2001,** *42* (9), 3995-4004.

47. Cywar, R. M.; Rorrer, N. A.; Hoyt, C. B.; Beckham, G. T.; Chen, E. Y. X., *Nat. Rev. Mater.* **2022,** *7* (2), 83-103.

48. CHEMnetBASE - Polymers: a Property Database. http://poly.chemnetbase.com/faces/polymers/PolymerSearch.xhtml (accessed Feb 22).

49. Peña Carrodeguas, L.; González-Fabra, J.; Castro-Gómez, F.; Bo, C.; Kleij, A. W., *Chem. Eur. J.* **2015,** *21* (16), 6115-6122.

50. Byrne, C. M.; Allen, S. D.; Lobkovsky, E. B.; Coates, G. W., *J. Am. Chem. Soc.* **2004,** *126* (37), 11404-11405.

51. Carrodeguas, L. P.; Chen, T. T. D.; Gregory, G. L.; Sulley, G. S.; Williams, C. K., *Green Chem.* **2020,** *22* (23), 8298-8307.

52. Neumann, S.; Däbritz, S. B.; Fritze, S. E.; Leitner, L.-C.; Anand, A.; Greiner, A.; Agarwal, S., *Polym. Chem*, **2021,** *12* (6), 903-910.

53. Neumann, S.; Leitner, L.-C.; Schmalz, H.; Agarwal, S.; Greiner, A., *ACS Sustain. Chem. Eng.* **2020,** *8* (16), 6442-6448.

54. Lee, S. H.; Cyriac, A.; Jeon, J. Y.; Lee, B. Y., *Polym. Chem*, **2012,** *3* (5), 1215-1220.

55. Langanke, J.; Wolf, A.; Hofmann, J.; Böhm, K.; Subhani, M. A.; Müller, T. E.; Leitner, W.; Gürtler, C., *Green Chem.* **2014,** *16* (4), 1865-1870.

56. Xian, W.; Song, L.; Liu, B.; Ding, H.; Li, Z.; Cheng, M.; Ma, L., *J. Appl. Polym. Sci.* **2018,** *135* (11), 45974.

57. Zhang, J.; Wang, L.; Liu, S.; Li, Z., *Angew. Chem. Int. Ed.* **2022,** *61* (4), e202111197.

58. Zhang, Y.-Y.; Yang, G.-W.; Wang, Y.; Lu, X.-Y.; Wu, G.-P.; Zhang, Z.-S.; Wang, K.; Zhang, R.-Y.; Nealey, P. F.; Darensbourg, D. J.; Xu, Z.-K., *Macromolecules* **2018,** *51* (3), 791-800.

59. Deacy, A. C.; Moreby, E.; Phanopoulos, A.; Williams, C. K., *J. Am. Chem. Soc.* **2020,** *142* (45), 19150-19160.

Chapter 5

Synthesis and Study of Novel Nickel(II) Complexes in Polymerisation Catalysis

"Catalysts are the conductors who choreograph the chemical dance that results in the formation of new structures."

Robert H. Grubbs

5.1 Introduction

Polyethylene (PE") is the most widely used polymer with a multitude of applications in commodity goods ranging from food packaging to water pipes. It benefits from low cost, easy processability, and high versatility. There are three main classes of polyethylene: high-density polyethylene (HDPE), low density polyethylene (LDPE), and linear low-density polyethylene (LLDPE) (Figure 5.1). Each possesses different microstructures, and hence offers different thermal and mechanical properties.

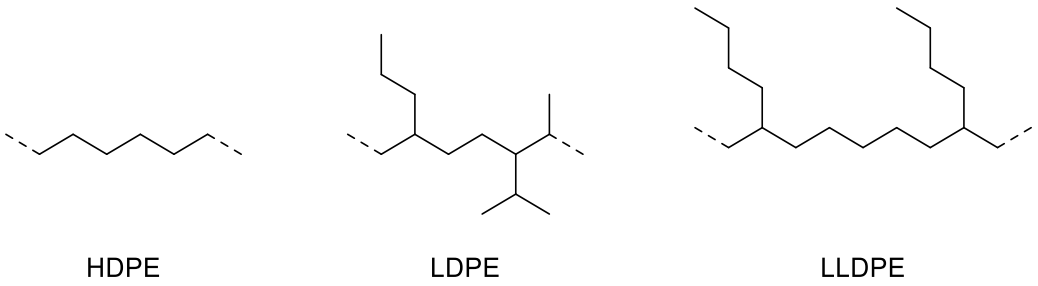

Figure 5.1: Classes of polyethylene with varying mechanical properties and applications. HDPE = high-density polyethylene, LDPE = low density polyethylene, and LLDPE = linear low-density polyethylene

PE" can be efficiently synthesised by early transition metal (TM) complexes, such as Ziegler Natta catalysts.[1-2] Alternatively, late TM (*i.e.* Ni and Pd) catalysts are also possible and have the benefit of being tolerant to alkenes featuring polar functional groups.[3-6] They may produce more branched PE", by a mechanism called “chain walking”. This process is characterised by a series of sequential β-hydrogen eliminations (BHE) and 2,1-alkene reinsertions which lead to the apparent migration of a metal active site along the growing hydrocarbon chain. The chain walking process may be enhanced or supressed by tuning the properties of the ancillary ligand.

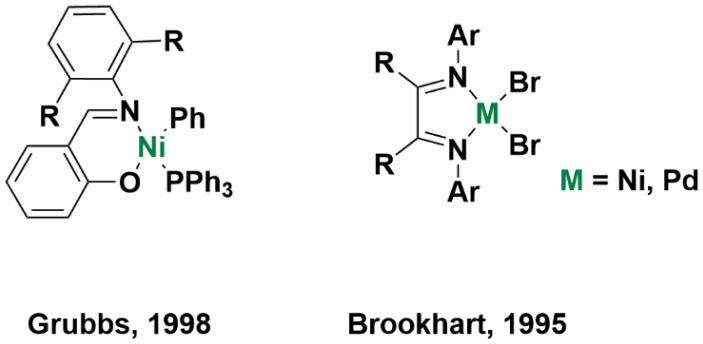

Figure 5.2: Structures of the Group 10 metal catalysts for ethylene polymerisation developed by Grubbs and Brookhart.[7-8]

Nickel-based catalysts for the synthesis of linear and branched PE" have been widely explored since their first report by Grubbs and co-workers in the form of a neutral Ni(II) complex and by Brookhart and co-workers as a cationic Ni(II) species in 1998 and 1995, respectively (Figure 5.2).[7-9] Grubbs's catalyst system, using a phenoxyiminato ligand, was particularly important as it was the first example of a neutral catalyst which did not require a co-catalyst to initiate olefin polymerisation. For neutral Ni catalysts, polymer microstructures can be varied by tuning the steric hinderance at axial sites with respect to the tetra-coordinated nickel centre, controlling the electron density of the metal centre, or controlling the steric bulk of *ortho*-phenoxy ring substituents.[10-12] Near-complete inhibition of β-hydrogen elimination can be achieved by introducing electron-withdrawing groups on N-terphenyl motifs of the ancillary ligand. These catalysts exhibit living polymerisation behaviour, in which one linear chain of PE" grows per metal centre, producing ultra-high molecular weight polyethylene (UHMWPE) with high degree of crystallinity.[13-14]

The accumulation of durable polyethylene plastics and their persistence in our environment has led to a growing interest in degradable polymers. One solution is to use oxygen-containing polyethylene mimetics, which exhibit similar physical properties but with the added benefit of being hydrolytically, enzymatically, or photolitically degradable. Successful examples include polyesters comprised of long-chain aliphatic units, such as

polycondensates,[15-16] products of ring-opening polymerisation (ROP) of lactones and macrolactones,[17] co-polymerisation of ethylene and CO to make polyketones,[18-19] and block polymers of polyethylene. Block polymers of polyethylene and oxygenated polymers may be able to combine the beneficial properties of polyethylene with the degradation capability of the oxygenated polymer. They could also be suitable as blend compatibalisers,[20] as the homopolymers are usually immiscible. The importance for the synthesis of such block copolymers containing polyolefin units has grown and several approaches have been reported.[21-22] The most common approach is based on the anionic polymerisation of butadiene followed by post-polymerisation, hydrogenation, and coordination-insertion polymerisation of lactide.[23] Alternatively, PE" synthesised in a living manner allows creation of end-functionalised macromolecules,[24] which can be used as macroinitiators capable of reacting with polar monomers. This method suffers from low productivity as only one chain is grown per metal centre,[24] although this drawback can be alleviated by using chain transfer agents such as zinc or aluminium alkyls.[25] Another approach is to use traditional non-living PE" catalysts, in which polymer chains terminate *via* BHE, yielding olefinic end groups which can be subject to post-polymerisation functionalisation.[21]

The methods outlined above require multiple steps, including purification of intermediates, and use of different catalysts, making the process more time consuming and expensive with each manipulation. An alternative strategy would be to “switch” from a metal carbon bond of a growing PE" chain to a metal-oxygen bond which can initiate oxygenate polymerisation, e.g. ROP, with a single catalyst. One recent example is a cobalt catalyst capable of switching between organometallic-mediated radical polymerisations and ROCOP, but it requires at least one workup and a change in Co oxidation state.[26]

Organometallic complexes using Group 4 and Group 10 metals may be interesting candidates to such a route as they have precedence in ethylene polymerisation.[9, 27] The first

challenge is to find a system that can accomplish both modes of catalysis. There are examples of Group 4 complexes for lactone ROP and epoxide ROCOP.[28-30] One study, from our group, investigated Ti(IV) complexes coordinated by *ortho*-vanillin derived phenoxyiminato ligands and two isopropoxide co-ligands. The complexes were active for both ROP of lactones and chain growth of ethylene.[31] Proving that both catalyses work separately with a single catalyst system is the first step towards achieving tandem catalysis. Such reactions have not been established using a Group 10 metal complex, such as Ni(II), but there are some complexes reported for lactone ROP or epoxide/CO_2 ROCOP catalysis.[32-34] Nickel alkoxides could function as initiators for both types of polymerisation. Few examples of nickel alkoxide complexes have been isolated and characterised; complexes are either very reactive or form dimers, so stabilising co-ligands such as pincer-type ligands are commonly utilised.[35-42] Nevertheless, the synthesis of such complexes is underexplored, as well as their application in ROP and ROCOP.

5.2 Aims

This work seeks to prepare phenoxyiminato ligated Ni(II) complexes for both ethylene and lactone polymerisation. A series of simple (single-step synthesis) ligands based on *ortho*-vanillin will be prepared with a range of commercially available amines, and subsequently complexed with Ni(II) precursors to make neutral Ni(II) complexes. They will be tested for ethylene polymerisation at different pressures and temperatures, and the resulting polymers will be analysed by NMR spectroscopy, GPC, and DSC.

Following this, different strategies to make nickel alkoxide complexes will be investigated, using the same phenoxyiminato ligand. If successful, they will be fully characterised and tested for lactone ROP.

5.3 Synthesis and Characterisation of O*rtho*-vanillin Phenoxyiminato Ni(II) Complexes

The Ni(II) complexes featuring an *ortho*-vanillin-derived ligand were prepared from an adapted literature procedure.[8] The target ligands (**HL$_n$**) were synthesised by the reaction of *ortho*-vanillin and the appropriate amine, in refluxing ethanol, with catalytic amounts of formic acid (Scheme 5.1), and were obtained in high yields (80–98%). The sodium salt of the ligands (**NaL$_n$**) were subsequently formed by treatment of **HL$_n$** with NaH, in THF, and were isolated in quantitative yields and used without further purification. The target complexes were synthesised, using an adapted literature procedure,[43] through the reaction with *trans*-[NiClPh(PPh$_3$)$_2$] with **NaL$_n$**, in toluene (Scheme 5.1). After washing the crude product with hexane, the desired complexes **11a**, **12a**, and **13a** were obtained in moderate yields (30–55 %). In the case of the complex with the adamantly substituent, **HL$_4$**, NMR scale experiments produced paramagnetic compounds and protonated ligand, and hence further investigations were not undertaken.

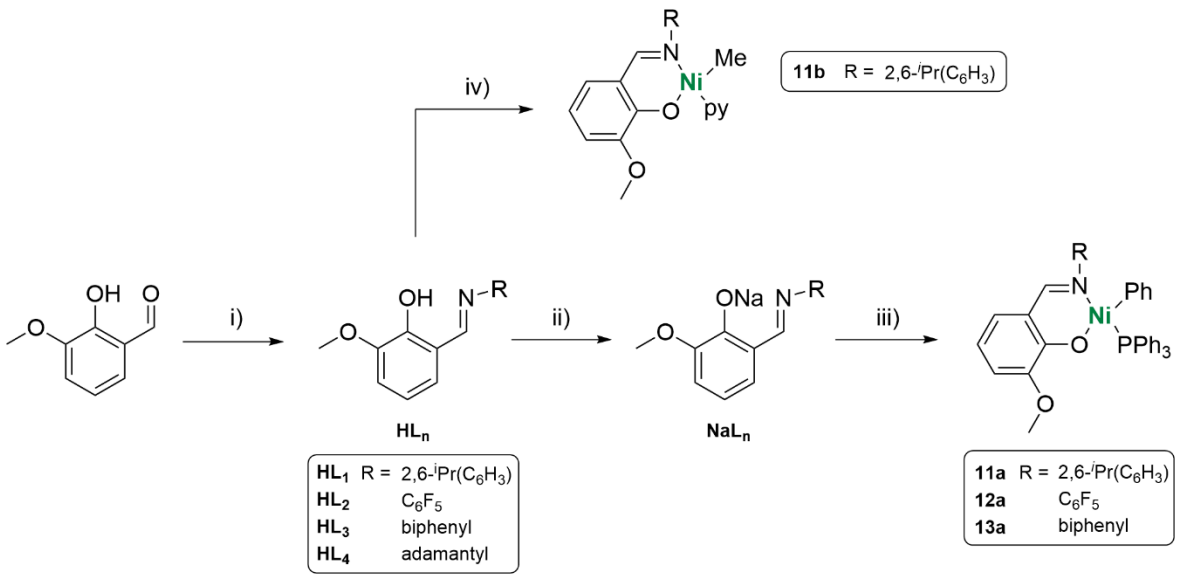

Scheme 5.1: Synthesis of complexes **11a, 12a, 13a, 13b**. i) H_2NR, cat. formic acid, EtOH, reflux. ii) NaH, THF, RT. iii) *trans*-[NiClPh(PPh$_3$)$_2$], toluene. iv) [(TMEDA)Ni(Me)$_2$], pyridine (20 equiv.), benzene, RT, 30 min.

Complexes **11a**–**13a** were characterised by ^{1}H, ^{31}P, and ^{13}C NMR spectroscopy (Figure S5.1–S5.10). In the ^{1}H NMR spectrum of each compound, a doublet was observed for the imine proton, as a result of $^{4}J_{HP}$ coupling (7.9–8.9 Hz) between HC=N–Ni–PPh$_3$, which indicates these ligands are in a trans disposition.[8] An example ^{1}H NMR spectrum is presented in Figure 5.3 for complex **11a**. The diisopropyl groups are diastereotopic, with two doublet resonances for the two sets of methyl protons (a and b in Figure 5.3), which couple to the corresponding proton at 4.07 ppm (c). The synthesis of **11a** has already been reported, however it was not fully characterised.[44]

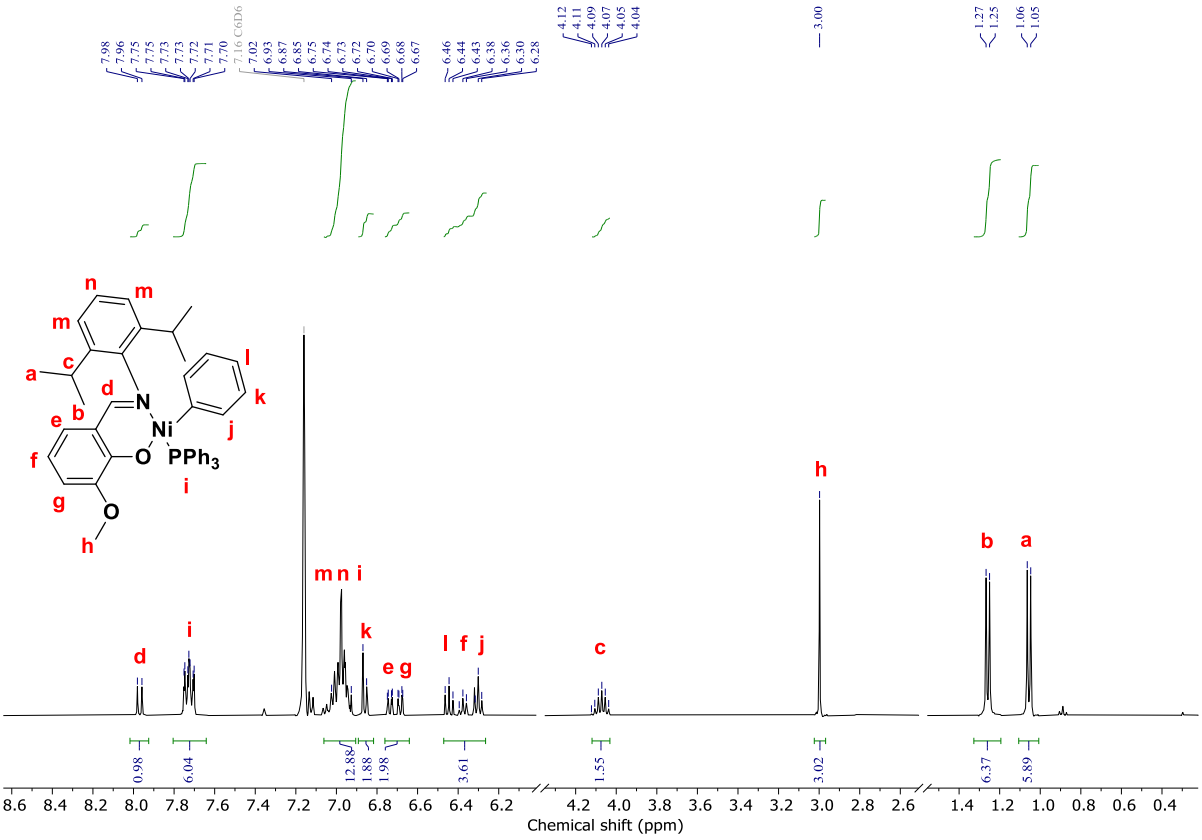

Figure 5.3: ^{1}H NMR (C_6D_6, 400 MHz) spectrum of **11a** (Figure S5.1 for full spectrum).

Crystals, suitable for X-ray diffraction, were obtained by cooling a saturated solution of the complexes in hexane to −30 °C: the solid-state structures are presented in Figure 5.4. The complexes display square planar geometries, which can be expected for a Ni(II) (d^8) complex, with the N and P atoms disposed *trans* to each other. The bond lengths and angles

for these complexes are similar (Table 5.1). Comparing **11a** with a complex possessing a ^{t}Bu group instead of methoxy group to the phenolate, the Ni-P bond is shorter (2.1931(12) compared to 2.1815(4) Å), which could have implications in the subsequent catalysis.[45]

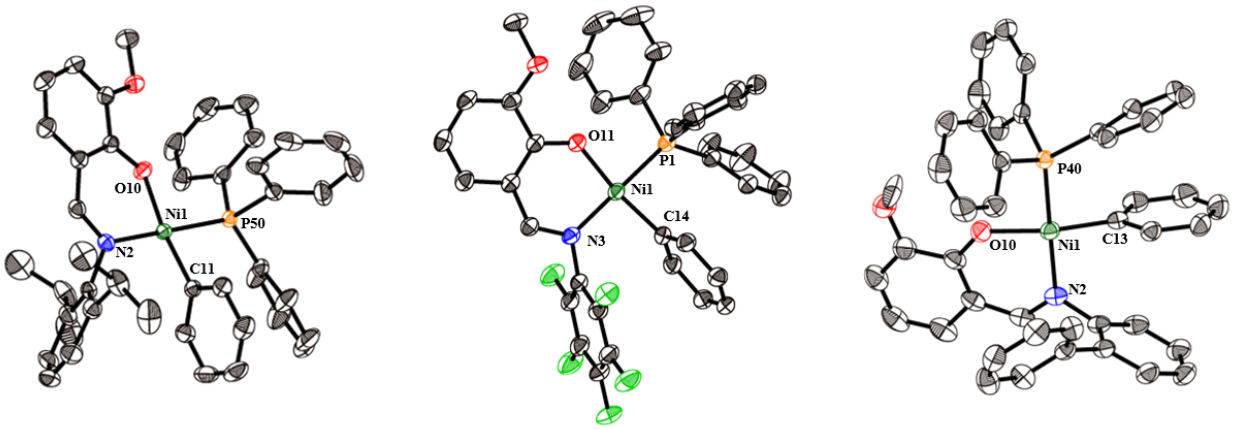

11a **12a** **13a**

Figure 5.4: Solid state structures solved by XRD of complexes **11a**–**13a**. H atoms omitted for clarity. Thermal ellipsoids at the 50 % probability level. Ni = dark green, P = orange, O = red, N = blue, F = green, C = grey.

Table 5.1: Selected bond lengths and angles of complexes **11a**, **12a**, and **13a**.

Bond/Angle	**11a**	**12a**	**13a**
Ni-P (Å)	2.1815(4)	2.1704(6)	2.1695(4)
Ni-C (Å)	1.8991(3)	1.8973(19)	1.8875(16)
Ni-O (Å)	1.8941(3)	1.8920(14)	1.9010(12)
Ni-N (Å)	1.9275(1)	1.9222(17)	1.9184(13)
P-Ni-N (°)	179.56(4)	175.94(5)	174.41(4)
O-Ni-C (°)	172.33(5)	167.79(8)	167.71(7)
P-Ni-O (°)	87.90(3)	87.93(5)	88.57(4)
C-Ni-N (°)	92.94(5)	92.47(7)	91.68(5)

"Phosphine-free" nickel phenoxyiminato complexes were also synthesised using a modified literature procedure with pyridine as co-ligand (Scheme 5.1). The pyridine is reported as

being a labile dissociating ligand and hence leads to more active ethylene polymerisation catalysts.[46-47] Treatment of [(TMEDA)Ni(CH_3)$_2$], which was synthesised according to a literature procedure (Figure S5.11),[48] with ligand **HL$_1$** and pyridine (20 equiv.) yielded complex **11b**. Characterisation by ^{1}H NMR spectroscopy shows three new signals for coordinated pyridine (8.78, 6.61, and 6.27 ppm) and one new signal at –0.66 ppm diagnostic of metal bound methyl group (Figure 5.5).

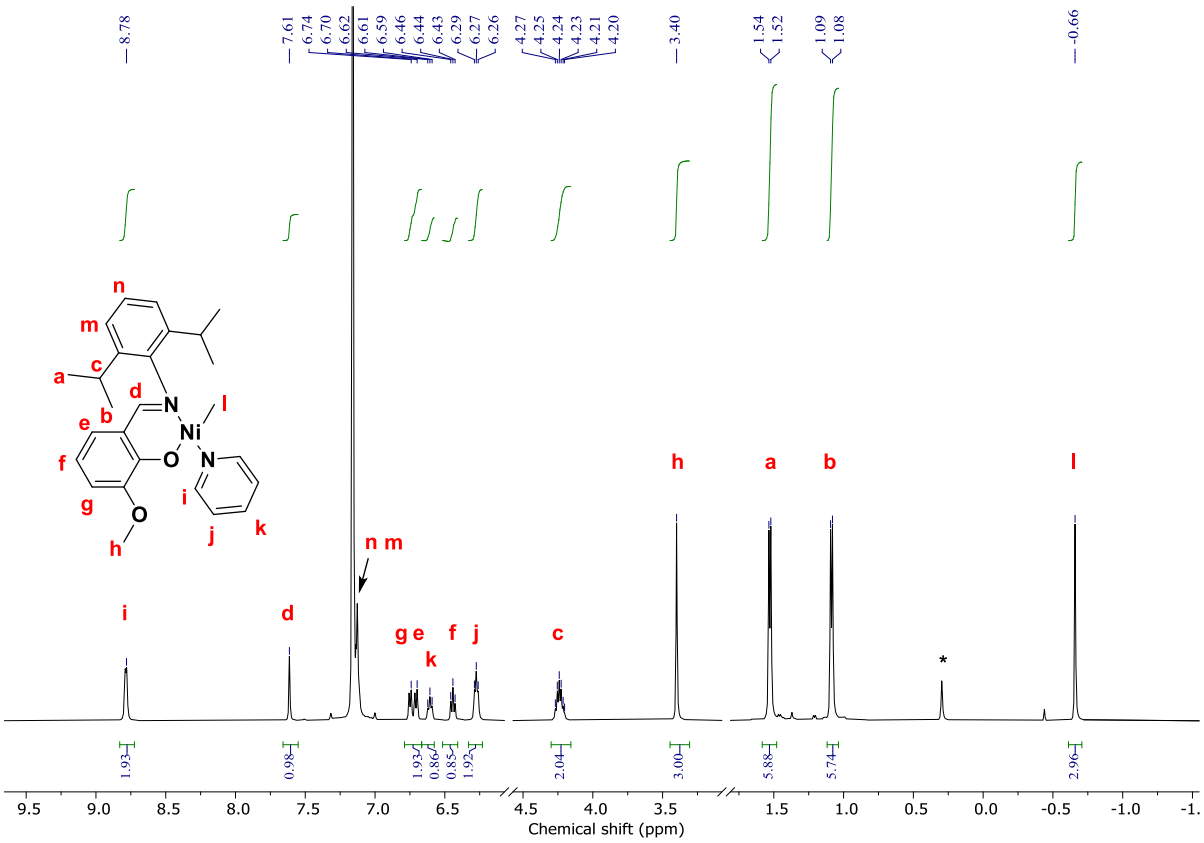

Figure 5.5: ^{1}H NMR spectrum (C_6D_6, 400 MHz) of complex **11b**. * denotes silicone grease peak (Figure S5.12 for full spectrum).

5.4 Ethylene Polymerisation

The complexes **11a**, **11b**, **12a**, and **13a** were subject to ethylene polymerisation, in toluene, under a range of conditions. For complexes with PPh_3 as the labile co-ligand, Ni(COD)$_2$ is often used as a phosphine scavenger to activate the catalyst and promote coordination of

ethylene.[8] Data for polymerisation at low (2 bar) and high (40 bar) pressures are reported in Table 5.2.

Table 5.2: Ethylene homopolymerisation data with catalysts **11a**, **11b**, **12a**, and **13a**.[a]

Entry	Cat.	Ethylene Pressure (bar)	Co-catalyst	T (˚C)	t (min)	Yield (g)	TOF (h^{-1})[b]	M_n (kg mol^{-1}) [$Đ$][c]	Branching/1000 C[c]	T_m (˚C)[f]
1	**11a**	2	✓	25	90	0.09	103	3.6 [1.58]	23	101
2	**11a**	2	-	25	90	0.14	154	8.6 [1.51]	30	92
3	**11a**	2	✓	60	90	0.57	648	5.1[d] [-]	57[e]	/ [h]
4	**11a**	40	-	25	60	0.10	175	4.3 [2.5]	9	116
5	**11a**	40	-	45	60	0.49	835	11.5 [1.49]	12	111
6	**11a**	40	-	60	60	6.51	11043	10.3 [1.70]	18	106
7	**11b**	40	-	25	60	0.04	68	4.4 [1.89]	9	118
8	**11b**	40	-	45	60	0.47	800	13.7 [1.65]	13	111
9	**11b**	40	-	60	60	5.29	8979	28.7 [1.92]	15	107
10	**12a**	2	✓	25	90	0.02	20	-	-	/ [h]
11	**12a**	2	✓	60	90	0.01	9	-	-	/ [h]
12	**12a**	2	-	25	90	0	-	-	-	/ [h]
13	**13a**	2	✓	25	90	traces	-	-	-	/ [h]
14	**13a**	2	✓	60	90	traces	-	-	-	/ [h]
15	**13a**	40	-	25	60	0.30	501	0.3 [1.37]	65[e]	/ [h]
16	**13a**	40	-	45	30	0.06	217	0.3 [1.30]	/ [g]	/ [h]
17	**13a**	40	-	60	30	0.14	465	0.2 [1.30]	/ [g]	/ [h]

[a] Polymerisations carried out with 21 µmol of catalyst, and 2.0 equivalents of $Ni(COD)_2$ co-catalyst where stated (✓). Reactions using 2 bar of C_2H_4 were carried out in 50 mL of toluene in a glass vessel, whereas reactions at 40 bar were carried out in 100 mL of toluene in a stainless steel autoclave reactor. [b] mol[C_2H_4] x mol^{-1} [Ni] x h^{-1}. [c] Determined by GPC at 160 ˚C *vs.* narrow polystyrene standards, unless stated otherwise (Figures S5.13–S5.19). [d] Determined by ^{1}H NMR (Figure S5.20).[49] [e] Determined by quantitative $^{13}C\{^1H\}$ NMR (inverse gated decoupled) (Figure S5.21 and Figure 5.8). [f] Determined by DSC, using the second heating curve at 10 ˚C min^{-1} (Figures S5.22–S5.28). [g] Beyond upper detection limit of the GPC. [h] No melt detectable.

It was found that for catalyst **11a**, the addition of 2 equiv. of $Ni(COD)_2$ did not improve the activity (Table 5.2, entries 1 and 2), and hence it was not used in further reactions at 40 bar ethylene pressure. Across all experiments, the degree of branching increased with

temperature. This correlation is expected, as BHE is more pronounced at higher temperatures, and is the key step for chain transfer and branching processes. Pressure also has an influence on catalytic activity and degree of branching, clearly observed in the data for polymerisations at 2 bar compared to 40 bar. This phenomenon has been reported by Brookhart *et al.*, who found that polymerisation temperature and ethylene pressure control the amount of branching.[11] At higher pressures, the equilibrium between the active nickel ethylene complex and resting nickel co-ligand complex lies towards the active species (Scheme 5.6).

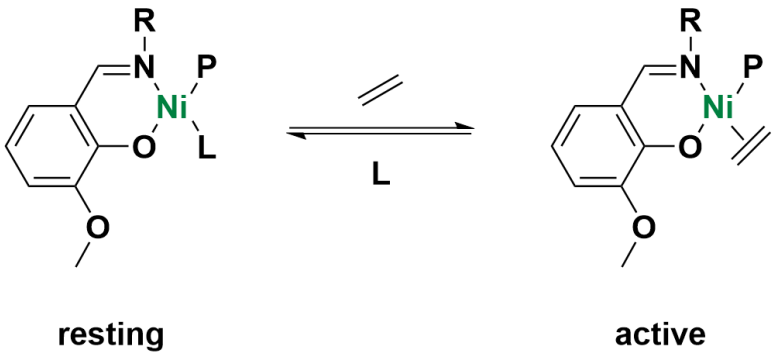

Figure 5.6: Equilibrium between resting and active state of neutral Ni(II) species during ethylene polymerisation catalysis. P = growing polymer chain, L = labile co-ligand PPh_3 or pyridine.

Catalysts **11a** and **11b**, with the same R group and different labile co-ligands, displayed similar polymerisation profiles at 40 bar of ethylene pressure. The similarity most likely arises from the comparable binding strength of the pyridine and triphenyl phosphine co-ligands.[50] Both complexes produce solid polymer, with a melting point (106–118 ˚C). Complex **11a** is more active compared to **11b** (11,043 h^{-1} *vs.* 8979 h^{-1}), although at 60 °C exhibits a higher degree of chain transfer as the M_n is less than half (Table 5.2, entries 6 and 9). For both, activity increases 100-fold from 25 to 60 °C, suggesting that there is an activation energy for the dissociation of the labile ligands PPh_3 and pyridine. To assess the effect of the OMe group *ortho* to the phenol, a Ni(II) catalyst with an H at the ortho position and 2,6-diisopropylphenyl (Dipp) R group was synthesised and compared to **11a** for

polymerisation of ethylene.[8] The polymerisations were conducted under identical conditions, with 42 μmol of catalyst, 2 equivalents of $Ni(COD)_2$ co-catalyst, 2 bar pressure of ethylene, at 25 ˚C for 90 minutes. The results were very similar, with the Ni(II) catalyst showing a slightly greater TOF (125 *vs.* 113 h^{-1}), signifying that the OMe group did not have a significant positive effect on the polymerisation.

Ethylene mass flow profiles of entries 4–9 and 15–17 in Table 5.2 were recorded, which were useful to monitor ethylene uptake throughout the reaction (Figure 5.7 and Figures S5.29–S5.33). For both catalysts **11a** and **11b**, at 25 and 45 °C the consumption of ethylene was mostly in the first few minutes upon pressurising the reactor. At 60 °C, the mass flow shows high activity (TOF of ~2400 h^{-1}) in the first 15 minutes, and decreases over time, most likely due to catalyst decomposition.[51]

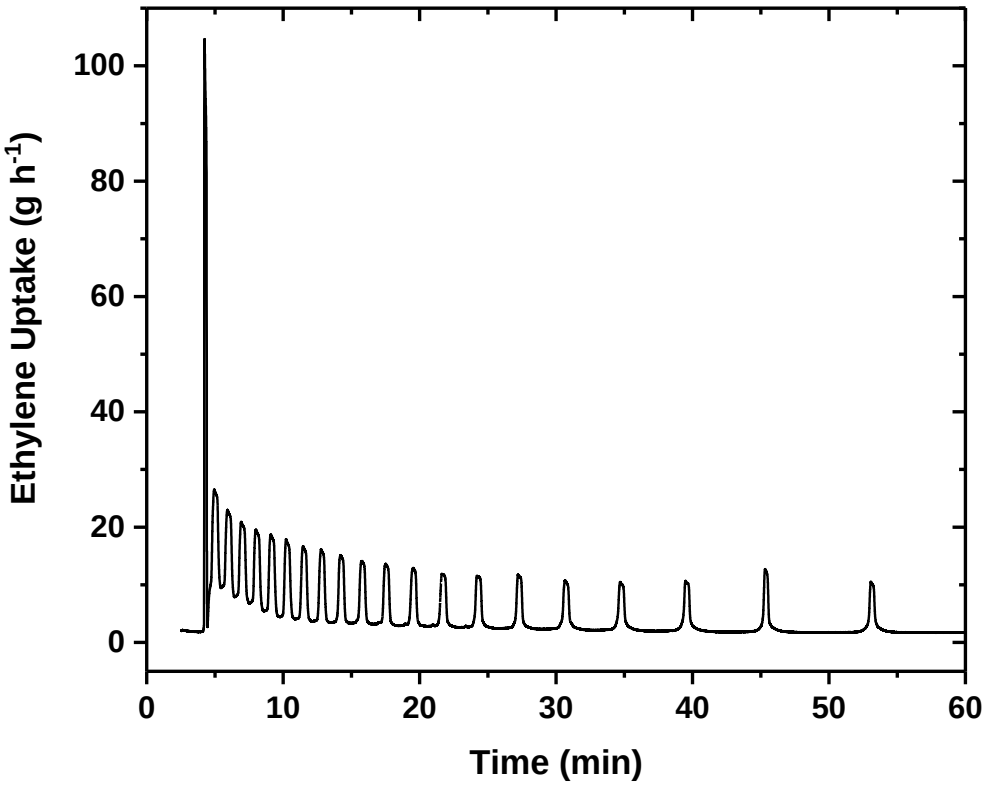

Figure 5.7: Ethylene uptake for the polymerisation of ethylene with catalyst **11a** at 60 ˚C (Table 5.2, entry 6).

At 2 bar of ethylene, complexes **12a** and **13a** displayed poor activity and very low yield of polymer (Table 5.2, entries 10–14). However, at 40 bar, complex **13a** produced an oily polymer, indicative of a highly branched oligomer, with molecular weights between 280 and 400 g mol^{-1} (Table 5.2, entry 13–17). Mecking and co-worker's experimental and theoretical studies find that, for pendant phenyl groups sitting close to the axial position of the Ni centre, there is possibility of a weak π-interaction between the aryl group and the metal.[46] As a result, there is an energetically favourable pathway towards branch formation.[46] For **12a**, the TOF was a fifth of what was obtained for **11a** at 20 ˚C (Table 5.2, entries 10 and 1). Ni(II) phenoxyiminato complexes with fluorinated N-terphenyl groups have been successful in synthesising high MW linear PE" and enhancing the TOF, owing to the electron-withdrawing nature of fluorinated aryl group as well as weak H-bonding between ortho-fluorine atoms and coordinated ethylene.[52] In the case of **12a**, the fluorine groups are not appropriately located for such an effect.

Microstructure analysis of the PE" by quantitative ^{13}C NMR spectroscopy revealed the polymers' branching patterns. Peak assignments were made according to literature reports.[49, 53-54] Using this method, it is possible to identify resonances of methyl, ethyl, and propyl branches, as well as the end group of sec-butyl motifs. An example of an assigned spectrum for an amorphous hyperbranched and a semicrystalline branched polymer is presented in Figure 5.8, corresponding to the PE" formed in entries 15 and 6, respectively, in Table 5.2. Quantitative ^{13}C NMR can also be used to measure the degree of branching of polyethylene, using equation 5.1.[55] This was necessary for hyperbranched polymers that are not accurately measured by GPC. The amorphous polymer is highly branched, displaying branches of varying lengths, with an approximate degree of 65 branches per 1000 C. The semicrystalline polymer displays almost exclusively methyl branches, with an approximate of 17 branches per 1000 C using equation 5.1, in close agreement with the result by GPC analysis.

$$\frac{branches}{1000\,C} = \frac{I\,{}^{1}{}_{B_1} + I\,{}^{1}{}_{B_2} + I\,{}^{1}{}_{B_3} + I_{B_{secB}}}{I_{tot}}$$

Equation 5.1

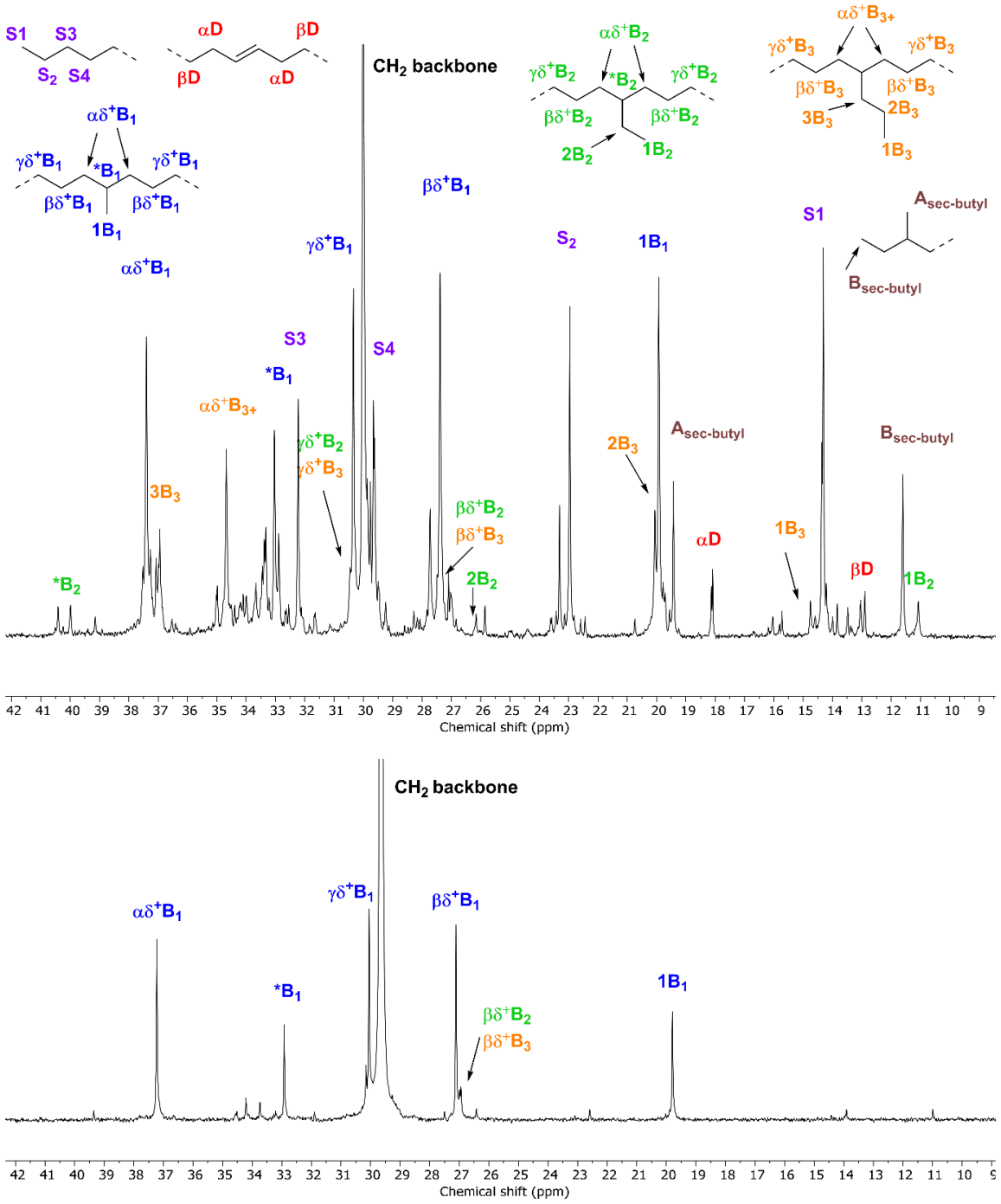

Figure 5.8: Selected region of the $^{13}C\{^{1}H\}$ NMR spectra (101 MHz, $C_2D_2Cl_4$, 383 K) of amorphous (top) and semicrystalline (bottom) polyethylene obtained with catalyst **13a** and **11a**, respectively. Assignments are numbered according to a method developed by J. C. Randall.[53] Branches are labelled as xB_y, where y is the branch length, x is the carbon (starting from the methyl end which is 1). The methine groups for the different branch lengths are labelled with $*B_y$, and the protons along the backbone are identified by two Greek letters indicating the locations of the nearest methine carbons in either direction; δ indicates it is four or more carbons away.

5.5 Towards the Synthesis of Nickel Alkoxides

In order to generate a complex capable of initiating the ROP of lactones, nickel alkoxide species were targeted. Three strategies were investigated: protonolysis of a nickel alkyl with an alcohol, salt metathesis of a nickel halide species with potassium alkoxide, and insertion of an epoxide into a nickel hydride species.

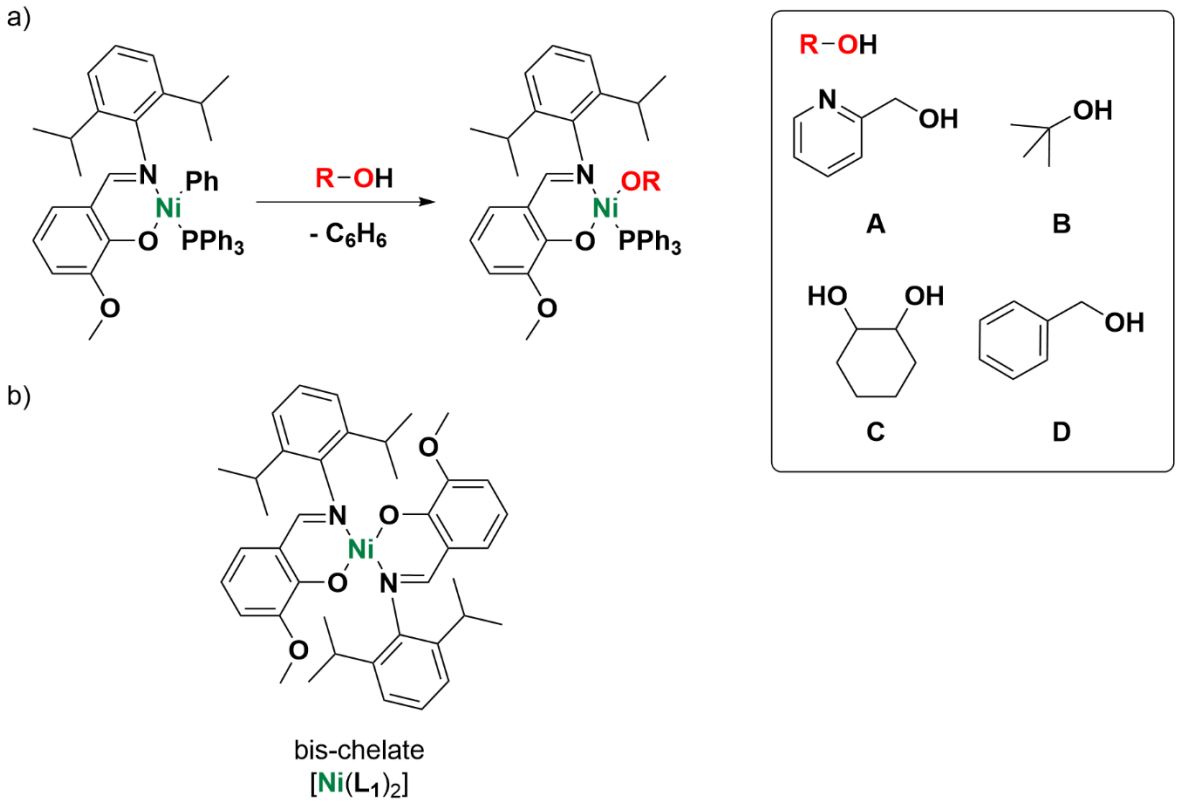

Scheme 5.2: a) Scheme for the protonolysis reaction of **11a** with alcohols **A**-**D** b) bischelate product [Ni(L_1)$_2$].

For the first strategy, complex **11a** was treated with four alcohols (**A**, **B**, **C**, and **D**), each with different pK_a values and steric profiles, in an NMR tube (Scheme 5.2a). Alcohol **A** (2-pyridine methanol) was selected as a chelating alcohol which could offer more stability to the complex, or form dimeric species such as in the case of the work by Schaper and co-workers with copper.[56] Upon reacting **11a** with **A**, it was found that the major product was the diamagnetic bis-chelate, [Ni(**L**$_1$)$_2$] (Scheme 5.2b), as well as one other minor species, (Figure S5.34). The alcohol can protonate the ligand, which de-coordinates and irreversibly

reacts with another molecule of the complex, liberating benzene and PPh_3. Bis-chelates are often observed as catalyst deactivation products during ethylene polymerisation, as they are not active for ethylene polymerisation, and are thermodynamic sinks for this class of nickel compounds.[47, 51] On the other hand, alcohols **B**, **C**, and **D** did not react with the complex, either stoichiometrically or in excess.

The second strategy involving salt metathesis is outlined in Scheme 5.3. There are several procedures in the literature to make Ni(II) chloro phenoxyiminato complexes, synthesised *via* $[NiCl_2(PPh_3)_2]$ or $[NiCl_2(py)_4]$, which are intermediates for hydride and nickel alkyl species.[11, 45, 57] Treatment of $[NiCl_2(PPh_3)_2]$, $[NiBr_2(PPh_3)_2]$, or $[NiCl_2(py)_4]$ with either **NaL₁** or **HL₁** with NEt_3 at 0 °C gives the bis-chelate $[Ni(\mathbf{L_1})_2]$ as a green compound, identified by ^{1}H NMR spectroscopy (Figure S5.35). As mentioned above, bis-chelates are thermodynamically favourable and formed relatively quickly. Grubbs and co-workers proposed that increasing the steric congestion around the metal, specifically *ortho* to the phenoxy ring, stabilises mono-ligated complexes and hinders coordination of two chelating ligands on the same metal centres.[47]

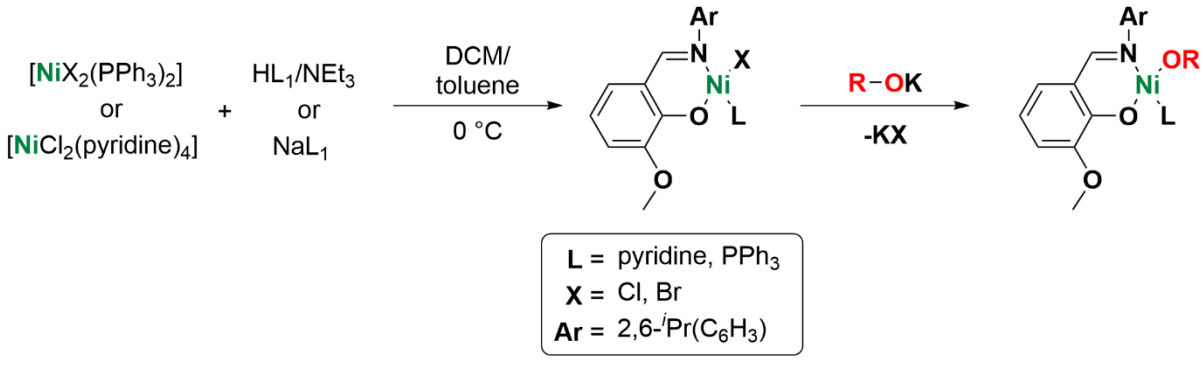

Scheme 5.3: Strategy for the synthesis of nickel alkoxide by salt metathesis with a potassium alkoxide.

A final strategy is to insert an epoxide into a Ni-H bond, of which there are examples in the literature with different ligand systems.[58] Nickel hydrides bearing phenoxyiminato ligands can be accessed via reduction of $[LNiCl(PPh_3)]$ with $NaBH(OMe)_3$, which was previously

reported for studying intermediates in nickel catalysed ethylene polymerisation (Scheme 5.4).[45] Here, the *ortho*-methoxy group was substituted for a ^{t}Bu group (**HL$_5$**) given the difficulties in accessing [L_nNiCl(PPh$_3$)] using **HL$_1$**. Whilst the intermediate chloro species is tetrahedral and hence paramagnetic, reduction to the hydride species makes it square planar and, thus, diamagnetic. The hydride was identified in the ^{1}H NMR spectrum as a doublet at −27.6 ppm, with a $^{2}J_{HP}$ of 140 Hz, and the same *J* coupling is also present in the ^{31}P NMR for the PPh$_3$ co-ligand (Figures S5.36 and S5.37). A preliminary reaction with styrene oxide was performed at the NMR scale, but no reaction was observed.

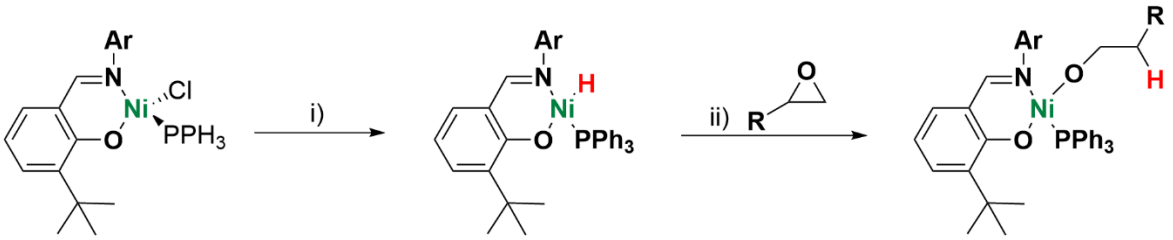

Scheme 5.4: Schematic for the synthesis of Ni(II) alkoxide complex *via* a Ni hydride. i) NaBH(OMe)$_3$ (3 equiv.), THF, RT overnight. ii) epoxide (2 equiv.), THF, RT.

5.6 Summary and Outlook

5.6.1 Summary

In summary, 4 novel Ni(II) phenoxyiminato complexes have been synthesised and fully characterised. They have been tested for ethylene polymerisation at 2 and 40 bar pressure to make branched polyethylene. The *ortho*-methoxy group did not have a significant effect on the polymerisation rate compared to having no substituent at that position, although the polymer exhibited less branching. The complexes **11a** and **11b** with the symmetrical 2,6-diisopropyl substituted aromatic R group on the ligand displayed the highest activity at 40 bar, the highest being for **11a** (TOF = 11,043 h^{-1}, 60 ˚C, 40 bar of C_2H_4) whilst **11b** displayed

a higher M_n under those conditions (28.7 kg mol^{-1}). The complexes **12a** and **13a** were significantly less active and yielded highly branched PE".

Several approaches towards nickel alkoxide complexes were attempted, using $\mathbf{L_1}$ as the model ancillary ligand. These included alcoholysis of a Ni-C, salt metathesis of Ni-X (X = halide) with potassium alkoxide, and insertion of an epoxide with a Ni-H species. It was evident from this work that the bis-chelate is a thermodynamic sink, which was facilitated by the *ortho*-methoxy group.

5.6.2 Outlook

Future work should focus on developing the three strategies to make nickel alkoxides described in this work. Changing the *ortho* group in the phenoxy ring to bulkier group such as anthryl, ^{t}Bu (**HL_5**) or iodo (Figure 5.9) in all synthesis routes may be beneficial to prevent bis-chelate formation.

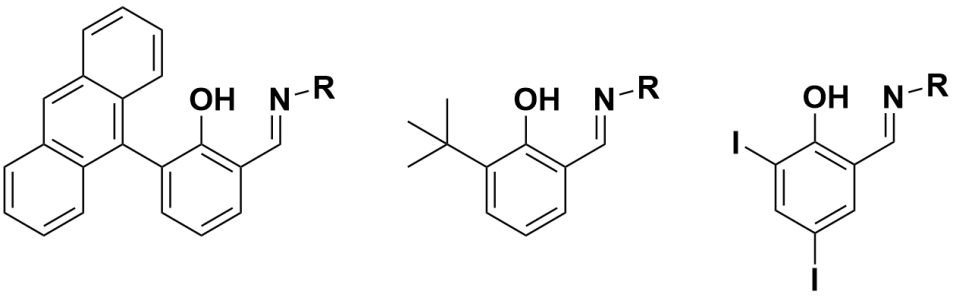

Figure 5.9: Ligands reported in the literature which introduce more steric bulk around the Ni(II) centre.

A potentially interesting class of compounds are the hydroxide-bridged dinuclear nickel complexes, which are nucleophilic.[59] The synthesis of the dinuclear Ni(II) complex with a phenoxyiminato ligand has already been isolated and characterised, although no reactivity studies were conducted (Figure 5.10).[45] It would be worth testing for in oxygenated monomer polymerisation catalysis.

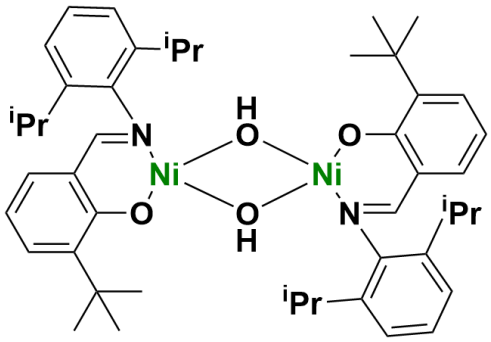

Figure 5.10: Structure of Ni(II) dimer with bridging OH groups.

Longer term, investigation of heterobimetallic complexes should be explored as a route towards switch catalysis. Cooperation of two or more metal centres has many benefits for ethylene polymerisation,[60-61] and homo and hetero-bimetallic catalysis developed by Williams and co-workers have made ROP/ ROCOP switch catalysis possible.[62]

5.7 References

1. Britovsek, G. J. P.; Gibson, V. C.; Wass, D. F., *Angew. Chem. Int. Ed.* **1999,** *38* (4), 428-447.

2. Collins, R. A.; Russell, A. F.; Mountford, P., *Appl. Petrochem. Res.* **2015,** *5* (3), 153-171.

3. Chen, Z.; Brookhart, M., *Acc. Chem. Res.* **2018,** *51* (8), 1831-1839.

4. Chen, C., *Nat. Rev. Chem.* **2018,** *2* (5), 6-14.

5. Mu, H.; Pan, L.; Song, D.; Li, Y., *Chem. Rev.* **2015,** *115* (22), 12091-12137.

6. Ito, S.; Nozaki, K., *Chem. Rec.* **2010,** *10* (5), 315-325.

7. Johnson, L. K.; Killian, C. M.; Brookhart, M., *J. Am. Chem. Soc.* **1995,** *117* (23), 6414-6415.

8. Wang, C.; Friedrich, S.; Younkin, T. R.; Li, R. T.; Grubbs, R. H.; Bansleben, D. A.; Day, M. W., *Organometallics* **1998,** *17* (15), 3149-3151.

9. Ittel, S. D.; Johnson, L. K.; Brookhart, M., *Chem. Rev.* **2000,** *100* (4), 1169-1204.

10. Göttker-Schnetmann, I.; Wehrmann, P.; Röhr, C.; Mecking, S., *Organometallics* **2007,** *26* (9), 2348-2362.

11. Jenkins, J. C.; Brookhart, M., *J. Am. Chem. Soc.* **2004,** *126* (18), 5827-5842.

12. Delferro, M.; McInnis, J. P.; Marks, T. J., *Organometallics* **2010,** *29* (21), 5040-5049.

13. Kenyon, P.; Wörner, M.; Mecking, S., *J. Am. Chem. Soc.* **2018,** *140* (21), 6685-6689.

14. Schnitte, M.; Lipinski, S.; Schiebel, E.; Mecking, S., *Organometallics* **2020,** *39* (1), 13-17.

15. Stempfle, F.; Ortmann, P.; Mecking, S., *Macromol. Rapid Commun.* **2013,** *34* (1), 47-50.

16. Häußler, M.; Eck, M.; Rothauer, D.; Mecking, S., *Nature* **2021,** *590* (7846), 423-427.

17. Myers, D.; Witt, T.; Cyriac, A.; Bown, M.; Mecking, S.; Williams, C. K., *Polym. Chem,* **2017,** *8* (37), 5780-5785.

18. Brubaker, M. M.; Coffman, D. D.; Hoehn, H. H., *J. Am. Chem. Soc.* **1952,** *74* (6), 1509-1515.

19. Baur, M.; Lin, F.; Morgen, T. O.; Odenwald, L.; Mecking, S., *Science* **2021,** *374* (6567), 604-607.

20. Macosko, C. W.; Guégan, P.; Khandpur, A. K.; Nakayama, A.; Marechal, P.; Inoue, T., *Macromolecules* **1996,** *29* (17), 5590-5598.

21. Yan, T.; Walsh, D. J.; Qiu, C.; Guironnet, D., *Macromolecules* **2018,** *51* (24), 10167-10173.

22. Goring, P. D.; Morton, C.; Scott, P., *Dalton Trans.* **2019,** *48* (11), 3521-3530.

23. Wang, Y.; Hillmyer, M. A., *J. Polym. Sci., Part A: Polym. Chem.* **2001,** *39* (16), 2755-2766.

24. Domski, G. J.; Rose, J. M.; Coates, G. W.; Bolig, A. D.; Brookhart, M., *Prog. Polym. Sci.* **2007,** *32* (1), 30-92.

25. Valente, A.; Mortreux, A.; Visseaux, M.; Zinck, P., *Chem. Rev.* **2013,** *113* (5), 3836-3857.

26. Zhao, Y.; Wang, Y.; Zhou, X.; Xue, Z.; Wang, X.; Xie, X.; Poli, R., *Angew. Chem. Int. Ed.* **2019,** *0* (0).

27. Takeuchi, D., *Dalton Trans.* **2010,** *39* (2), 311-328.

28. Lord, R. M.; Janeway, F. D.; Bird, L.; McGowan, P. C., *Polyhedron* **2022,** *211*, 115520.

29. Bakewell, C.; Fateh-Iravani, G.; Beh, D. W.; Myers, D.; Tabthong, S.; Hormnirun, P.; White, A. J. P.; Long, N.; Williams, C. K., *Dalton Trans.* **2015,** *44* (27), 12326-12337.

30. Seo, C. C. Y.; Ahmed, M.; Oliver, A. G.; Durr, C. B., *Inorg. Chem.* **2021,** *60* (24), 19336-19344.

31. Durr, C. B.; Williams, C. K., *Inorg. Chem.* **2018,** *57* (22), 14240-14248.

32. Chang, C.-H.; Tsai, C.-Y.; Lin, W.-J.; Su, Y.-C.; Chuang, H.-J.; Liu, W.-L.; Chen, C.-T.; Chen, C.-K.; Ko, B.-T., *Polymer* **2018,** *141*, 1-11.

33. Routaray, A.; Mantri, S.; Nath, N.; Sutar, A. K.; Maharana, T., *Polyhedron* **2016,** *119*, 335-341.

34. Reis, N. V.; Deacy, A. C.; Rosetto, G.; Durr, C. B.; Williams, C. K., *Chem. Eur. J.* **2022,** *28*, e202104198.

35. Martínez-Prieto, L. M.; Palma, P.; Cámpora, J., *Dalton Trans.* **2019,** *48* (4), 1351-1366.

36. Treadwell, L. J.; Boyle, T. J.; Phelan, W. A.; Parkes, M. V.; Young, D. P., *Dalton Trans.* **2017,** *46* (18), 5806-5815.

37. Chadha, S. L.; Sharma, V., *Inorg. Chim. Acta* **1987,** *131* (1), 101-103.

38. Dodd, N. A.; Bacsa, J.; Sadighi, J. P., *Polyhedron* **2021,** *208*, 115408.

39. Bellow, J. A.; Yousif, M.; Fang, D.; Kratz, E. G.; Cisneros, G. A.; Groysman, S., *Inorg. Chem.* **2015,** *54* (12), 5624-5633.

40. LaPierre, E. A.; Piers, W. E.; Spasyuk, D. M.; Bi, D. W., *Chem. Commun.* **2016,** *52* (7), 1361-1364.

41. Klein, H.-F.; Dal, A.; Jung, T.; Braun, S.; Röhr, C.; Flörke, U.; Haupt, H.-J., *Eur. J. Inorg. Chem.* **1998,** *1998* (5), 621-627.

42. Sacco, A.; Mastrorilli, P., *J. Chem. Soc., Dalton Trans.* **1994,** (19), 2761-2764.

43. Zeller, A.; Herdtweck, E.; Strassner, T., *Eur. J. Inorg. Chem.* **2003,** *2003* (9), 1802-1806.

44. Cai, Z.; Xiao, D.; Do, L. H., *J. Am. Chem. Soc.* **2015,** *137* (49), 15501-15510.

45. Ölscher, F.; Göttker-Schnetmann, I.; Monteil, V.; Mecking, S., *J. Am. Chem. Soc.* **2015,** *137* (46), 14819-14828.

46. Falivene, L.; Wiedemann, T.; Göttker-Schnetmann, I.; Caporaso, L.; Cavallo, L.; Mecking, S., *J. Am. Chem. Soc.* **2018,** *140* (4), 1305-1312.

47. Connor, E. F.; Younkin, T. R.; Henderson, J. I.; Waltman, A. W.; Grubbs, R. H., *Chem. Commun.* **2003,** (18), 2272-2273.

48. Göttker-Schnetmann, I.; Mecking, S., *Organometallics* **2020,** *39* (18), 3433-3440.

49. Wiedemann, T.; Voit, G.; Tchernook, A.; Roesle, P.; Göttker-Schnetmann, I.; Mecking, S., *J. Am. Chem. Soc.* **2014,** *136* (5), 2078-2085.

50. Kenyon, P.; Falivene, L.; Caporaso, L.; Mecking, S., *ACS Catal.* **2019,** *9* (12), 11552-11556.

51. Berkefeld, A.; Mecking, S., *J. Am. Chem. Soc.* **2009,** *131* (4), 1565-1574.

52. Wang, J.; Yao, E.; Chen, Z.; Ma, Y., *Macromolecules* **2015,** *48* (16), 5504-5510.

53. Randall, J. C., *J. Polym. Sci., Part C* **1989,** *29* (2-3), 201-317.

54. Galland, G. B.; de Souza, R. F.; Mauler, R. S.; Nunes, F. F., *Macromolecules* **1999,** *32* (5), 1620-1625.

55. Schiebel, E.; Santacroce, S.; Falivene, L.; Göttker-Schnetmann, I.; Caporaso, L.; Mecking, S., *ACS Catal.* **2019,** *9* (5), 3888-3894.

56. Fortun, S.; Daneshmand, P.; Schaper, F., *Angew. Chem. Int. Ed.* **2015,** *54* (46), 13669-13672.

57. Voit, G. Higher Alkyl and Hemilabile-Substituted N-Terphenyl Nickel(II) Salicylaldiminato Catalyst Precursors. University of Konstanz, 2015.

58. Wenz, J.; Wadepohl, H.; Gade, L. H., *Chem. Commun.* **2017,** *53* (31), 4308-4311.

59. Bertini, S.; Albrecht, M., *Organometallics* **2020,** *39* (18), 3413-3424.

60. Delferro, M.; Marks, T. J., *Chem. Rev.* **2011,** *111* (3), 2450-2485.

61. Smith, A. J.; Kalkman, E. D.; Gilbert, Z. W.; Tonks, I. A., *Organometallics* **2016,** *35* (15), 2429-2432.

62. Chen, T. T. D.; Zhu, Y.; Williams, C. K., *Macromolecules* **2018,** *51* (14), 5346-5351.

Chapter 6

Thesis Conclusions and Outlook

6.1 Thesis Summary

In this thesis, the activity, selectivity, and modification of Mg(II)M(II) heterodinuclear catalysts have been studied for the ROCOP of CO_2/epoxide and anhydride/epoxide, (Figure 6.1). The main aims and results from each chapter were the following:

Chapter 2. Investigating the activity of Mg(II)M(II) (M = Mg, Cr, Mn, Fe, Co, Ni, Cu, Zn) heterodinuclear complexes for the ROCOP of NA and CHO. The most active was Mg(II)Co(II), with a TOF of 610 h^{-1}, followed by Mg(II)Mn(II) (TOF = 272 h^{-1}) and Mg(II)Ni(II) (TOF = 244 h^{-1}). A similar trend was reported for CO_2/CHO ROCOP, with the exception of Mg(II)Fe(II), which was less active for NA/CHO ROCOP compared to most of the other metal combinations (TOF = 109 h^{-1}) (Figure 6.1a).[1]

Determining the selectivity in CO_2/anhydride/epoxide ROCOP with Mg(II)M(II) (M = Zn, Co) heterodinuclear complexes. The one pot polymerisation of TCA, CHO, and CO_2 with these complexes resulted in a random copolymer using Mg(II)Zn(II), and polycarbonate using Mg(II)Co(II). Comparing these results to the previously reported reactions of homodinuclear complexes Mg(II)Mg(II) and Zn(II)Zn(II), the rate of CO_2 insertion follows the order Mg(II)Co(II) > Mg(II)Mg(II) > Mg(II)Zn(II) > Zn(II)Zn(II) (Figure 6.1b).

Chapter 3. Synthesising ROCOP- and ROP-derived multi-block copolymers. Using the heterodinuclear Mg(II)Co(II) catalyst, which was the most active and selective catalyst in Chapter 2 for CO_2/epoxide and anhydride/epoxide ROCOP, multi-block copolymers were constructed in one pot by switching between CO_2 and N_2 gas. Using a bifunctional CTA, triblock, pentablock, and heptablock copolymers were afforded, depending on the number of gas switches performed. This presents a novel and facile way of constructing multi-block copolymers of polycarbonates and polyesters (Figure 6.1c).

Adding a fourth monomer, CL, to the one-pot reaction yielded a pentablock copolymer with one switch from CO_2 to N_2. After switching to N_2, TCA/CHO ROCOP commenced and, once all the anhydride was consumed, ROP of lactone followed to form a CABAC block copolymer. The resulting T_g was 86 ˚C, which was significantly lower than the ABA triblock (T_g = 121 ˚C). Modulating the T_g of a polymer is useful and inclusion of CL could reduce the brittleness of the material.

Chapter 4. Synthesis of a Mg(II)Co(II) catalyst with non-initiating co-ligands and application to the ROCOP of CO_2/epoxide. Organometallic C_6F_5 co-ligands were installed in the heterodinuclear Mg(II)Co(II) framework to replace the acetate groups. The novel complex was characterised *via* NMR spectroscopy, X-ray crystallography, CV, and SQUID magnetometry. Using MALDI-ToF spectroscopy, it was confirmed that the C_6F_5 groups do not initiate the polymerisation. The complex, in combination with bifunctional protic CTAs, allowed for the synthesis of high molar mass polycarbonates with monodisperse distributions (Figure 6.1d). The highest molar mass achieved was 163 kg mol^{-1} PvCHC, prepared at 0.01 mol % catalyst loading with vCHO at 20 bar of CO_2. Tensile properties of this polymer were measured, which displayed a tensile strength of 23 MPa, strain at break of 18.8 % and Young's Modulus of 1.0 GPa.

Chapter 5. Investigating Ni(II) alkyl complexes for ethylene polymerisation and the synthesis of Ni(II) alkoxide. Four novel Ni(II) complexes with an *ortho*-vanillin derived ligand were synthesised and characterised, and subsequently studied for ethylene homopolymerisation. Polyethylene with varying degree of branching was produced, dependant on the substituents on the ligand. Various synthetic strategies towards Ni(II) alkoxide complexes with the same supporting ligand were attempted, as they could act as ROP initiators, but success was limited as the bis-chelated complex was predominately formed.

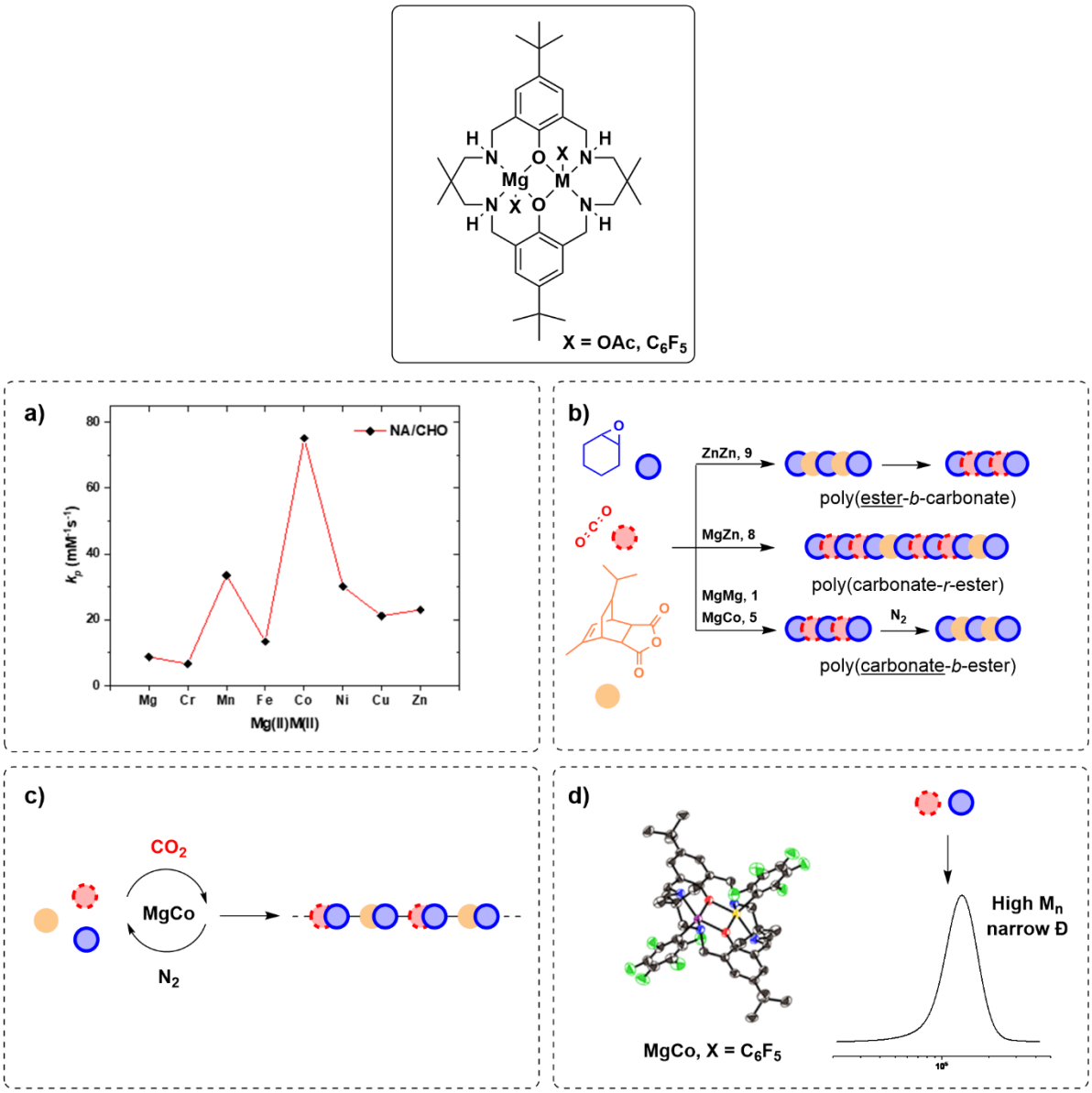

Figure 6.1: Thesis summary covering Chapters 2–4.

6.2 Outlook

6.2.1 Catalysis Applications

The thesis has primarily focussed on the catalysis of heterodinuclear complexes and novel approaches towards the synthesis of CO_2-derived polymers. A clear future opportunity is to explore the application/properties of these materials. The multi-block copolymers prepared in Chapter 3 feature two high T_g and rigid blocks which, in that molar mass regime, are phase miscible. As seen with the CABAC pentablock copolymer, incorporating an aliphatic polyester block, with a much lower T_g, changed the thermal properties of the polymer considerably. Hence, one future direction is to make multi-block copolymers with structurally diverse aliphatic polyesters, e.g. succinic anhydride or diglycolic anhydride ROCOP so as to target multi-block polymers with controllable T_g and mechanical properties. Another possibility is to post-functionalise the polymer backbone, which can be employed to alter polymer properties and add functional groups. The alkene functionality in TCA is not readily reactive due to the methyl group.[2] In contrast, norbornene anhydride and a citraconic anhydride-based tricyclic anhydride can be subject to post-polymerisation modification reactions, such as thiol-ene click chemistry.[2-3] Given that they are tricyclic anhydrides, it is likely that they exhibit the same insertion selectivity as TCA, such that selective block copolymer formation would take place (Figure 6.2a).[4]

Microphase-separated multi-block polymers prepared by switch catalysis should be investigated, as studies have shown changes in properties and enhanced performance compared to di- or triblocks.[5-9] For example, a study with alternating $(AB)_n$ phase-separating blocks of isoprene and 4-methylstyrene showed that the strain at break increased significantly from 4 to 1150 % from a diblock (n = 1) to decablock (n = 5).[9] This strategy could be applied to switch catalysis, using polycarbonates derived from CO_2/epoxide

ROCOP and aliphatic polyesters from the ROP of lactones, which have been reported to exhibit microphase separation (Figure 6.2b).[10-11] In either example of multi-block copolymers, the novel organometallic Mg(II)Co(II) complex described in Chapter 4 should be employed, as it would enable chain-end fidelity and yield polymers with higher molar masses.

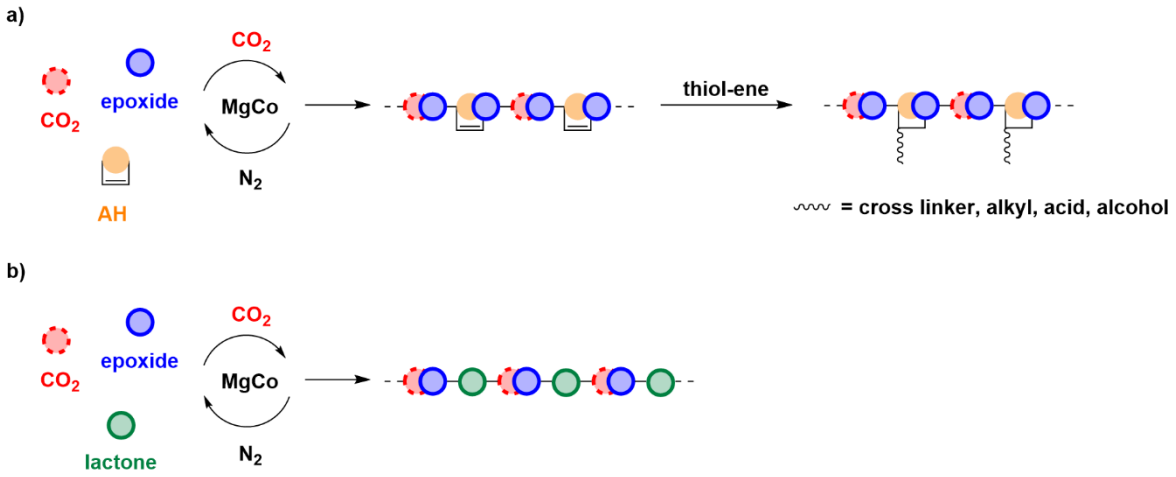

Figure 6.2: a) Post-polymerisation modification of alkene functionalities in the anhydride moiety of mutli-block copolymers. b) Multi-gas switches to afford multi-block copolymers of polycarbonate and aliphatic polyester *via* switch catalysis.

A final future target is to determine the stability and depolymerisation process of oxygenated multiblock polymers. An important motivation for the synthesis of these polymers was the possibility of chemical and biological degradation of oxygen-rich polymers with hydrolysable linkages. Recently, Carrodeaguas *et al.* reported the degradation of PLC back into its monomers using the macrocyclic Zn(II)Zn(II) catalyst with phenyl co-ligands, and Chen *et al.* reported the degradation of TCA-based polyesters using *p*-toluenesulphonic acid under mild conditions (1 M, 60 °C).[11-12] Both these strategies could be combined to completely degrade the multi-blocks described in this thesis and enable closed-loop recycling.

6.2.2 Catalyst Design

One limitation of the catalysts with the studied macrocyclic ligand scaffold is that they are inactive for the ROCOP of acyclic epoxides (e.g. PO) and CO_2. This narrows the scope of accessible polycarbonates.[13] Recently our group reported a macrocyclic heterodinuclear catalyst with Co(III) and K(I) metal centres which shows high activity for CO_2/PO ROCOP at low catalyst loadings (TOF = 800 h^{-1}, 0.025 mol %, 20 bar of CO_2) and selectivity of polymer over cyclic carbonate byproducts.[14] Given that the catalyst possesses acetate co-ligands, only low molar mass polyols were obtained with added CTAs, or bimodal molar mass distributions without them. Hence, it would be beneficial to install non-initiating, organometallic co-ligands, as was done similarly with the Mg(II)Co(II) complex.

Developing catalysts that would facilitate metal-carbon and metal-oxygen intermediates for ethylene and ROP or ROCOP polymerisations, respectively, remains a challenge. Examples of block polymers consisting of polyolefin and polyester/carbonate are rare, and involve intermediary purification steps or multiple catalysts.[15-16] Phenoxyiminato complexes of Ni(II) should be further explored, as Ni(II) complexes are active for both polymerisation cycles. Preventing the formation of the bis-chelate complex is an immediate aim, and could be achieved by replacing the *ortho*-methoxy substituent on the ligand with a more sterically hindered group.

6.3 References

1. Reis, N. V.; Deacy, A. C.; Rosetto, G.; Durr, C. B.; Williams, C. K., *Chem. Eur. J.* **2022,** *28,* e202104198.

2. Sanford, M. J.; Van Zee, N. J.; Coates, G. W., *Chem. Sci.* **2018,** *9* (1), 134-142.

3. Yi, N.; Chen, T. T. D.; Unruangsri, J.; Zhu, Y.; Williams, C. K., *Chem. Sci.* **2019,** *10* (43), 9974-9980.

4. Saini, P. K.; Fiorani, G.; Mathers, R. T.; Williams, C. K., *Chem. Eur. J.* **2017,** *23* (18), 4260-4265.

5. Zhang, J.; Deubler, R.; Hartlieb, M.; Martin, L.; Tanaka, J.; Patyukova, E.; Topham, P. D.; Schacher, F. H.; Perrier, S., *Macromolecules* **2017,** *50* (18), 7380-7387.

6. Spontak, R. J.; Smith, S. D., *J. Polym. Sci., Part B: Polym. Phys.* **2001,** *39* (9), 947-955.

7. Bates, C. M.; Bates, F. S., *Macromolecules* **2017,** *50* (1), 3-22.

8. Lee, I.; Bates, F. S., *Macromolecules* **2013,** *46* (11), 4529-4539.

9. Grune, E.; Appold, M.; Müller, A. H. E.; Gallei, M.; Frey, H., *ACS Macro Lett.* **2018,** *7* (7), 807-810.

10. Sulley, G. S.; Gregory, G. L.; Chen, T. T. D.; Peña Carrodeguas, L.; Trott, G.; Santmarti, A.; Lee, K.-Y.; Terrill, N. J.; Williams, C. K., *J. Am. Chem. Soc.* **2020,** *142* (9), 4367-4378.

11. Carrodeguas, L. P.; Chen, T. T. D.; Gregory, G. L.; Sulley, G. S.; Williams, C. K., *Green Chem.* **2020,** *22* (23), 8298-8307.

12. Chen, T. T. D.; Carrodeguas, L. P.; Sulley, G. S.; Gregory, G. L.; Williams, C. K., *Angew. Chem. Int. Ed.* **2020,** *59* (52), 23450-23455.

13. Wang, Y.; Darensbourg, D. J., *Coord. Chem. Rev.* **2018,** *372*, 85-100.

14. Deacy, A. C.; Moreby, E.; Phanopoulos, A.; Williams, C. K., *J. Am. Chem. Soc.* **2020,** *142* (45), 19150-19160.

15. Zhao, Y.; Wang, Y.; Zhou, X.; Xue, Z.; Wang, X.; Xie, X.; Poli, R., *Angew. Chem. Int. Ed.* **2019,** *0* (0).

16. Yan, T.; Walsh, D. J.; Qiu, C.; Guironnet, D., *Macromolecules* **2018,** *51* (24), 10167-10173.

Chapter 7

Experimental Section

7.1 Materials and General Considerations

All manipulations, unless otherwise stated, were carried out under inert conditions, either in a N_2 filled MBraun glovebox or a dual manifold N_2-vacuum Schlenk line. Solvents used in air-sensitive synthesis were collected from a solvent purification system (SPS), degassed by three freeze-pump-thaw cycles, and stored under 3 Å molecular sieves under an N_2 atmosphere. THF was additionally dried over CaH_2 and distilled.

All chemicals purchased, purified, or synthesised were stored under an inert atmosphere. $NiCl_2 \cdot 6H_2O$ (Strem chemicals, 99.999 %) and $Ni(COD)_2$ (Strem chemicals, 98+%), $CoBr_2$ (Sigma Aldrich, 98 %), bromopentafluorobenzene (Fluorochem, 99 %), were used as received. Triphenylphosphine (Sigma Aldrich) was purified by recrystallisation from ethanol. [Mg{N[Si(Me3)$_3$]$_2$}o$_2$] (Sigma Aldrich, 97 %) was recrystallised from hexane. 1,2-Cyclohexanediol (Sigma Aldrich, 98 %) was recrystallized from ethyl acetate. Pyridine (Sigma Aldrich) was dried over CaH_2 and fractionally distilled prior to use. 4-Fluorophenol (Sigma Aldrich, 99 %) was sublimed under high vacuum at room temperature prior to use. LH_2 was synthesised according to a literature procedure, and was recrystallised form methanol and dried under vacuum prior to use.[1] [NiClPh(PPh_3)$_2$] was synthesised according to a literature procedure.[2] [Co(C_6F_5)$_2$(THF)$_2$] was synthesised according to a literature procedure, and recrystallised twice from a 1:6 THF/hexane mixture at –30 ˚C prior to use.[3-4] [$NiCl_2$(py)$_4$] was synthesised according to a literature procedure.[5] Complexes **1**, **5**, **8**, and **9** were synthesised according to reported procedures.[1, 6-8] Complexes **2**–**4**, **6** and **7** were prepared and characterised by Dr. Natalia Reis.[9]

Deuterated solvents were purchased from Cambridge Isotope Laboratories Inc., and were dried over CaH_2, degassed by three freeze-pump-thaw cycles, and dried under 3 Å molecular sieves prior to use.

7.1.1 Monomer Purification Procedures

Cyclohexene oxide (CHO, Acros Organics, 98 %) was stirred over CaH_2 for three days, followed by fractional distillation under an N_2 atmosphere at 140 ˚C. It was subsequently distilled from ^{n}BuLi (2.5 M in hexanes) at 40 ˚C and 35 mbar, and then fractionally distilled at 40 ˚C and 35 mbar. 4-Vinyl-cyclohexene oxide (vCHO, Sigma Aldrich, 98 %) was dried and distilled once over CaH_2 at 50 ˚C under 10 mbar. ε-Caprolactone (CL, Sigma Aldrich, 97 %) was dried and distilled over CaH_2 at 65 ˚C and 1.2 mbar. ε-Decalactone (DL, Sigma Aldrich, >99 %) was purified by stirring over CaH_2, followed by fraction distillation at 70 °C and 0.1 mbar. Phthalic anhydride (PA, Sigma Aldrich, >99 %) was purified through a three-step procedure; first *via* solvent extraction into toluene, recrystallisation from hot chloroform, and finally sublimation under vacuum at 80 °C. Norbornene anhydride (NA, Sigma Aldrich, >99 %) was purified by recrystallisation from dry ethyl acetate, followed by sublimation under vacuum at 80 °C. Tricyclic anhydride (TCA) was synthesised according to the method by Mathers and co-workers, and was purified by recrystallisation from dry hexane followed by sublimation under vacuum at 90 °C.[10] CO_2 gas (BOC, CP grade, 99.995 %) was passed through two carbon dioxide purifiers (VICI) at point of use. For experiments at 40 bar of ethylene, ethylene gas (Air Liquide, grade 3.5) was used as obtained.

7.2 Methods

Nuclear Magnetic Resonance (NMR) Spectroscopy

^{1}H, COSY, HSQC, HMBC, ^{31}P{^{1}H}, ^{19}F{^{1}H} NMR spectra were obtained using a Bruker AVIII HD 400 NMR. ^{13}C{^{1}H} NMR spectra were obtained using a Bruker AV III 500 equipped with a cryoprobe. All spectra were recorded at 298 K, unless stated otherwise.

Abbreviations for observed signal splitting: singlet = s, doublet = d, triplet = t, quartet = q, sept = septet, multiplet = m, broad = br.

NMR spectra of polyethylene samples were recorded in either $CDCl_3$ or $C_2D_2Cl_4$, with addition of 5 mg mL^{-1} of $Cr(acac)_3$ as paramagnetic relaxation agent, and $^{13}C\{^1H\}$ spectra were recorded as inverse gated spectra.

NMR spectra were processed and analysed using MestReNova and Bruker TopSpin software packages.

In situ Infrared (IR) Spectroscopy

In situ IR spectroscopy experiments were measured with a Mettler-Toledo ReactIR ic.10 spectrometer equipped with an MCT detector and a silver halide DiComp probe. Polymerisations monitored by *in situ* IR spectroscopy were performed either in a glass Schlenk flask (1 bar of CO_2 or N_2) or in a 25 mL Parr 5500 HP compact reactor (20 bar of CO_2).

Cyclic Voltammetry (CV)

Electrochemical studies were carried out using a PalmSens EmStat Blue potentiostat. Cyclic voltammetry experiments were performed in N_2 glovebox using a three-electrode configuration: with an Au disc (2.0 mm^2) as the working electrode, a Pt wire as the counter electrode and a Ag wire as the pseudo-reference electrode. Sample solutions were prepared by dissolving the analyte (*ca.* 5 mM), in THF (10 mL), followed by addition of a supporting electrolyte $[^nBu_4N][PF_6]$. The reported mid-peak potential was recorded at a scan rate of 0.1 V s^{-1} and is referenced internally to the $FeCp^+/FeCp$ redox couple, which was measured by adding FeCp (*ca*. 1 mg) to the sample solution.

Superconducting Quantum Interference Device (SQUID) Magnetometry

SQUID measurements were carried out on powdered samples using a Quantum Design MPMS-3 Magnetometer, with a field of 0.1 T, at temperatures from 2 to 300 K. The sample (*ca.* 15 mg) was placed into a gelatine capsule and then loaded into a diamagnetic plastic straw under inert atmosphere prior to placing it in the cryostat. Magnetic susceptibility values were corrected using the diamagnetic Pascal constants.

Elemental Analysis (EA)

EA was carried out by Mr. Stephen Boyer at the London Metropolitan University.

X-Ray Crystallography

Crystallographic data were collected, and structures solved, by Dr. Ryan Kerr (Chapter 4) and Dr. Kirsten Christensen (Chapter 5). Air sensitive samples were isolated in a glovebox and immersed in fluorinated oil before analysis. Crystalline samples were mounted on a MiTeGen Micromount and cooled to 150 K with dry nitrogen using an Oxford Cryostream.[11] Data was collected with an Oxford Diffraction Supernova diffractometer using Cu Kα (λ = 1.5417 Å) radiation. The resulting reflection data was processed with CrysAlis Pro.[12] Structures in Chapter 4 were solved using the SHELXT program and least-square refined using the SHELXL program within the Olex2 system suite.[13-15] Structures in Chapter 5 were solved with *CRYSTALS* using SUPERFLIP software.[16-17] Complete experimental details for each structure can be found in Tables S4.2 and S5.1.

Gel Permeation Chromatography (GPC)

GPC analysis was carried out on a Shimadzu LC-20AD instrument, equipped with a Refractive Index (RI) detector and two PSS SDV 5 μm linear M columns, with an eluent of HPLC-grade THF, heated to 30 °C and at a flow rate of 1.0 mL min^{-1}. For polyethylene

synthesised in Chapter 5, molar masses were determined by high temperature GPC in 1,2-dichlorobenzene at 160 ˚C on a Polymer Char GPC-IR instrument, equipped with PSS Polefin Linear XL columns (3 x 30 cm), an infrared detector (IR5 MCT, concentration signal) and a viscometer. The instrument was calibrated versus narrow polystyrene standards from PSS Polymer Standards (software: PSS WinGPC, version 8.32). The infrared detector was equipped with interference filters of different wavelengths that enabled the selective and simultaneous measurements of methyl and methylene bands, which allows for determination of the methyl branch content from GPC measurements (calibrated versus samples with known degree of branching, determined *via* high temperature $^{13}C\{^{1}H\}$ NMR experiments).

Matrix Assisted Laser Desorption/Ionisation – Time of Flight Mass Spectrometry (MALDI-ToF MS)

MALDI-ToF was carried out on a Bruker Autoflex Speed instrument. A 1:1:4 solution of polymer (20 mg mL^{-1} in THF), potassium trifluoroacetate (20 mg mL^{-1} in THF), and dithranol (20 mg mL^{-1} in THF) was prepared and spotted twice on a MALDI plate. The samples were allowed to dry completely before being subjected to analysis.

Differential Scanning Calorimetry (DSC)

Carried out using either a DSC3+ (Mettler-Toledo Ltd.) or a DSC 25 (TA Instruments). Samples were heated to 200 °C for 5 minutes to remove thermal history, before heating and cooling from 30 °C to 200 °C at a rate of 20 °C min^{-1} under an N_2 atmosphere. Each sample was run for three heating and cooling cycles. Glass transition temperatures (T_g) and melt temperatures (T_m) were recorded from the midpoint of the transition during the second heating curve.

Thermal Gravimetric Analysis (TGA)

TGA was carried out on a Discovery TGA 5500 (TA Instruments) at 10 ˚C min^{-1} between 30–700 ˚C, under continuous N_2 flow. Polymer samples subject to TGA were purified by column chromatography and dried in a 60 ˚C vacuum oven prior to use.

Tensile Testing

Polymer samples were analysed using an EZ-LX Universal Testing Instrument (Shimadzu). The polymer was solvent cast into a rectangular-shaped PTFE mould and cut into dumbbell-shaped specimens using a Zwick ZCP020 cutting press equipped with a cutting die for ISO 527-2 type 5B. Uniaxial extension experiments (10 mm min^{-1} cross-head speed) were run according to ISO 527.

CO_2 Mass Flow Measurements

From the raw mass flow data obtained in millilitre normal per minute (mLn min^{-1}) using a Bronkhorst F-100C Mass Flow Meter, the number of times CO_2 mass flow increased to a maximum was calculated and used qualitatively to show CO_2 uptake. The pressure of CO_2 was kept constant at 1 bar using a Bronkhorst P-602CV/P-612CV Pressure Controller.

7.3 General Polymerisation Procedures

7.3.1 Chapter 2 – NA/CHO Copolymerisation

A Schlenk was charged with CHO (3.0 mL, 30.0 mmol), catalyst (15.0 μmol), NA (246 mg, 1.5 mmol) and CHD (35 mg, 0.3 mmol) in a glovebox. The Schlenk was connected to a CO_2-N_2-vacuum triple manifold glass Schlenk line through three vacuum-N_2 cycles. The reaction was placed under 1 bar of N_2 atmosphere, and an IR probe was fitted in the Schlenk flask. The reaction was heated to 100 °C until full consumption of the anhydride, which could be observed from the *in situ* IR trace. After completion, the reaction was quenched

through cooling to 25 °C and opening to air. The conversion was confirmed by ^{1}H NMR spectroscopy of an aliquot taken at the end of the reaction.

7.3.2 Chapter 2 – Anhydride/CHO/CO_2 Copolymerisation

The catalyst (8 μmol), anhydride (0.8 mmol), epoxide (1.6 mL, 16.0 mmol) and CHD (9.2 mg, 0.08 mmol) were combined in a 3-neck screw cap Schlenk tube, with a screw-capped sidearm, in a glovebox. The Schlenk tube was cycled three times between vacuum and 1 bar of CO_2 to a CO_2-N_2-vacuum triple manifold glass Schlenk line, and the headspace was evacuated and refilled with 1 bar of CO_2 three times before placing the flask in a pre-heated 100 ˚C oil bath. The *in situ* IR spectroscopy probe was fitted to the Schlenk tube and was used to monitor the polymerisation. Aliquots for ^{1}H NMR spectroscopy and GPC analysis were taken by extracting 0.1 mL of the mixture with a syringe under a positive flow of gas using the screw-cap sidearm. To stop the reaction, the CO_2 source was closed and the Schlenk flask was opened to air. The polymers were precipitated in acidified methanol and dried in a 60 ˚C vacuum oven.

7.3.3 Chapter 3 – TCA/CHO/CO_2 Copolymerisation

Complex **5** (9 mg, 12 μmol), TCA, CHO, CHD (14 mg, 0.12 mmol), and toluene were combined in a 3-neck screw cap Schlenk tube with a screw-capped sidearm equipped with a rare-earth magnetic stirrer bar in a glovebox. The Schlenk tube was cycled three times on a CO_2-N_2-vacuum triple manifold steel Schlenk line, between vacuum and CO_2, and the headspace was evacuated and refilled with CO_2 three times before placing the flask in a pre-heated 100 ˚C oil bath. To switch to a N_2 atmosphere after the allotted time, CO_2 was removed by applying 6 rapid vacuum/N_2 cycles to the reaction flask. The reaction was left under N_2 for the desired time. The same procedure applies when switching back to CO_2. Aliquots were taken prior to switching reaction gas by extracting 0.1 mL of the mixture with

a syringe, under a positive flow of gas, using the screw-cap sidearm. The experiments were conducted at constant pressure (1 bar of CO_2) throughout the polymerisation. The CO_2 feed was controlled by a Bronkhorst pressure controller, and the CO_2 mass flow was monitored by a Bronkhorst mass flow metre. The experiments were repeated on a CO_2-N_2-vacuum triple manifold glass Schlenk line to monitor the polymerisations by *in situ* IR spectroscopy.

7.3.4 Chapter 4 – Epoxide/CO_2 Copolymerisation

For polymerisations run at 1 bar of CO_2, the catalyst, vCHO, CHD, and toluene were combined in a Rotaflo ampoule equipped with a rare-earth magnetic stirrer bar in a glovebox. The ampoule was cycled three times on a triple manifold steel Schlenk line, between vacuum and CO_2, and the headspace was evacuated and refilled with CO_2 three times before placing the flask in a pre-heated 100 ˚C oil bath.

For polymerisations run at 20 bar of CO_2, complex **10**, epoxide, CHD, and toluene were combined in a 25 mL or 100 mL stainless steel Parr pressure vessel and sealed in a glovebox. The vessel was heated to 80 ˚C and pressurised to 20 bar of CO_2 once the temperature was reached. To stop the reaction, the vessel was cooled to room temperature and the remaining CO_2 pressure was vented. A sample of the crude polymer was collected for analysis by ^{1}H NMR spectroscopy. The viscous solution was diluted with DCM and the polymer was isolated from precipitation from acidified methanol and dried in a 60 ˚C vacuum oven.

7.3.5 Chapter 5 – Low pressure (2 bar) Ethylene Polymerisation

Polymerisation experiments at 2 bar of ethylene were conducted in a high-pressure Rotaflo ampoule, which was charged with a 50 mL solution of catalyst and co-catalyst in toluene, prepared in a glovebox. The headspace of the ampoule was degassed under vacuum, after which ethylene at 2 bar was passed to the flask whilst stirring at 1000 rpm at the designated temperature in an oil bath. After the polymerisation time, the reaction was quenched by

stopping the ethylene flow and venting the ampoule. Acidified methanol (50 mL) was added to the mixture and stirred for 1 h. The white solid precipitate was collected by centrifugation and dried in a 60 ˚C vacuum oven.

7.3.6 Chapter 5 – High pressure (40 bar) Ethylene Polymerisation

Polymerisation experiments at 40 bar of ethylene were conducted at the University of Konstanz, during a 1 month research placement, in a Büchi miniclave reactor with a 280 mL vessel. The reactor was equipped with a mechanical stirrer, a heating and cooling jacket connected to a thermostat, a thermocouple dipping into the polymerisation mixture and a nitrogen/vacuum supply. Prior to all polymerisation experiments, the reactor was evacuated and heated up by setting the thermostat to 90 ˚C. When the reactor temperature was > 60 °C, the reactor was flushed with nitrogen and evacuated three times. The reactor was brought 3 °C below the desired reaction temperature and filled with 100 mL of toluene via cannula transfer and stirred at 500 rpm. The catalyst was dissolved in 5 mL of toluene and transferred into the reactor *via* syringe. Immediately after addition, the stirring rate was increased to 1000 rpm and the reactor was pressurised to 40 bar of ethylene. During the pressurisation procedure, the desired temperature was set. All experiments were conducted at constant pressure over the entire polymerisation experiment with the ethylene feed controlled and monitored by a Bronkhorst mass flow meters. After the desired reaction time, the ethylene flow was stopped and the reactor vented to air. The content of the reactor was poured into a beaker with 300 mL of MeOH, and the precipitated polymer was collected by filtration and dried in a 60 ˚C vacuum oven overnight.

7.4 Synthesis and Characterising Data

7.4.1 Chapter 4

Synthesis of [LMgCo(C_6F_5)$_2$] (10)

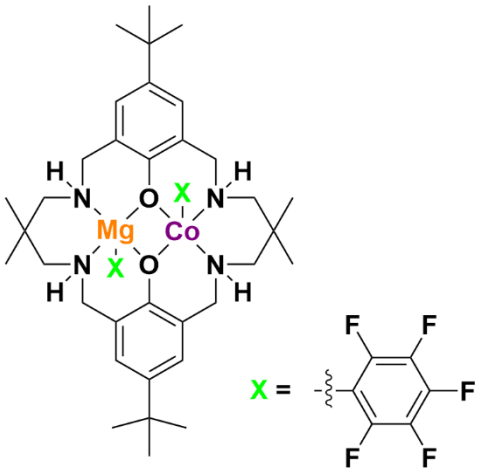

10

Macrocyclic tetraamine-based ligand [LH_2] (143 mg, 0.29 mmol, 1 equiv.) and [Mg{N[Si(Me3)$_3$]$_2$}$_2$] (98 mg, 0.29, 1 equiv.) were stirred in anhydrous THF (15 mL) in a sealed vial for 2 h in a glovebox. A concentrated solution of [Co(C_6F_5)$_2$(THF)$_2$] (153 mg, 0.29 mmol, 1 equiv.) was added dropwise and stirred overnight at room temperature, observing a colour change from aquamarine to black/purple. The solution was cooled to −30 ˚C for 24 h to afford a purple crystalline solid. The solution was decanted and the solid residue was washed with cold (– 30 ˚C) THF and hexane, and dried *in vacuo* overnight at room temperature (0.15 mmol, 52 % yield). The product was stored at −30 ˚C. Crystals suitable for X-ray diffraction were afforded from a −30 ˚C solution in THF after 48 h. ^{1}H NMR (toluene-d_8, 400 MHz): δ 264.51, 220.88, 148.51, 75.08, 29.42, 25.13, 10.29, 7.77, 6.34, 3.28, 2.58, -0.42, -1.98, -16.60, -56.33 ppm. ^{19}F{^{1}H} NMR (toluene-d_8, 377 MHz) -68.45 (s, 4 F), -153.63 (t, 2 H, J = 19.1 Hz), -155.50 (br, 4 H) ppm.

Complex **10** was further characterised by SQUID magnetometry, X-ray crystallography, and CV (see Chapter 4).

Synthesis of [$LCo_2(C_6F_5)_2$]

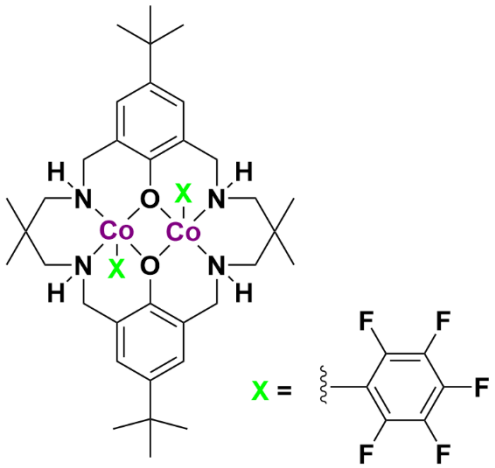

$[Co(C_6F_5)_2(THF)_2]$ (39 mg, 0.073 mmol, 2 equiv.) was added to a cold (−30 ˚C) suspension of $[LH_2]$ (20 mg, 0.036 mmol, 1 equiv.) in toluene-d_8 (0.6 mL). After stirring for 5 minutes, the solution turned dark/deep purple. Quantitative conversion of the ligand was determined by ^{1}H NMR spectroscopy. Crystals suitable for X-ray diffraction were afforded from a −30 ˚C solution in toluene-d_8. ^{1}H NMR (toluene-d_8, 400 MHz): δ 269.93, 229.57, 187.21, 94.15, 25.46, 5.92, -0.30, -27.11, -75.77 ppm. ^{19}F{^{1}H} NMR (toluene-d_8, 377 MHz): δ -71.2 ppm.

7.4.2 Chapter 5

General Synthesis of ligands HL_n[18]

Salicylaldehyde (1 equivalent) and aniline (1 equivalent) were refluxed in ethanol (50 mL) overnight under air. The product either precipitates upon cooling the solution, or is precipitated from hexane after removal of ethanol.

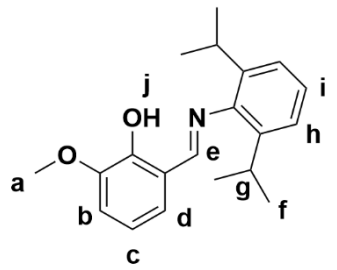

HL_1

HL_1: yellow powder, 89 % yield. ^{1}H NMR ($CDCl_3$, 400 MHz): δ 13.54 (s, 1H, j), 8.32 (s, 1H, e), 7.19 (m, 3H, h, i), 7.05–6.90 (m, 3H, b, c, d), 3.97 (s, 3H, a), 3.01 (sept, 2H, *J* = 6.5 Hz, g), 1.18 (d, 12H, *J* = 6.5 Hz, f) ppm.

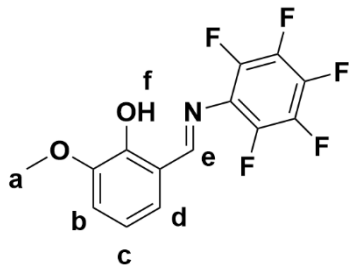

HL_2

HL_2: bright orange powder, 91 % yield. ^{1}H NMR ($CDCl_3$, 400 MHz) δ 12.57 (s, 1H, f), 8.85 (s, 1H, e), 7.08–6.89 (m, 3H, b, c, d), 3.93 (s, 3H, a) ppm. ^{19}F{^{1}H} NMR ($CDCl_3$, 377 MHz): δ -151.68 (dd, *J* = 21.5, 6.4 Hz, *ortho*), -158.00 (t, *J* = 21.3 Hz, *para*), -162.34 (td, *J* = 21.6, 6.5 Hz, *meta*) ppm.

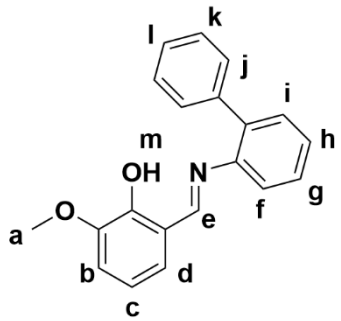

HL_3

HL$_3$: red/orange powder, 94 % yield. ^{1}H NMR ($CDCl_3$, 400 MHz): δ 12.90 (s, 1H, m), 8.61 (s, 1H, e), 7.47–7.20 (m, 9H, f-l), 7.02–6.83 (m, 3H, b, c, d), 3.90 (s, 3H, a) ppm.

General Synthesis of ligand salts

To a vial charged with **HL$_n$** (1 equiv.) dissolved in anhydrous THF, NaH (1.8 equiv.) was added in portion wise. The suspension was stirred overnight, filtered, and dried in vacuo at room temperature. The white/pale yellow solids (**NaL$_n$**) were isolated and used without further purification.

General Synthesis of [L$_n$NiPh(PPh$_3$)][18]

To a Schlenk tube charged with **NaL$_n$** (1.1 equiv) in toluene (50 mL), [NiClPh(PPh_3)$_2$] (1 equiv.) was added. The mixture was stirred at room temperature for 24 h, which turned deep red over time. The mixture was filtered and the solvent removed *in vacuo*. The crude solid was dissolved in hexane, filtered, and stored at −30 ˚C overnight. The red crystalline solid produced was isolated by filtration, washed with cold hexane, and dried *in vacuo* at room temperature.

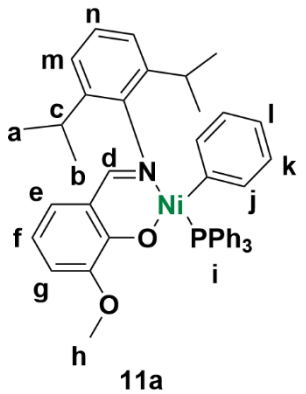

11a

11a: 55 % yield. Anal. Calcd: C, 74.59; H, 6.26; N, 1.98. Found: C, 74.66; H, 6.17; N, 1.91. ^{1}H NMR (C_6D_6, 400 MHz): δ 7.97 (d, 1H, $^4J_{PH}$ = 8.9 Hz, d), 7.80–7.69 (m, 6H, i), 7.02–6.85 (m, 14H, i, m, n, k), 6.74 (dd, 1H, *J* = 8.0, 1.7 Hz, e), 6.68 (dd, 1H, *J* = 7.5, 1.7 Hz, g), 6.66 (t, 1H, *J* = 7.7 Hz, l), 6.38 (t, 1H, *J* = 7.1 Hz, f), 6.30 (dd, 2H, *J* = 8.0, 6.6 Hz, j), 4.07 (sept,

2H, *J* = 6.8 Hz, c), 3.00 (s, 3H, h), 1.26 (d, 6H, *J* = 6.8 Hz, b), 1.06 (d, 6H, *J* = 6.8 Hz, a) ppm. $^{31}P\{^{1}H\}$ NMR (C_6D_6, 162 MHz): δ 22.56 ppm. $^{13}C\{^{1}H\}$ (C_6D_6, 126 MHz): δ 166.3, 159.1, 153.6, 152.6, 149.8, 149.5, 140.5, 139.1, 136.5, 135.4, 134.9, 134.9, 132.4, 132.1, 131.2, 129.8, 129.6, 128.5, 128.4, 127.4, 127.1, 127.0, 125.9, 125.4, 125.25, 124.7, 121.4, 120.5, 117.8, 113.3, 56.5 ppm.

Complex **11a** was further characterised by X-ray crystallography (see Chapter 5).

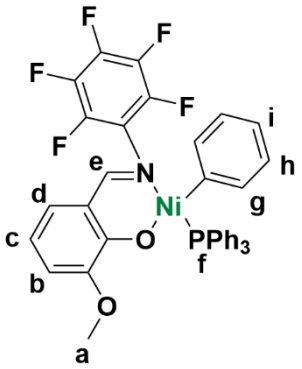

12a

12a: 50 % yield. Anal. Calcd: C, 63.90; H, 3.81; N, 1.96. Found: C, 63.99; H, 3.94; N, 1.85. ^{1}H NMR (C_6D_6, 500 MHz): δ 7.73 (d, 1H, $^{4}J_{HP}$ = 7.9 Hz, e), 7.63–7.65 (m, 6H, f), 7.19 (d, 2H, *J* = 7.5 Hz, h), 6.97–6.87 (m, 9H, f), 6.70 (dd, 1H, *J* = 8.2, 1.7 Hz, d), 6.61 (dd, 1H, *J* = 7.5, 1.7 Hz, b), 6.43 (t, 1H, *J* = 7.8 Hz, c), 6.33 – 6.26 (m, 3H, g, i) ppm. ^{19}F (470 MHz, C_6D_6) *δ* -147.49 (dd, *J* = 24.5, 6.2, *ortho*), -161.80 (t, *J* = 21.8, *para*), -165.15 (dd, *J* = 23.3, 5.0, *meta*) ppm. $^{31}P\{^{1}H\}$ NMR (C_6D_6, 162 MHz): δ 25.75 ppm. $^{13}C\{^{1}H\}$ NMR (C_6D_6, 126 MHz): δ 168.7, 160.7, 153.7, 151.2, 150.7, 137.6, 134.9, 134.8, 131.7, 131.2, 129.8, 128.8, 126.6, 125.7, 122.4, 119.4, 116.8, 114.1, 56.1 ppm.

Complex **12a** was further characterised by X-ray crystallography (see Chapter 5).

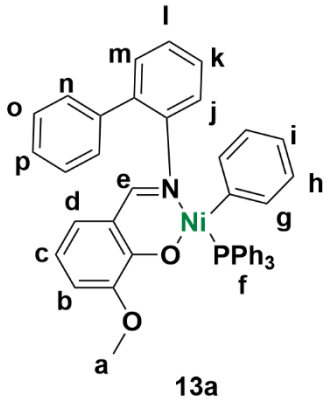

13a

13a: 30 % yield. ^{1}H NMR (C_6D_6, 400 MHz): δ 7.91 (d, 1H, $^{4}J_{HP}$ = 8.4 Hz, e), 7.84 (d, 2H, *J* = 7.1 Hz, o), 7.60–7.51 (m, 6H, f), 7.3 (t, 2H, *J* = 7.4 Hz, h), 7.22 (t, 1H, *J* = 6.7 Hz, p), 7.1 (dd, 1H, *J* = 7.8, 1.5 Hz, m) 7.06–6.92 (m, 10H, f), 6.77 (t, 1H, *J* = 7.8 Hz, c), 6.69–6.61 (m, 3H, d, j, k), 6.44 (t, 1H, *J* = 6.9 Hz, n), 6.38 (m, 2H, *J* = 7.8 Hz, b, l), 2.92 (s, 3H, a) ppm. ^{31}P{^{1}H} NMR (C_6D_6, 162 MHz): δ 24.76 ppm. ^{13}C{^{1}H} NMR (C_6D_6, 126 MHz): δ 166.3, 159.1, 153.6, 152.6, 149.8, 149.4, 140.45, 139.1, 136.5, 135.4, 134.9, 134.7, 132.4, 132.1, 131.2, 129.8, 129.6, 127.3, 127.1, 127.0, 125.9, 125.4, 125.3, 124.7, 121.4, 120.5, 117.8, 113.3, 56.5 ppm.

Complex **13a** was further characterised by X-ray crystallography (see Chapter 5).

Synthesis of [(TMEDA)Ni(Me)$_2$][19]

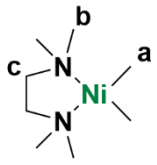

TMEDA (37.2 g, 320 mmol) was added to a solution of $Ni(OAc)_2{\cdot}4H_2O$ (72.1 g, 289.7 mmol) in methanol (350 mL) under air, resulting in a rapid colour change from green to blue-green. The solution was concentrated to dryness to yield blue-green solid $[(TMEDA)_4Ni_2(OAc)_4(H_2O)]$. This was re-dissolved in toluene (300 mL), filtered over celite, and concentrated to *ca.* 250 mL. The reaction flask was connected to a Dean-Stark

apparatus, purged with N_2, and refluxed for 4 h at 150 ˚C, until around 18 mL of water was collected in the Dean-Stark apparatus. Additional 150 mL of solvent was distilled into the trap, and the rest was concentrated dryness. A dark green solid [(TMEDA)Ni(OAc)$_2$] was collected and stored under N_2 (84.2 g, 287.4 mmol, 99 % yield).

[(TMEDA)Ni(OAc)$_2$] (23.44 g, 80.0 mmol) was grinded and dissolved in a 4:1 mixture of toluene and THF (600 mL) and cooled to –40 ˚C. Methyl lithium (160 mmol, 100 mL, 1.6 M in Et_2O) was added using a dropping funnel over the course of 30 min in an inert atmosphere. The funnel was washed with Et_2O (10 mL) and the mixture was stirred for a further 10 min, after which half of the solvent volume was removed in vacuo. The dark mixture was filtered through celite, and the filter cake was washed thoroughly with toluene (50 mL). The solution was concentrated to dryness to give a dark yellow solid and stored under at –30 ˚C (11.76 g, 57.7 mmol, 72 % yield). ^{1}H NMR (C_6D_6, 400 MHz): δ 1.94 (s, 12H, b), 1.39 (s, 4H, c), -0.45 (s, 6H, a) ppm.

Synthesis of 11b

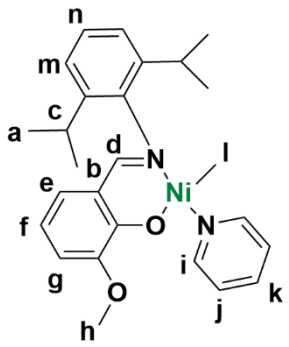

11b

HL$_1$ (93 mg, 0.30 mmol, 1 equiv.), [(TMEDA)NiMe$_2$] (69 mg, 0.33 mmol, 1.1 equiv.), and pyridine (480 mg, 6.00 mmol, 20 equiv.) were combined in benzene and stirred for 30 min. The mixture was centrifuged, and the supernatant was concentrated to dryness to produce a red solid (69.5 mg, 0.15 mmol, 51 % yield.); ^{1}H NMR (C_6D_6, 400 MHz): δ 8.79 (d, 2H, *J* =

5.1 Hz, i), 7.61 (s, 1H, d), 6.75–6.67 (m, 2H, g, e), 6.61 (t, 1H, *J* = 7.8 Hz, k), 6.44 (t, 1H, *J* = 7.8, f), 6.27 (t, 2H, *J* = 6.8 Hz, j), 4.23 (sept, 2H, *J* = 6.8 Hz, c), 3.40 (s, 3H, h), 1.53 (d, 6H, *J* = 6.9 Hz, a), 1.08 (d, 6H, *J* = 6.9 Hz, b) -0.66 (s, 3H, l) ppm.

7.5 References

1. Kember, M. R.; Knight, P. D.; Reung, P. T. R.; Williams, C. K., *Angew. Chem. Int. Ed.* **2009,** *48* (5), 931-933.

2. Zeller, A.; Herdtweck, E.; Strassner, T., *Eur. J. Inorg. Chem.* **2003,** *2003* (9), 1802-1806.

3. Smith, C. F.; Tamborski, C., *J. Organomet. Chem.* **1971,** *32* (2), 257-262.

4. Royo, P.; Vazquez, A., *J. Organomet. Chem.* **1981,** *204* (2), 243-247.

5. Jezorek, R. L.; Zhang, N.; Leowanawat, P.; Bunner, M. H.; Gutsche, N.; Pesti, A. K. R.; Olsen, J. T.; Percec, V., *Org. Lett.* **2014,** *16* (24), 6326-6329.

6. Deacy, A. C.; Kilpatrick, A. F. R.; Regoutz, A.; Williams, C. K., *Nat. Chem.* **2020,** *12* (4), 372-380.

7. Garden, J. A.; Saini, P. K.; Williams, C. K., *J. Am. Chem. Soc.* **2015,** *137* (48), 15078-15081.

8. Kember, M. R.; Williams, C. K., *J. Am. Chem. Soc.* **2012,** *134* (38), 15676-15679.

9. Reis, N. V.; Deacy, A. C.; Rosetto, G.; Durr, C. B.; Williams, C. K., *Chem. Eur. J.* **2022,** *28*, e202104198.

10. Dakshinamoorthy, D.; Weinstock, A. K.; Damodaran, K.; Iwig, D. F.; Mathers, R. T., *ChemSusChem* **2014,** *7* (10), 2923-2929.

11. Cosier, J.; Glazer, A., *J. Appl. Crystallogr.* **1986,** *19* (2), 105-107.

12. CrysAlisPRO, Oxford Diffraction /Agilent Technologies UK Ltd, Yarnton, England.

13. Sheldrick, G., *Acta Crystallographica Section C* **2015,** *71* (1), 3-8.

14. SHELXTL v5.1, Bruker AXS, Madison, WI, **1998**.

15. Dolomanov, O. V.; Bourhis, L. J.; Gildea, R. J.; Howard, J. A. K.; Puschmann, H., *J. Appl. Crystallogr.* **2009,** *42* (2), 339-341.

16. Betteridge, P. W.; Carruthers, J. R.; Cooper, R. I.; Prout, K.; Watkin, D. J., *J. Appl. Crystallogr.* **2003,** *36* (6), 1487.

17. Palatinus, L.; Chapuis, G., *J. Appl. Crystallogr.* **2007,** *40* (4), 786-790.

18. Wang, C.; Friedrich, S.; Younkin, T. R.; Li, R. T.; Grubbs, R. H.; Bansleben, D. A.; Day, M. W., *Organometallics* **1998,** *17* (15), 3149-3151.

19. Göttker-Schnetmann, I.; Mecking, S., *Organometallics* **2020,** *39* (18), 3433-3440.

Appendix

Supplementary Figures and Data for Chapter 2

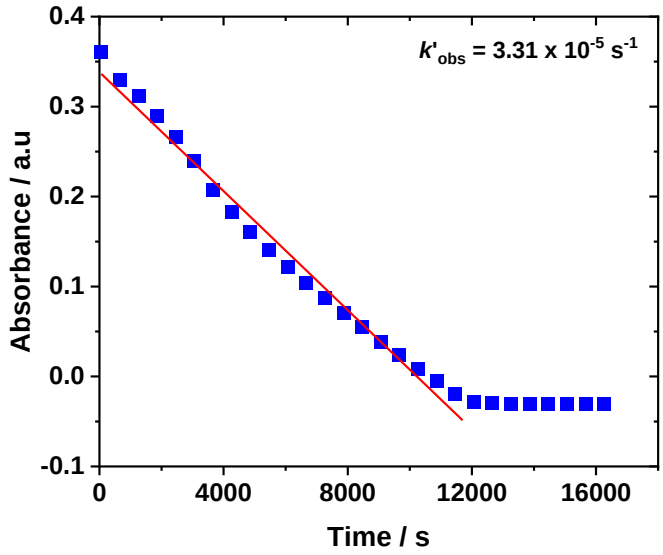

Figure S2.1: Plot of absorbance (1785 cm^{-1}) *vs.* time for the ROCOP of NA/CHO using complex **2** (Table 2.1, entry 2).

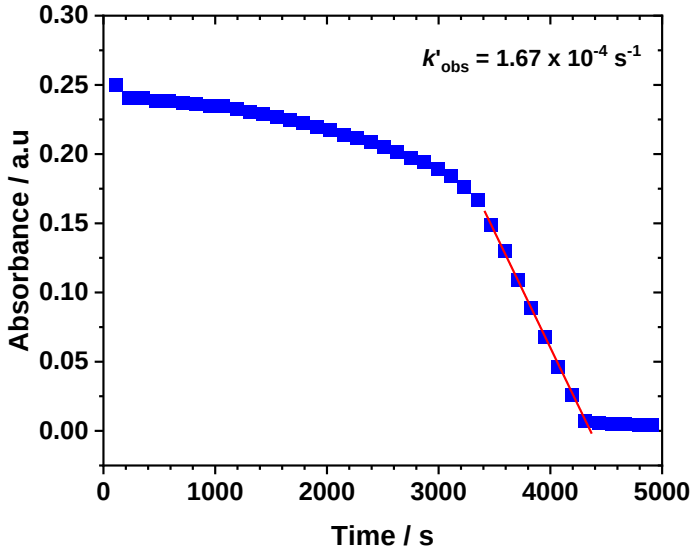

Figure S2.2: Plot of absorbance (1785 cm^{-1}) *vs.* time for the ROCOP of NA/CHO using complex **3** (Table 2.1, entry 3).

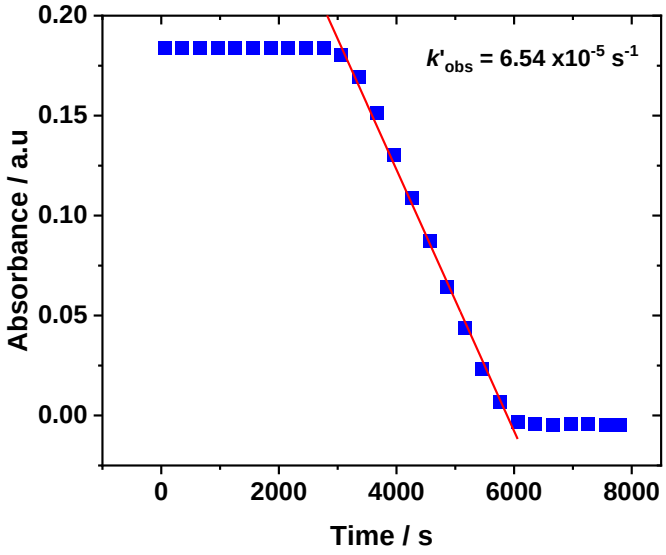

Figure S2.3: Plot of absorbance (1785 cm^{-1}) *vs.* time for the ROCOP of NA/CHO using complex **4** (Table 2.1, entry 4).

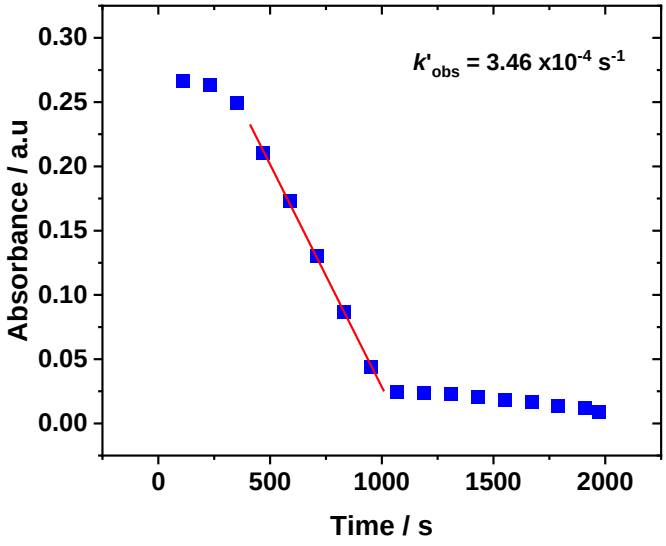

Figure S2.4: Plot of absorbance (1785 cm^{-1}) *vs.* time for the ROCOP of NA/CHO using complex **5** (Table 2.1, entry 5).

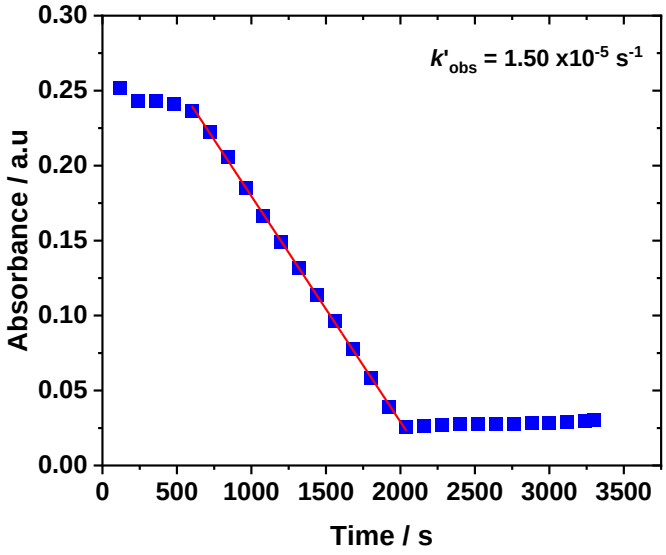

Figure S2.5: Plot of absorbance (1785 cm^{-1}) *vs.* time for the ROCOP of NA/CHO using complex **6** (Table 2.1, entry 6).

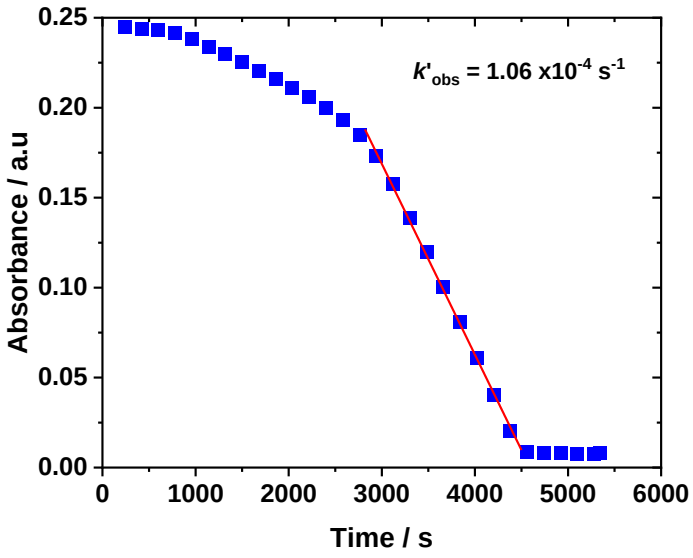

Figure S2.6: Plot of absorbance (1785 cm^{-1}) *vs.* time for the ROCOP of NA/CHO using complex **7** (Table 2.1, entry 7).

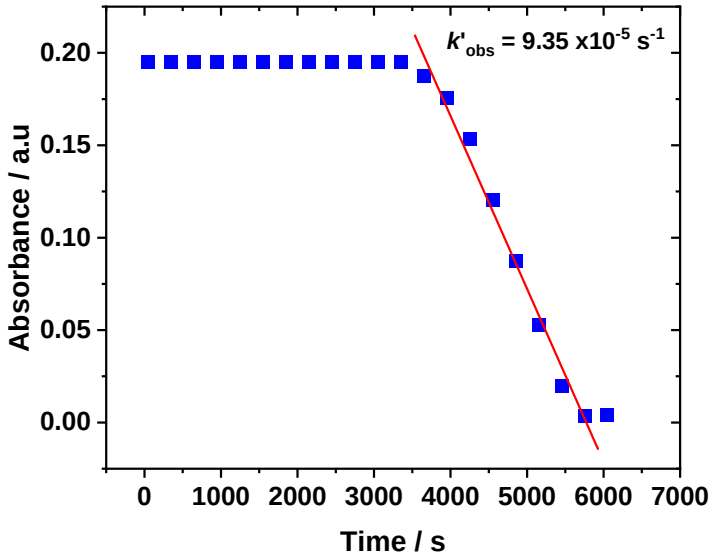

Figure S2.7: Plot of absorbance (1785 cm^{-1}) versus time for the ROCOP of NA/CHO using complex **8** (Table 2.1, entry 8).

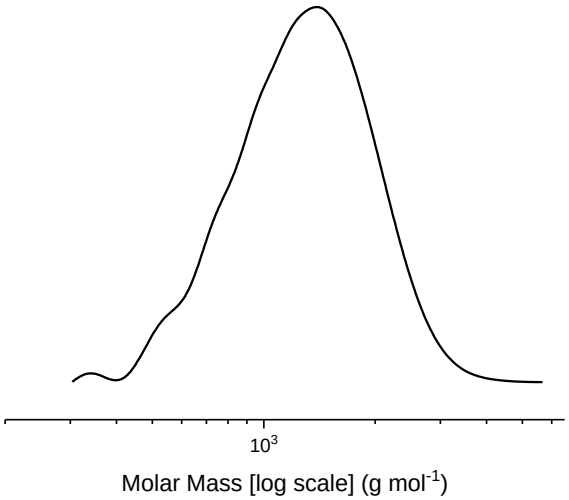

Figure S2.8: Example GPC trace for NA/CHO copolymerisation.

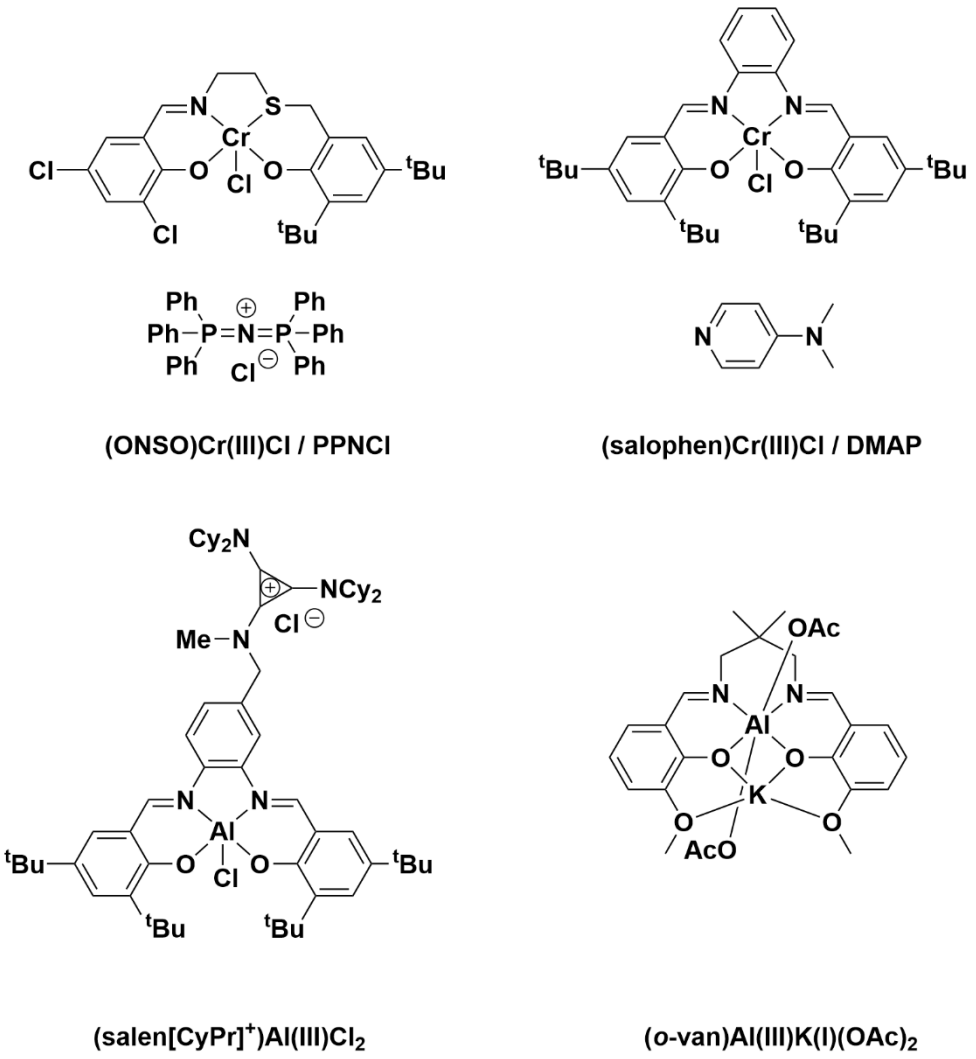

Figure S2.9: Illustration of literature catalysts for NA/CHO ROCOP featured in Table 2.1: (ONSO)Cr(II)Cl/PPNCl,[1] (salophen)Cr(III)Cl/DMAP,[2] (salen[CyPr]$^{+}$)Al(III)Cl_2,[3] (o-van)Al(III)K(I)$(OAc)_2$.[4]

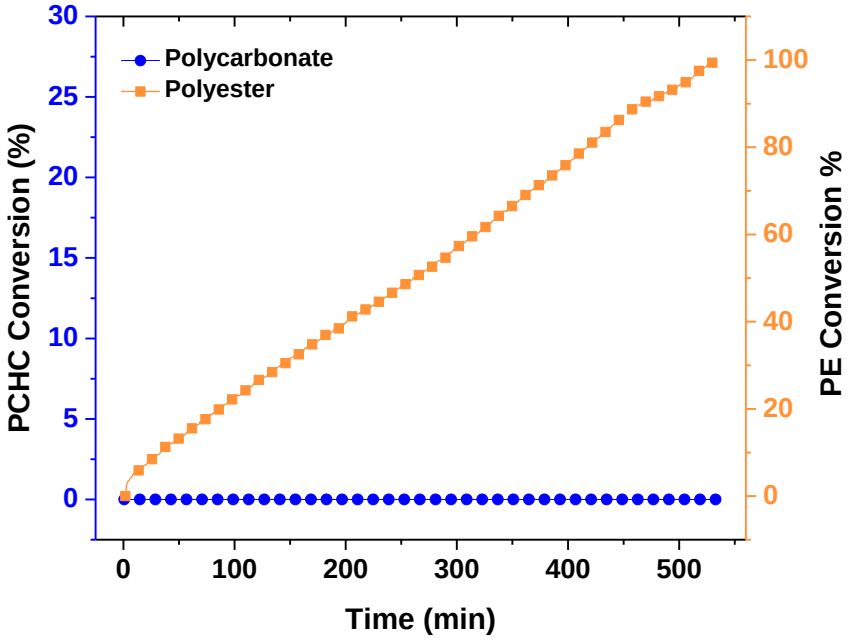

Figure S2.10: Conversion *vs.* time plot using data from *in situ* IR spectroscopy for the polymerisation of TCA/CHO/CO_2 with catalyst **9** (Table 2.2, entry 1).

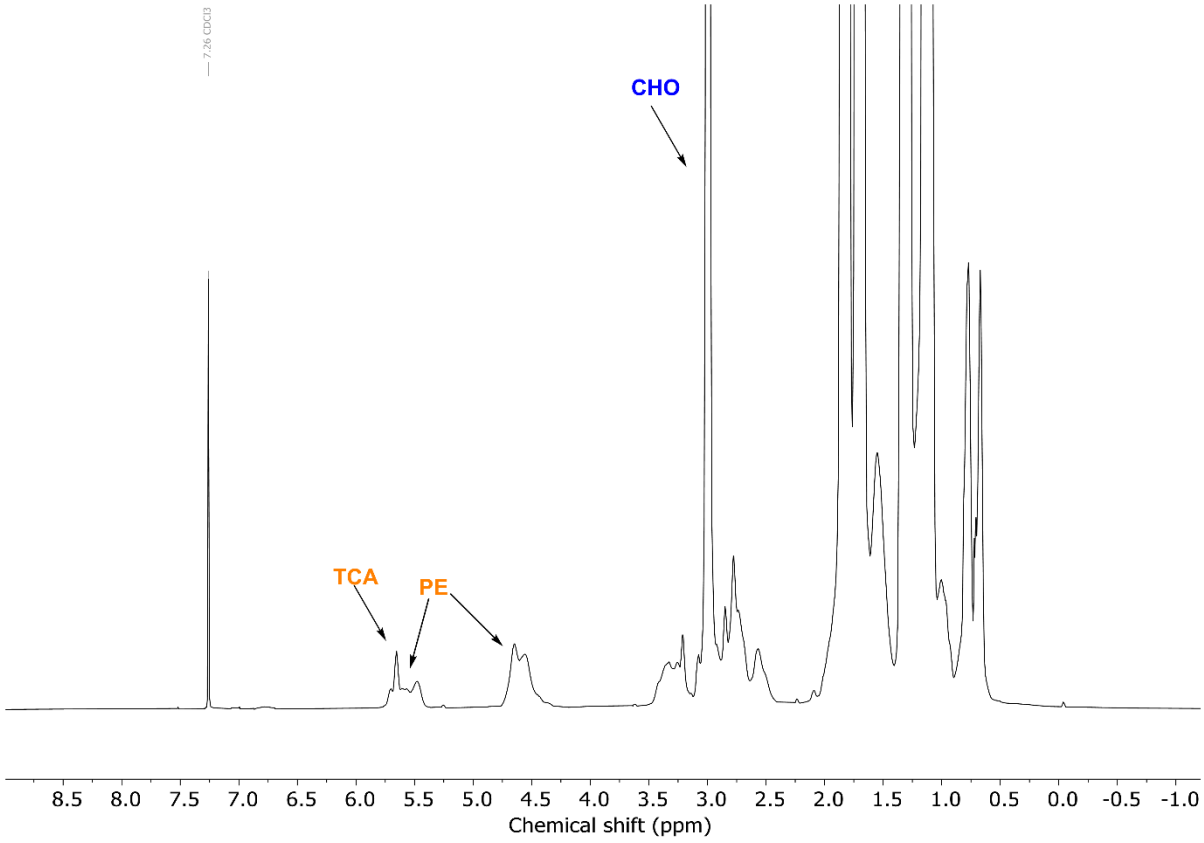

Figure S2.11: ^{1}H NMR spectrum ($CDCl_3$, 400 MHz) of an aliquot taken at 7.7 h for the polymerisation of TCA/CHO/CO_2 with catalyst **9** (Table 2.2, entry 1).

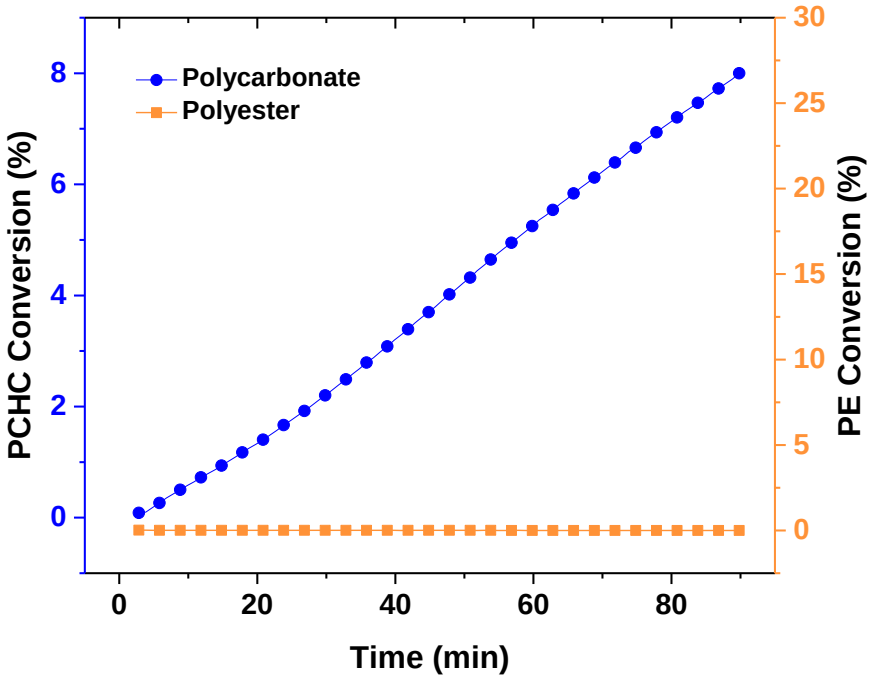

Figure S2.12: Conversion *vs.* time plot using data from *in situ* IR spectroscopy for the polymerisation of TCA/CHO/CO_2 with catalyst **1** (Table 2.2, entry 2).

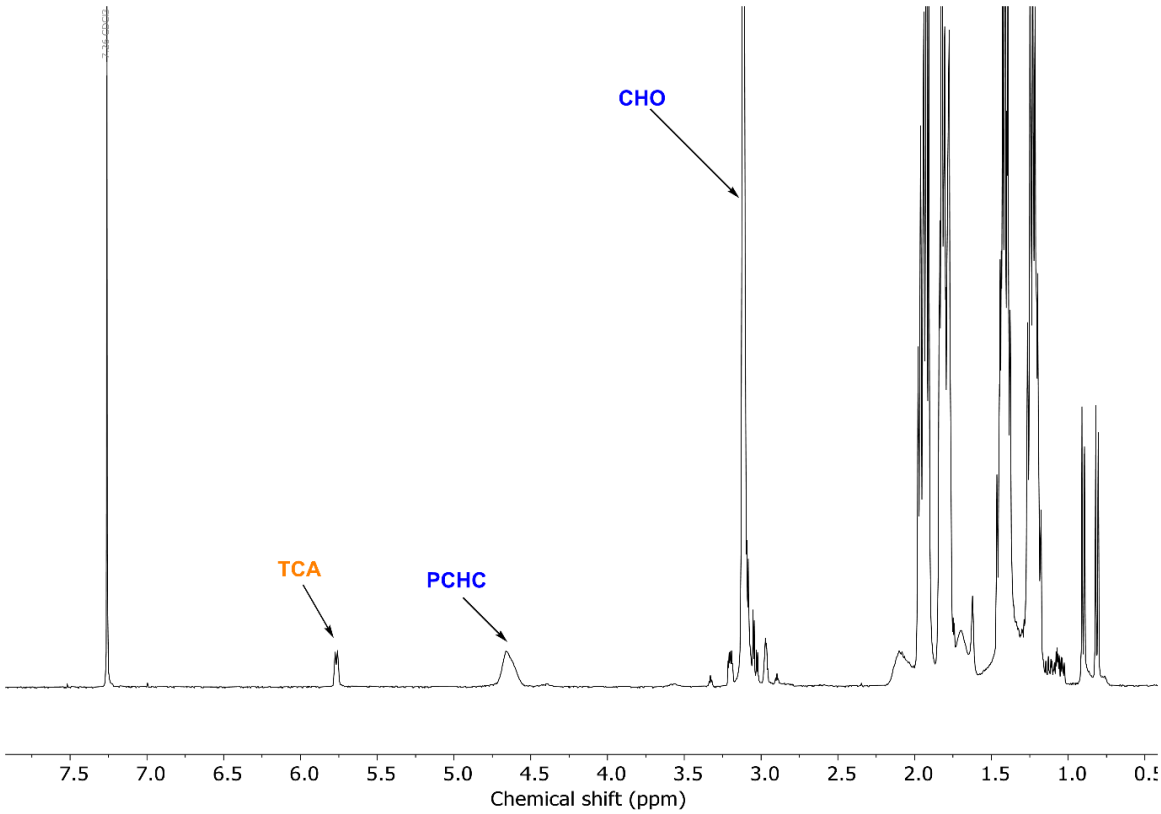

Figure S2.13: ^{1}H NMR spectrum ($CDCl_3$, 400 MHz) of an aliquot taken for the polymerisation of TCA/CHO/CO_2 with catalyst **1** (Table 2.2, entry 2).

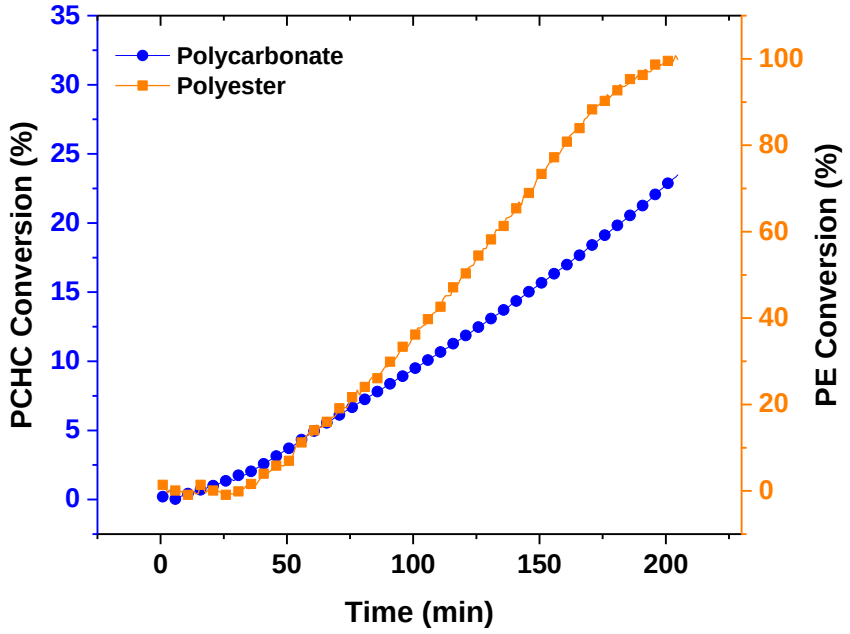

Figure S2.14: Conversion *vs.* time plot using data from *in situ* IR spectroscopy for the polymerisation of TCA/CHO/CO_2 with catalyst **8** (Table 2.2, entry 3).

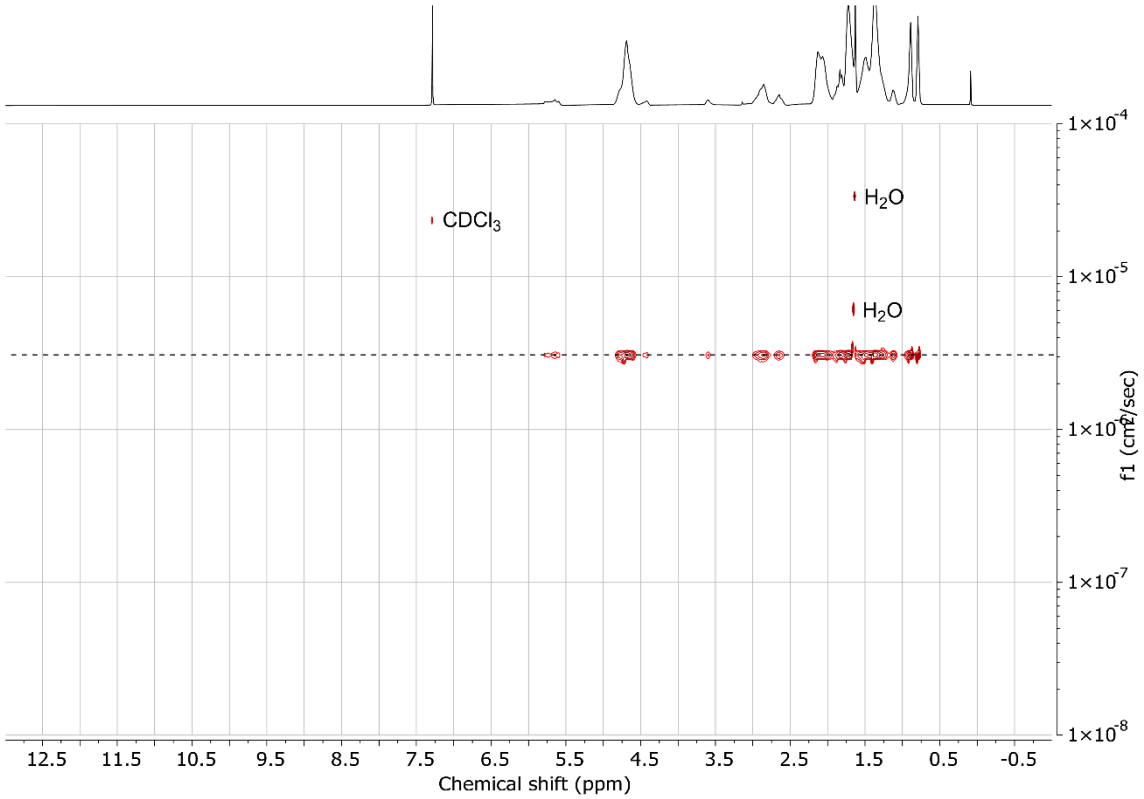

Figure S2.15: ^{1}H DOSY spectrum ($CDCl_3$, 500 MHz) of the purified random copolymer obtained from the polymerisation of TCA/CHO/CO_2 with catalyst **8**.

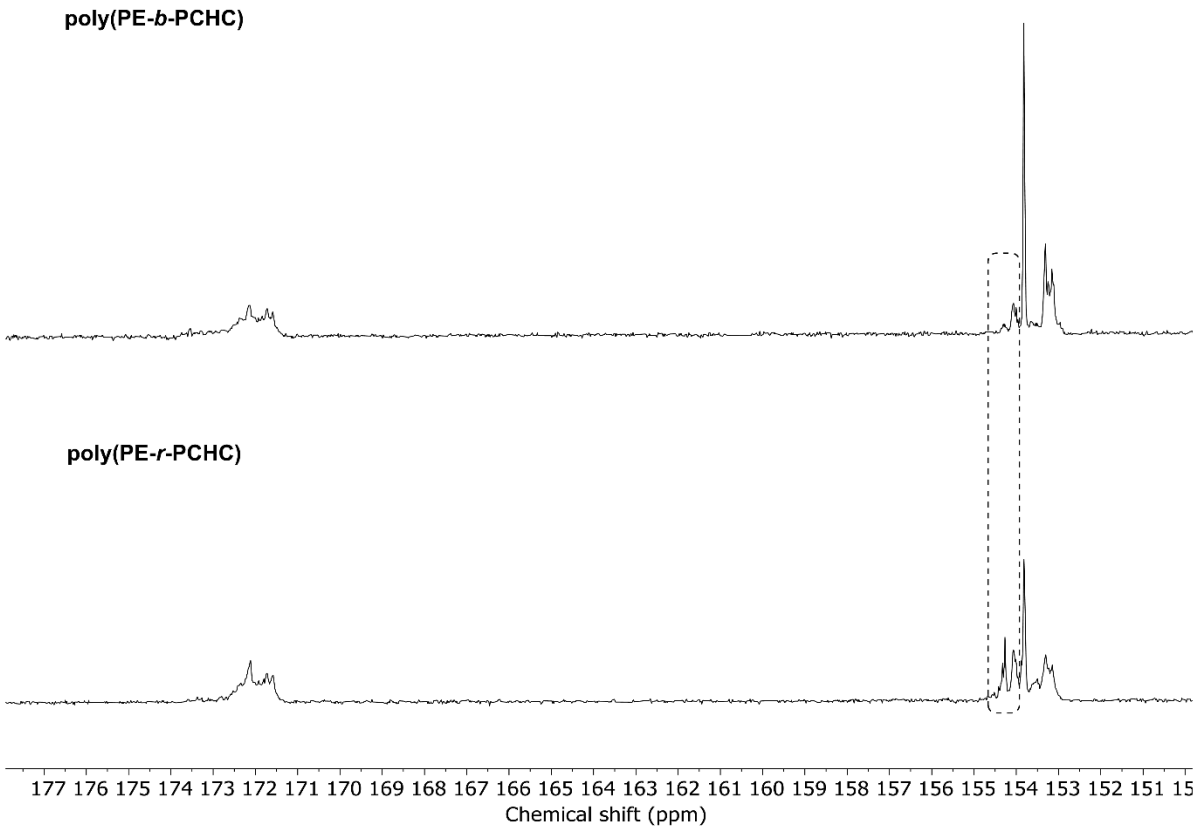

Figure S2.16: Portion of the $^{13}C\{^{1}H\}$ NMR spectrum ($CDCl_3$, 126 MHz) of poly(PE-*b*-PCHC) (top) and poly(PE-*r*-PCHC) (bottom). New carbonyl signals can be observed at 154 ppm for the random copolymer.

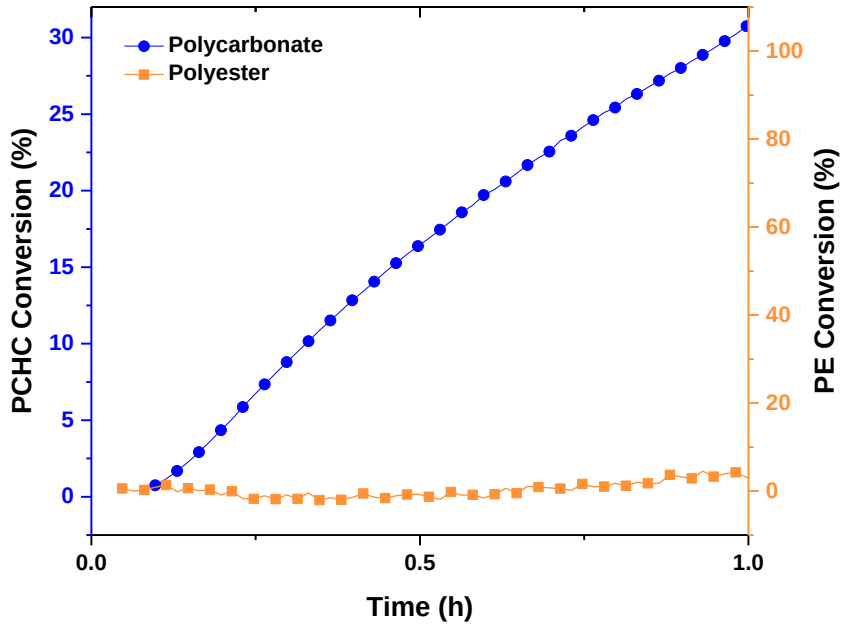

Figure S2.17: Conversion *vs.* time plot using data from *in situ* IR spectroscopy for the polymerisation of TCA/CHO/CO_2 with catalyst **5** (Table 2.2, entry 4).

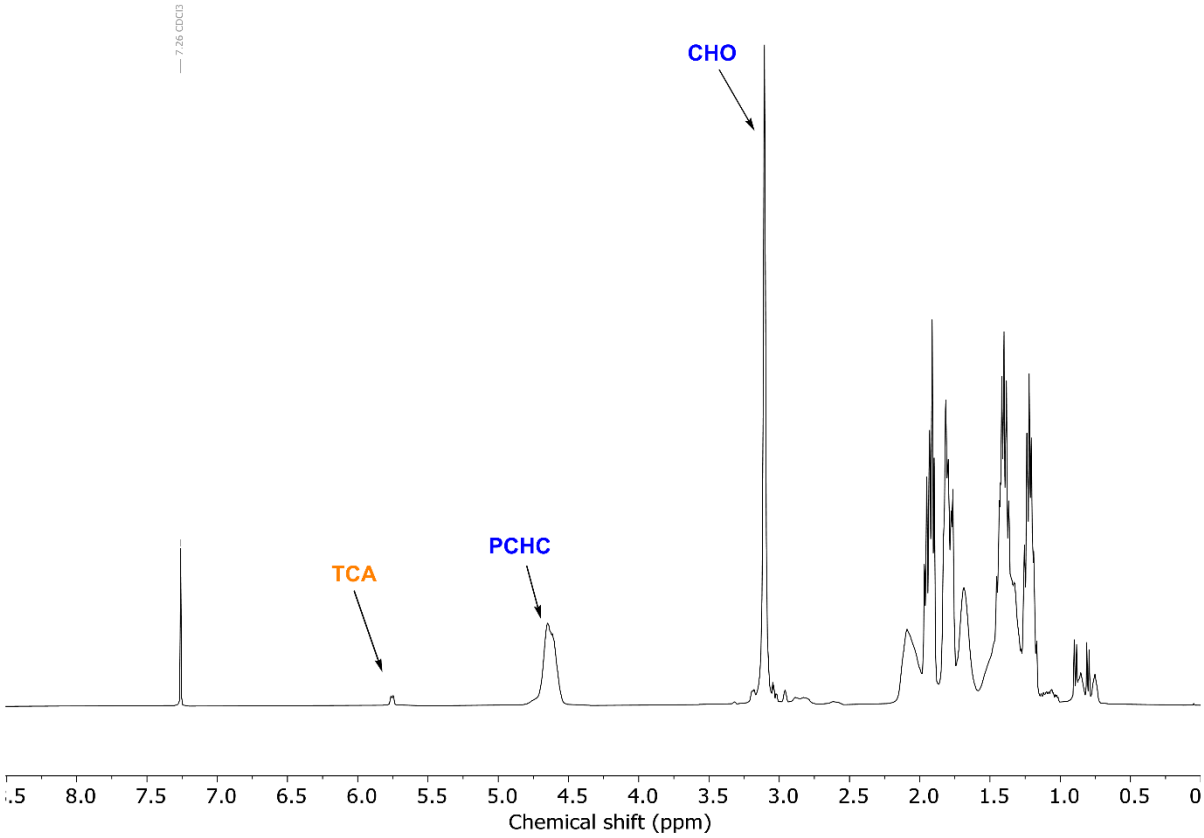

Figure S2.18: ^{1}H NMR spectrum ($CDCl_3$, 400 MHz) of an aliquot taken for the polymerisation of TCA/CHO/CO_2 with catalyst **5** (Table 2.2, entry 4).

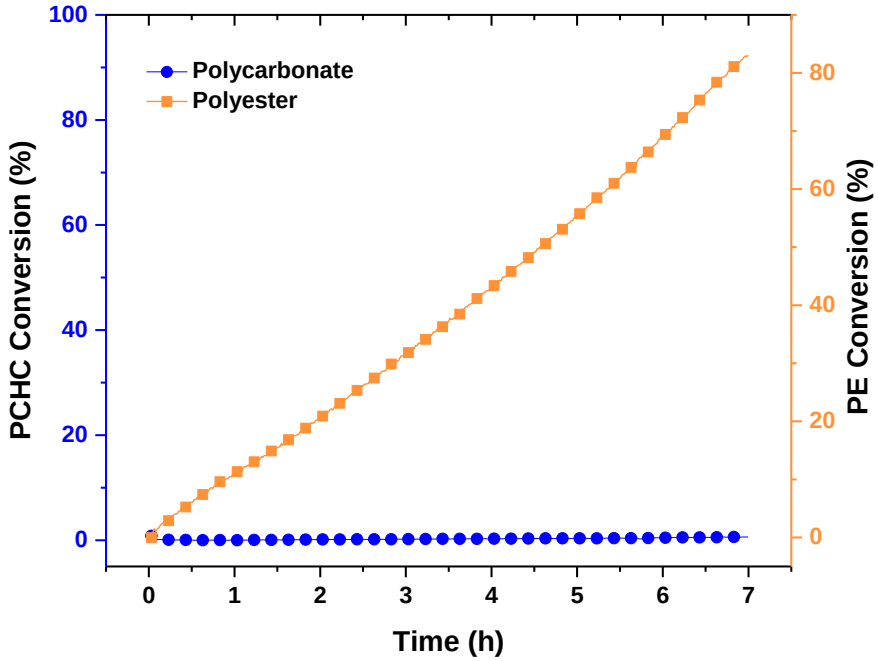

Figure S2.19: Conversion *vs.* time plot using data from *in situ* IR spectroscopy for the polymerisation of PA/CHO/CO_2 with catalyst **9** (Table 2.3, entry 1).

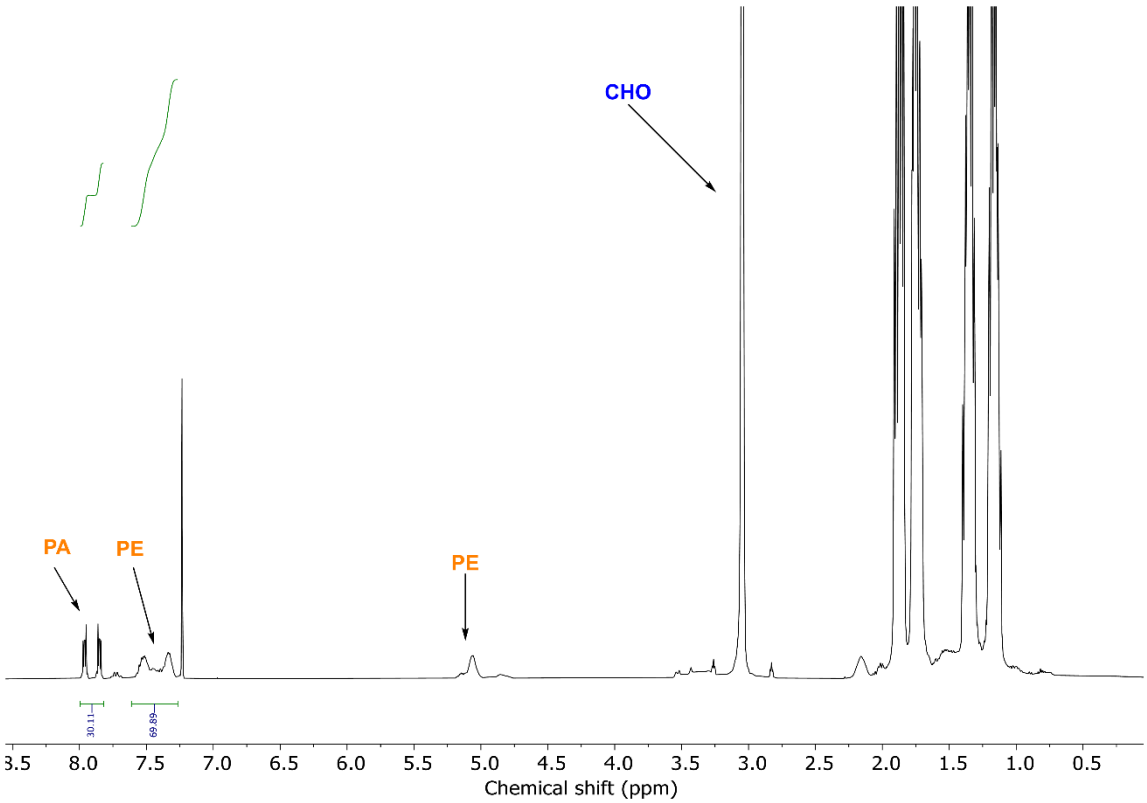

Figure S2.20: ^{1}H NMR spectrum ($CDCl_3$, 400 MHz) of an aliquot taken for the polymerisation of PA/CHO/CO_2 with catalyst **9** (Table 2.3, entry 1).

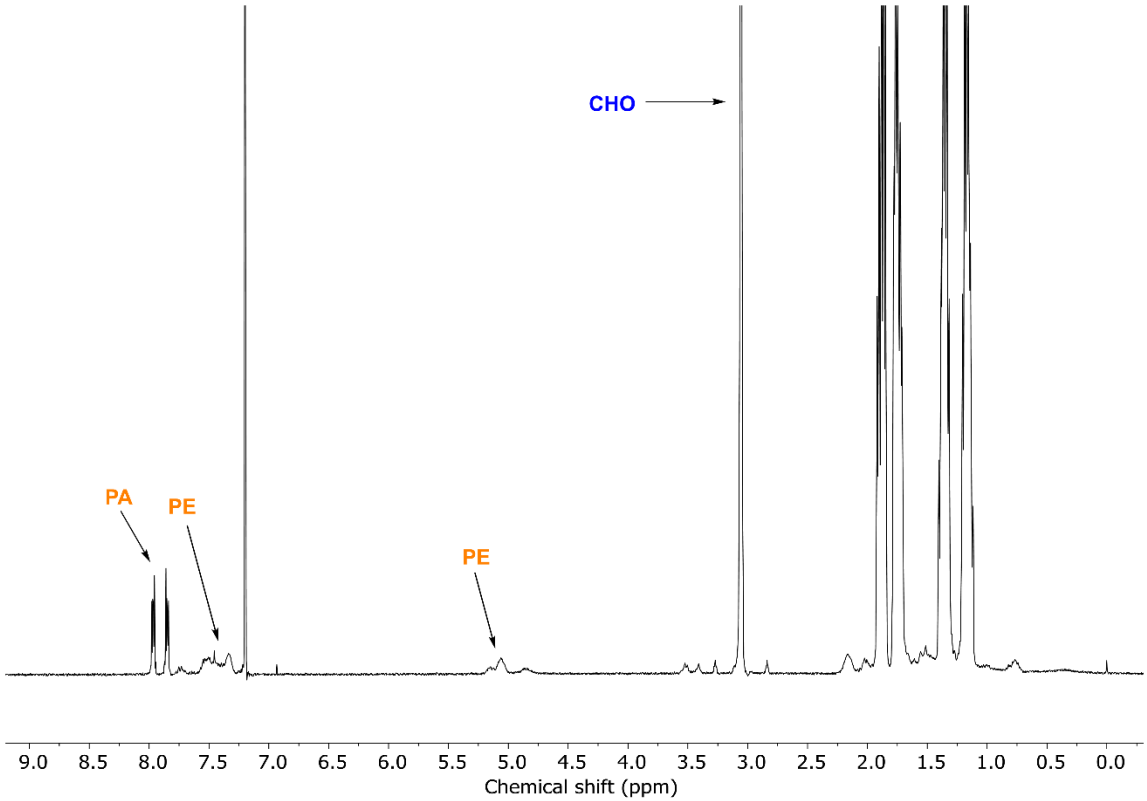

Figure S2.21: ^{1}H NMR spectrum ($CDCl_3$, 400 MHz) of an aliquot taken for the polymerisation of PA/CHO/CO_2 with catalyst **8** (Table 2.3, entry 3).

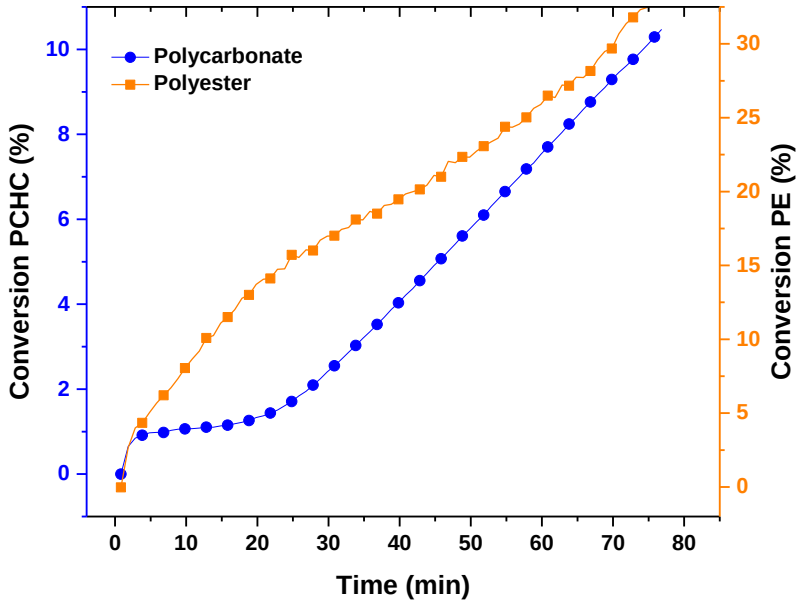

Figure S2.22: Conversion *vs.* time plot using data from *in situ* IR spectroscopy for the polymerisation of PA/CHO/CO_2 with catalyst **1** (Table 2.3, entry 2).

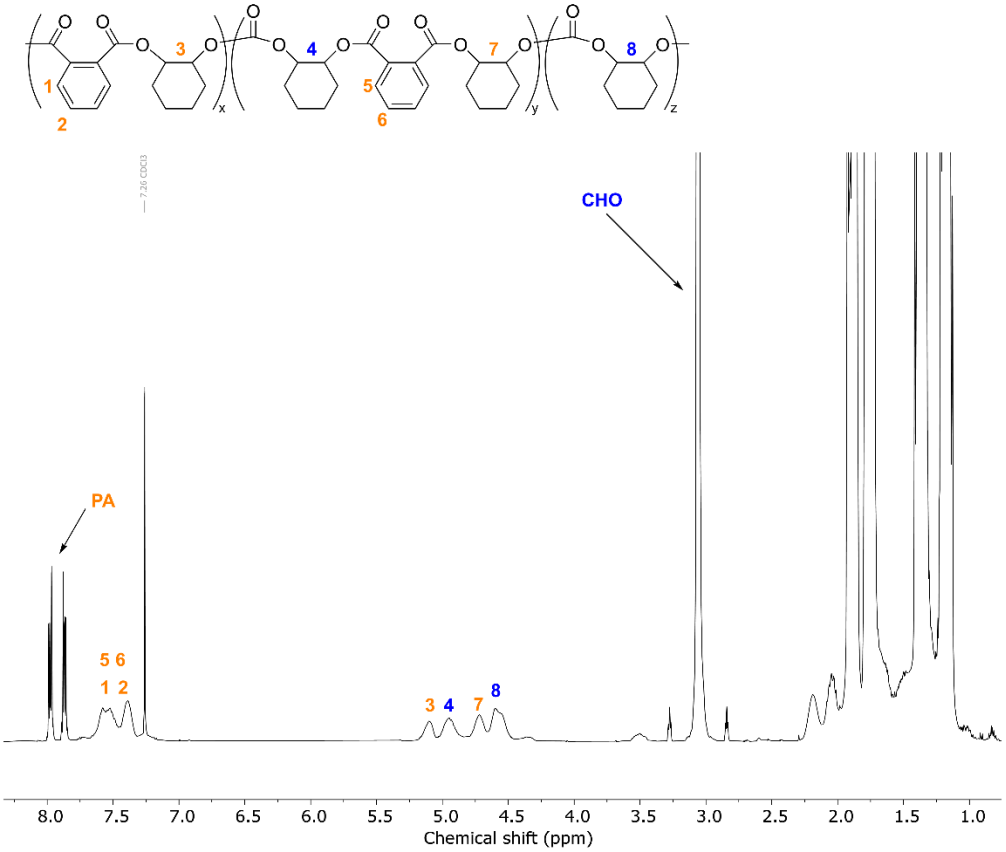

Figure S2.23: ^{1}H NMR spectrum ($CDCl_3$, 400 MHz) of an aliquot taken for the polymerisation of PA/CHO/CO_2 with catalyst **1** (Table 2.3, entry 2).

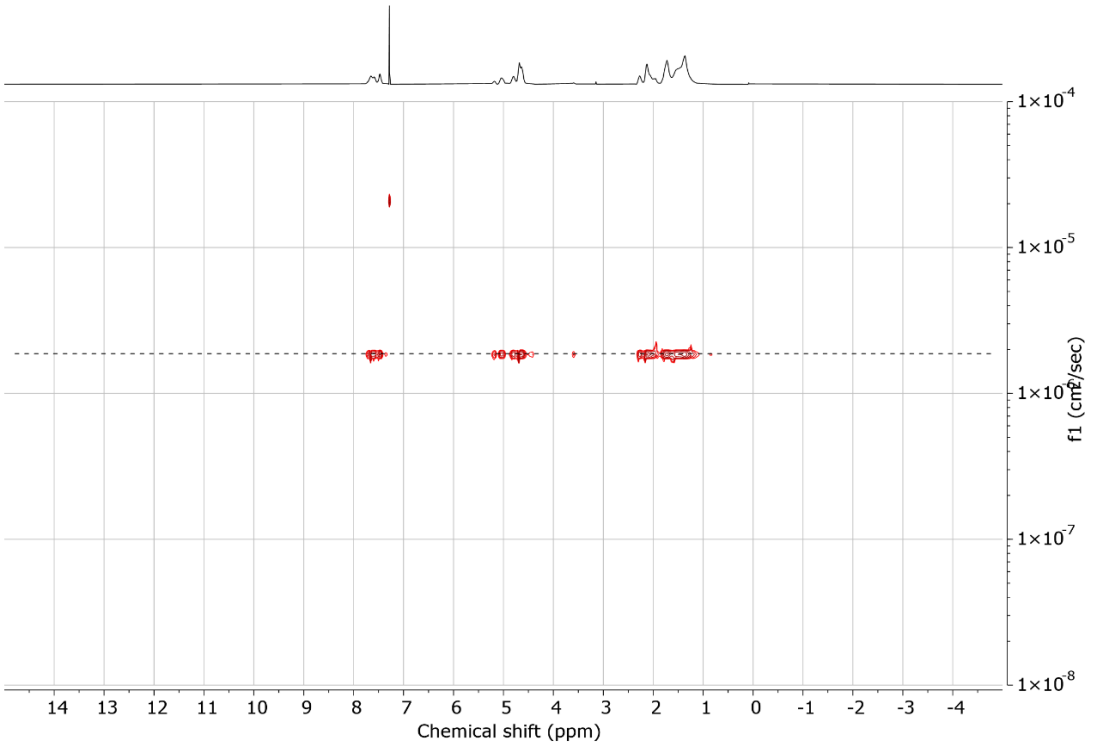

Figure S2.24: ^{1}H DOSY spectrum ($CDCl_3$, 500 MHz) of the purified random copolymer obtained from the polymerisation of PA/CHO/CO_2 with catalyst **5**.

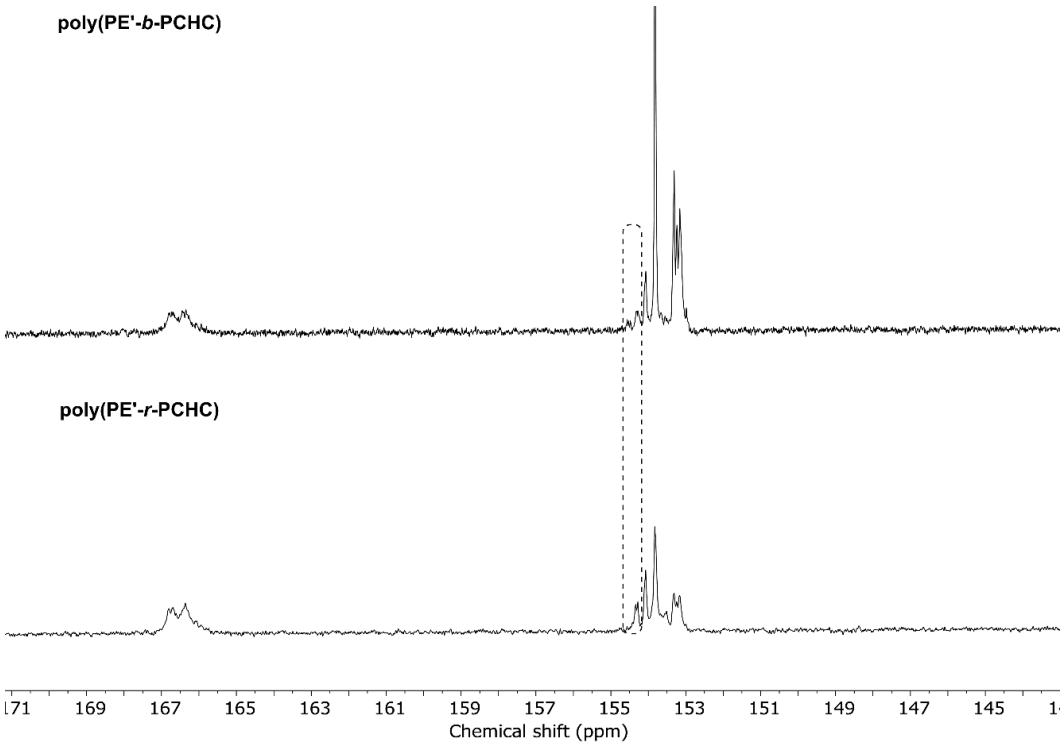

Figure S2.25: Portion of the ^{13}C NMR ($CDCl_3$, 126 MHz) spectrum of poly(PE'-*b*-PCHC) (top) and poly(PE'-*r*-PCHC) (bottom). A sharper peak for the polycarbonate junction unit can be observed at 154 ppm for the random copolymer.

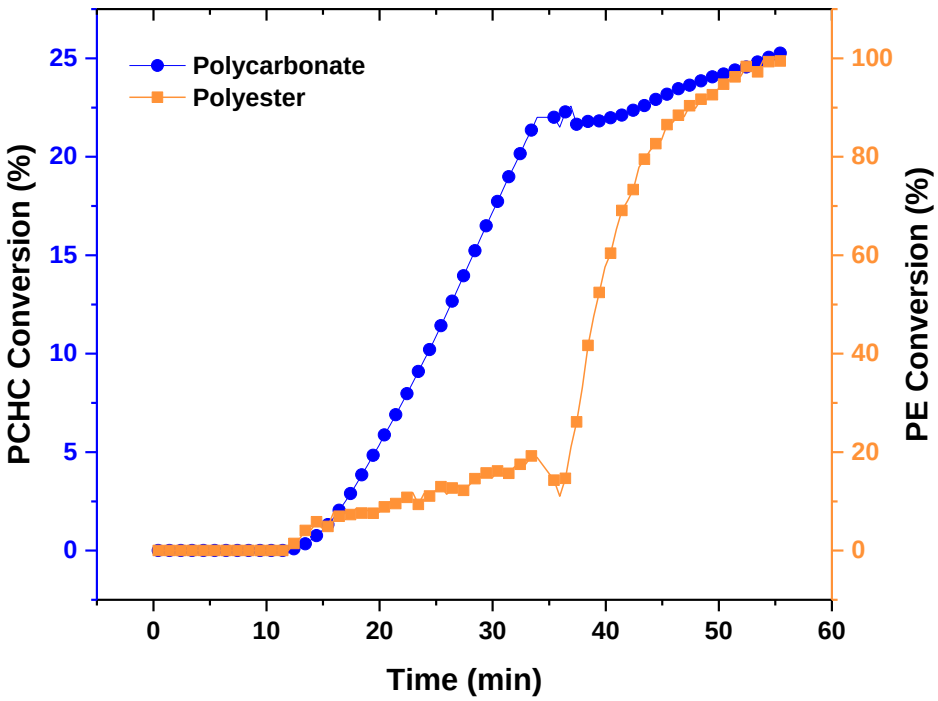

Figure S2.26: Conversion *vs.* time plot using data from *in situ* IR spectroscopy for the polymerisation of PA/CHO/CO_2 (20 bar) with catalyst **5** (Table 2.3, entry 5).

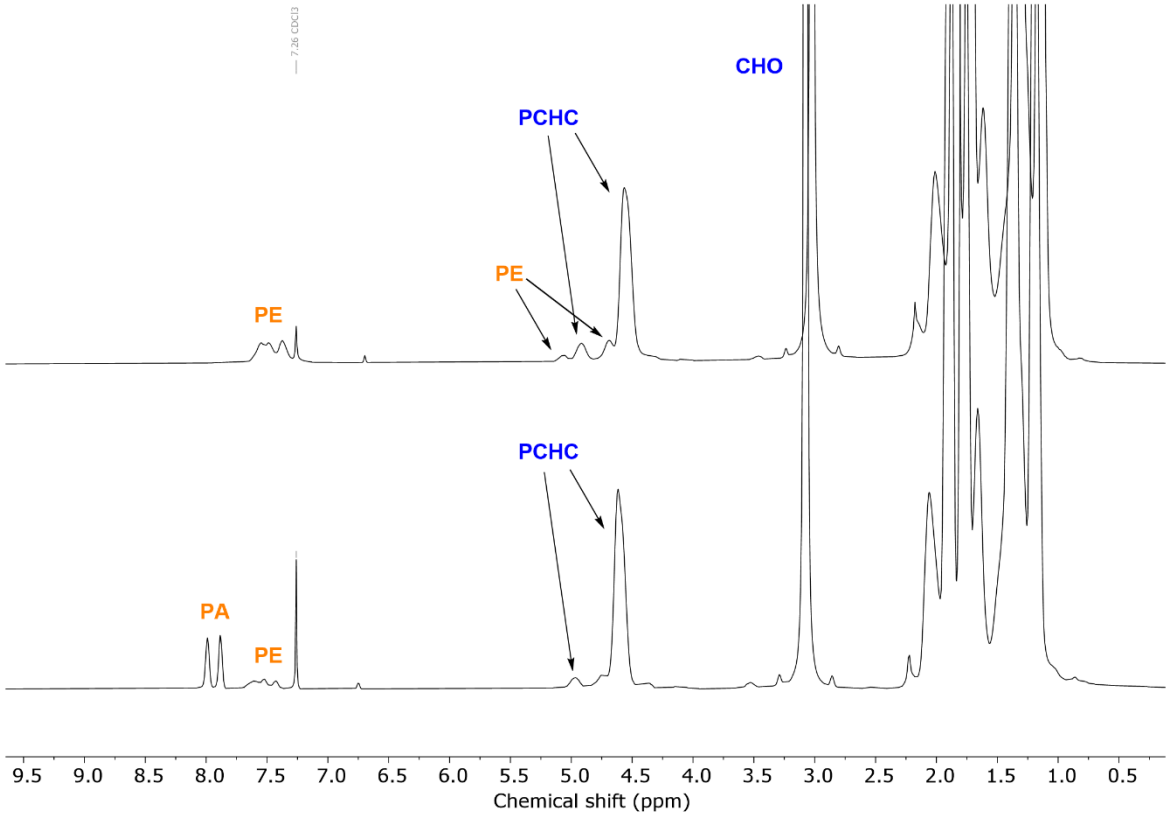

Figure S2.27: ^{1}H NMR ($CDCl_3$, 400 MHz) of aliquots taken for the polymerisation of PA/CHO/CO_2 (20 bar) with catalyst **5**. Below: after 35 min under 20 bar of CO_2 (Table 2.3, entry 5). Above: after 20 min under air (full conversion of anhydride)

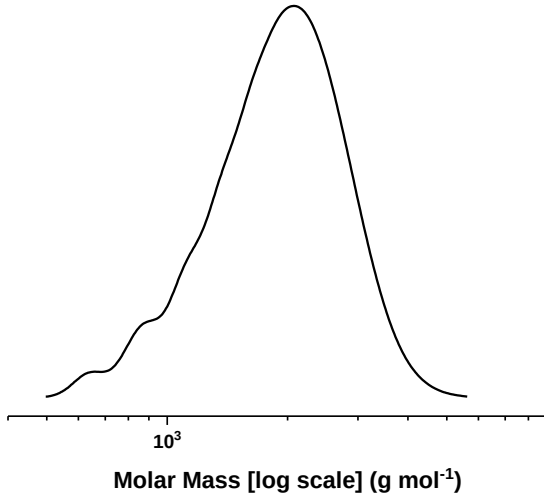

Figure S2.28: GPC trace of the polymer synthesised from TCA/CHO/CO_2 with catalyst **9**, M_n = 1.7, $Đ$ = 1.16 (Table 2.2, entry 1).

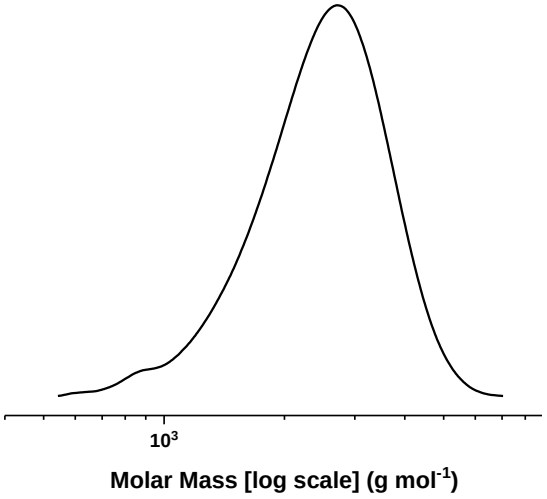

Figure S2.29: GPC trace of the polymer synthesised from TCA/CHO/CO_2 with catalyst **1**, M_n = 2.3, $Đ$ = 1.15 (Table 2.2, entry 2).

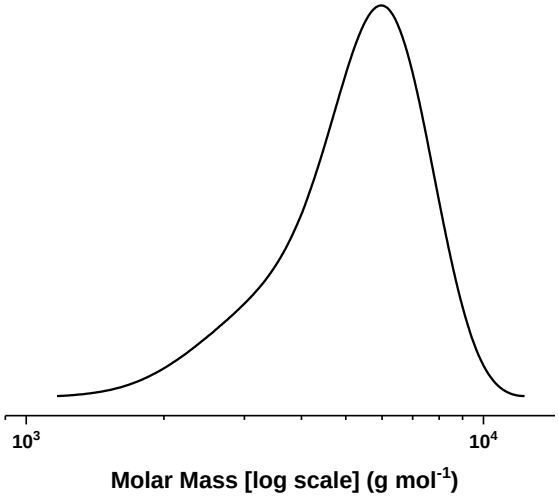

Figure S2.30: GPC trace of the polymer synthesised from TCA/CHO/CO_2 with catalyst **8**, M_n = 4.8, $Đ$ = 1.14 (Table 2.2, entry 3).

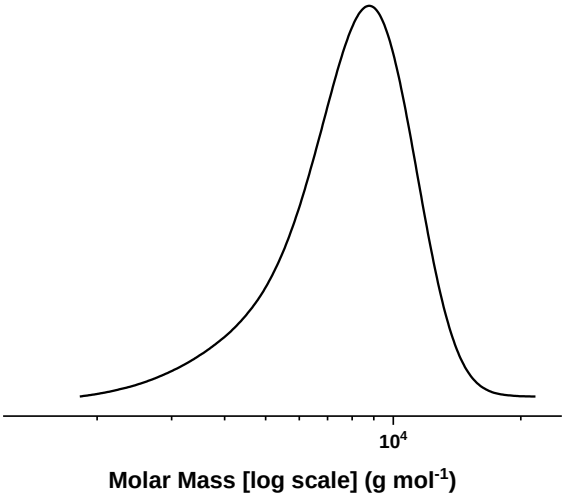

Figure S2.31: GPC trace of the polymer synthesised from TCA/CHO/CO_2 with catalyst **5**, M_n = 7.2, $Đ$ = 1.13 (Table 2.2, entry 4).

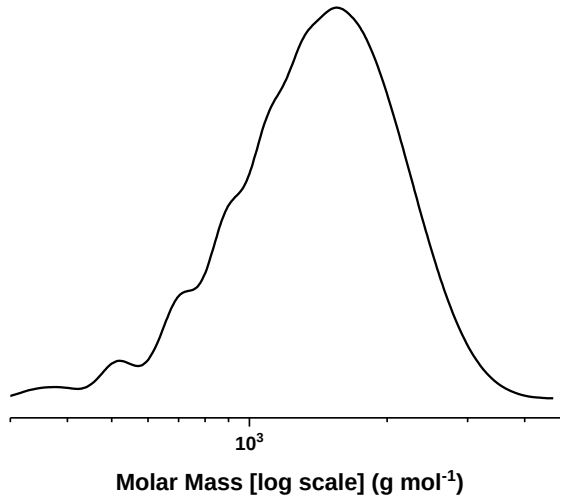

Figure S2.32: GPC trace of the polymer synthesised from PA/CHO/CO_2 with catalyst **9**, M_n = 1.3, $Đ$ = 1.19 (Table 2.3, entry 1).

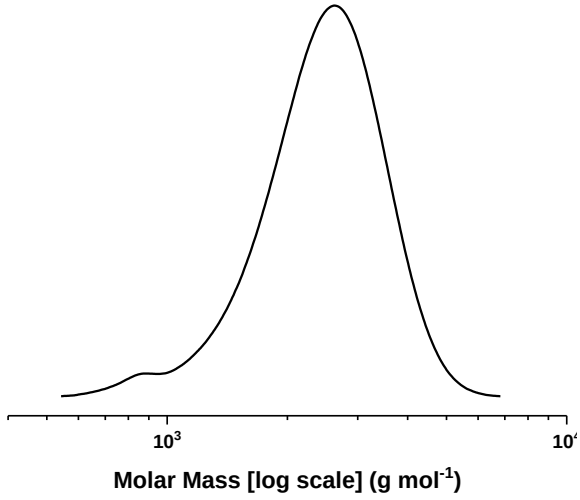

Figure S2.33: GPC trace of the polymer synthesised from PA/CHO/CO_2 with catalyst **1**, M_n = 2.3, $Đ$ = 1.14 (Table 2.3, entry 2).

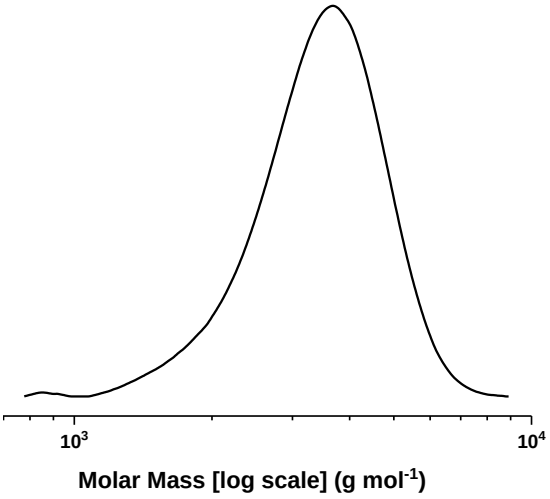

Figure S2.34: GPC trace of the polymer synthesised from PA/CHO/CO_2 with catalyst **8**, M_n = 3.2, $Đ$ = 1.11 (Table 2.3, entry 3).

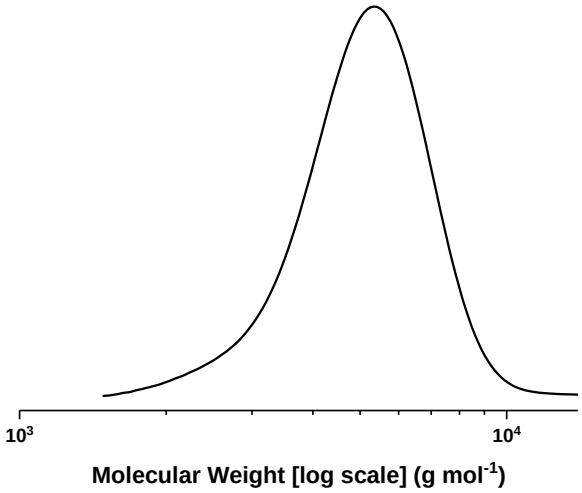

Figure S2.35: GPC trace of the polymer synthesised from PA/CHO/CO_2 with catalyst **5**. M_n = 5.3, $Đ$ = 1.09 (Table 2.3, entry 4).

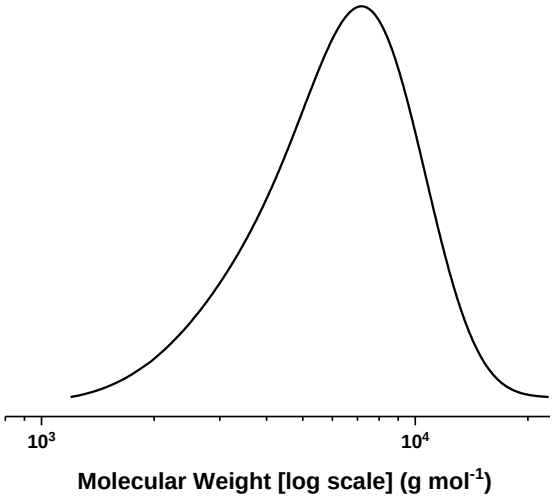

Figure S2.36: GPC trace of the polymer synthesised from PA/CHO/CO_2 at 20 bar with catalyst **5**, M_n = 5.4, $Đ$ = 1.25 (Table 2.3, entry 5).

Supplementary Figures and Data for Chapter 3

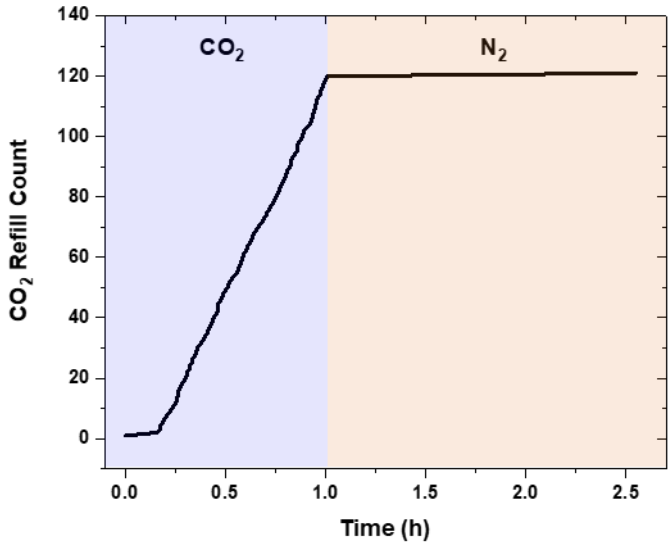

Figure S3.1: Frequency of CO_2 refill extracted from mass flow data for the polymerisation of TCA/CHO/CO_2 with catalyst **5**, with one gas switch.

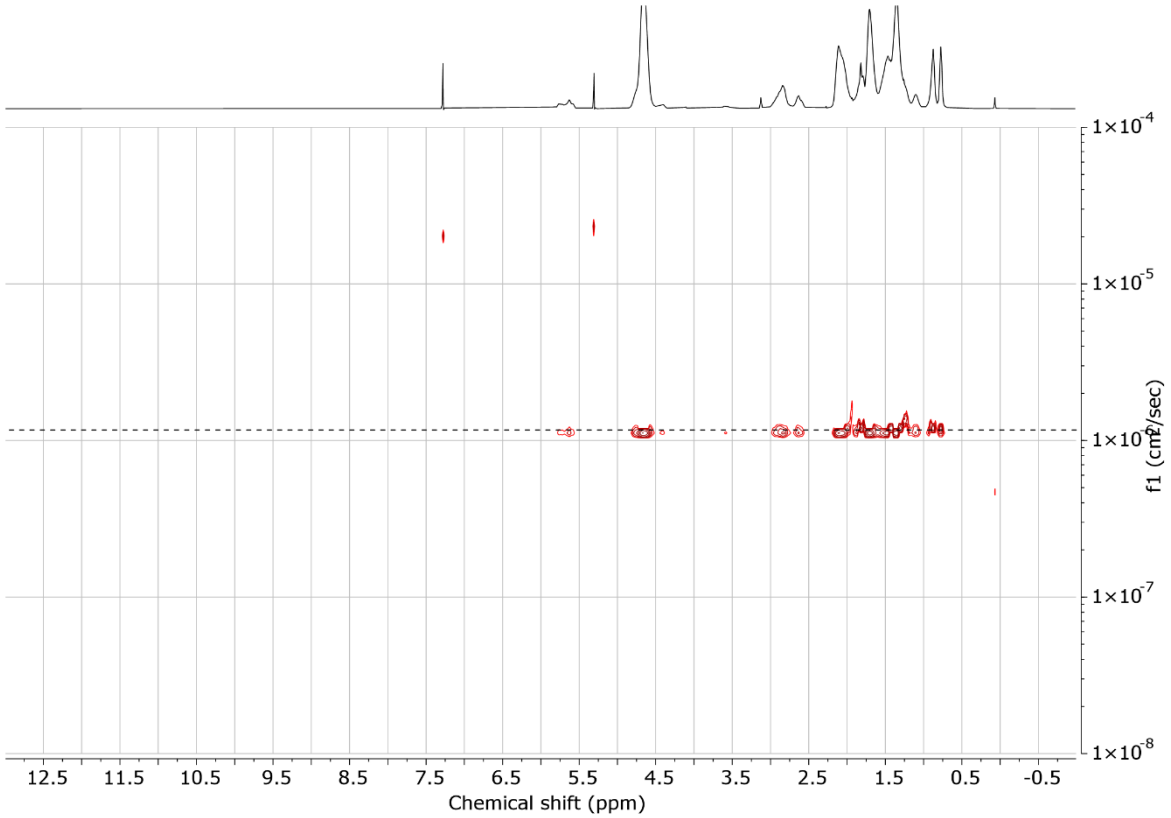

Figure S3.2: ^{1}H DOSY NMR spectrum of the purified ABA block copolymer, displaying a single diffusion coefficient.

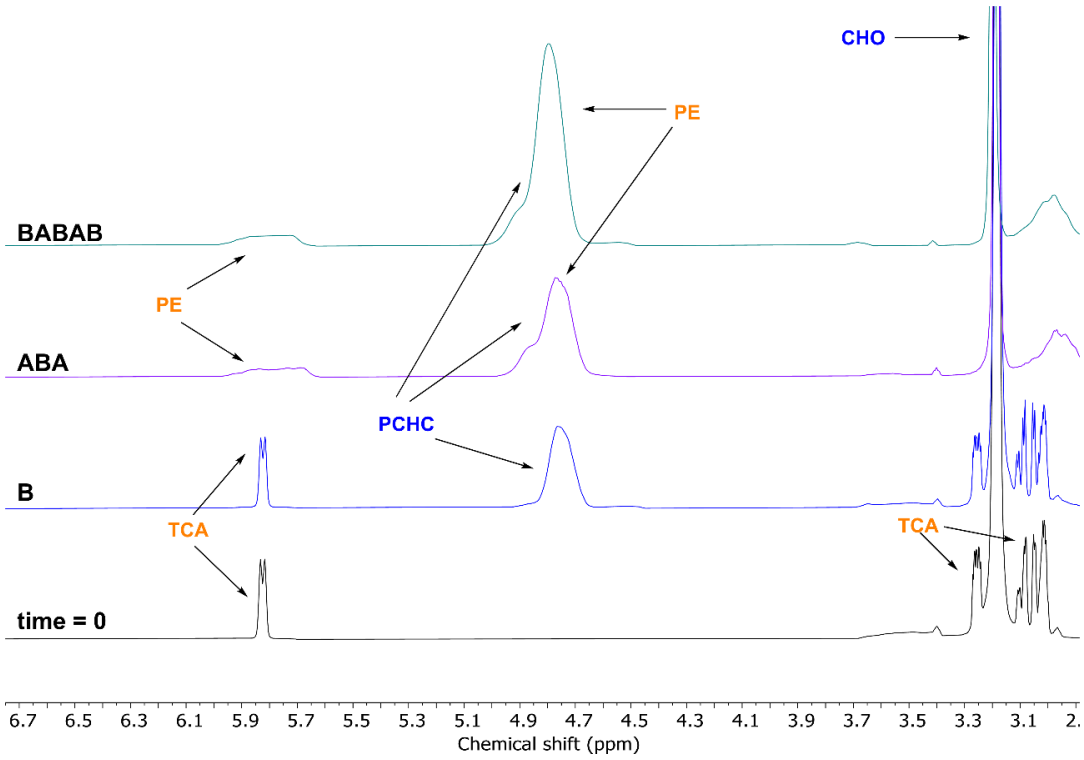

Figure S3.3: Selected region of the ^{1}H NMR spectra throughout polymerisation stages of the BABAB pentablock copolymer.

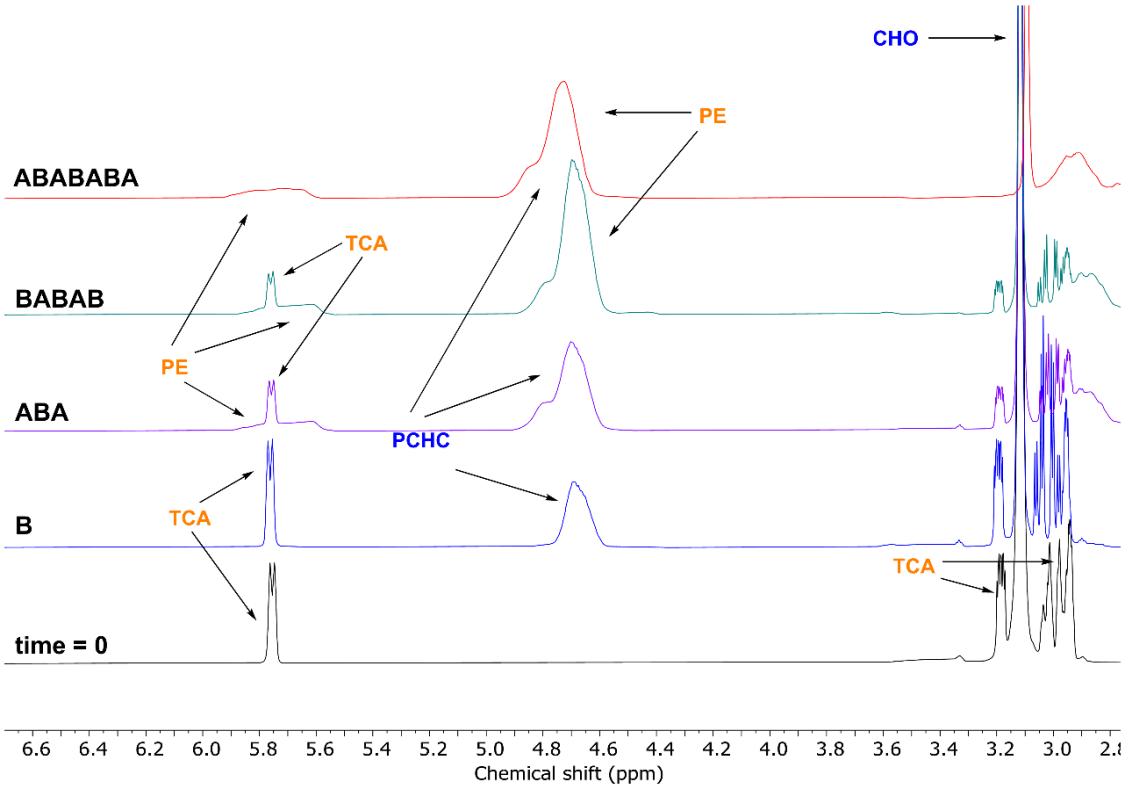

Figure S3.4: Selected region of the ^{1}H NMR spectra throughout polymerisation stages of the ABABABA heptablock copolymer.

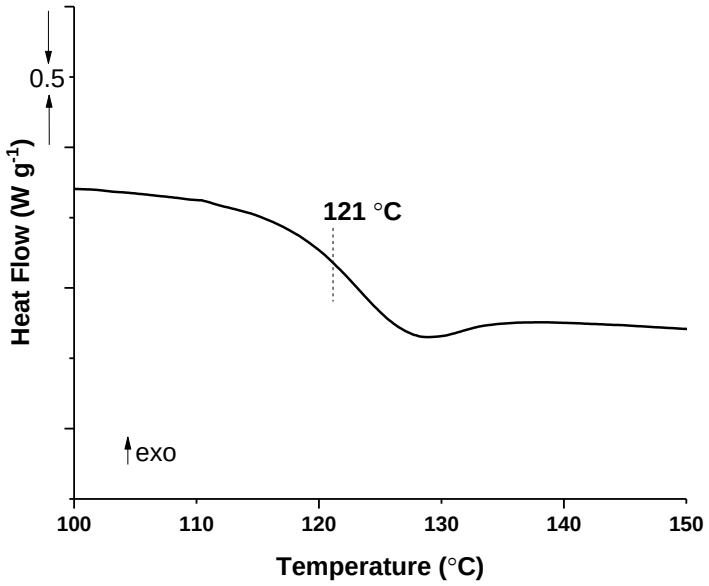

Figure S3.5: DSC data for the purified ABA triblock copolymer, determined at 20 ˚C/min heating rate, and taken from the second heating/cooling cycle.

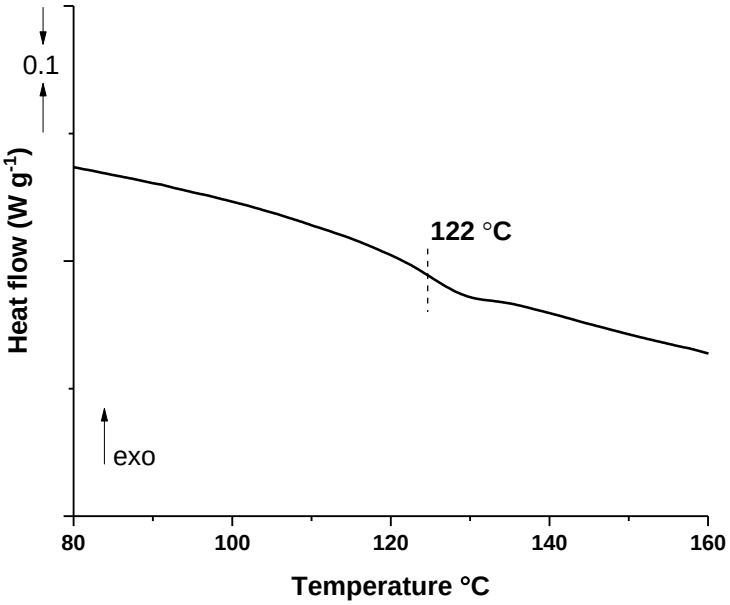

Figure S3.6: DSC data for the purified BABAB pentablock copolymer, determined at 20 ˚C/min heating rate, and taken from the second heating/cooling cycle.

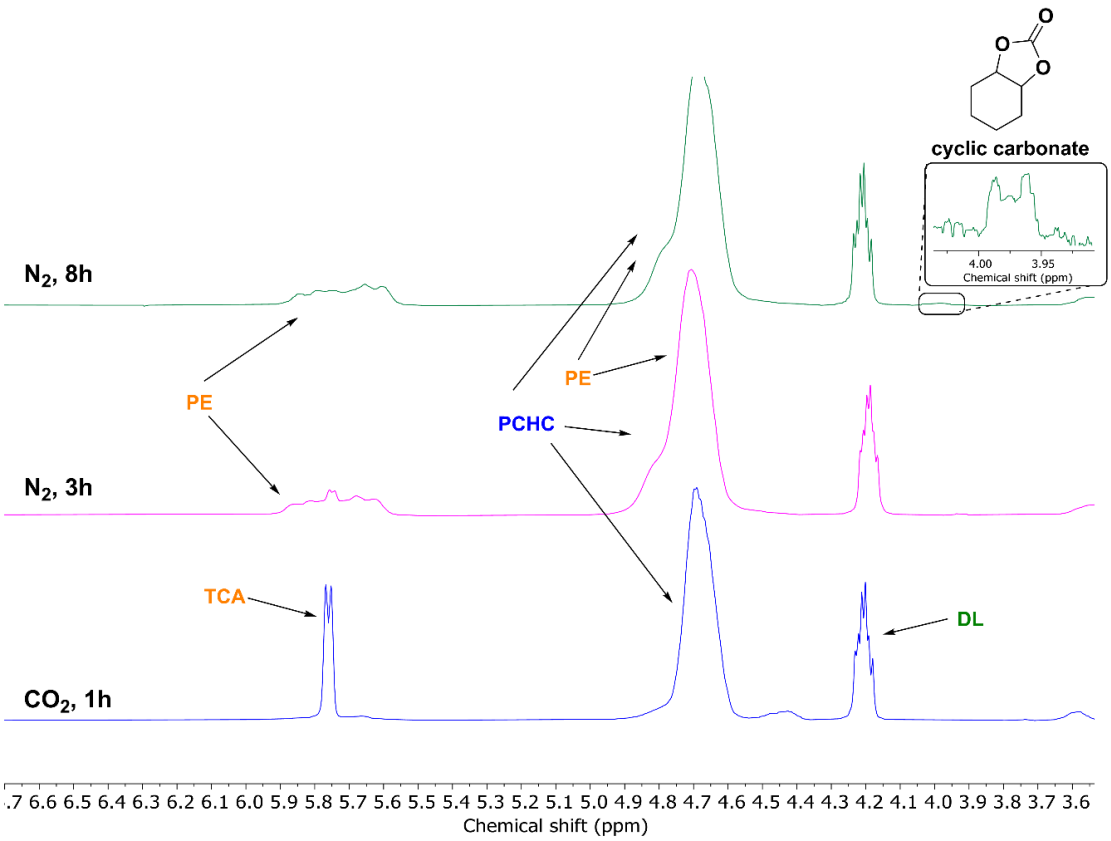

Figure S3.7: Selected region of the ^{1}H NMR spectra of reaction aliquots illustrating the changes in resonances during the different stages of the CHO/TCA/CO_2/DL copolymerisation with **5**.

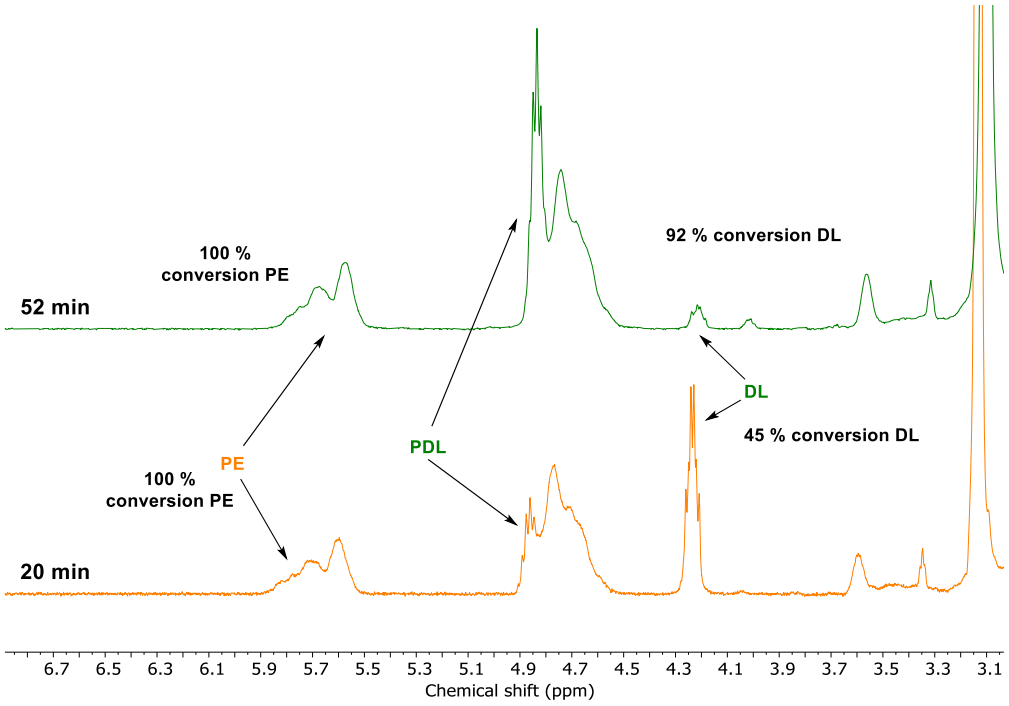

Figure S3.8: Selected region of the ^{1}H NMR spectra of reaction aliquots illustrating the changes in resonances during CHO/TCA /DL copolymerisation with **5**.

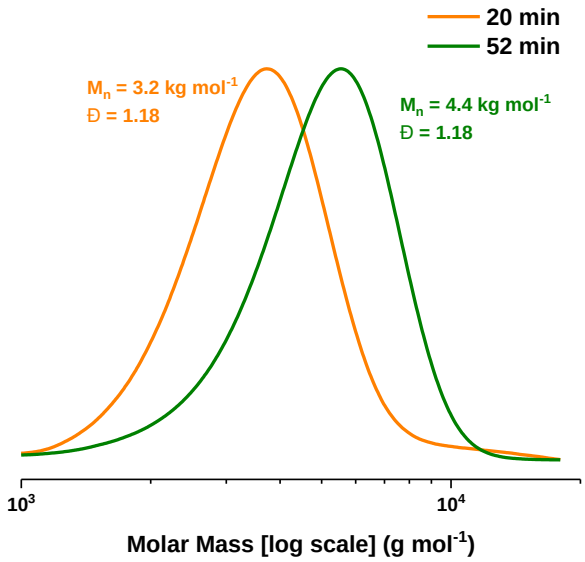

Figure S3.9: GPC traces corresponding to two aliquots taken during the polymerisation of CHO/TCA/DL with **5**.

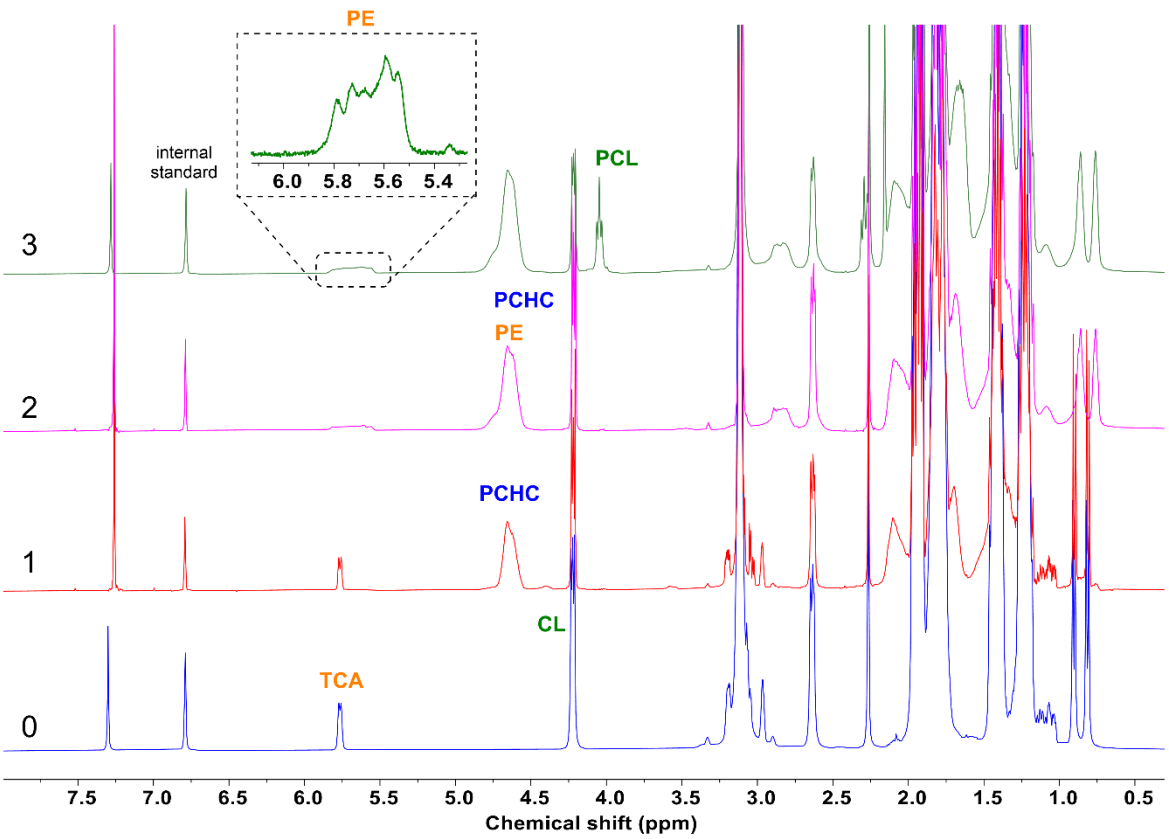

Figure S3.10: Stack plot showing the ^{1}H NMR spectra of aliquots removed during formation of the polymer blocks. 0 = mixture before polymerisation. 1 = formation of PCHC under CO_2. 2 = formation of PE block when switching to N_2. 3 = formation of PCL block once TCA is fully converted.

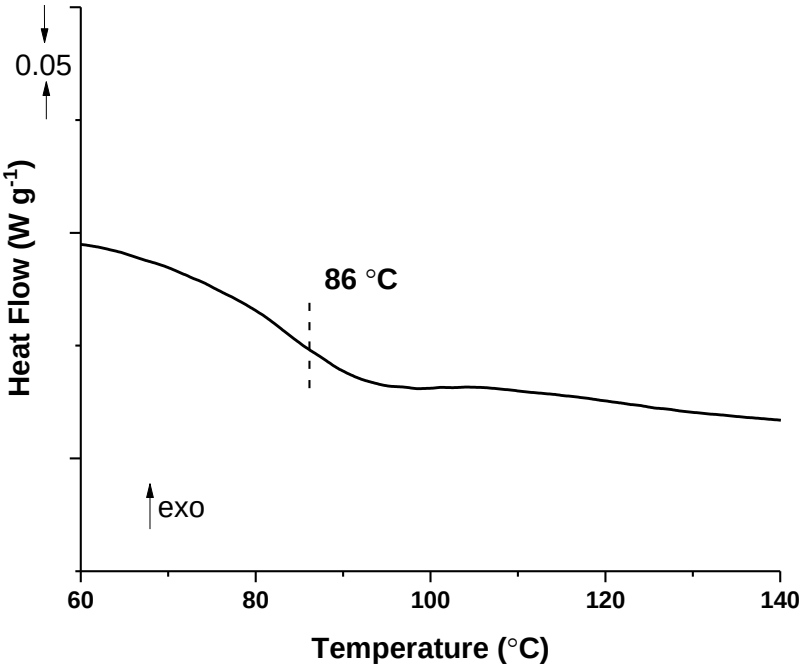

Figure S3.11: DSC data for the purified CABAC pentablock copolymer, determined at 20 ˚C/min heating rate, and taken from the second heating/cooling cycle

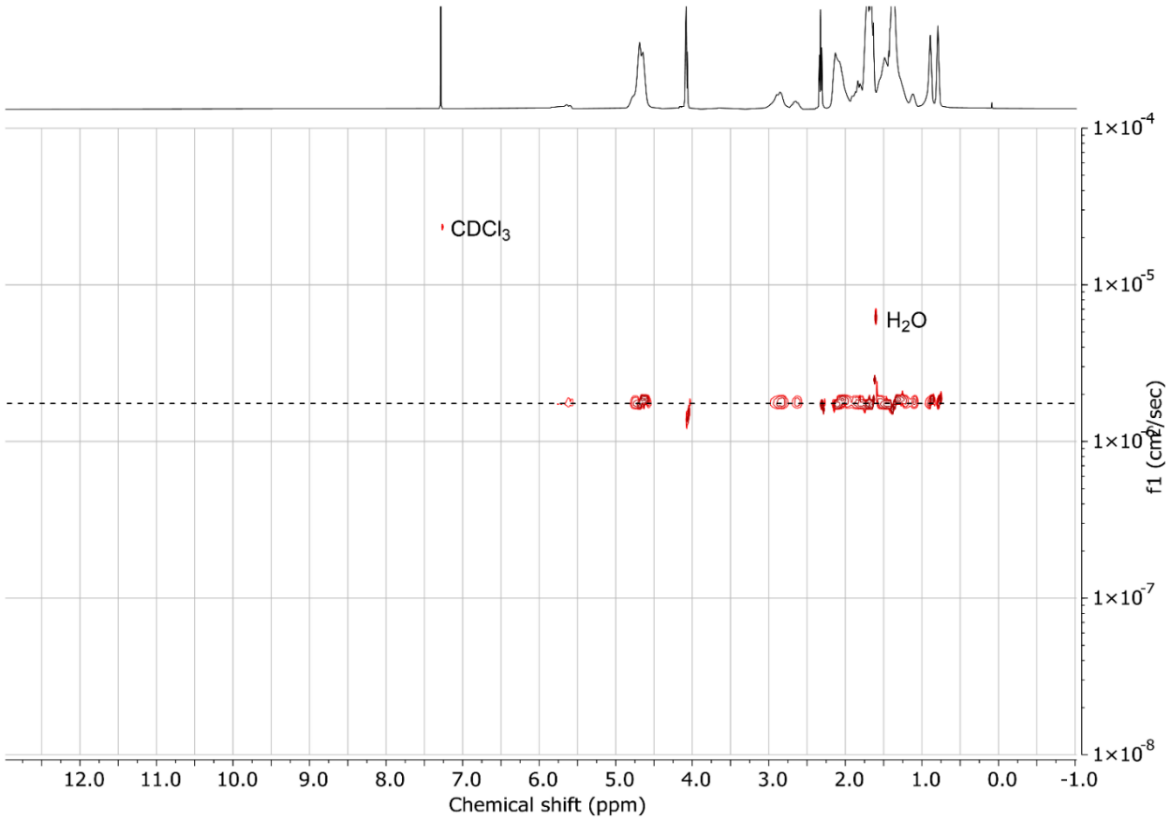

Figure S3.12: ^{1}H DOSY spectrum ($CDCl_3$, 500 MHz) of the purified CABAC polymer.

Supplementary Figures and Data for Chapter 4

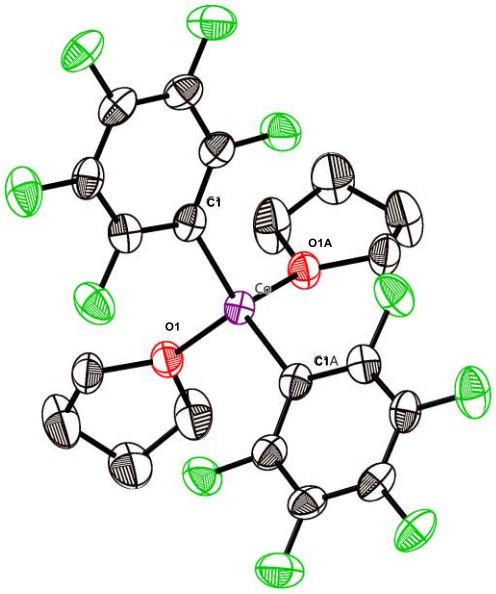

Figure S4.1: Molecular structure of **[Co(C$_6$F$_5$)$_2$(THF)$_2$]**. H atoms omitted for clarity. Thermal ellipsoids at the 50 % probability level. Figure on the right shows the "S" shape of the ligand. Co = purple, O = red, F = green, C = grey.

Table S4.1: Selected bond lengths and angles of **[Co(C$_6$F$_5$)$_2$(THF)$_2$]**.

Bond	**Length (Å)**	**Bond**	**Angle (˚)**
Co-O(1)	2.031(3)	O(1)-Co-C(1)	112.45(14)
		C(1)-Co-C(1A)	114.2(2)
Co-C(1)	2.030(4)	O1-Co-O(1A)	92.12(18)
		C(1)-Co-O(1A)	111.82(14)

Table S4.2: Summary of crystallographic experimental details for the refinement of **[Co(C$_6$F$_5$)$_2$(THF)$_2$]**, **10**, and **[LCo$_2$(C$_6$F$_5$)$_2$]**.

Complex	**[Co(C$_6$F$_5$)$_2$(THF)$_2$]**	**10**	**[LCo$_2$(C$_6$F$_5$)$_2$]**
Local code	001rwfk20	010rwfk21	001rwfk22
Crystal data			
Chemical formula	1.33($C_{20}H_{16}CoF_{10}O_2$)	$C_{46}H_{54}CoF_{10}MgN_4O_2$·2($C_4H_8O$)·2($C_4H_7O$)	$C_{46}H_{54}Co_2F_{10}N_4O_2$·2($C_7H_8$)
M_r	569.26	1254.57	1187.06
Crystal system, space group	Monoclinic, *I*2/*a*	Triclinic, *P*1	Monoclinic, *Cc*
a, *b*, *c* (Å)	17.2511 (12), 7.1979 (3), 19.7651 (15)	10.7864 (7), 11.9681 (7), 13.1272 (7)	12.0771 (3), 22.9816 (5), 20.9792 (6)
α, β, γ (°)	118.933 (10)	70.242 (5), 84.445 (5), 73.579 (5)	100.875 (2)
V (Å^3)	2147.9 (3)	1529.81 (17)	5718.2 (3)
Z	3	1	4
Radiation type	Cu *K*α	Cu *K*α	Cu *K*α
μ (mm^{-1})	5.50	3.02	5.21
Data collection			
Absorption correction	Multi-scan *CrysAlis PRO* 1.171.39.46e (Rigaku Oxford Diffraction, 2018) Empirical absorption correction using spherical harmonics, implemented in SCALE3 ABSPACK scaling algorithm.	Multi-scan *CrysAlis PRO* 1.171.41.81a (Rigaku Oxford Diffraction, 2020) Empirical absorption correction using spherical harmonics, implemented in SCALE3 ABSPACK scaling algorithm.	Gaussian *CrysAlis PRO* 1.171.40.53 (Rigaku Oxford Diffraction, 2019) Numerical absorption correction based on gaussian integration over a multifaceted crystal model Empirical absorption correction using spherical harmonics, implemented in SCALE3 ABSPACK scaling algorithm.
T_{min}, T_{max}	0.409, 1.000	0.901, 1.000	0.768, 1.000

No. of measured independent and observed [$I > 2\sigma(I)$] reflections	10558, 2249, 1799	20972, 6309, 4400	47744, 11882, 10939
R_{int}	0.077	0.074	0.045
$(\sin \theta/\lambda)_{max}$ ($Å^{-1}$)	0.632	0.631	0.630
Refinement			
$R[F^2 > 2\sigma(F^2)]$, $wR(F^2)$, S	0.058, 0.179, 1.07	0.059, 0.168, 1.03	0.033, 0.084, 1.03
No. of reflections	2249	6309	11882
No. of parameters	150	387	819
No. of restraints	0	3	8
$\Delta\rho_{max}$, $\Delta\rho_{min}$ (e $Å^{-3}$)	1.01, −0.41	0.57, −0.33	0.46, −0.27
Absolute structure	–	–	Flack x determined using 5131 quotients $[(I+)-(I-)]/[(I+)+(I-)]$[5]

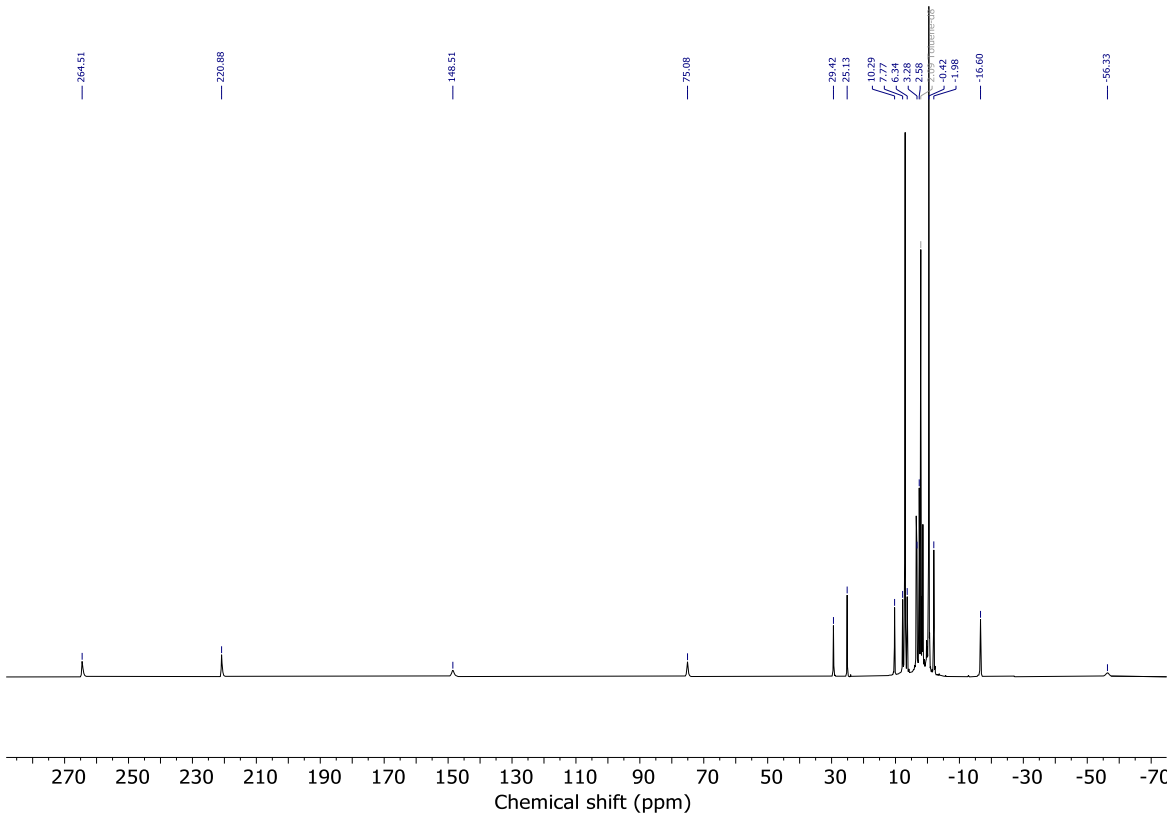

Figure S4.2: ^{1}H NMR spectrum (toluene-d_8, 400 MHz) of complex **10**.

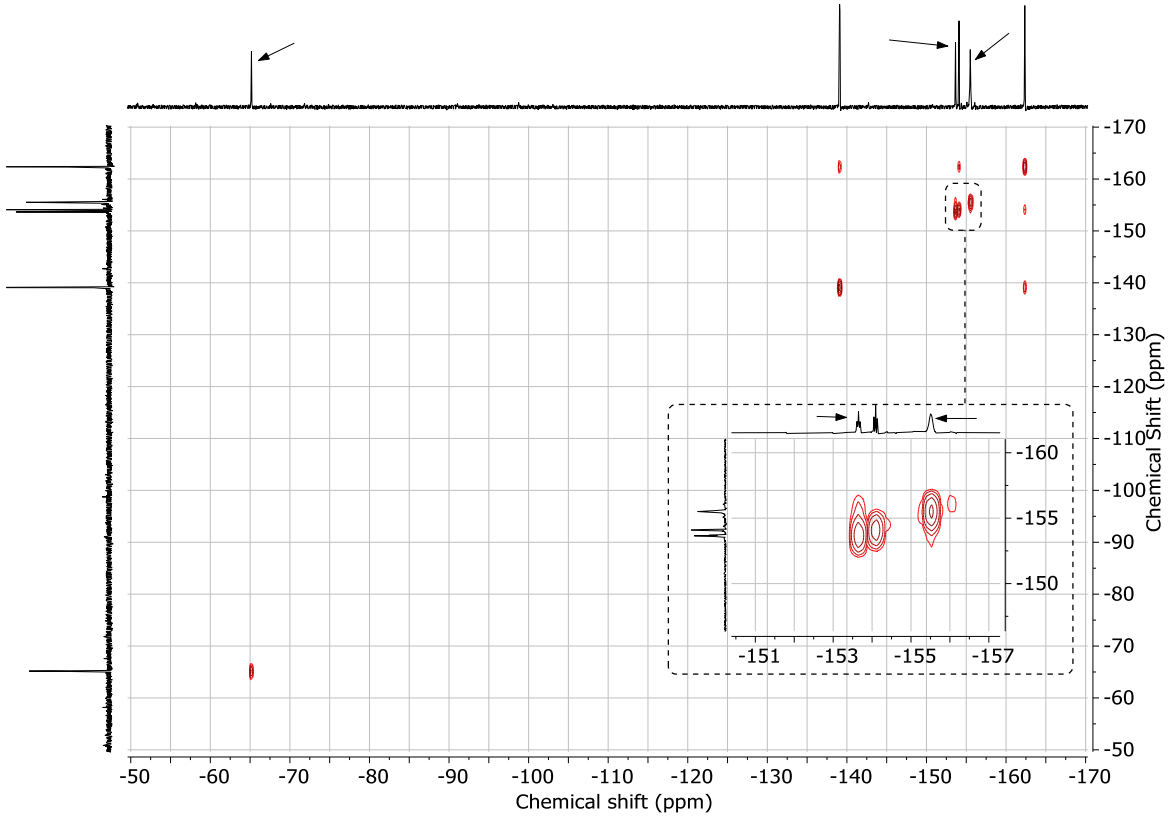

Figure S4.3: ^{19}F COSY NMR spectrum (toluene-d_8, 470 MHz) of complex **10**. Resonances of **10** are indicated by an arrow.

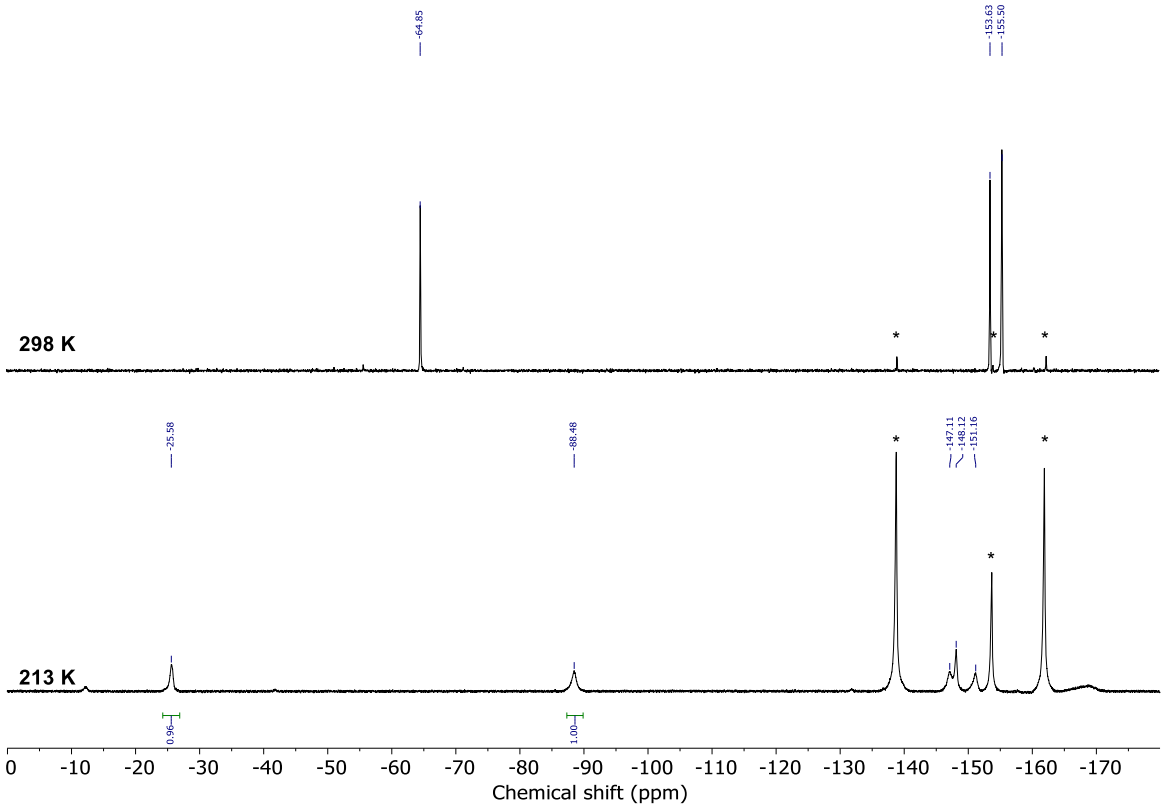

Figure S4.4: VT $^{19}F\{^{1}H\}$ NMR spectra (toluene-d_8, 470 MHz) of **10**. HC_6F_5 denoted by *.

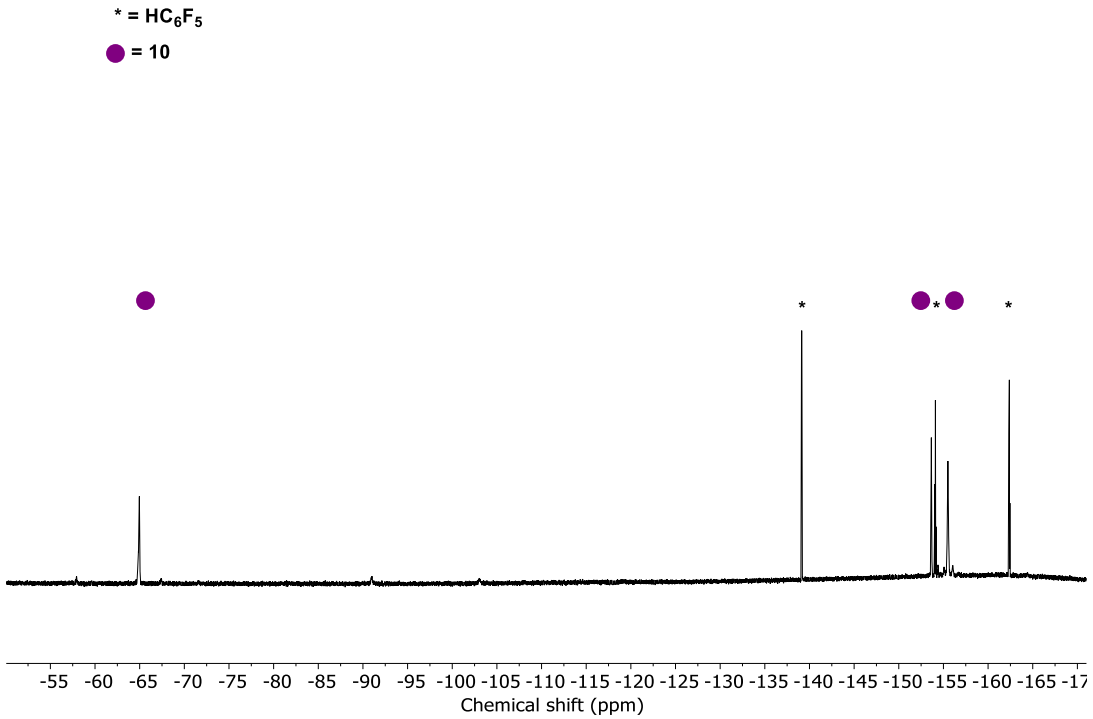

Figure S4.5: $^{19}F\{^{1}H\}$ NMR spectrum (toluene-d_8, 377 MHz) of **10** after 3.5 days in a Young's tap NMR tube.

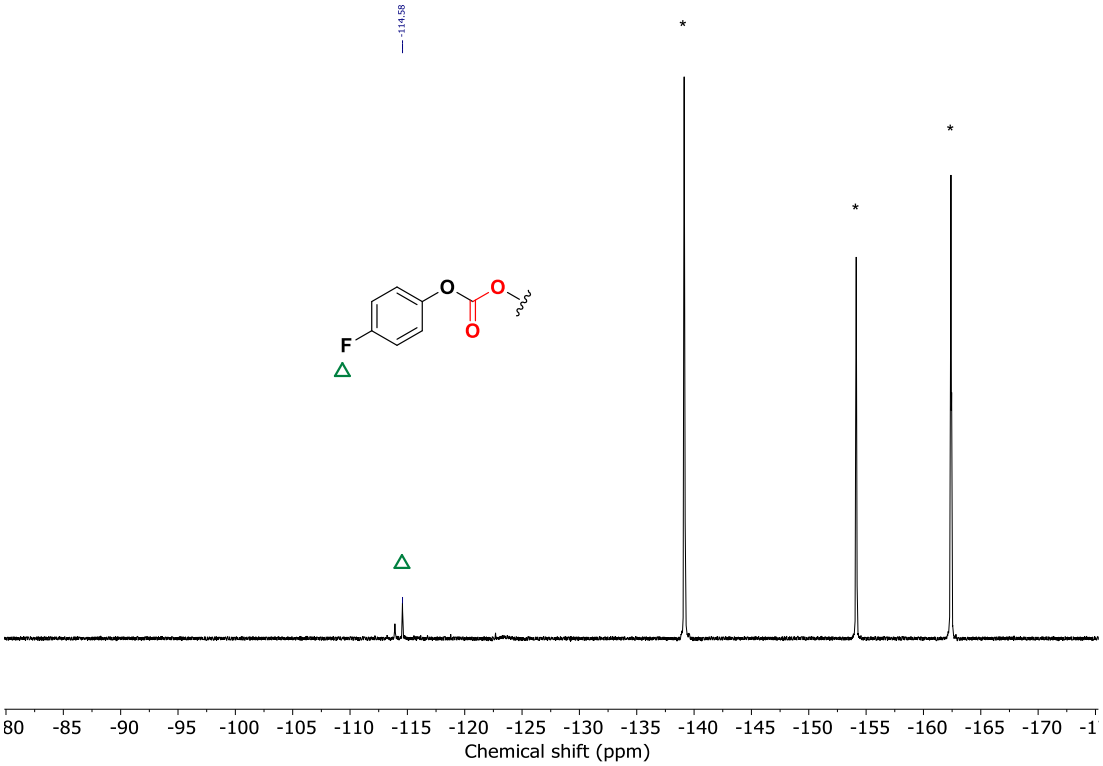

Figure S4.6: $^{19}F\{^{1}H\}$ NMR spectrum (toluene-d_8, 377 MHz) of reaction of **10**, 4-fluorophenol, and 1 bar of CO_2. HC_6F_5 denoted by *.

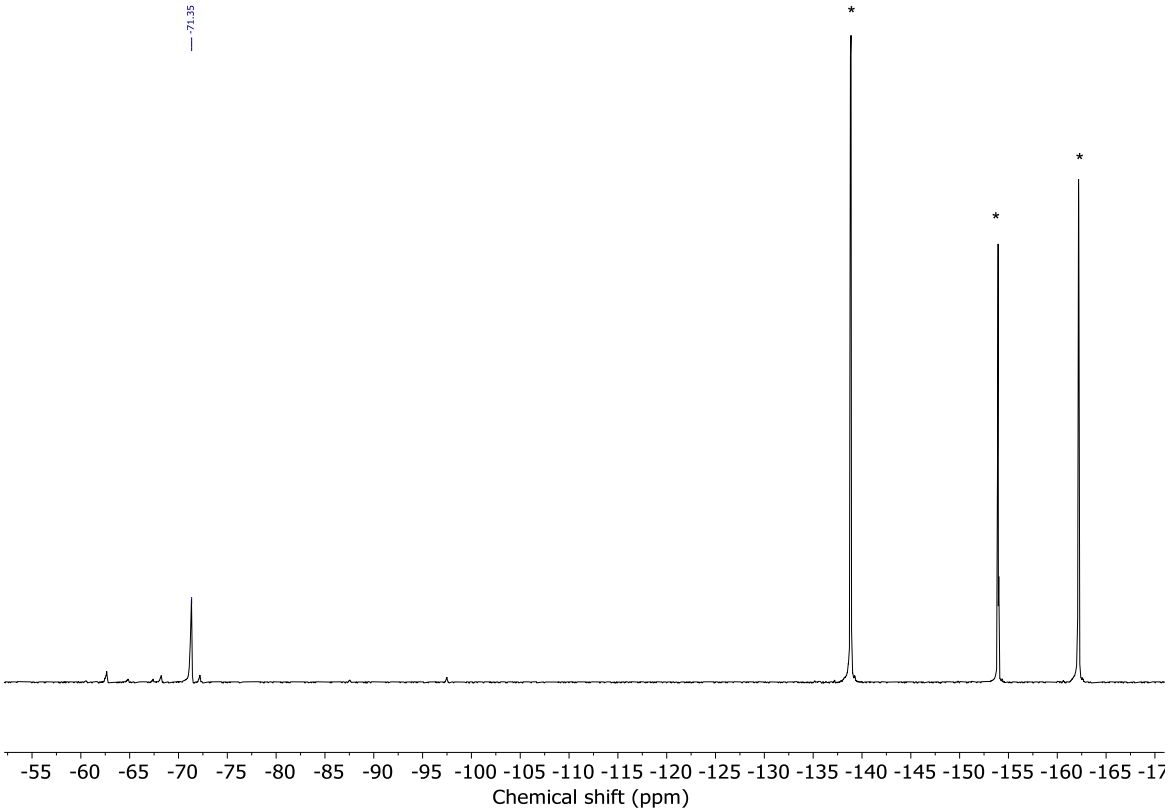

Figure S4.7: Crude $^{19}F\{^{1}H\}$ NMR spectrum (toluene-d_8, 377 MHz) of **[LCo$_2$(C$_6$F$_5$)$_2$]**.

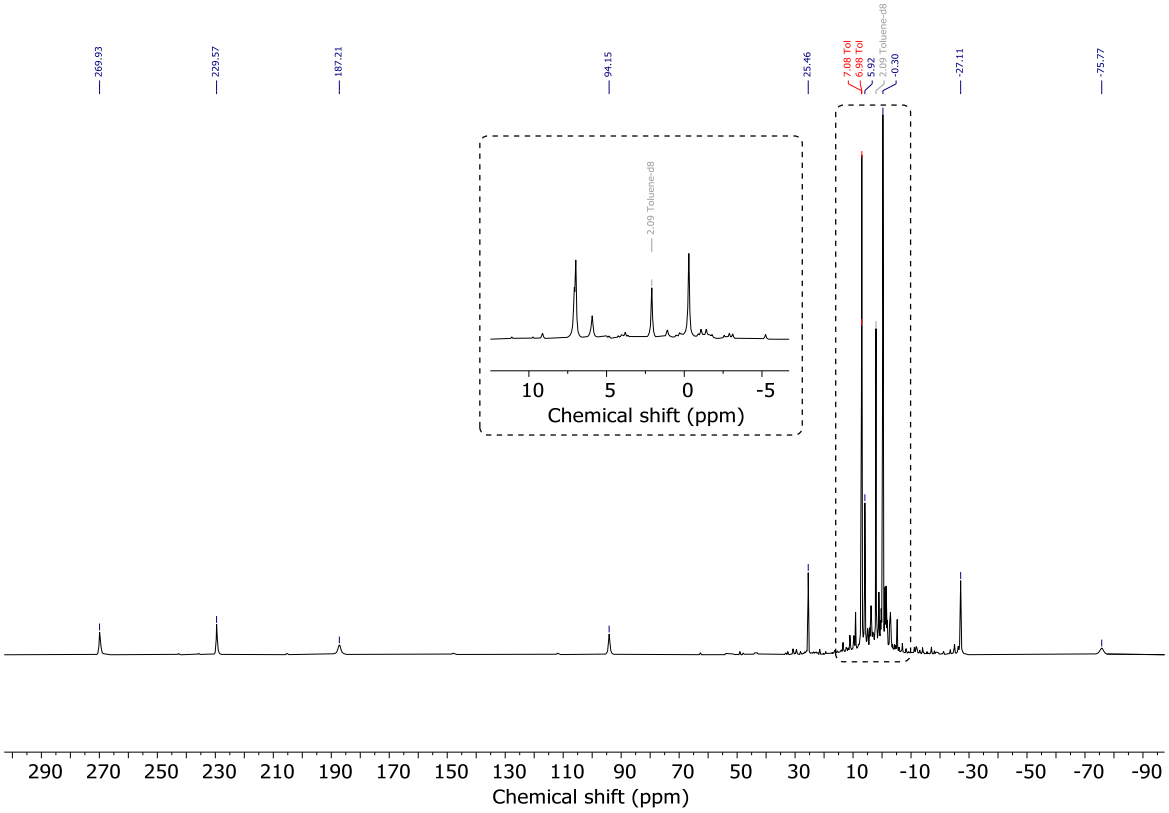

Figure S4.8: ^{1}H NMR spectrum (toluene-d_8, 400 MHz) of [LCo$_2$(C$_6$F$_5$)$_2$].

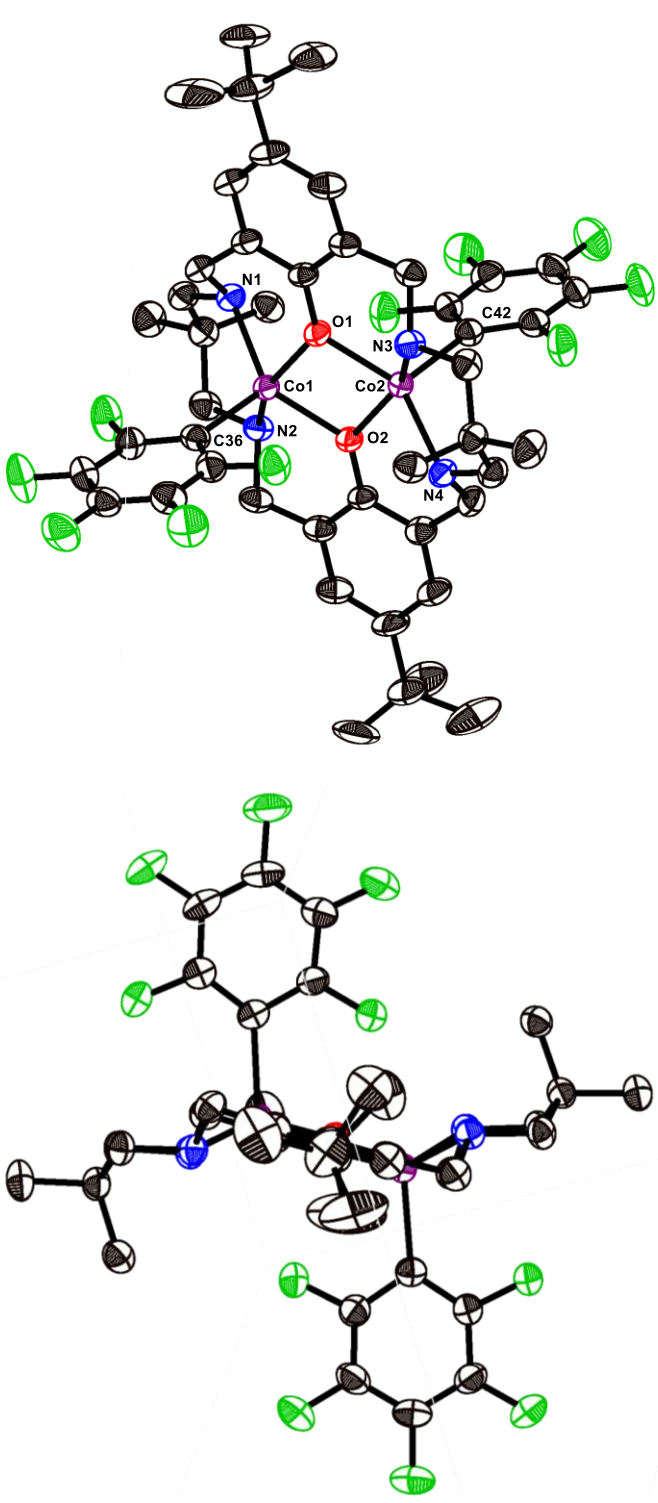

Figure S4.9: Molecular structure of [$LCo_2(C_6F_5)_2$]. H atoms and two toluene molecule have been omitted for clarity. Thermal ellipsoids at the 50 % probability level. Co = purple, O = red, N = blue, F = green, C = grey.

Table S4.3: Selected bond length and angles for [$LCo_2(C_6F_5)_2$].

Bond	**Length (Å)**	**Bond**	**Angle (˚)**
Co(1)-O(1)	2.046(2)	N(1)-Co(1)-O(2)	143.69(11)
Co(1)-O(2)	2.010(2)	N(2)-Co(1)-O(2)	83.44(11)
Co(2)-O(2)	2.054(2)	N(2)-Co(1)-O(1)	149.31
Co(2)-O(1)	2.014(2)	N(3)-Co(2)-O(1)	139.97(11)
Co(1)-N(1)	2.115(3)	N(4)-Co(2)-O(1)	83.2511)
Co(1)-N(2)	2.167(3)	N(4)-Co(2)-O(2)	149.40(11)
Co(2)-N(3)	2.111(3)		
Co(2)-N(4)	2.147(3)		
Co(1)-C(36)	2.104(4)		
Co(2)-C(42)	2.094(3)		

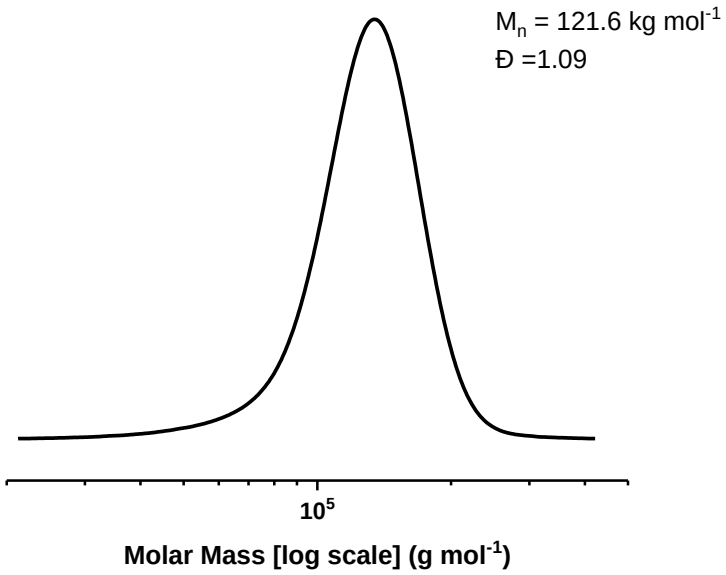

Figure S4.10: GPC trace of **P8**.

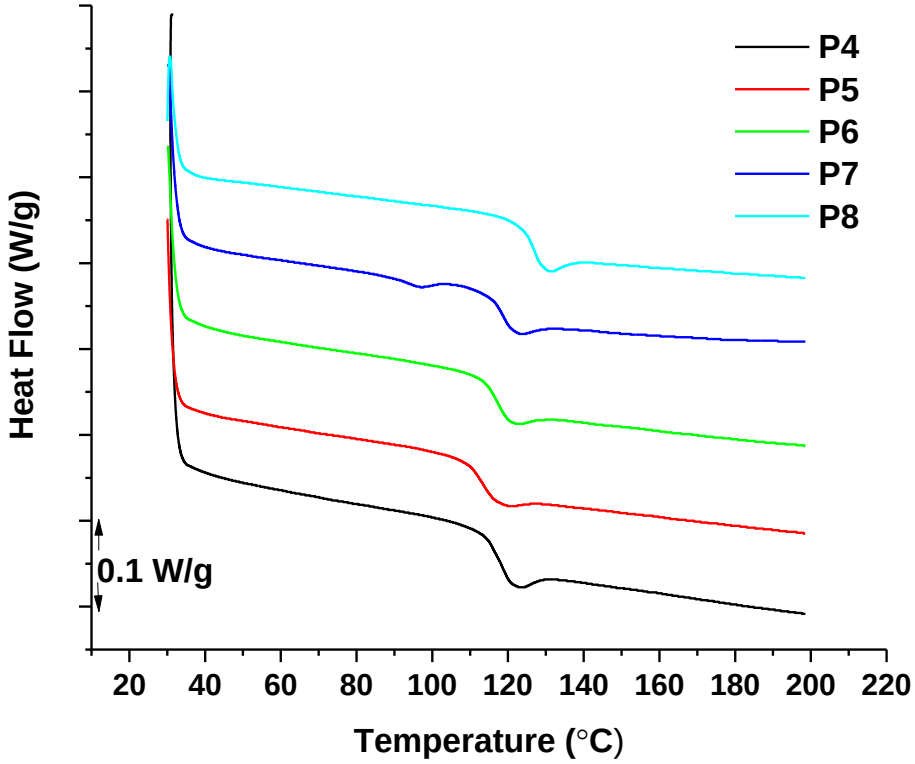

Figure S4.11: DSC data for polymers **P4**-**P8**

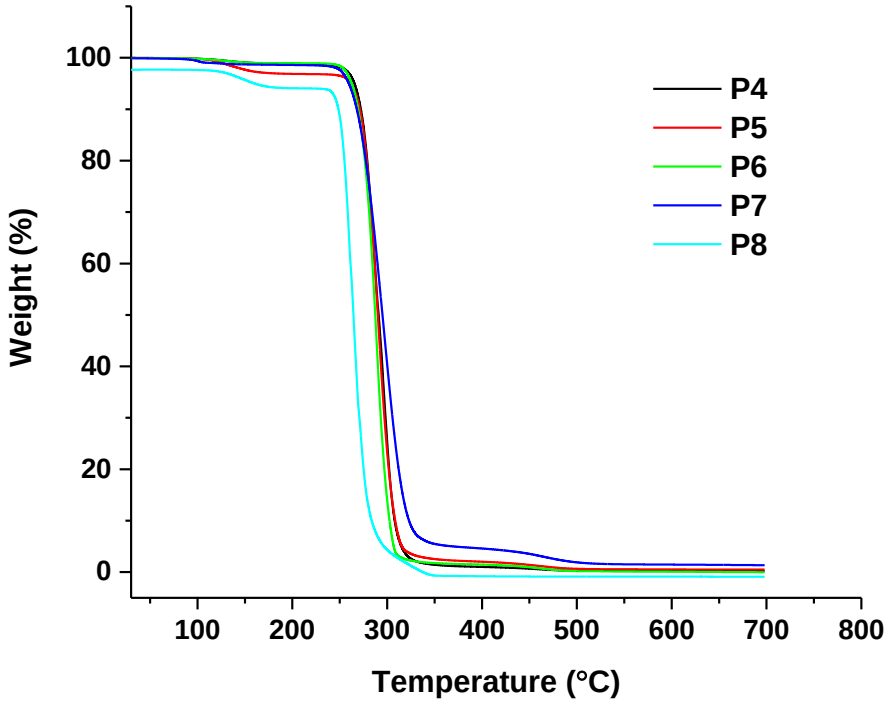

Figure S4.12: TGA data for polymers **P4**-**P8**.

Supplementary Figures and Data for Chapter 5

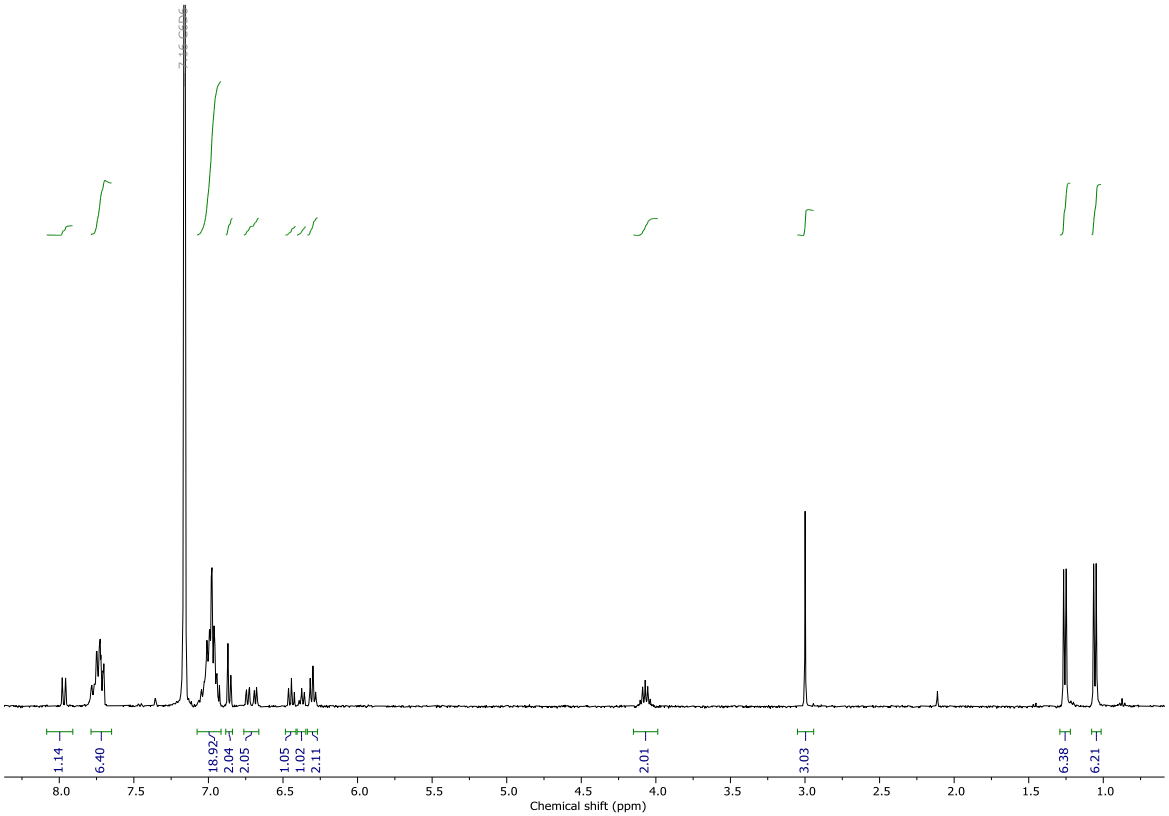

Figure S5.1: ^{1}H NMR spectrum (C_6D_6, 400 MHz) of **11a**.

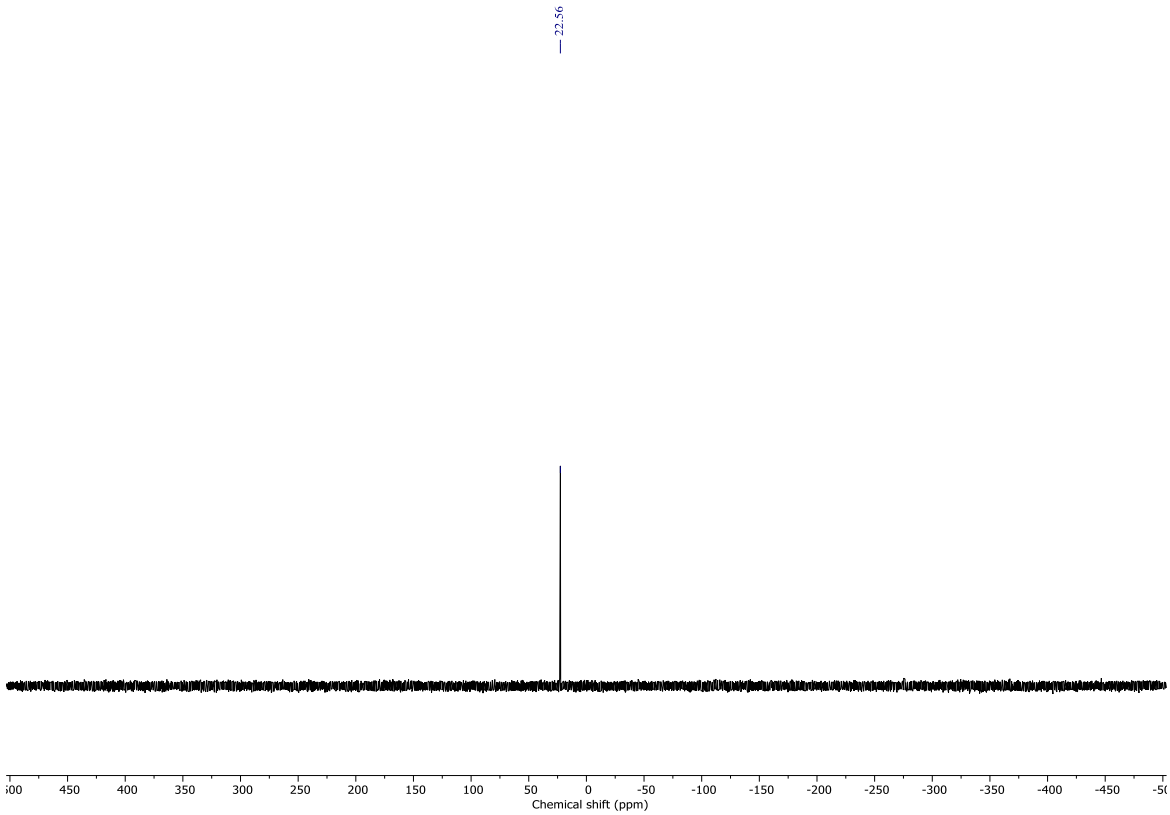

Figure S5.2: $^{31}P\{^{1}H\}$ NMR spectrum (C_6D_6, 162 MHz) of complex **11a**.

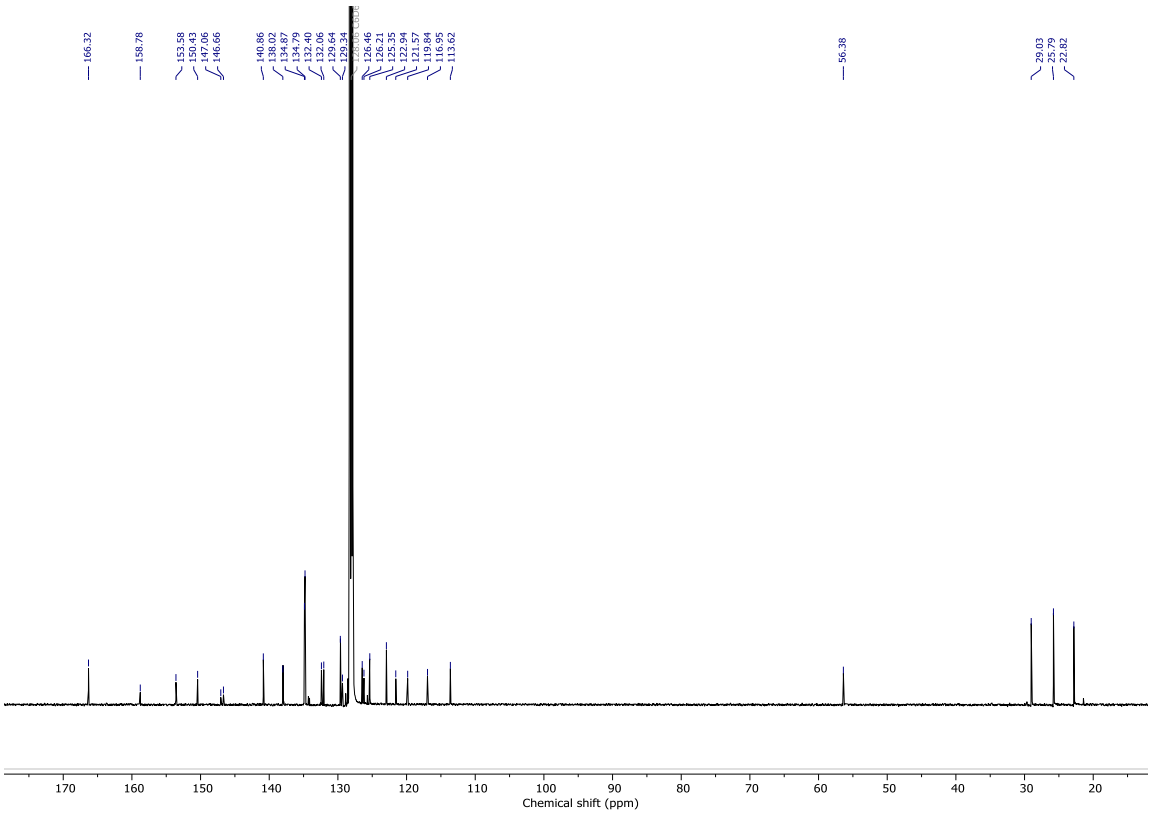

Figure S5.3: $^{13}C\{^{1}H\}$ NMR spectrum (C_6D_6, 126 MHz) of complex **11a**.

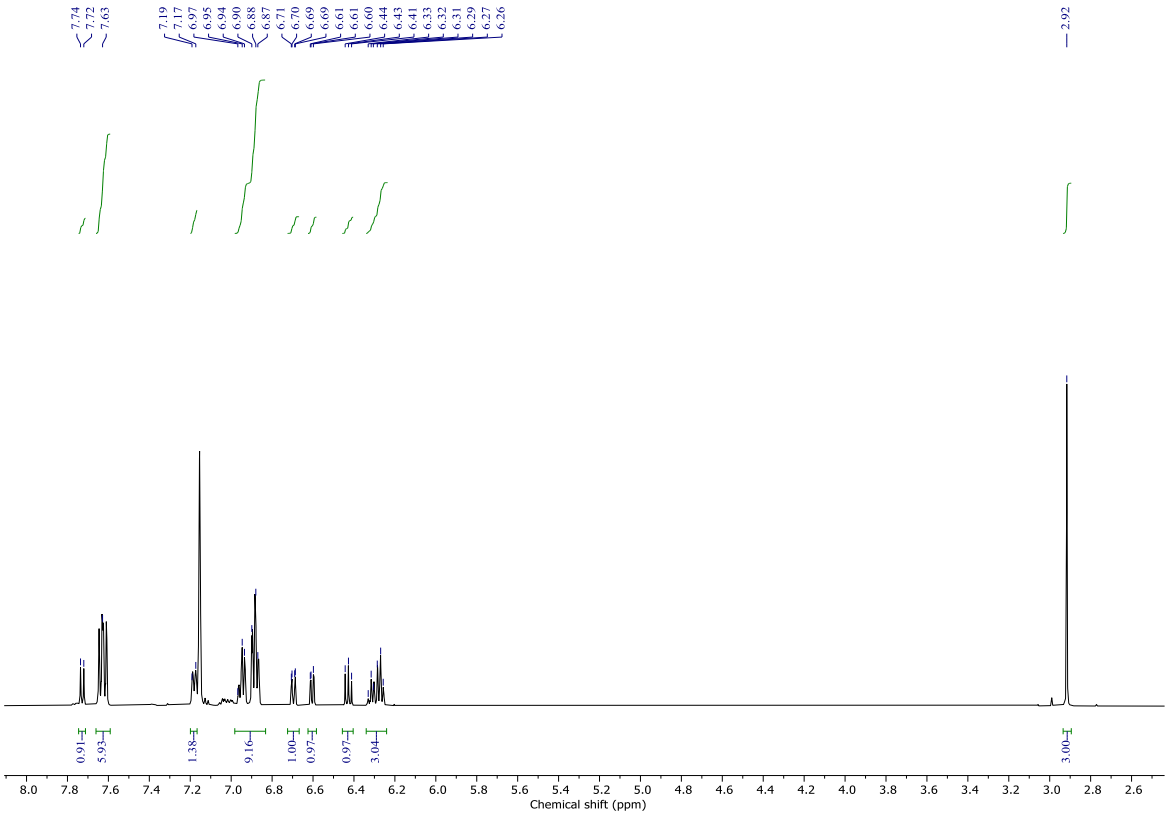

Figure S5.4: ^{1}H NMR spectrum (C_6D_6, 400 MHz) of **12a**.

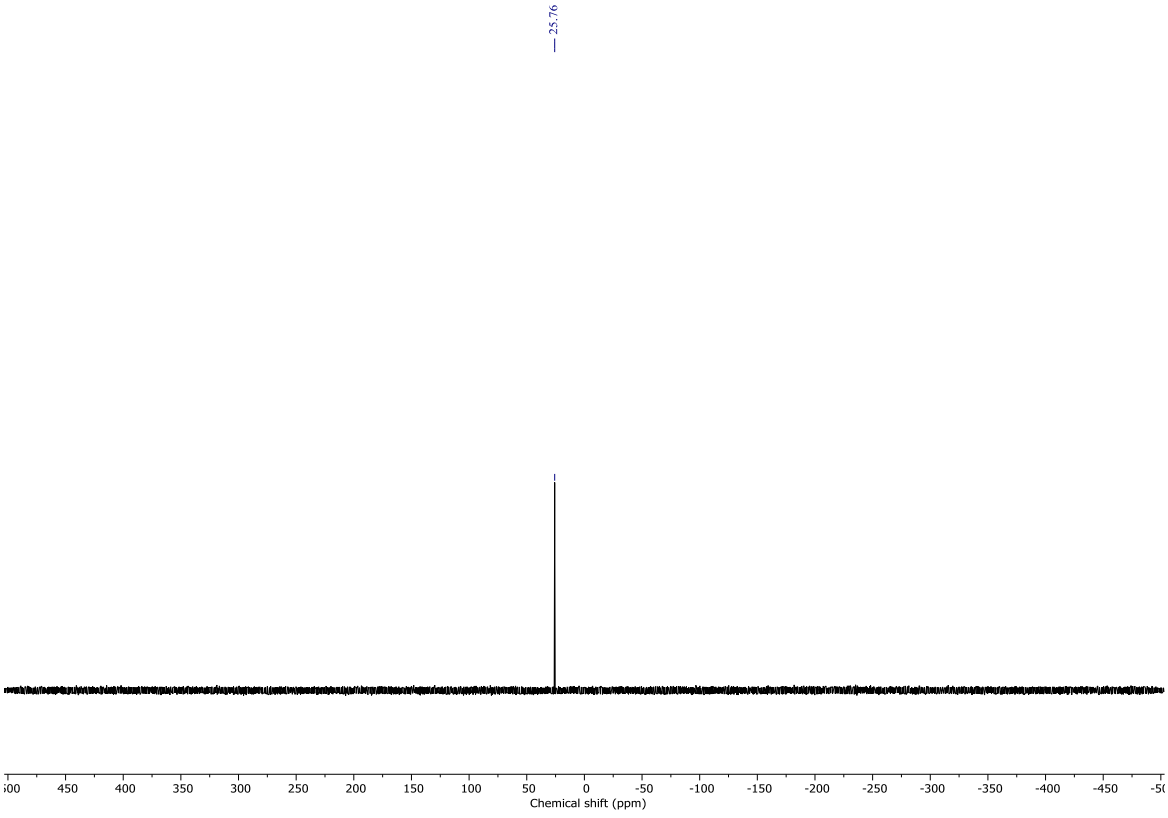

Figure S5.5: $^{31}P\{^{1}H\}$ NMR spectrum (C_6D_6, 162 MHz) of complex **12a**.

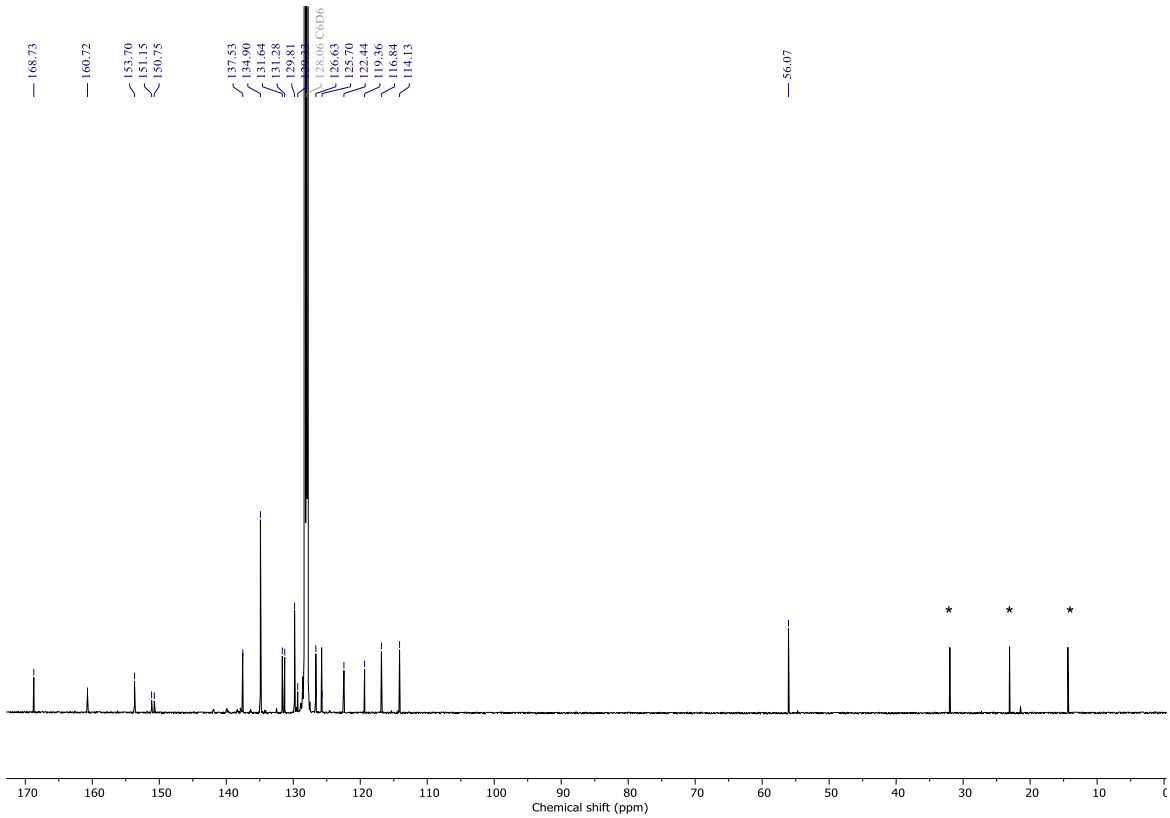

Figure S5.6: $^{13}C\{^{1}H\}$ NMR spectrum (C_6D_6, 126 MHz) of complex **12a**. * = residual hexane

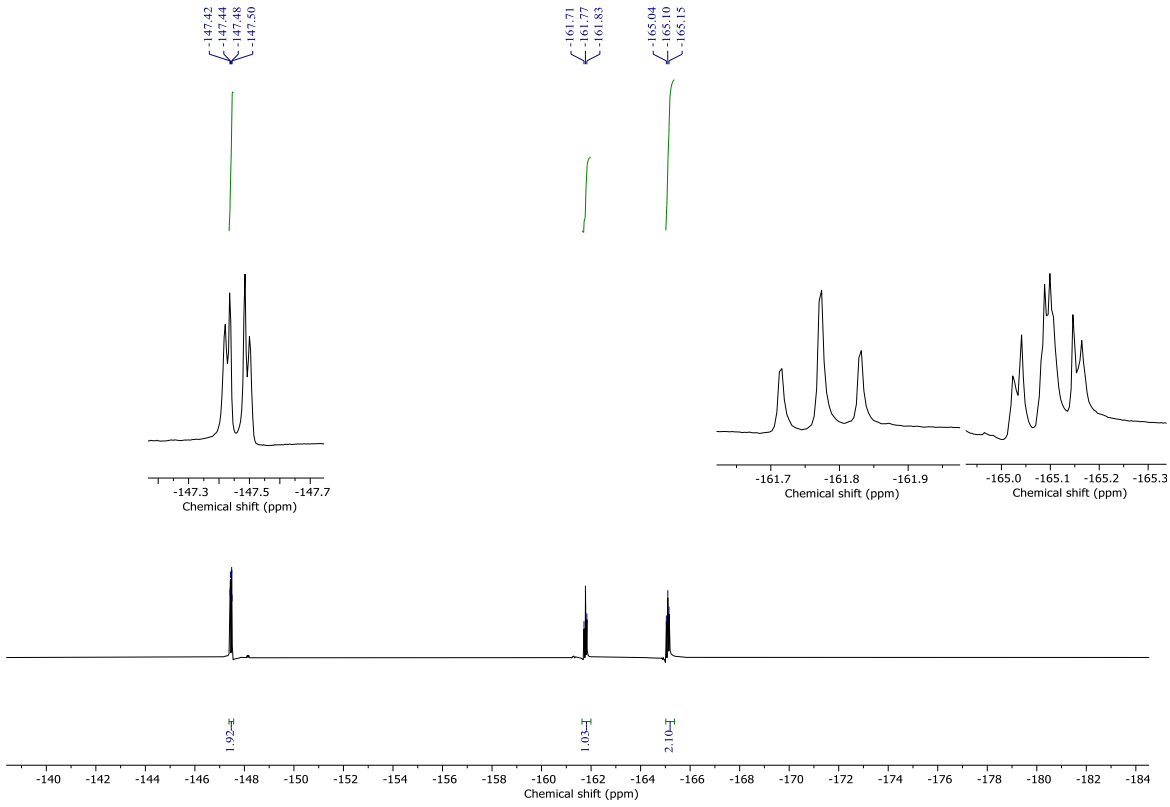

Figure S5.7: $^{19}F\{^{1}H\}$ NMR spectrum (C_6D_6, 377 MHz) of complex **12a**.

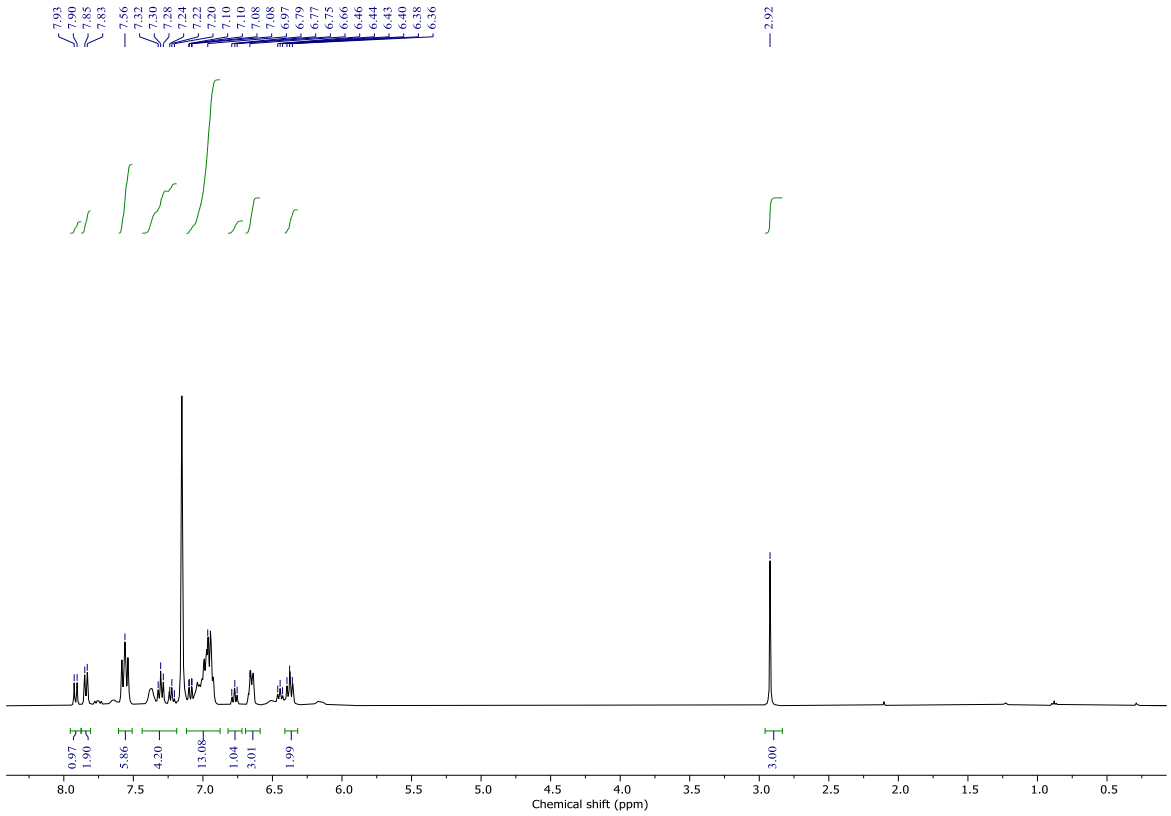

Figure S5.8: ^{1}H NMR spectrum (C_6D_6, 400 MHz) of **13a**.

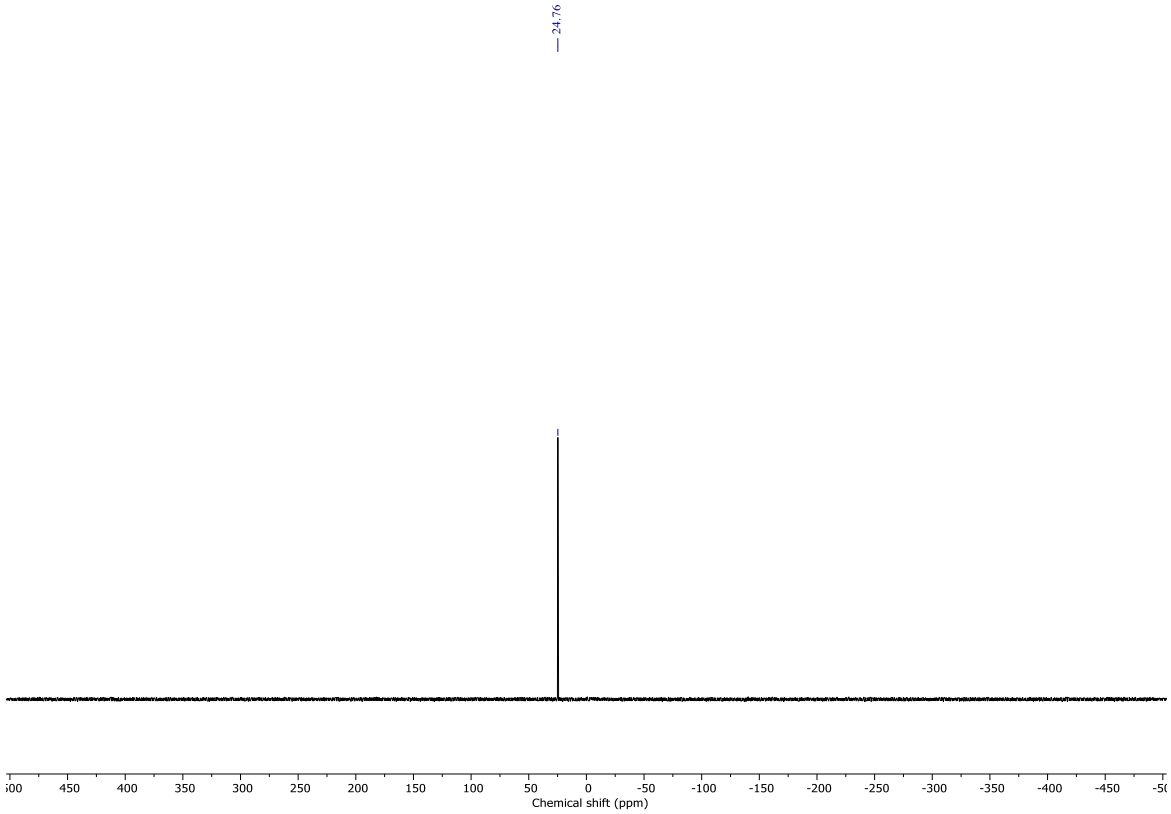

Figure S5.9: $^{31}P\{^{1}H\}$ NMR spectrum (C_6D_6, 162 MHz) of complex **13a**.

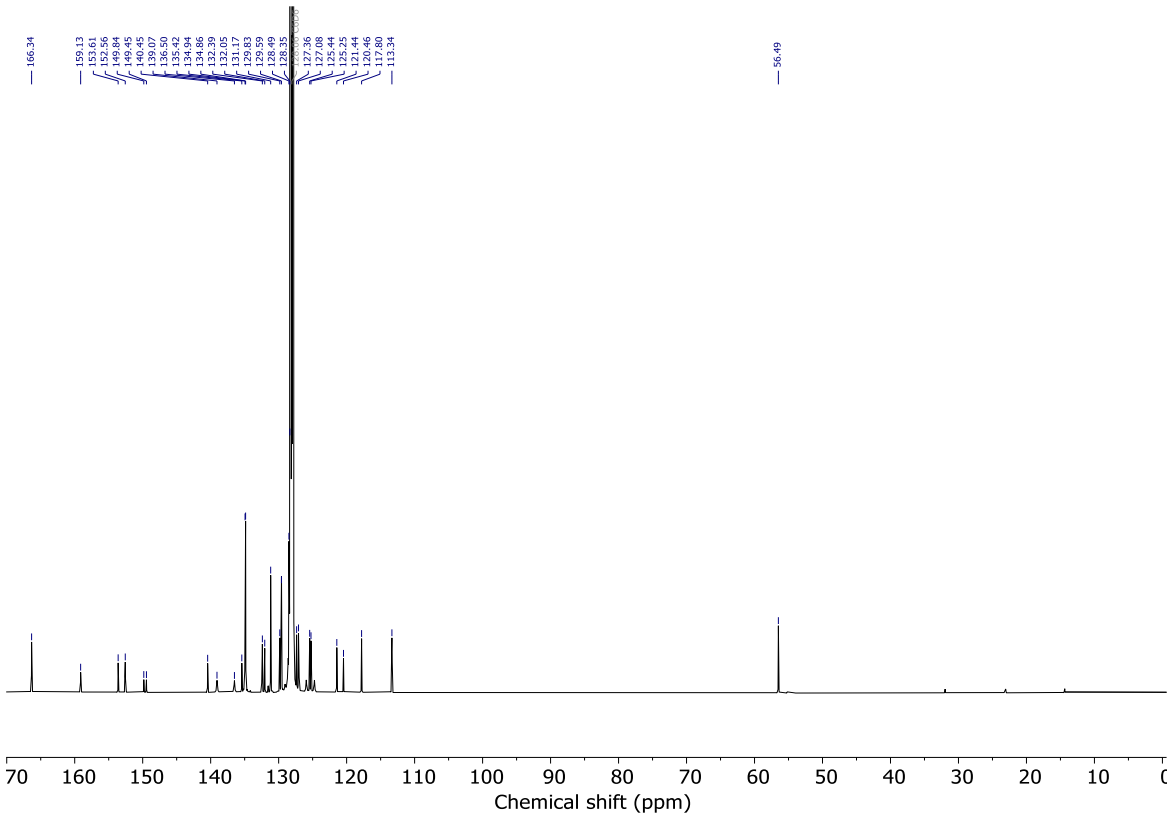

Figure S5.10: $^{13}C\{^{1}H\}$ NMR spectrum (C_6D_6, 126 MHz) of complex **13a**.

Table S5.1: Crystallographic Data for complexes **11a**, **12a**, and **13a**.

Complex	**11a**	**12a**	**13a**
Local Code	7086	7135	7161
Crystal Data			
Chemical formula	$C_{44}H_{44}NNiO_2P$	$C_{38}H_{27}F_5NNiO_2P$	$C_{44}H_{36}NNiO_2P$
M_r	708.52	714.31	700.46
Crystal system, space group	Monoclinic, $P2_1/n$	Triclinic, $P\bar{1}$	Monoclinic, $P2_1/c$
a, b, c (Å)	9.8242 (1) 9.7189 (1), 38.5197 (3)	11.6551 (4) 17.5552 (5) 18.6026 (5)	13.5717 (1) 9.4725 (1), 27.0123 (2)
α, β, γ (°)	94.9248 (6)	91.265 (2), 102.040 (3), 101.801 (3)	90.3479 (7)
V (Å^3)	3664.30 (6)	3635.5 (2)	3472.58 (5)
Z	4	4	4
Radiation type	Cu $K\alpha$	Cu $K\alpha$	Cu $K\alpha$
μ (mm^{-1})	1.46	1.69	1.54
Data collection			
T_{min}, T_{max}	0.90, 0.93	0.57, 0.84	0.73, 0.86
No. of measured, independent and observed [$I > 2.0\sigma(I)$] reflections	46065, 7657, 6871	32465, 15135, 12644	45125, 7217, 6394
R_{int}	0.032	0.033	0.039
$(\sin\theta/\lambda)_{max}$ (Å^{-1})	0.630	0.632	0.630
Refinement			
$R[F^2 > 2\sigma(F^2)]$, $wR(F^2)$, S	0.031, 0.081, 1.01	0.043, 0.119, 0.99	0.035, 0.095, 1.00
No. of reflections	7655	15132	7217
No. of parameters	442	967	449
No. of restraints	0	108	4
$\Delta\rho_{max}$, $\Delta\rho_{min}$ (e Å^{-3})	0.40, −0.28	1.31, −0.38	0.49, −0.43

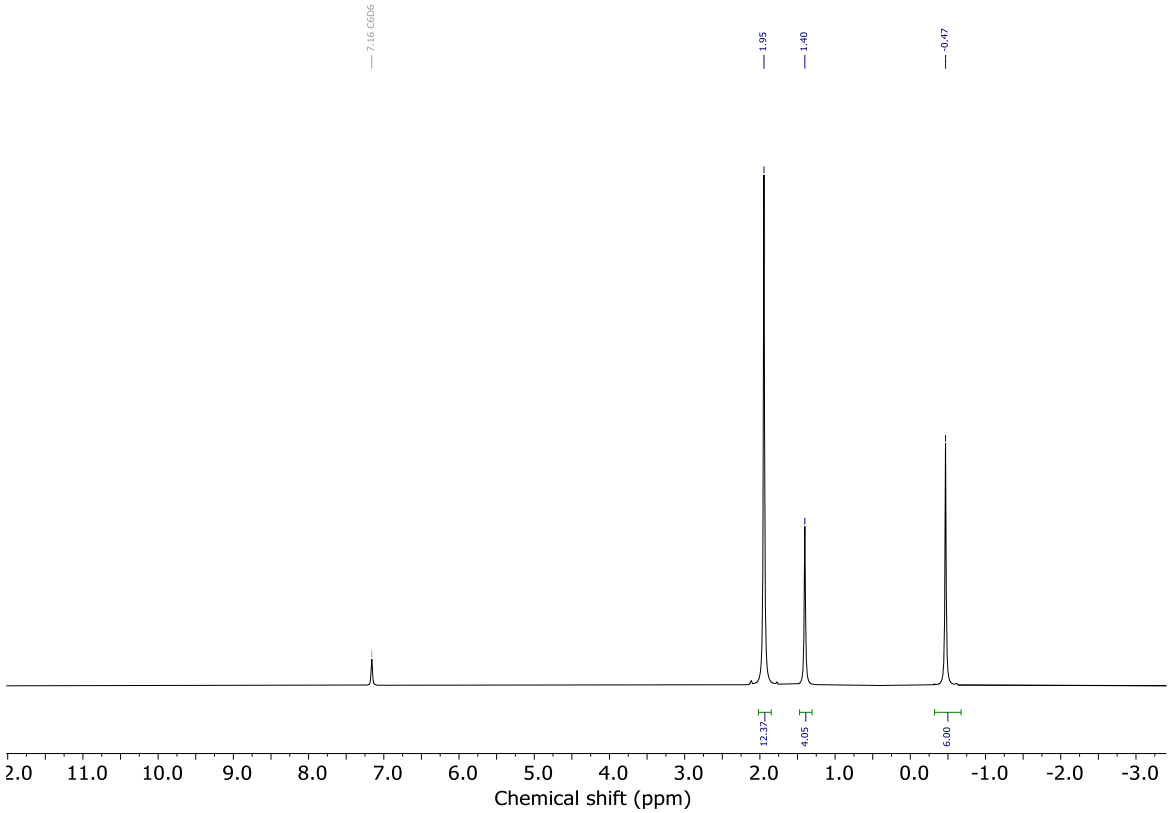

Figure S5.11: ^{1}H NMR spectrum (C6D6, 400 MHz) of [(Tmeda)Ni(CH_3)$_2$].

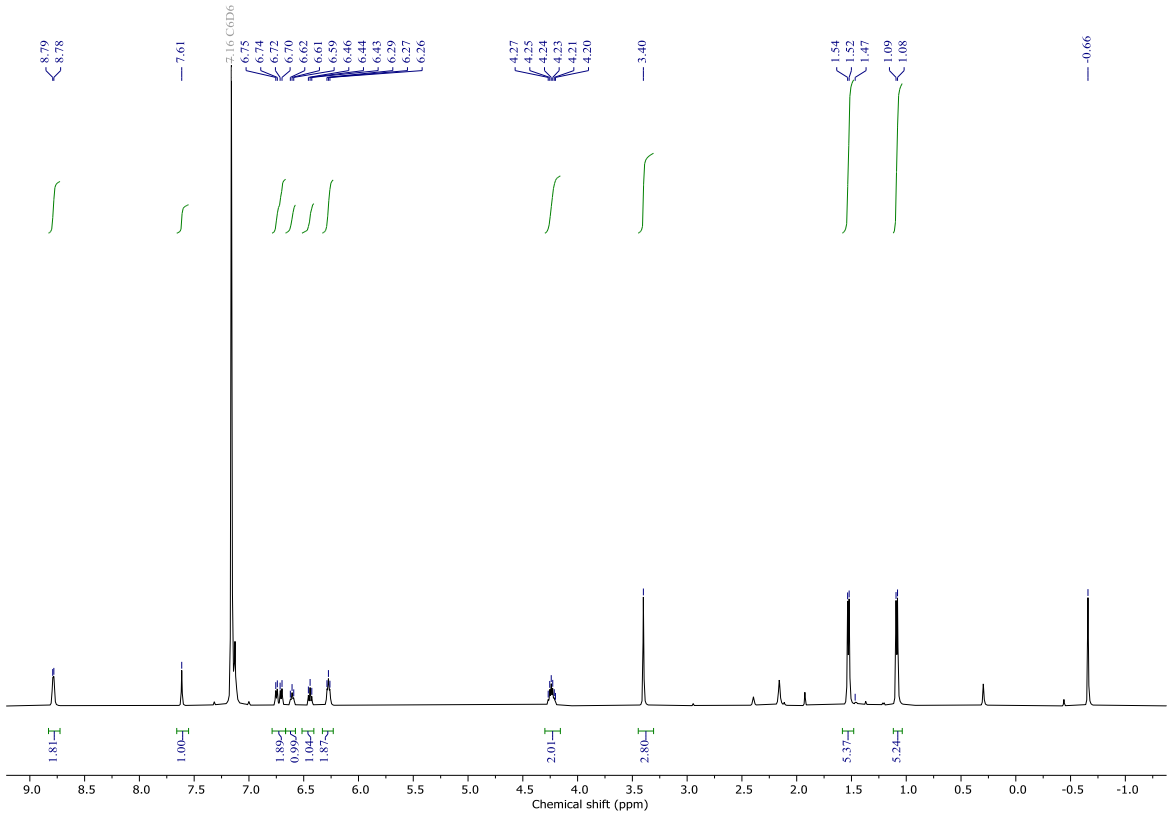

Figure S5.12: ^{1}H NMR spectrum (C_6D_6, 400 MHz) of **11b**.

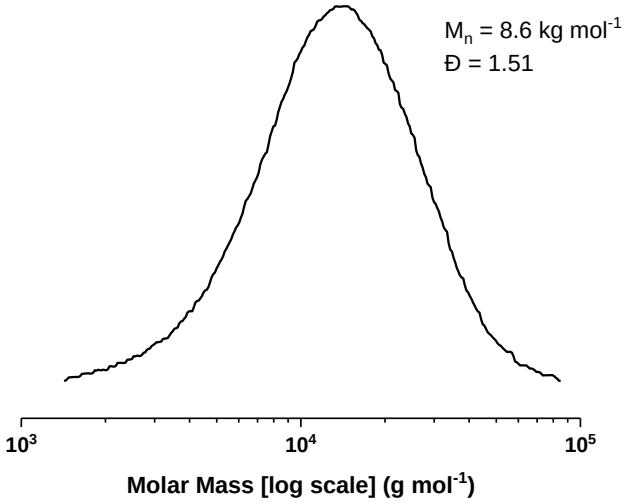

Figure S5.13: GPC trace for the polyethylene obtained with **11a** at 25 ˚C at 2 bar of ethylene (Table 5.2, entry 2).

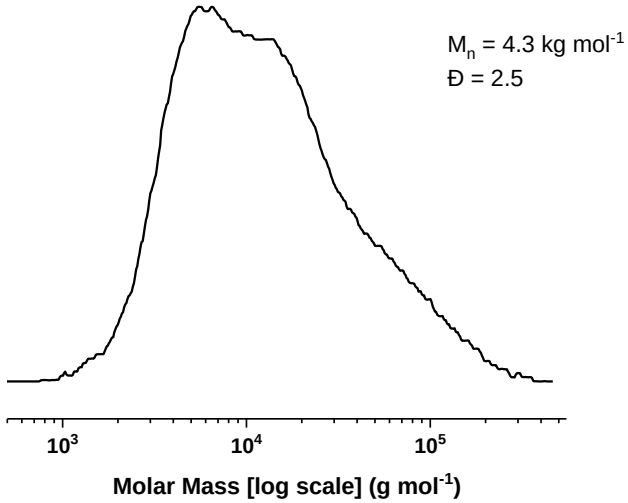

Figure S5.14: GPC trace for the polyethylene obtained with **11a** at 25 ˚C at 40 bar of ethylene (Table 5.2, entry 4).

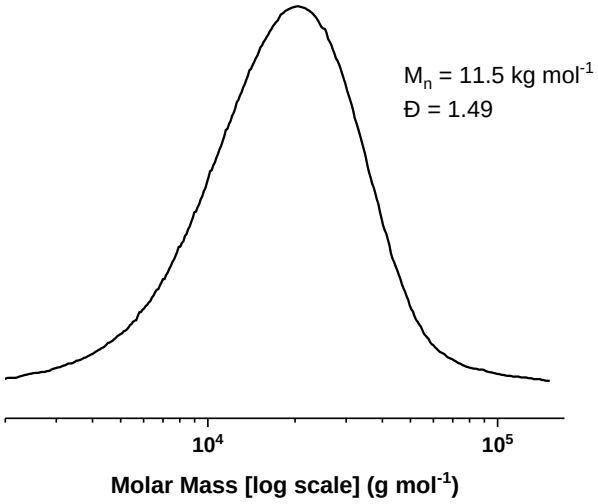

Figure S5.15: GPC trace for the polyethylene obtained with **11a** at 45 ˚C at 40 bar of ethylene (Table 5.2, entry 5).

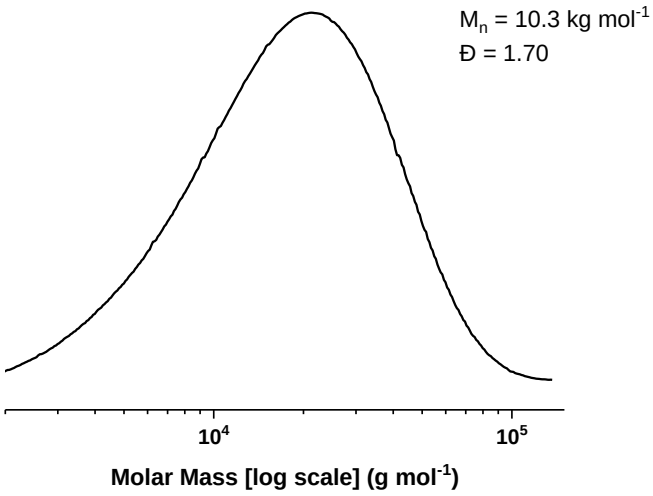

Figure S5.16: GPC trace for the polyethylene obtained with **11a** at 60 ˚C at 40 bar of ethylene (Table 5.2, entry 6).

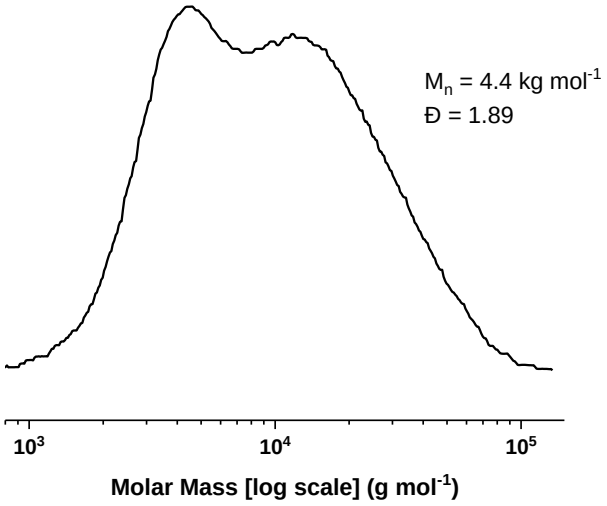

Figure S5.17: GPC trace for the polyethylene obtained with **11b** at 25 ˚C at 40 bar of ethylene (Table 5.2, entry 7).

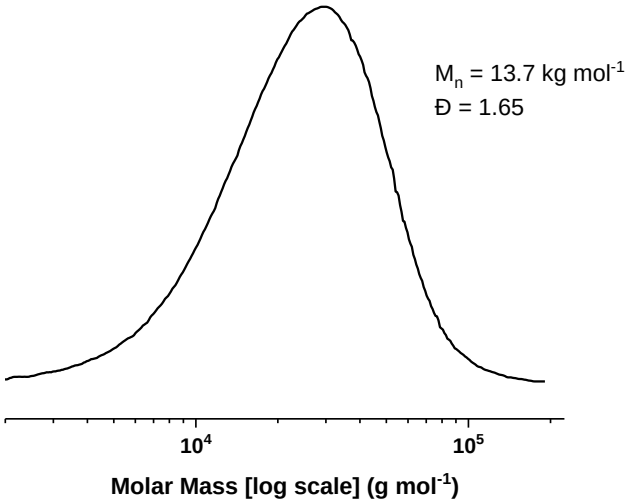

Figure S5.18: GPC trace for the polyethylene obtained with **11b** at 45 ˚C at 40 bar of ethylene (Table 5.2, entry 8).

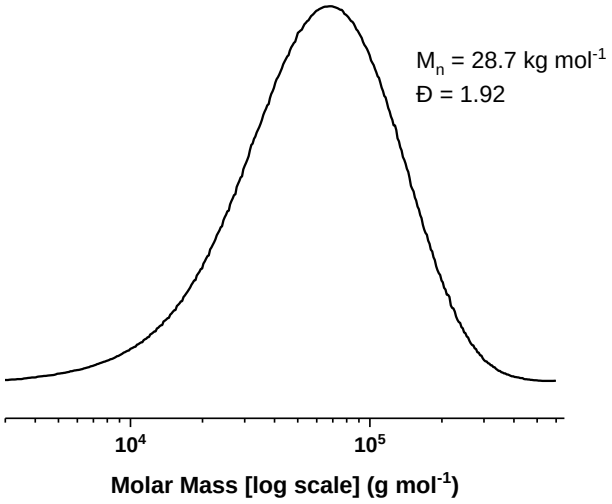

Figure S5.19: GPC trace for the polyethylene obtained with **11b** at 60 ˚C at 40 bar of ethylene (Table 5.2, entry 9).

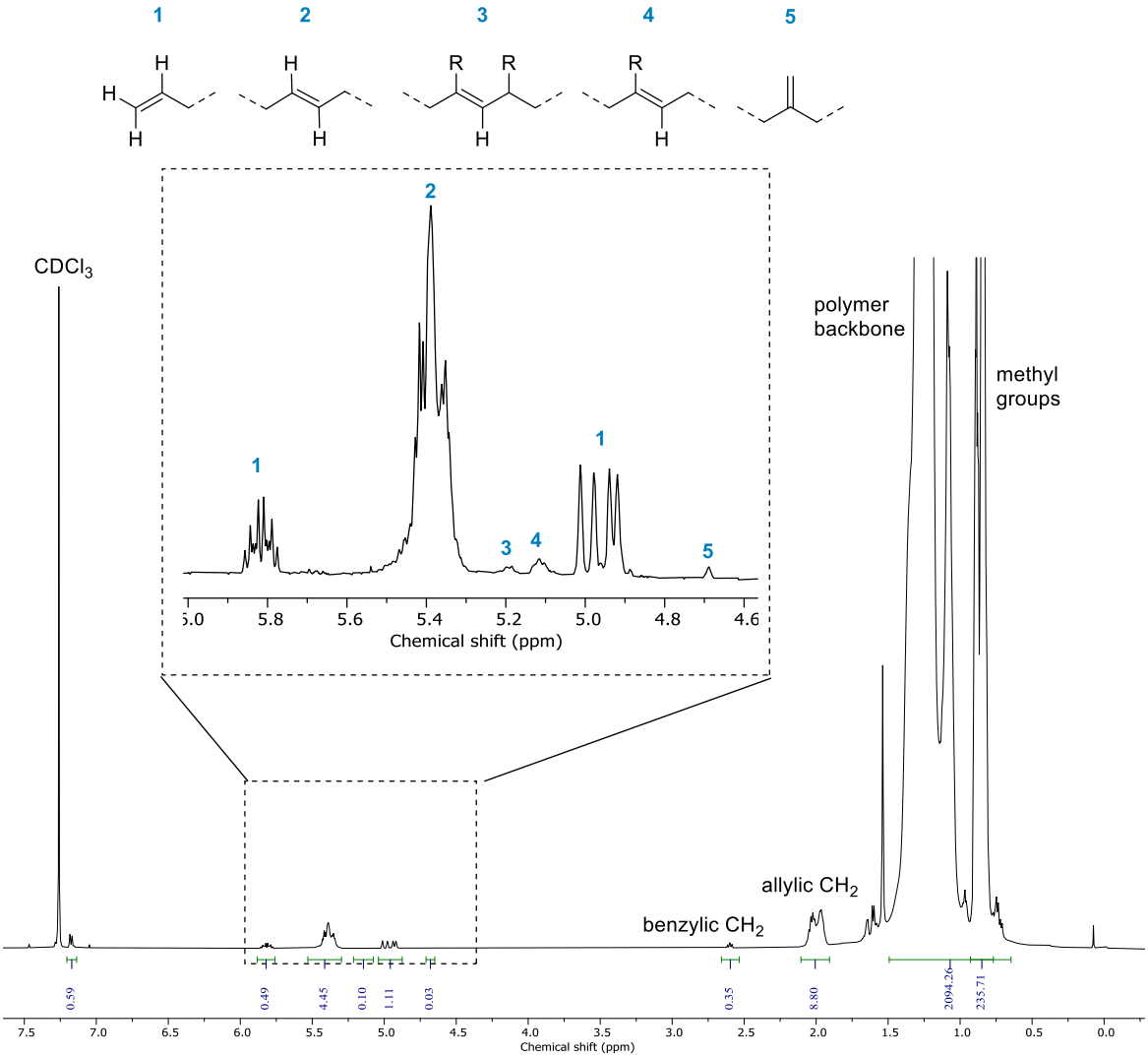

$$M_n = \frac{\left(\frac{I_{tot}}{4}\right)}{\left(\frac{I_1 + I_2 + 2I_3 + 2I_4 + I_5}{2}\right)} \cdot 28\ g mol^{-1} = 5063\ g\ mol^{-1}$$

Figure S5.20: ^{1}H NMR spectrum ($CDCl_3$, 400 MHz) used to calculate M_n (using equation) of polyethylene obtained with **11a** at 60 ˚C with 2 bar of ethylene (Table 5.2. entry 3).

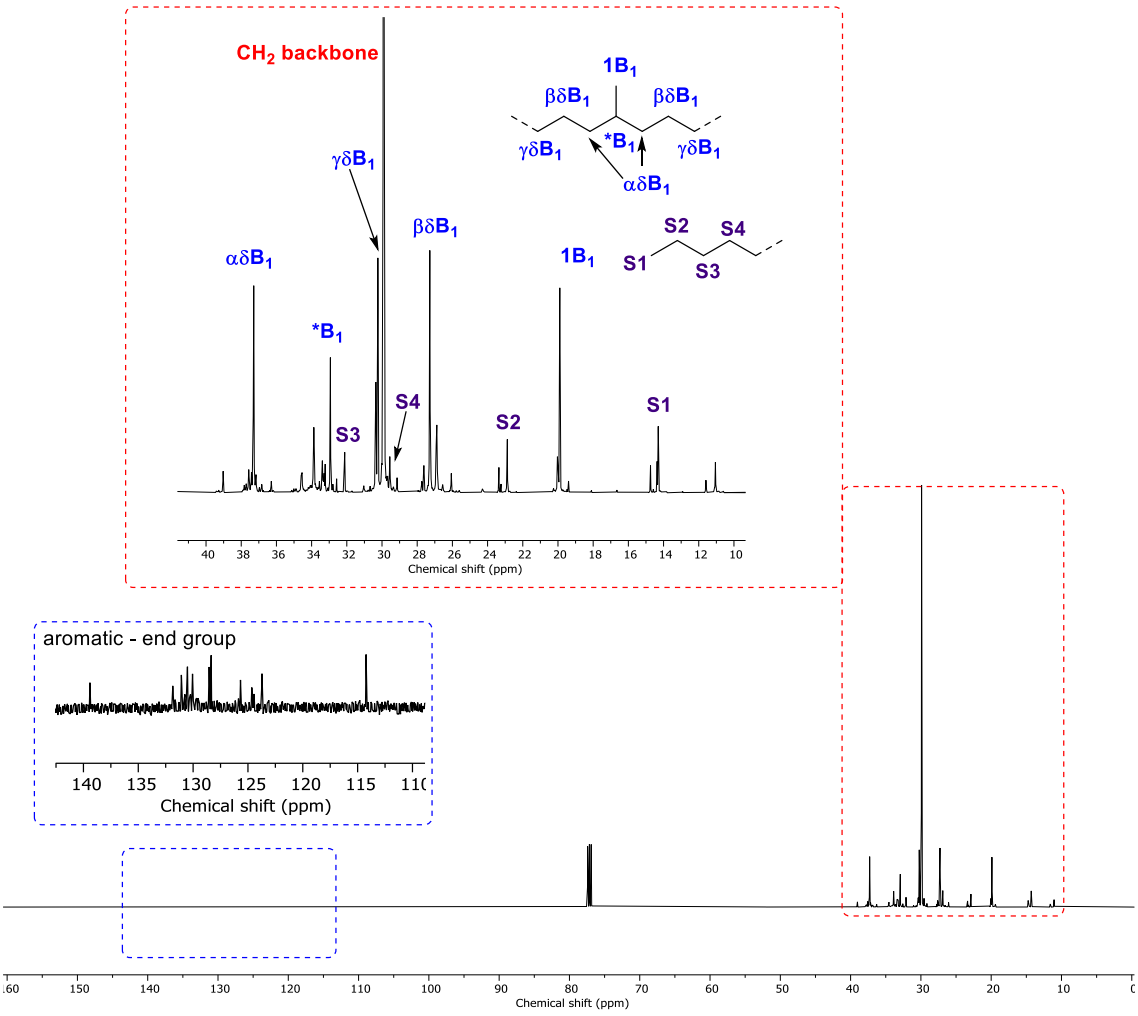

Figure S5.21: $^{13}C\{^{1}H\}$ NMR spectrum ($CDCl_3$, 126 MHz) used to calculate degree of branching of polyethylene obtained with **11a** at 60 ˚C with 2 bar of ethylene (Table 5.2. entry 3).

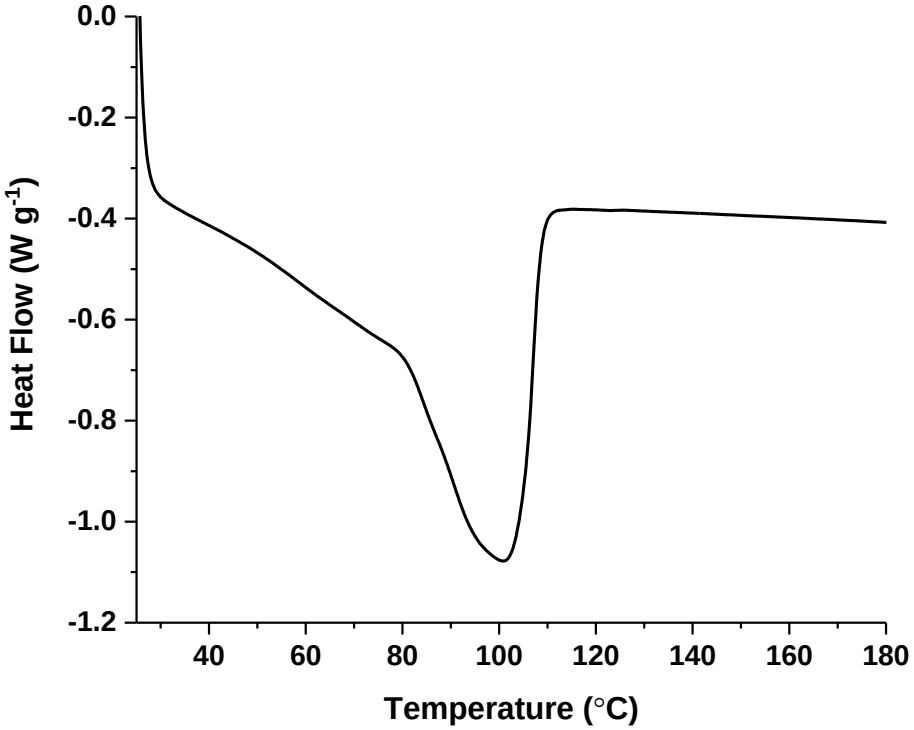

Figure S5.22: DSC data for the polyethylene obtained with **11a** at 25 ˚C at 2 bar of ethylene (Table 5.2, entry 1).

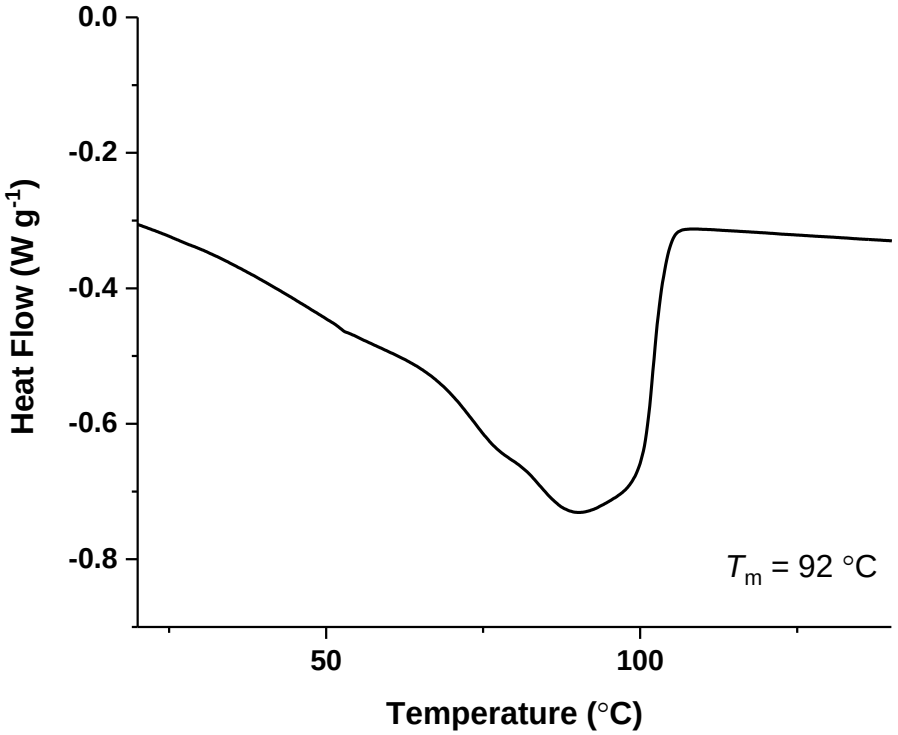

Figure S5.23: DSC data for the polyethylene obtained with **11a** at 25 ˚C at 2 bar of ethylene (Table 5.2, entry 2).

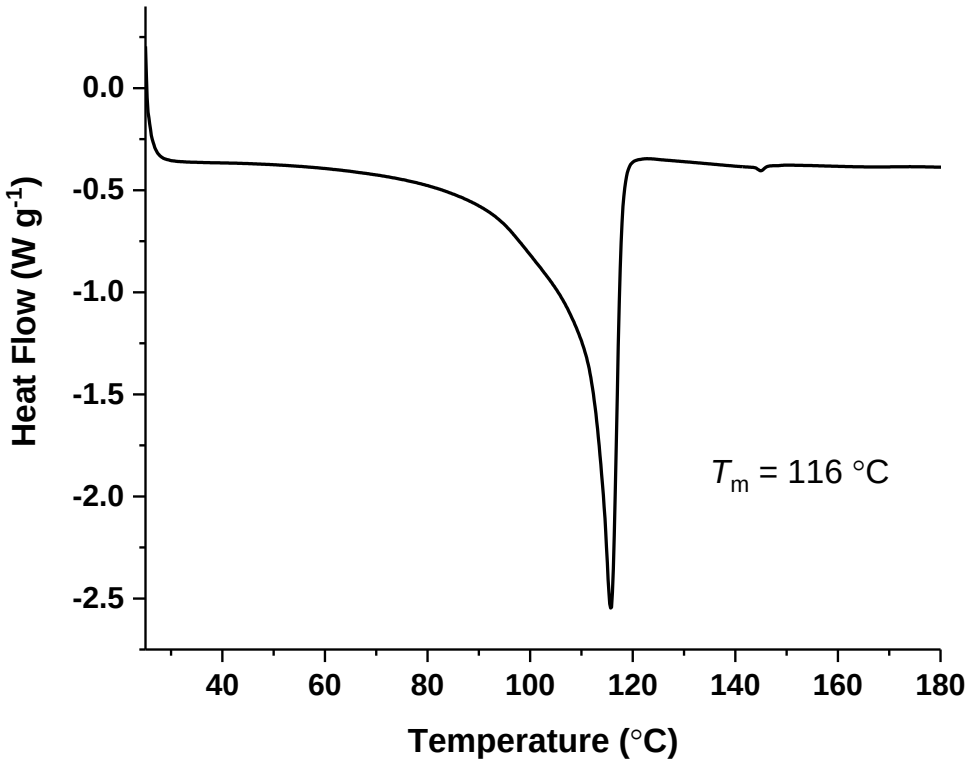

Figure S5.24: DSC data for the polyethylene obtained with **11a** at 25 ˚C at 40 bar of ethylene (Table 5.2, entry 4).

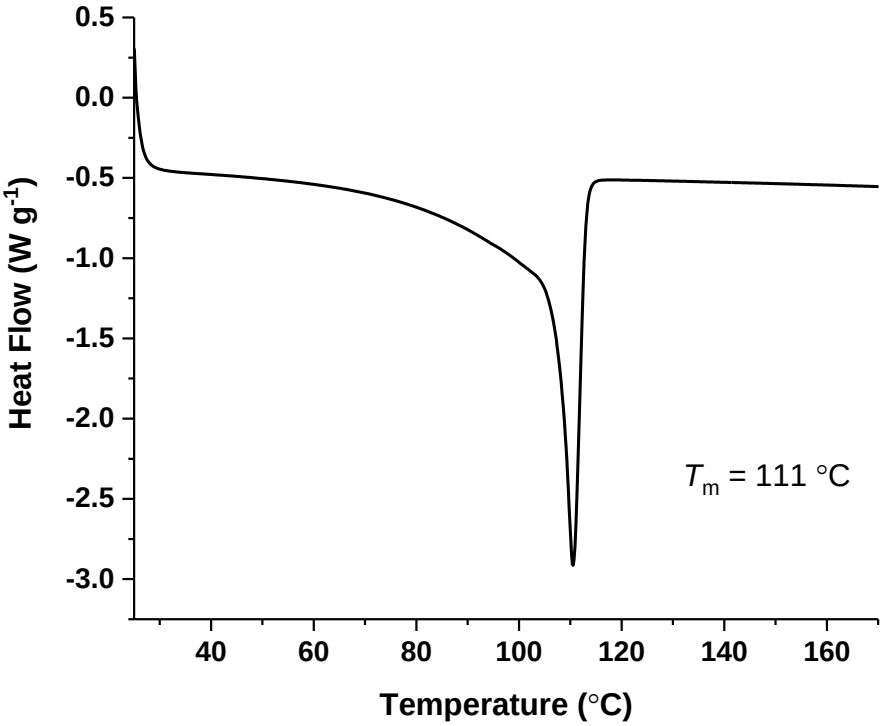

Figure S5.25: DSC data for the polyethylene obtained with **11a** at 45 ˚C at 40 bar of ethylene (Table 5.2, entry 5).

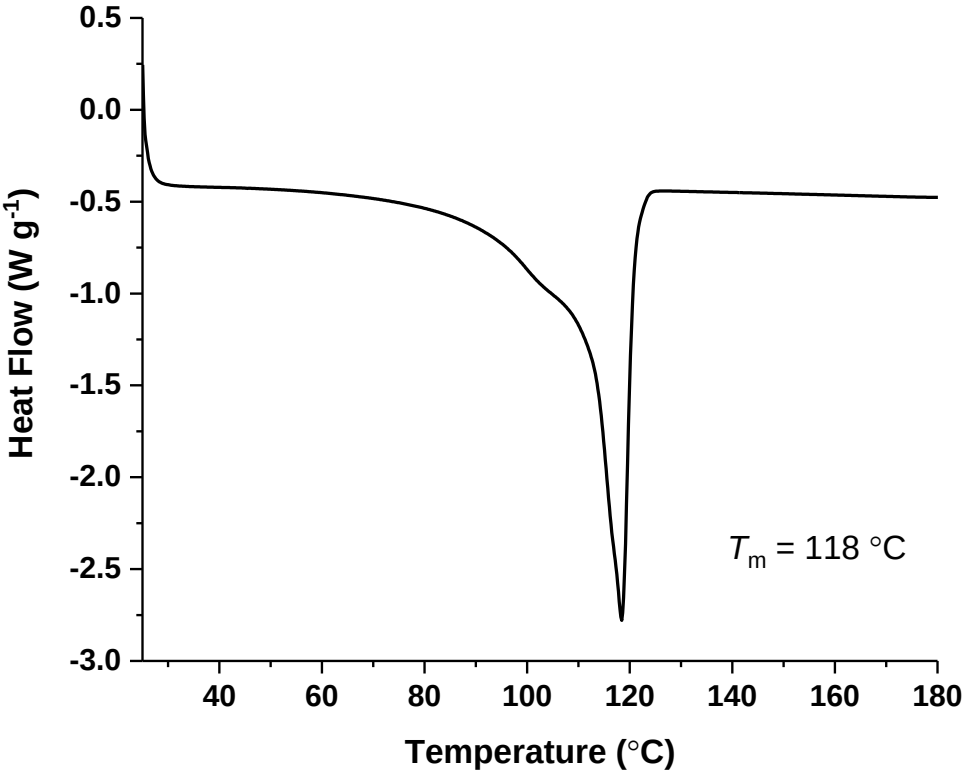

Figure S5.26: DSC data for the polyethylene obtained with **11b** at 25 ˚C at 40 bar of ethylene (Table 5.2, entry 7).

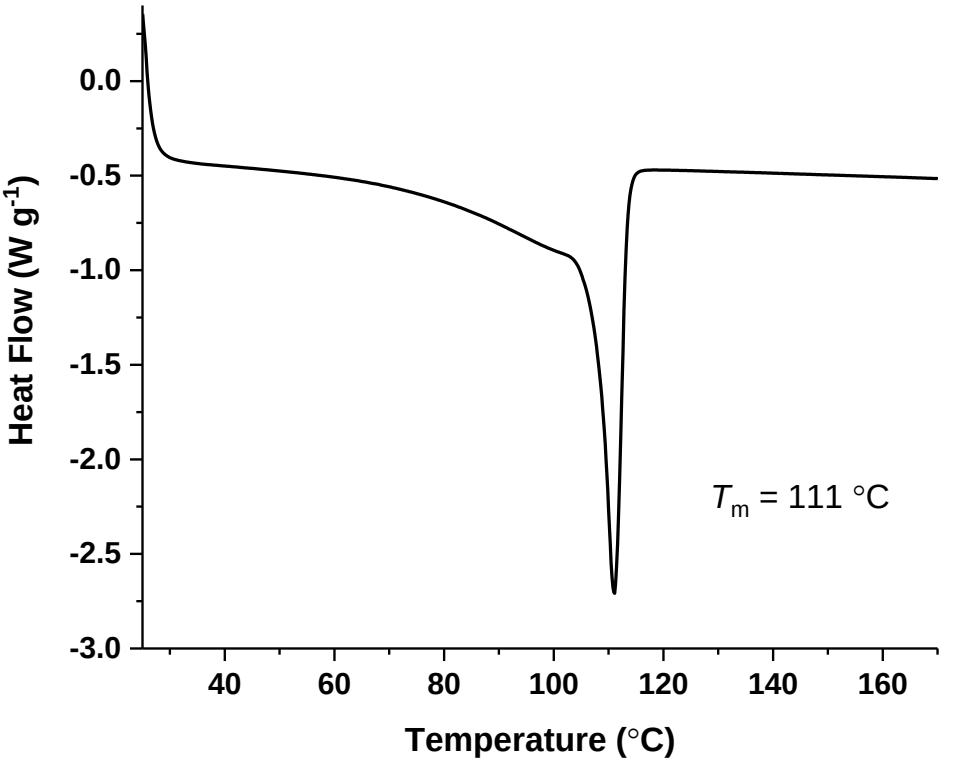

Figure S5.27: DSC data for the polyethylene obtained with **11b** at 45 ˚C at 40 bar of ethylene (Table 5.2, entry 8).

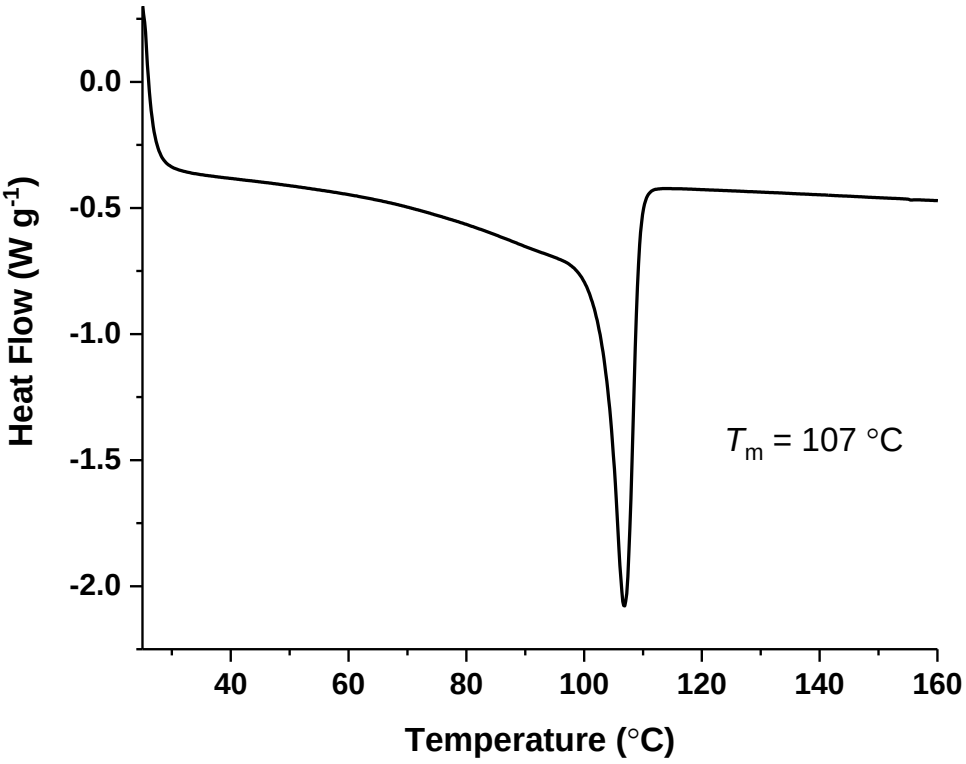

Figure S5.28: DSC data for the polyethylene obtained with **11b** at 60 ˚C at 40 bar of ethylene (Table 5.2, entry 9).

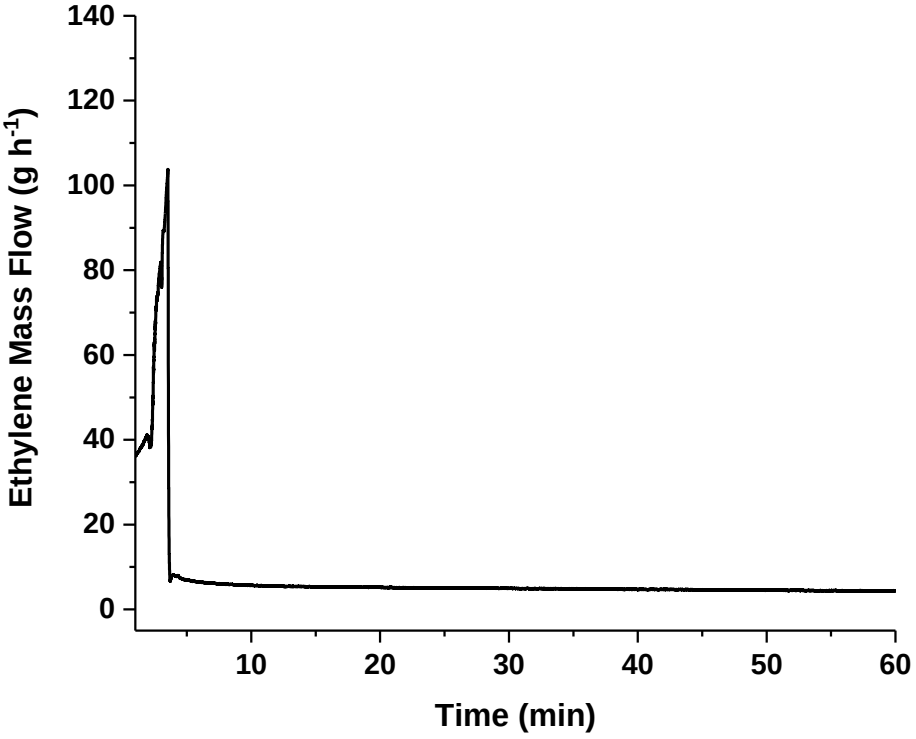

Figure S5.29: Ethylene mass flow data for the polymerisation with catalyst **11a** at 25 ˚C (Table 5.2 entry 4).

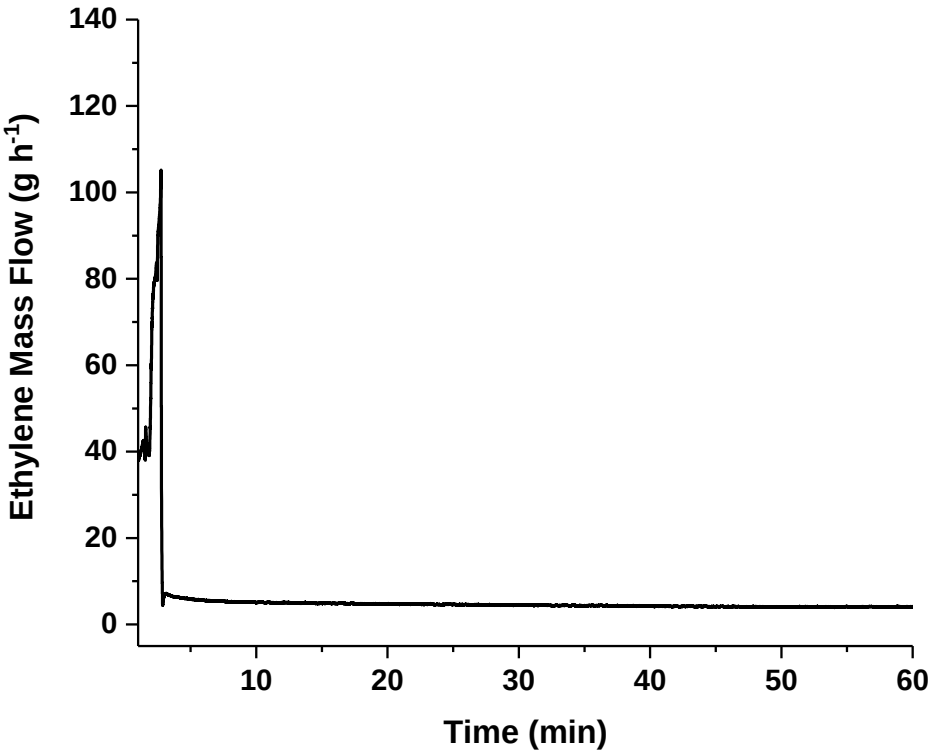

Figure S5.30: Ethylene mass flow data for the 40 bar ethylene polymerisation with catalyst **11a** at 45 ˚C (Table 5.2 entry 5).

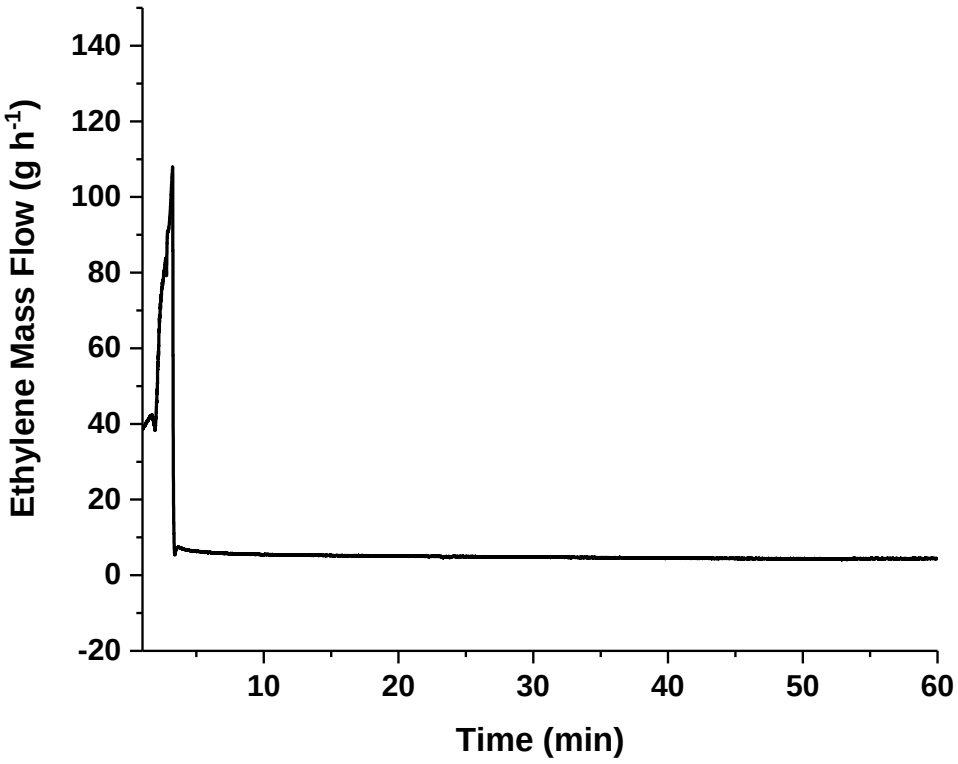

Figure S5.31: Ethylene mass flow data for the polymerisation with catalyst **11b** at 25 ˚C (Table 5.2 entry 7).

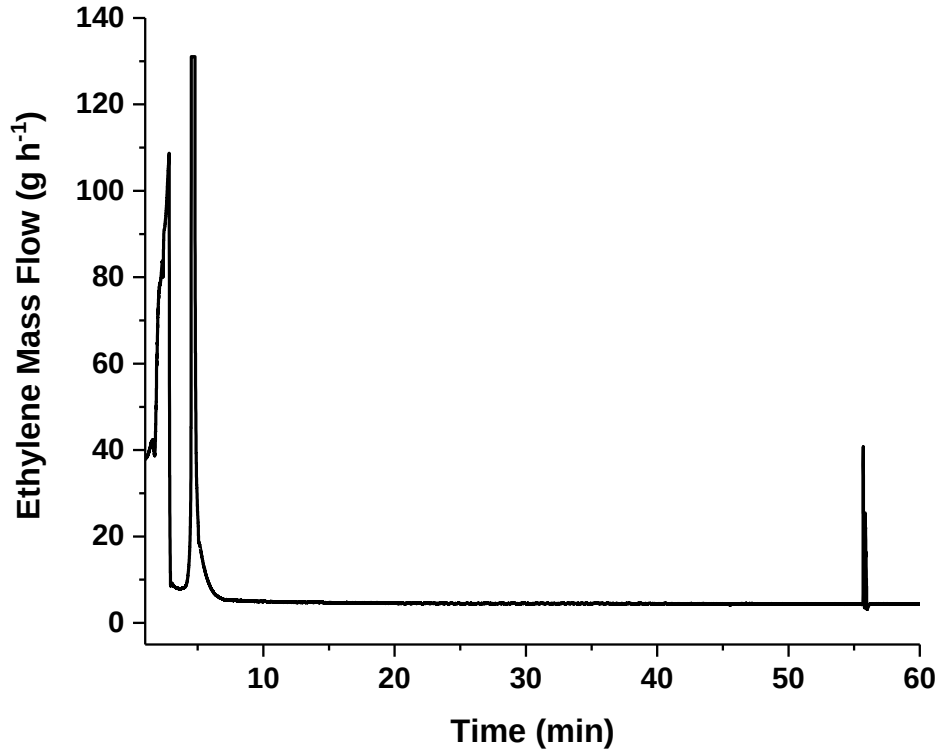

Figure S5.32: Ethylene mass flow data for the polymerisation with catalyst **11b** at 45 ˚C (Table 5.2 entry 8).

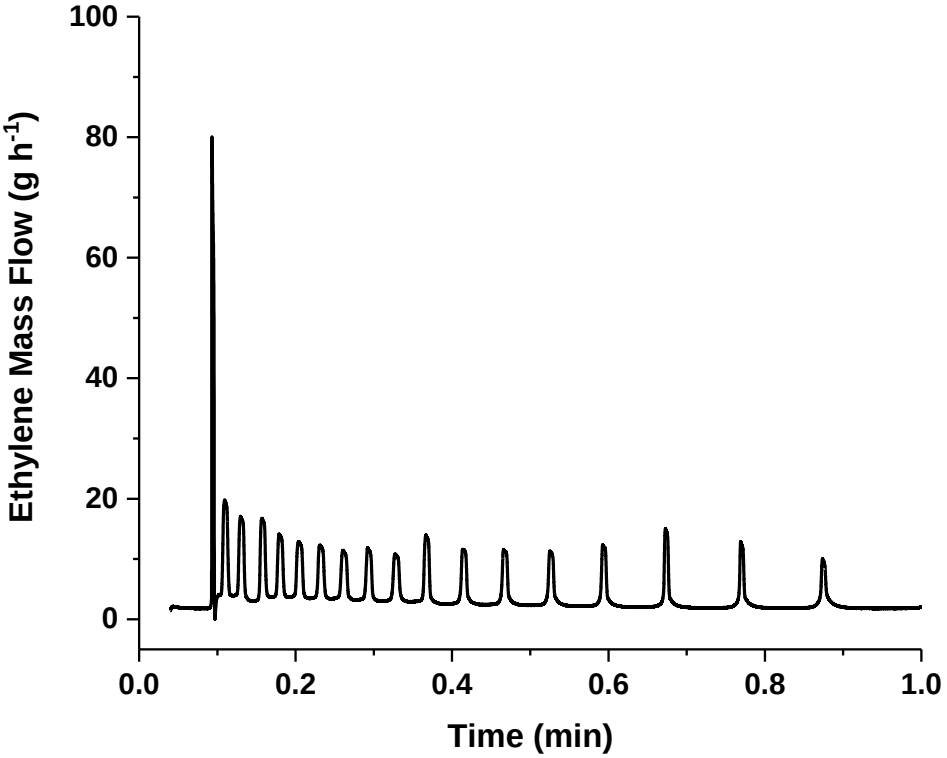

Figure S5.33: Ethylene mass flow data for the polymerisation with catalyst **11b** at 60 ˚C (Table 5.2 entry 9).

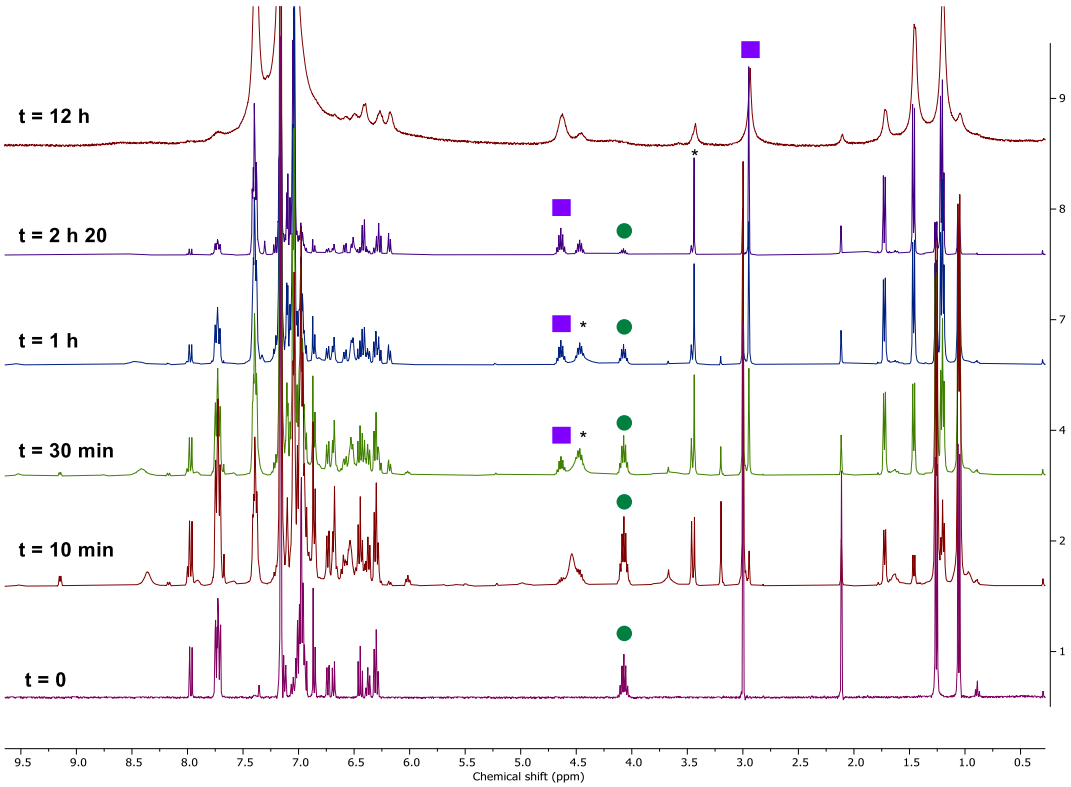

Figure S5.34: Stacked ^{1}H NMR plot (C_6D_6, 400 MHz) of **11a** (green circle) with 2-pyridinemethanol over time. Bis-chelate = purple square, * = not assigned.

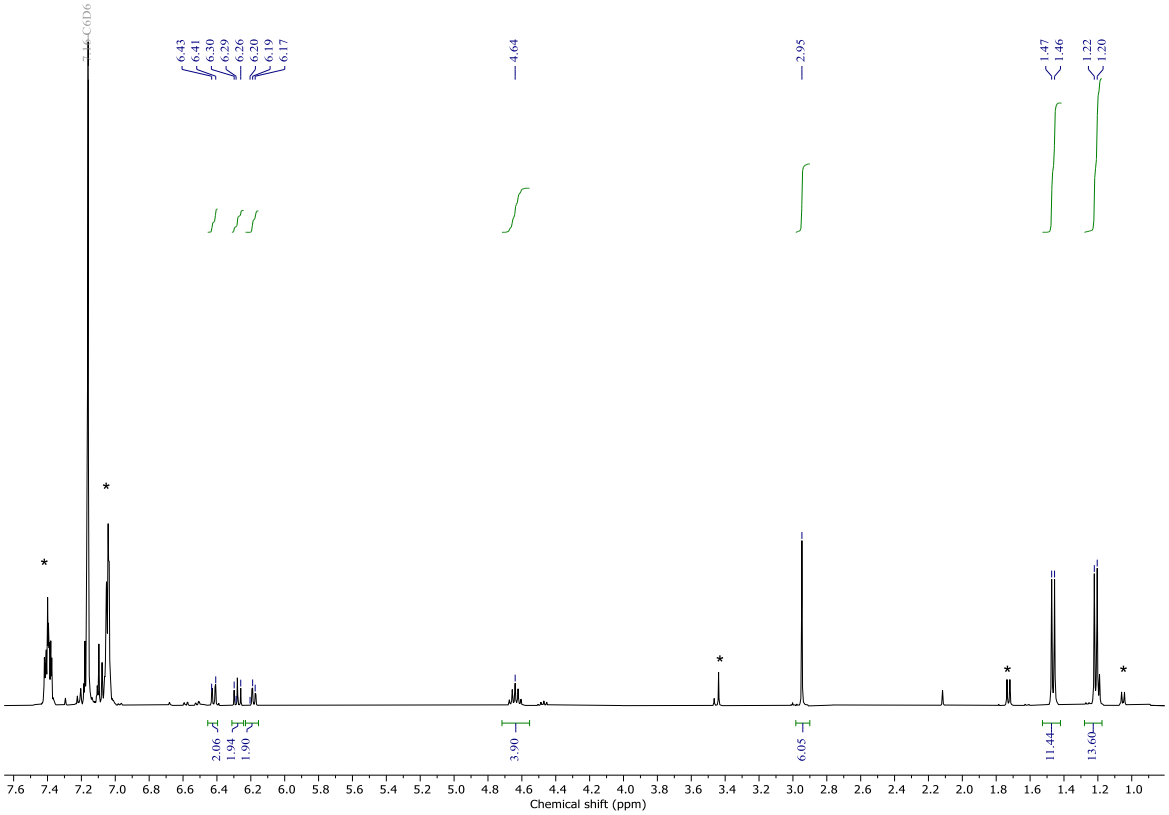

Figure S5.35: ^{1}H NMR spectrum (C_6D_6, 400 MHz) of **[Ni(L$_1$)$_2$]**. **L$_1$** and PPh_3 byproducts are denoted by *.

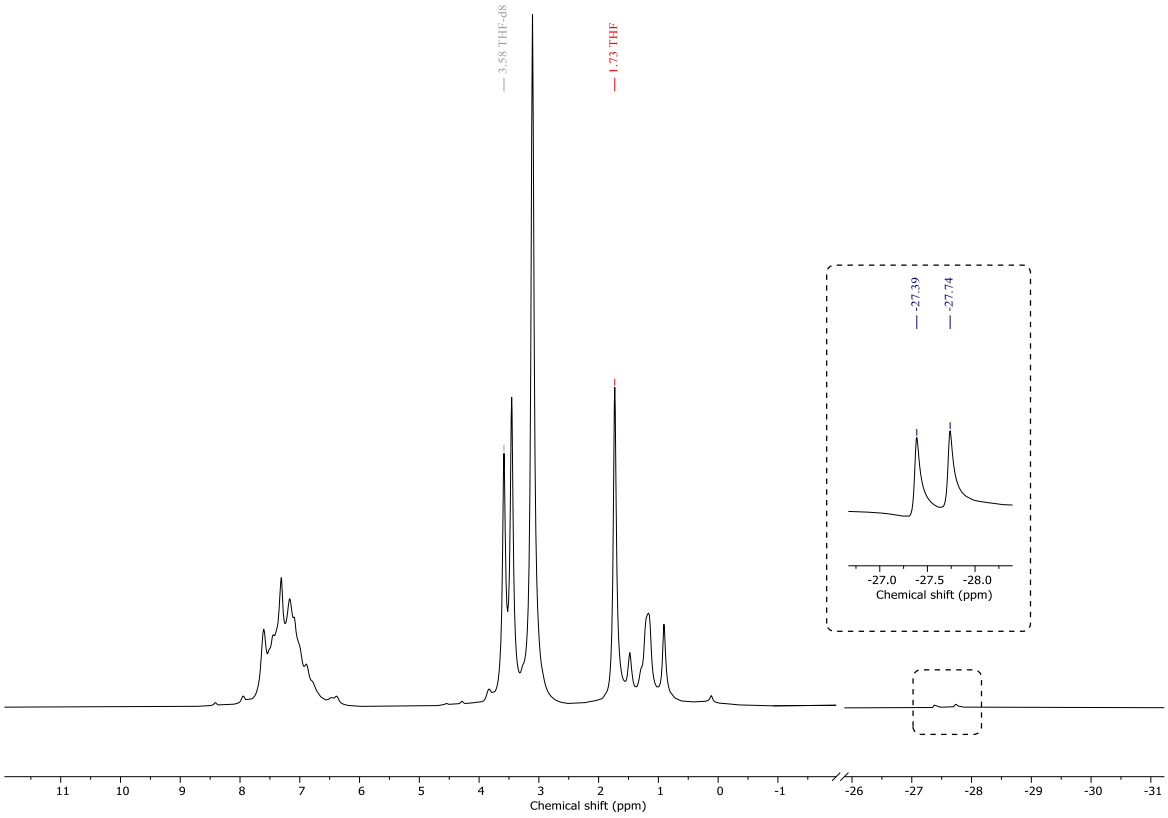

Figure S5.36: Wide scan ^{1}H NMR spectrum (THF-d_8, 400 MHz) of Ni(H) species.

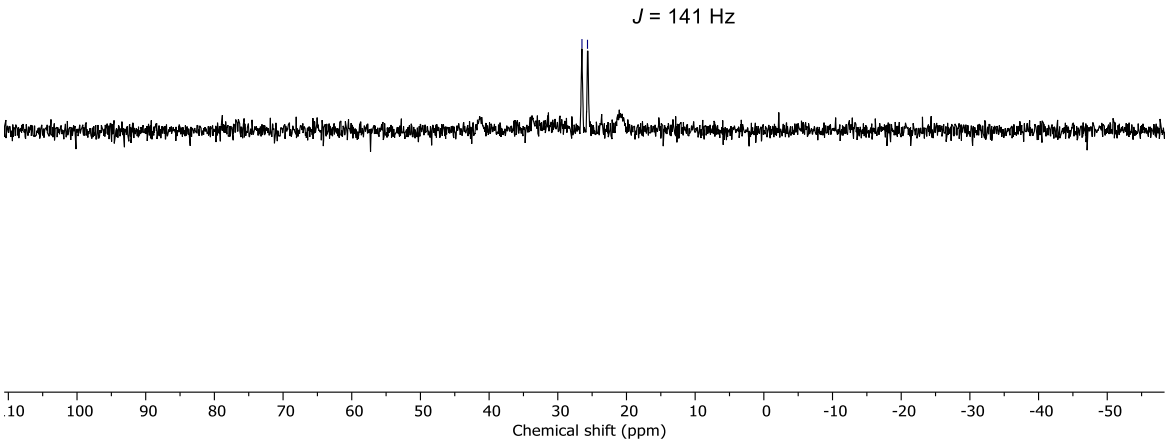

Figure S5.37: ^{31}P NMR spectrum (THF-d_8, 162 MHz) of Ni(H) species.

References

1. Han, B.; Zhang, L.; Yang, M.; Liu, B.; Dong, X.; Theato, P., *Macromolecules* **2016,** *49* (17), 6232-6239.

2. Baumgartner, R.; Song, Z.; Zhang, Y.; Cheng, J., *Polym. Chem,* **2015,** *6* (19), 3586-3590.

3. Abel, B. A.; Lidston, C. A. L.; Coates, G. W., *J. Am. Chem. Soc.* **2019,** *141* (32), 12760-12769.

4. Diment, W. T.; Gregory, G. L.; Kerr, R. W. F.; Phanopoulos, A.; Buchard, A.; Williams, C. K., *ACS Catal.* **2021,** *11* (20), 12532-12542.

5. Parsons, S.; Flack, H. D.; Wagner, T., *Acta Crystallographica Section B* **2013,** *69* (3), 249-259.